NASA Technical Memorandum 87640

SHORT-WAVELENGTH BUCKLING AND SHEAR FAILURES FOR COMPRESSION-LOADED COMPOSITE LAMINATES

MARK J. SHUART

NOVEMBER 1985

National Aeronautics and Space Administration

Langley Research Center
Hampton, Virginia 23665

TABLE OF CONTENTS

LIST OF TABLES

LIST OF FIGURES

LIST OF SYMBOLS

a	laminate length
A_{jk}	fiber-plate extensional stiffnesses
A^{T}_{jk}	laminate extensional stiffnesses
b	laminate width
c_1	parameter determined by lamina location
D_{jk}	fiber-plate bending stiffnesses
$\overline{D}$	bending stiffness operator
$\tilde{D}$	bending stiffness parameter
E	Young's modulus
E^*	material constant for matrix-foundation
G	shear modulus
G_1^*, G_2^*	material constants for matrix-foundation
h	fiber diameter
h_{mn}	material constant for fiber-plate
H_{mn}	material constant for fiber-plate
k	bonding parameter
k_m	material constant for fiber-plate

L_m	material constant for idealized lamina
$\overline{M}$	material constant for matrix-foundation
M_x, M_y, M_{xy}	moment resultants for fiber-plate
N	number of laminae in laminate
$\overline{N}$	material constant for matrix-foundation
N_x, N_y, N_{xy}	inplane stress resultants for fiber-plate
P_o	load in a 0° lamina
P_θ	load in a θ-oriented lamina
Q_{jk}	reduced stiffnesses for fiber-plate
$\overline{Q}_{jk}$	transformed reduced stiffnesses for fiber-plate
t	lamina thickness
u, v, w	displacements
$\overline{u}$, $\overline{v}$, $\overline{w}$	displacements
$\overline{u}_o$	applied end shortening for the laminate
U	strain energy
V_f	fiber volume fraction
V_y	transverse shear stress resultant
$\overline{w}$	amplitude of w displacement
$\overline{w}_{max}$	maximum w displacement for the laminate
w_1	w displacement due to loading
w_o	initial imperfection for a lamina

$\bar{w}_o$	amplitude of initial imperfection
x, y, z	laminate coordinates
$\bar{x}$	translated x-coordinate
$\bar{z}$	through-the-thickness coordinate for a fiber-plate
$\tilde{z}$	through-the-thickness coordinate for a matrix-foundation
β	slope
γ_{xy}, γ_{xz}, γ_{yz}	shear strains in laminate coordinate system
γ_{12}	shear strain in principal material coordinate system
δ	variational operator
ε	infinitesimal parameter
ε_x, ε_y, ε_z	normal strains in laminate coordinate system
ε_1, ε_2	normal strains in principal material coordinate system
θ	lamina fiber orientation
κ_x, κ_y, κ_{xy}	fiber-plate curvatures
λ	half-wavelength of the short-wavelength buckling mode shape
ν	Poisson's ratio
Π	potential energy
σ	laminate compressive stress
σ_c, σ_{lam}	compressive strength of a laminate

σ_c^*	laminate compressive stress for short-wavelength buckling at $V_f = 0.55$
σ_m^*	shear instability limit of the matrix
σ_R	laminate compressive strength using Rosen's equation
σ_x, σ_y, σ_z	normal stresses in laminate coordinate system
σ_0	compressive strength of a 0° lamina
σ_1, σ_2	normal stresses in principal material coordinate system
σ_o	compressive stress at short-wavelength buckling for a four-lamina laminate
τ_{xy}, τ_{xz}, τ_{yz}	shear stresses in laminate coordinate system
τ_{12}	shear stress in principal material coordinate system
ϕ	skew angle for short-wavelength buckling mode shape of an anisotropic fiber-plate

Superscripts

i	ith fiber-plate or matrix-foundation between ith and (i+1)th fiber-plates
$\circ$	fiber-plate middle surface

Subscripts

a	adjacent equilibrium
c	coefficient of cosine function
cr	short-wavelength buckling
f	fiber
fp	fiber-plate
m	matrix, matrix-foundation
s	coefficient of sine function
1	first-order term
o	prebuckling or zeroth-order term

ABSTRACT

This investigation studies the short-wavelength buckling (or the microbuckling) and the interlaminar and inplane shear failures of multi-directional composite laminates loaded in uniaxial compression. A laminate model is presented that idealizes each lamina. The fibers in the lamina are modeled as a plate, and the matrix in the lamina is modeled as an elastic foundation. The out-of-plane w displacement for each plate is expressed as a trigonometric series in the half-wavelength of the mode shape for laminate short-wavelength buckling. Nonlinear strain-displacement relations are used. The model is applied to symmetric laminates having linear material behavior. The laminates are loaded in uniform end shortening and are simply supported.

A linear analysis is used to determine the laminate stress, strain, and mode shape when short-wavelength buckling occurs. The equations for the laminate compressive stress at short-wavelength buckling are dominated by matrix contributions. The effects of fiber volume fraction on the compressive stress at short-wavelength buckling is reported for a laminate with any stacking sequence and any

thickness. The laminate mode shape at short-wavelength buckling is discussed.

A nonlinear analysis for laminae with initial imperfections is used to determine laminate stresses and interlaminar strains. Results are presented for imperfection-amplitude-to-lamina-thickness ratios of 0.1 and 0.5. The nonlinear behavior of $[0_2]_s$, $[0/90]_s$, $[\pm 45]_s$, and $[+45/0/-45/90]_s$ laminates is discussed. Results are presented for laminate stress, end shortening, and w displacement. The w displacement gradients cause significant interlaminar shear strains γ_{xz} at laminate stresses that are much lower than the laminate stress at short-wavelength buckling, and the distribution of these strains is described. The effect of fiber volume fraction on the nonlinear laminate response is presented for $[0_2]_s$ and $[\pm 45]_s$ laminates.

A failure criterion for compression-loaded laminates is discussed. Laminate failure that is initiated by outer-lamina buckling, by interlaminar shear strains from lamina imperfections, or by inplane matrix shearing is considered. The laminate strength is calculated as a function of lamina orientation for $[\pm\theta]_s$ laminates. A simple method referred to as the stiffness-ratio method is described for predicting the strength of 0°-dominated laminates.

CHAPTER 1

INTRODUCTION

Composite materials are being widely used in a variety of applications ranging from sporting equipment to primary structures for commercial transport aircraft. The design of composite structures is often a combination of traditional practices used for metal structures and empirical criteria. This design technique is easy to use but neglects the unique mechanisms that dominate the behavior of composite structures. The most efficient composite structures are designed using a thorough understanding of the basic response mechanisms of these materials.

The uniaxial compressive strength of a composite laminate is a fundamental property. The mechanics of uniaxial compressive failure have been studied by many researchers for unidirectional laminates having fibers parallel to the loading direction. These laminates fail when short-wavelength buckling (or microbuckling) of the fibers occurs or when shear failure at the fiber-matrix interface occurs. Few similar investigations have been conducted for multi-directional composite laminates although multi-directional laminates are more

widely used than unidirectional laminates in composite structural components. This study investigates the short-wavelength buckling of multi-directional composite laminates loaded in compression. This study also addresses the interlaminar shear failures due to short-wavelength imperfections and the inplane shear failures in these laminates. The results of this study are reported herein.

1.1 Chronological Review of the Literature

This section reviews the literature on models for predicting the compressive strength of composite materials. This review focuses on studies that emphasize the short-wavelength buckling phenomenon and the interlaminar shear failures due to short-wavelength initial imperfections. The review is chronological except that similar subsequent publications by an author are discussed with the first reference. A summary of the review is found at the end of this section.

In 1960 Dow and Gruntfest [1] postulated that the compressive failure of unidirectional laminates was the result of either of the following two phenomena: (1) high tensile stresses perpendicular to the loading direction and at the fiber-matrix interface; or (2) buckling of the fibers within the matrix. The former phenomenon is often called transverse tension failure, and the latter phenomenon is often called microbuckling. An equation to predict the laminate

compressive strength at microbuckling was derived using reference 2 and is based on a model consisting of columns supported by an elastic foundation. An empirical constant was included in this equation. This reference was the first to associate fiber instability with the compressive strength of unidirectional laminates.

Fried [3], Fried and Kaminetsky [4], and Fried [5] studied the influence of the matrix, the reinforcement, and the matrix-reinforcement interface on the compressive failure of composite materials. Experimental results from unidirectional laminates were reported in reference 3 and led Fried to suggest the following failure sequence: the reinforcement phase in a composite material carries the compressive load until the rigid matrix phase yields; upon yielding, the matrix flows and no longer supports the reinforcement; the reinforcement buckles; and the composite material fails catastrophically. The laminate compressive strength was expressed as a linear function of the matrix yield stress by assuming that (1) the maximum stress in the matrix is its yield stress and that (2) the strain in the matrix is the same as the strain in the reinforcement. In his investigation Fried also identified the straightness of the reinforcement and the bond between the reinforcement and the matrix as secondary effects on the compressive strength.

Experimental results in a subsequent study [4] supported Fried's initial conclusions. The results in reference 4 showed that

the compressive strength for unidirectional laminates increases with increasing matrix yield stress for the materials studied. The yield stress for each matrix material was presented, but no other properties (e.g., Young's modulus or shear modulus) of the matrix were discussed.

Fried [5] also studied the compressive failure of filament wound $[0/90]_s$-class laminates. He observed interlaminar cracking in failed compression specimens. This failure mode for specimens loaded in compression was similar to the failure mode for specimens loaded in interlaminar shear, and Fried assumed that failure was the result of debonding at the matrix-reinforcement interface for both load cases. Fried suggested that debonding initiated at voids. Experimental results showed that laminate compressive strength was inversely proportional to void content. As discussed in references 3 and 4, the compressive strength for laminates with very low void contents was limited by the matrix yield stress.

Leventz [6] studied the influence of fiber diameter on the compressive strength of glass-epoxy composite materials. Experimental results showed that the compressive strength was maximized using a 0.005-in.-diameter glass fiber. The range of fiber diameters for this study was from 0.001 inches to 0.010 inches. Leventz reported that the failure mode for the unidirectional composite materials in his study appeared to be a combination of fiber instability and matrix

shear failure. He suggested that the laminate compressive strength was proportional to the square of the fiber diameter although the experimental results did not support this theory. Leventz reported that the larger diameter fibers were more collimated than the smaller diameter fibers, but he did not investigate the influence of fiber straightness on the laminate compressive strength.

In 1965 Rosen [7] reported on his classic study of the compressive failure of unidirectional composite materials. This study focused on fiber instability in glass-epoxy laminates using a two-dimensional model. The fibers were modeled as columns supported by an elastic matrix foundation. Rosen suggested that compressive failure for a unidirectional composite material occurred when the fibers buckled into either of two possible short-wavelength modes, the extension mode or the shear mode. These mode shapes are shown in figure 1.1. For the extension mode, the deformation of the matrix material between fibers is extension in the direction perpendicular to the fibers. For the shear mode, shear deformation occurs in the matrix material. The wavelength is short compared to the length or the width of the test specimen for both buckling modes. Using an energy formulation, Rosen obtained

$$\sigma_c = 2V_f \left[\frac{V_f E_m E_f}{3(1-V_f)} \right]^{1/2} \qquad (1.1)$$

for the extension mode and

$$\sigma_c = \frac{G_m}{1-V_f} + \frac{\pi^2 E_f h^2}{12\lambda^2} \qquad (1.2)$$

for the shear mode where

σ_c = compressive strength of the unidirectional composite material

V_f = fiber volume fraction

E_m = Young's modulus for the matrix

E_f = Young's modulus for the fiber

G_m = shear modulus for the matrix

h = fiber diameter

λ = half-wavelength of the buckling mode shape

The magnitude of the second term in equation (1.2) is small compared to the magnitude of the first term since the half-wavelength is much larger than the fiber diameter. Neglecting the second term, Rosen obtained the approximate (and more familiar) equation for the shear mode

$$\sigma_c = \frac{G_m}{1-V_f} \qquad (1.3)$$

The composite material compressive strength was predicted using the lower value from equations (1.1) and (1.3). Equation (1.3) gives the lower prediction for most composite materials.

Rosen recognized that equation (1.3) gave predicted strengths that were two to three times greater than experimental strengths when the elastic shear modulus of the matrix was used. He obtained more realistic strength predictions by assuming the matrix shear modulus was a function of the applied load.

Unlike previous theories, Rosen's analysis did not use empirical factors for predicting compressive strength. Also, equation (1.3) illustrates that the composite material compressive strength is a function of the matrix shear modulus for fiber-instability-initiated failures.

The results from reference 7 were also included in a subsequent report by Dow and Rosen [8]. Also, Dow, Rosen, and Hashin [9] modified equation (1.3) to account for an elastic-perfectly-plastic response of the matrix. The matrix material was assumed to be isotropic and incompressible after yielding. The authors of reference 9 obtained

$$\sigma_c = \left[\frac{V_f \, E_f \, \sigma_f}{3(1-V_f)} \right]^{1/2} \qquad (1.4)$$

where σ_y is the yield stress of the matrix, and the other variables are defined above. The use of equation (1.4) is limited since many matrix materials do not exhibit elastic-perfectly-plastic behavior.

Ekvall [10] also studied fiber instability for glass-epoxy laminates loaded in compression. He observed that the matrix yielded well before laminate failure. This observation contradicted the theory in reference 3. Ekvall predicted the buckling wavelength for fiber instability to be on the order of a fiber diameter, and this prediction agreed with his experimental results.

Hayashi [11] reported on a "shear instability failure" for orthotropic materials. He postulated that such a failure occurred when a material's flexural rigidity was significantly greater than its shear rigidity. This concept of a shear-deformation-dominated instability for orthotropic materials is the same as that discussed by Rosen [7] for fiber-reinforced composite materials. Hayashi minimized the potential energy of a compression-loaded orthotropic material and obtained an expression for the strength associated with the shear instability failure

$$\sigma_c = G \tag{1.5}$$

where σ_c is the compressive strength and G is the shear modulus of the material. The shear modulus for a unidirectional composite material can be calculated as a function of constituent properties from

$$G_c = \frac{G_m}{V_f \frac{G_m}{G_f} + (1-V_f)} \tag{1.6}$$

where G_c is the shear modulus for a unidirectional composite material and G_f is the shear modulus of the fiber (see reference 12). The other variables are defined in the preceeding paragraphs. The shear modulus of the fiber is much greater than the shear modulus of the matrix for most fiber-reinforced composite materials, and the first term in the denominator of equation (1.6) can be neglected. The shear modulus for a unidirectional composite material is approximated by

$$G_c = \frac{G_m}{1-V_f} \tag{1.7}$$

When equation (1.7) is substituted into equation (1.5) (Note: $G = G_c$ for composite materials), equation (1.3) is obtained.

Independent of Rosen, Schuerch [13] also obtained equations (1.1) and (1.3) for the short-wavelength buckling of unidirectional composite materials. Schuerch tested boron-magnesium laminates and obtained good correlation between theory and experiment.

In 1966 Foye [14] showed that the upper bound for any material's compressive strength was its shear modulus (cf., equation (1.5)). Also, he showed that this upper bound could be approximated by equation (1.3) for unidirectional composite materials. Foye suggested that differences between experimental strengths and predicted strengths for composite materials were due to "local imperfections." He observed fiber instability in randomly located regions throughout the material. He also modified his compressive strength predictions by including the effects of voids and matrix fillers.

Some researchers attempted to isolate fiber instability in a laminate by studying a single fiber surrounded by matrix. Hermann, Mason, and Chan [15] developed a beam model that included initial waviness of the beam. The authors of reference 15 found that the short-wavelength buckling loads predicted by their model agreed with similar loads for the extension mode in reference 13. Also, the response of the model was significantly influenced by the initial waviness of the beam. Sadowsky, Pu, and Hussain [16] developed a model to study fiber instability caused by manufacturing-induced

residual thermal stresses. The authors of reference 16 predicted the compressive strain for short-wavelength buckling of the fiber. They showed that the shear deformation of the fiber had a negligible effect on the fiber compressive strain at buckling for most composite materials. The predicted strains appear to be more than an order of magnitude greater than experimental results.

Crawford [17] studied the compressive behavior of a boron-polyimide-film layered composite material. Analytical and experimental results were presented. Crawford modified the analysis of reference 13 to account for any inplane-load-carrying capability of the matrix. The inplane axial stiffness of the boron layer was expressed as a function of the layer's initial waviness. Crawford suggested that this initial waviness caused interlaminar normal and shear stresses that resulted in laminate failure prior to short-wavelength buckling. He predicted the amplitude and half-wavelength of the initial waviness for this laminate to be approximately five times and eighty times the thickness of the boron layer, respectively.

Yue, et al. [18] studied the compressive behavior of Al-$CuAl_2$ eutectic composite materials. The authors of reference 18 expanded the results of reference 9 to model linear strain-hardened matrix

materials and obtained reasonable agreement between theoretical and experimental strengths.

Lager and June [19] used Rosen's results [7] to experimentally study the effect of matrix modulus and of fiber volume fraction on the unidirectional compressive strength of boron-epoxy laminates. Two matrix materials were used to fabricate specimens with fiber volume fractions ranging from 0.05 to 0.46. The authors of reference 19 modified equations (1.1) and (1.3) by including an "influence coefficient" that was determined empirically. They used the influence coefficient to account for softening of the matrix with increasing applied load. The coefficient was the same for both equations. The strength of specimens fabricated using the stiffer matrix were higher than the strength of similar specimens fabricated using the softer matrix. The experimental strengths for specimens having fiber volume fractions less than ten percent agreed with the predicted strengths from modified equation (1.1), and the experimental strengths for specimens having fiber volume fractions greater than ten percent agreed with the predicted strengths from modified equation (1.3).

Chung and Testa [20] applied Biot's mechanics of incremental deformations [21] to a model for fibrous composite materials in their study of short-wavelength buckling. The model consisted of fiber beams supported by an elastic matrix foundation. The authors of reference 20 calculated the laminate stress that buckled fibers into

either the extension mode or the shear mode (figure 1.1). The equations for these stresses reduced to Rosen's equations [7] (i.e., equations (1.1) and (1.3)) when the buckling wavelength was much greater than the thickness of the matrix between fibers. The authors of reference 20 also presented experimental results from specimens with fiber volume fractions less than 0.10 that agreed with their analytical results. The equations in reference 20 are useful but much more difficult to use than the equations in reference 7.

Russian researchers have also predicted the compressive strength of unidirectional composite materials [22-27]. They obtained equation (1.5) using nonlinear elasticity theory [22-24,26,27]. Skudra, Kalnays, and Bulavs [25] postulated that the laminate compressive strength was strictly a function of compressive and shear failures of the composite material's constituents. Limited experimental results are also presented in references 24 and 25.

De Ferran and Harris [28] studied the compressive strength of steel-wire - polyester-resin composite materials. They suggested that the laminate compressive failure was a function of the wire (or fiber) tensile strength and that a simple "rule-of-mixtures" analysis could predict the compressive strength. They obtained experimental strengths that agreed with their predicted strengths although the

analysis neglects any of the fiber instabilities or matrix failures documented in previous studies.

Kiusalaas and Jaunzemis [29] also used incremental deformation theory [21] to study short-wavelength buckling of composite materials. Their investigation was motivated by the beam-on-an-elastic-foundation model used by Chung and Testa [20]. Kiusalaas and Jaunzemis derived a continuum theory for buckling of a laminated medium. The medium consisted of alternating fiber and matrix layers. The results of reference 29 reduce to the results of reference 20.

Hayashi [30] and Hayashi and Koyama [31] expanded Hayashi's previous theory for the compressive strength of orthotropic materials [11] to unidirectional composite materials. Hayashi [30] assumed that a compression-loaded composite material fails when the axial stress in the matrix equals the "shear instability limit" of the matrix, σ_m^*. He defined this limit as the shear modulus of the matrix and calculated the compressive strength of a unidirectional composite material by assuming equal axial strain in the fiber and the matrix. Hayashi obtained the rule-of-mixtures equation

$$\sigma_c = \sigma_f V_f + \sigma_m^*(1-V_f) \tag{1.8}$$

where σ_f is the fiber stress corresponding to the axial strain at failure. The other variables are defined in the preceeding paragraphs. The fiber had linear elastic material response. This analysis considers matrix instability (instead of fiber instability) as the cause of laminate failure. The predicted strengths from equation (1.8) were compared to experimental strengths in references 30 and 31. Only some of the data agreed with the predictions, and no explanation was given for discrepancies between analytical and experimental results.

Independent of Hayashi, Orringer [32] also postulated that a matrix instability could cause compressive failure of composite materials. Orringer defined a "matrix critical strain" and calculated the composite material's strength at this strain using a rule-of-mixtures equation. He also studied short-wavelength buckling of fibers. Orringer suggested that "progressive buckling" of the fibers led to laminate failure. He assumed that the progressive buckling started at voids or at disbonds within the laminate.

In 1972 Greszczuk [33,34] reported on his experimental investigations of the effects of the constituents on the compressive strength of fiber- and lamina-reinforced composite materials. These investigations include the most thorough experimental results to date. The author varied the matrix material, the fiber material, the fiber diameter, the fiber volume fraction of the specimen, the initial

imperfections (i.e., initial waviness) in the specimen, the specimen geometry, and the specimen's boundary conditions for unidirectional fiber-reinforced specimens. Greszczuk performed similar studies for lamina-reinforced specimens with 6061-T6 aluminum laminae. He reported on the influence of constituent properties on the composite material's compressive failure mode. Short-wavelength buckling of the reinforcement occurred when the shear modulus of the matrix was low. Compressive strength failure of the reinforcement occurred when the shear modulus of the matrix was high. Initial imperfections significantly decreased the strength of all specimens. The results presented in references 33 and 34 were also presented in subsequent reports [35-39].

Suarez, Whiteside, and Hadcock [40] studied the compressive strength of multi-directional boron-epoxy laminates. This study was one of the first to investigate lamina instability in multi-directional laminates. The authors of reference 40 assumed that the outer-most laminae buckled in a short-wavelength mode; the remainder of the laminate was treated as an elastic foundation with both extensional and shearing stiffness. The fibers in the outer-most laminae were always oriented parallel to the direction of loading (i.e., 0-degree laminae). Some experimental results agreed with predicted strengths when the initial waviness of the outer laminae was included in the analysis. The authors assumed that the ratio of waviness amplitude to lamina thickness ranged from 0.2 to 0.4.

Filament failure and global instability of the specimen were also discussed.

Hackett, Tarpy, and Wood [41] studied fiber instability by performing tests on a single steel wire embedded in a block of epoxy resin. They obtained the load and stress distribution at buckling using a photoelastic stress analysis and compared these experimental results with analytical results they obtained using a finite element analysis. The authors of reference 41 reported reasonable agreement between the experimental and the analytical results. This study illustrates a useful test technique but has limited application to the short-wavelength buckling of composite laminates.

Lanir and Fung [42] considered the buckling and postbuckling response of cylindrical columns of matrix reinforced with parallel, straight fibers. They suggested that the compressive failure of a unidirectional laminate occurred at a load much greater than the buckling load of the fiber. They did not consider a short-wavelength buckling mode as the initial mode shape for the buckled fiber. The buckling mode shape changed with increasing load (the wavelength decreased with increasing load). They assumed that failure resulted from high stresses at the fiber-matrix interface.

Independent of references 11 and 14, Kao and Pipkin [43] showed that the critical stress for short-wavelength buckling was

equal to the shear modulus of the composite material (see equation (1.5)). They also showed that the shear mode for short-wavelength buckling was an admissible deformation for fiber-reinforced columns. This study discusses short-wavelength buckling as a basic response phenomenon for unidirectional laminates; the compressive failure of such laminates is not discussed.

Kulkarni, Rice, and Rosen [44,45] modified equation (1.3) to account for shear deformation of the fiber and for imperfect bonding at the fiber-matrix interface. They obtained an expression for the compressive strength of a unidirectional laminate,

$$\sigma_c = G_m \left[\frac{1-(1-k)V_f}{1-\left(1-\frac{G_m}{G_f}k\right)V_f} \right]^2 \left[1-\left(1-\frac{G_m}{G_f}\right)V_f \right] \qquad (1.9)$$

where G_f is the shear modulus of the fiber and k is a bonding parameter. They defined the range for k as

$$-\left(\frac{1-V_f}{V_f}\right) \leq k \leq 1 \qquad (1.10)$$

where the limits represent no bonding and perfect bonding, respectively. The authors showed that the compressive strength

predicted by equation (1.9) was less than the compressive strength predicted by equation (1.3).

Davis [46,47] included both nonlinear material behavior and initial waviness of the laminae in his analysis of the compressive strength of unidirectional composite materials. A model consisting of fiber layers and matrix layers was analyzed as a multilayered Timoshenko beam loaded in compression. The matrix material had a nonlinear shear stress-strain behavior. Davis measured the initial waviness of the laminae in his boron-epoxy specimens, and the ratio of initial waviness amplitude to lamina thickness ranged from 0.2 to 1.6. He assumed that failure was caused either by delamination or by short-wavelength of the lamina. Davis referred to thes short-wavelength buckling as a shear instability. He found that shear instability was the dominant cause of failure for these specimens. Compressive strength predictions based on equation (1.5) agreed with the experimental results.

Hanasaki and Hasegawa [48] and Wang [49] independently conducted studies similar to that conducted by Davis [46]. The results of references 48 and 49 are also similar to the results of reference 46.

Evans and Adler [50] suggested that fiber kinking was the dominant failure mechanism for unidirectional laminates. Kinking

occurred subsequent to short-wavelength buckling within the laminate. The authors of reference 50 studied the mechanics of fiber kinking and obtained a approximate expression for the "critical kink formation stress." They presented experimental results from three-dimensional carbon-carbon woven composite material specimens to illustrate kink geometry.

Similar to Evans and Adler, Maewal [51] studied the short-wavelength buckling and postbuckling behavior of unidirectional laminates in compression. He used a three-layer model consisting of a fiber layer surrounded by matrix layers to analyze the shear mode buckling and initial postbuckling of these laminates. Maewal found that his model predicted a postbuckling stiffness for the laminate that was approximately one-third of the prebuckling stiffness of the laminate. He suggested that initial waviness of the fiber layer did not significantly affect the short-wavelength buckling stress. These results contradict previous studies that show unidirectional laminates have no postbuckling stiffness and show that initial waviness of the laminae significantly affects the stress distribution in the laminate (e.g., reference 46).

Budiansky [52] used the results of the previous two studies [50,51] in his investigation of fiber kinking. He included matrix plasticity and initial waviness of the fibers in his analysis of kinking. Budiansky identified the shear stiffness and shear strength

of the composite material as the most important parameters affecting "kink strength." This reference contains a good discussion of the importance of understanding the role of the matrix and the role of initial waviness of the fibers in predicting the compressive strength of unidirectional laminates.

Hahn and Williams [53] studied the compressive failure mechanisms of unidirectional composite materials using a nonlinear model that included initial waviness of the fiber (called fiber curvature) and nonlinear material behavior for the matrix. The authors of reference 53 determined the loading on a single fiber surrounded by matrix and obtained

$$\sigma_c = V_f \, G_c \tag{1.11}$$

for the compressive strength of a unidirectional laminate with a linear elastic matrix and straight fibers. In equation (1.11) G_c is the composite material shear modulus. A laminate fails when short-wavelength buckling occurs. Equation (1.11) differs from previous predictions [7,11] by the factor V_f. Hahn and Williams suggest that this difference is the result of the free body diagram used in the analysis. As expected, they found that the compressive strength of composite laminates with matrix material nonlinearity and with initial waviness of the fiber was less that the compressive strength of

composite laminates with a linear elastic matrix and straight fibers. This reference also includes experimental results for compressive strength as a function of constituent properties. The authors of reference 53 observed changes in the laminate failure mode caused by changes in the material properties of the matrix.

In summary, researchers have studied the failure mechanisms for compression-loaded composite laminates for the past twenty-five years. Most of these studies have focused on the short-wavelength buckling of unidirectional laminates and on the interlaminar shear failures due to lamina imperfections in these laminates. Researchers have obtained reasonable correlation between theory and experiment using geometrically and/or materially nonlinear analyses. The short-wavelength buckling and shear failures of multi-directional laminates in compression have received very limited attention. These laminates were modeled as the outer-most lamina supported by an elastic foundation, and the short-wavelength buckling of the interior laminae was neglected. The outer-most laminae always had fibers parallel to the loading direction. No general theory exists for analyzing short-wavelength buckling and shear failures in compression-loaded symmetric multi-directional laminates.

1.2 Objective and Scope

The objective of this investigation is to study the short-wavelength buckling and the interlaminar shear failure due to short-wavelength imperfections of multi-directional laminates loaded in uniaxial compression. The inplane shear failure within anisotropic laminae is also addressed for these multi-directional laminates. A model that focuses on these specific phenomena is presented. The model is used to analyze laminates with orthotropic or anisotropic laminae. The stacking sequence of each laminate in this study is symmetric with respect to the laminate's middle surface. A linear analysis is used to determine the laminate stress, strain, and mode shape when short-wavelength buckling occurs. A nonlinear analysis that assumes initially imperfect (i.e., initially wavy) laminae is used to calculate the laminate stresses and interlaminar strains. The initial imperfection for each lamina has the same shape as the laminate's short-wavelength buckling mode. A result of this investigation is a failure criterion based on short-wavelength buckling of the laminae and shear failures within the laminate.

Chapter 2

ANALYSIS

This chapter presents a model for the short-wavelength buckling and shear response of compression-loaded composite laminates. The model considers the interlaminar shearing due to short-wavelength initial imperfections and the inplane shearing in these laminates. The governing equations of the model are derived from first principles using an energy formulation. The loading and boundary conditions of the model are discussed. The solution of the governing equations is described. A linear analysis is performed to obtain the eigenvalues and eigenvectors associated with short-wavelength buckling in the laminate. A nonlinear analysis is performed to obtain the stress distribution in a laminate with initially imperfect laminae.

2.1 Derivation of the Governing Equations

2.1.1 Model Description

The geometry of a typical laminate is shown in figure 2.1. The x-y-z coordinate system is referred to as the laminate coordinate

system. The laminate is rectangular having length a and width b. A $+\theta^{\circ}$ fiber orientation in the lamina is indicated in the figure. The laminate is symmetric with respect to the middle surface, the z=0 plane.

The fundamental element for the model in this study is a idealized lamina. The cross-sections of a typical lamina and of an idealized lamina are illustrated in figure 2.2. The typical lamina has thickness t, and the fibers are modeled as a plate (hereafter referred as the "fiber-plate") and the matrix is modeled as an elastic foundation (hereafter referred to as the "matrix-foundation"). The fiber-plate and matrix-foundation have uniform thicknesses t_f and t_m, respectively, where

$$t_f = V_f t$$

$$t_m = \frac{1}{2}(1-V_f)t \qquad (2.1)$$

V_f is the fiber volume fraction of the laminate. Combining equations (2.1),

$$t = t_f + 2t_m \qquad (2.2)$$

Idealized laminae are assembled to form the model for a laminate. The model for a typical laminate is shown in figure 2.3. The linear elastic properties used in this analysis are presented in Table 2.1. The fiber-plate properties are typical properties for a graphite-epoxy lamina. The matrix-foundation properties are neat resin properties from reference 54. The typical lamina thickness is 0.0052 inches.

Initial imperfections in the fiber-plate are also included in the model. Previous authors have referred to these initial imperfections as initial waviness of the fibers or as fiber curvature. The initial imperfections in this study have the same shape as the short-wavelength buckling mode shape for the laminate.

2.1.2 Fiber-Plate Contributions

A geometrically nonlinear plate theory is used for the fiber-plates. The ith fiber-plate has displacements $u^{(i)}$, $v^{(i)}$, and $w^{(i)}$ in the x, y, and z directions, respectively. The theory for the fiber-plates is derived using the Kirchhoff assumptions:

1. Normals to the undeformed middle surface of each fiber-plate remain straight, normal, and inextensional during deformation so that the transverse normal strains ε_z and

transverse shearing strains γ_{yz} and γ_{xz} in the fiber-plate may be neglected; and

2. Transverse normal stresses σ_z in the fiber-plate are small compared to the other normal stress components and may be neglected in the stress-strain relations.

The first assumption leads to the following expressions for the fiber-plate displacements,

$$\begin{aligned} u^{(i)}(x,y,\bar{z}) &= u^{(i)^\circ}(x,y) - \bar{z}w^{(i)^\circ}(x,y)_{,x} \\ v^{(i)}(x,y,\bar{z}) &= v^{(i)^\circ}(x,y) - \bar{z}w^{(i)^\circ}(x,y)_{,y} \\ w^{(i)}(x,y,\bar{z}) &= w^{(i)^\circ}(x,y) \end{aligned} \qquad (2.3)$$

where $u^{(i)^\circ}$, $v^{(i)^\circ}$, and $w^{(i)^\circ}$ are displacements in the x, y, and z directions, respectively, for the middle surface of the ith fiber-plate, $\bar{z}$ is the through-the-thickness coordinate of the fiber-plate such that $-\frac{t_f}{2} \leq \bar{z} \leq \frac{t_f}{2}$, and subscripts x and y preceeded by commas denote partial differentiation with respect to x or y. The $w^{(i)^\circ}$ displacement is the sum of the displacements due to the initial

imperfection of the fiber-plate $w_o^{(i)}$ and the displacement due to loading $w_1^{(i)}$, i.e.,

$$w^{(i)^\circ}(x,y) = w_o^{(i)}(x,y) + w_1^{(i)}(x,y) \tag{2.4}$$

The expressions for the normal and shear strains in the ith fiber-plate are

$$\begin{aligned} \varepsilon_x^{(i)} &= \varepsilon_x^{(i)^\circ} + \bar{z}\kappa_x^{(i)} \\ \varepsilon_y^{(i)} &= \varepsilon_y^{(i)^\circ} + \bar{z}\kappa_y^{(i)} \\ \gamma_{xy}^{(i)} &= \gamma_{xy}^{(i)^\circ} + \bar{z}\kappa_{xy}^{(i)} \end{aligned} \tag{2.5}$$

where $\varepsilon_x^{(i)^\circ}$, $\varepsilon_y^{(i)^\circ}$, and $\gamma_{xy}^{(i)^\circ}$ are the normal and shearing strains for the middle surface of the ith fiber-plate, and $\kappa_x^{(i)}$, $\kappa_y^{(i)}$, and $\kappa_{xy}^{(i)}$ are the curvatures of the ith fiber-plate. The middle surface strains are defined using the von Karman nonlinear strain-displacement relations and include the initial imperfections of the fiber-plate. These strain-displacement relations assume that the strains are small compared to unity, that rotations relative to the x and y

directions are moderately small, and that rotations relative to the z direction are negligibly small. The strain-displacement relations for the ith fiber-plate are

$$\begin{aligned}
\varepsilon_x^{(i)^\circ} &= u_{,x}^{(i)^\circ} + \frac{1}{2}\left(w_{1,x}^{(i)}\right)^2 + w_{o,x}^{(i)} w_{1,x}^{(i)} \\
\varepsilon_y^{(i)^\circ} &= v_{,y}^{(i)^\circ} + \frac{1}{2}\left(w_{1,y}^{(i)}\right)^2 + w_{o,y}^{(i)} w_{1,y}^{(i)} \\
\gamma_{xy}^{(i)^\circ} &= u_{,y}^{(i)^\circ} + v_{,x}^{(i)^\circ} + w_{1,x}^{(i)} w_{1,y}^{(i)} \\
&\quad + w_{o,x}^{(i)} w_{1,y}^{(i)} + w_{o,y}^{(i)} w_{1,x}^{(i)}
\end{aligned} \tag{2.6}$$

The normal and shearing strains are zero when the fiber-plate is unloaded. The curvatures are defined by

$$\begin{aligned}
\kappa_x^{(i)} &= -w_{1,xx}^{(i)} \\
\kappa_y^{(i)} &= -w_{1,yy}^{(i)} \\
\kappa_{xy}^{(i)} &= -2w_{1,xy}^{(i)}
\end{aligned} \tag{2.7}$$

The initial imperfection does not appear in the definition of the curvatures since the curvatures are determined by the change in slope of the middle surface from the initial middle surface geometry.

Each fiber-plate is homogeneous and has linear elastic material behavior. A fiber-plate has specially orthotropic material symmetry with respect to a principal material coordinate system. This coordinate system has axes that are parallel (1-axis) and perpendicular (2-axis) to the fiber orientation in the fiber-plate, and these axes are illustrated in figure 2.4 for a $+\theta$ fiber orientation ($-90^{\circ} \leq \theta \leq +90^{\circ}$). The laminate coordinate axes x and y are also illustrated in the figure. The constitutive relation for a specially orthotropic fiber-plate is

$$\begin{Bmatrix} \sigma_1 \\ \sigma_2 \\ \tau_{12} \end{Bmatrix} = \begin{bmatrix} Q_{11} & Q_{12} & 0 \\ Q_{12} & Q_{22} & 0 \\ 0 & 0 & Q_{66} \end{bmatrix} \begin{Bmatrix} \varepsilon_1 \\ \varepsilon_2 \\ \gamma_{12} \end{Bmatrix} \tag{2.8}$$

where $\{\sigma\}$ and $\{\varepsilon\}$ are the inplane stresses and strain, respectively, and $[Q]$ are the reduced stiffnesses for the fiber-plate. The reduced stiffnesses are calculated using material properties and

$$\begin{aligned} Q_{11} &= E_{11}/(1-\nu_{12}\nu_{21}) \\ Q_{12} &= \nu_{12}E_{22}/(1-\nu_{12}\nu_{21}) \\ Q_{22} &= E_{22}/(1-\nu_{12}\nu_{21}) \\ Q_{66} &= G_{12} \end{aligned} \tag{2.9}$$

where

E_{11} = Young's modulus in the direction parallel to the fibers

E_{22} = Young's modulus in the direction perpendicular to the fibers

G_{12} = shear modulus in the 1-2 plane

ν_{12} = major Poisson's ratio

ν_{21} = minor Poisson's ratio

The ith fiber-plate has generally orthotropic material symmetry with respect to the laminate coordinate system. The constitutive relation for the ith fiber-plate is

$$\begin{Bmatrix} \sigma_x \\ \sigma_y \\ \tau_{xy} \end{Bmatrix}^{(i)} = \begin{bmatrix} \bar{Q}_{11} & \bar{Q}_{12} & \bar{Q}_{16} \\ \bar{Q}_{12} & \bar{Q}_{22} & \bar{Q}_{26} \\ \bar{Q}_{16} & \bar{Q}_{26} & \bar{Q}_{66} \end{bmatrix}^{(i)} \begin{Bmatrix} \varepsilon_x \\ \varepsilon_y \\ \gamma_{xy} \end{Bmatrix}^{(i)} \qquad (2.10)$$

where $\{\sigma\}^{(i)}$ are the fiber-plate stresses in the laminate coordinate system, $\{\varepsilon\}^{(i)}$ are defined by equations (2.5) and (2.6), and $[\bar{Q}]^{(i)}$ are the transformed reduced stiffness of the ith fiber-plate. The

transformed reduced stiffnesses are calculated using equations (2.9) and

$$\bar{Q}_{11}^{(i)} = Q_{11}\cos^4\theta_i + 2(Q_{12}+2Q_{66})\cos^2\theta_i\sin^2\theta_i + Q_{22}\sin^4\theta_i$$

$$\bar{Q}_{12}^{(i)} = (Q_{11}+Q_{22}-4Q_{66})\sin^2\theta_i\cos^2\theta_i + Q_{12}(\sin^4\theta_i + \cos^4\theta_i)$$

$$\bar{Q}_{22}^{(i)} = Q_{11}\sin^4\theta_i + 2(Q_{12}+2Q_{66})\sin^2\theta_i\cos^2\theta_i + Q_{22}\cos^4\theta_i$$

$$\bar{Q}_{16}^{(i)} = (Q_{11}-Q_{12}-2Q_{66})\sin\theta_i\cos^3\theta_i + (Q_{12}-Q_{22}+2Q_{66})\sin^3\theta_i\cos\theta_i$$

$$\bar{Q}_{26}^{(i)} = (Q_{11}-Q_{12}-2Q_{66})\sin^3\theta_i\cos\theta_i + (Q_{12}-Q_{22}+2Q_{66})\sin\theta_i\cos^3\theta_i$$

$$\bar{Q}_{66}^{(i)} = (Q_{11}+Q_{22}-2Q_{12}-Q_{66})\sin^2\theta_i\cos^2\theta_i + Q_{66}(\sin^4\theta_i + \cos^4\theta_i) \qquad (2.11)$$

where θ_i is the fiber orientation of the ith fiber-plate. For convenience, fiber-plates with $\theta_i = 0^\circ$ or with $\theta_i = 90^\circ$ are subsequently referred to as orthotropic fiber-plates. Fiber-plates with any other θ_i are subsequently referred to as anisotropic fiber-plates.

The potential energy of the ith fiber-plate is the sum of the potential energy of the applied loads and the strain energy of the fiber-plate. The potential energy of the applied loads is zero for

this model as discussed in section 2.1.5 Model Loading and Boundary Conditions. The strain energy of the ith fiber-plate $U_{fp}^{(i)}$ is

$$U_{fp}^{(i)} = \frac{1}{2}\int_0^a\int_0^b\int_{-t_f/2}^{t_f/2} [\sigma_x^{(i)}\varepsilon_x^{(i)} + \sigma_y^{(i)}\varepsilon_y^{(i)} + \sigma_z^{(i)}\varepsilon_z^{(i)} + \tau_{yz}^{(i)}\gamma_{yz}^{(i)} + \tau_{xz}^{(i)}\gamma_{xz}^{(i)} + \tau_{xy}^{(i)}\gamma_{xy}^{(i)}]\, d\bar{z}\, dy\, dx \tag{2.12}$$

Using the Kirchhoff assumptions, equation (2.12) is simplified to

$$U_{fp}^{(i)} = \frac{1}{2}\int_0^a\int_0^b\int_{-t_f/2}^{t_f/2} [\sigma_x^{(i)}\varepsilon_x^{(i)} + \sigma_y^{(i)}\varepsilon_y^{(i)} + \tau_{xy}^{(i)}\gamma_{xy}^{(i)}]\, d\bar{z}\, dy\, dx \tag{2.13}$$

Using equations (2.5) and (2.10), equation (2.13) becomes

$$U_{fp}^{(i)} = \frac{1}{2}\int_0^a\int_0^b\int_{-t_f/2}^{t_f/2} [\bar{Q}_{11}^{(i)}(\varepsilon_x^{(i)^\circ} + \bar{z}\kappa_x^{(i)})^2 + \bar{Q}_{22}^{(i)}(\varepsilon_y^{(i)^\circ} + \bar{z}\kappa_y^{(i)})^2 + \bar{Q}_{66}^{(i)}(\gamma_{xy}^{(i)^\circ} + \bar{z}\kappa_{xy}^{(i)})^2 + 2\{\bar{Q}_{12}^{(i)}(\varepsilon_x^{(i)^\circ} + \bar{z}\kappa_x^{(i)})(\varepsilon_y^{(i)^\circ} + \bar{z}\kappa_y^{(i)}) +$$

$$\bar{Q}_{16}^{(i)}(\varepsilon_x^{(i)^\circ} + \bar{z}\kappa_x^{(i)})(\gamma_{xy}^{(i)^\circ} + \bar{z}\kappa_{xy}^{(i)}) +$$

$$\bar{Q}_{26}^{(i)}(\varepsilon_y^{(i)^\circ} + z\kappa_y^{(i)})(\gamma_{xy}^{(i)^\circ} + \bar{z}\kappa_{xy}^{(i)})\}] \, d\bar{z} \, dy \, dx \tag{2.14}$$

Equation (2.14) is integrated with respect to the through-the-thickness coordinate $\bar{z}$ to obtain

$$U_{fp}^{(i)} = \frac{1}{2}\int_0^a\int_0^b [A_{11}^{(i)}\varepsilon_x^{(i)^{\circ 2}} + A_{22}^{(i)}\varepsilon_y^{(i)^{\circ 2}} + A_{66}^{(i)}\gamma_{xy}^{(i)^{\circ 2}} +$$

$$2(A_{12}^{(i)}\varepsilon_x^{(i)^\circ}\varepsilon_y^{(i)^\circ} + A_{16}^{(i)}\varepsilon_x^{(i)^\circ}\gamma_{xy}^{(i)^\circ} +$$

$$A_{26}^{(i)}\varepsilon_y^{(i)^\circ}\gamma_{xy}^{(i)^\circ}) + D_{11}^{(i)}\kappa_x^{(i)^2} + D_{22}^{(i)}\kappa_y^{(i)^2} +$$

$$D_{66}^{(i)}\kappa_{xy}^{(i)^2} + 2(D_{12}^{(i)}\kappa_x^{(i)}\kappa_y^{(i)} + D_{16}^{(i)}\kappa_x^{(i)}\kappa_{xy}^{(i)}$$

$$+ D_{26}^{(i)}\kappa_y^{(i)}\kappa_{xy}^{(i)})] \, dy \, dx \tag{2.15}$$

where $A_{jk}^{(i)}$ and $D_{jk}^{(i)}$ are the extensional and bending stiffnesses, respectively, of the ith fiber-plate and are defined by

$$(A_{jk}^{(i)},\ D_{jk}^{(i)}) = \int_{-t_f/2}^{t_f/2} \bar{Q}_{jk}^{(i)}\ (1,\ \bar{z}^2)\ d\bar{z} \qquad (2.16)$$

The potential energy contribution of each fiber-plate to the total potential energy of the model is given by equation (2.15).

2.1.3 Matrix-Foundation Contributions

The matrix-foundations elastically support the fiber-plates. The ith matrix-foundation is located between the ith and the (i+1)th fiber-plates and has displacements $u_m^{(i)}$, $v_m^{(i)}$, and $w_m^{(i)}$ in the x, y, and z directions, respectively. The displacements of the ith matrix-foundation in this model are a linear function of the displacements of the adjacent fiber-plates and are defined by

$$u_m^{(i)}(x,y,\bar{z}) = \frac{1}{2t_m}\left[(t_m+\bar{z})u^{(i+1)}\Big|_{\bar{z}=-t_f/2} + (t_m-\bar{z})u^{(i)}\Big|_{\bar{z}=t_f/2}\right]$$

$$v_m^{(i)}(x,y,\bar{z}) = \frac{1}{2t_m}\left[(t_m+\bar{z})v^{(i+1)}\Big|_{\bar{z}=-t_f/2} + (t_m-\bar{z})v^{(i)}\Big|_{\bar{z}=t_f/2}\right]$$

$$w_m^{(i)}(x,y,\bar{z}) = \frac{1}{2t_m}\left[(t_m+\bar{z})w^{(i+1)} + (t_m-\bar{z})w^{(i)}\right] \qquad (2.17)$$

where the fiber-plate displacements are defined by equations (2.3), and $\bar{z}$ is the through-the-thickness coordinate of the matrix-foundation such that $-t_m \leq \bar{z} \leq t_m$. Evaluating the fiber-plate displacements, equations (2.17) become

$$u_m^{(i)} = u^{(i)^\circ} + \frac{t_f}{4t_m}\left[(t_m + \bar{z})w_{1,x}^{(i+1)} - (t_m - \bar{z})w_{1,x}^{(i)}\right]$$

$$v_m^{(i)} = v^{(i)^\circ} + \frac{t_f}{4t_m}\left[(t_m + \bar{z})w_{1,y}^{(i+1)} - (t_m - \bar{z})w_{1,y}^{(i)}\right]$$

$$w_m^{(i)} = \frac{1}{2t_m}\left[(t_m + \bar{z})w_1^{(i+1)} + (t_m - \bar{z})w_1^{(i)}\right] \qquad (2.18)$$

The initial imperfections of the adjacent fiber-plates do not appear in equations (2.18). Deformation in the matrix-foundation is the result of displacements due to loading of the adjacent fiber-plates.

The matrix-foundations in this model have extensional stiffness in the z direction and shearing stiffness in the y-z and x-z planes. The strain-displacement relations for the ith matrix-foundation are

$$\varepsilon_{mz}^{(i)} = w_{m,\bar{z}}^{(i)}$$

$$\gamma_{myz}^{(i)} = v_{m,\bar{z}}^{(i)} + w_{m,y}^{(i)} \qquad (2.19)$$

$$\gamma_{mxz}^{(i)} = u_{m,\bar{z}}^{(i)} + w_{m,x}^{(i)}$$

Equations (2.18) are substituted into equations (2.19) to obtain

$$\varepsilon_{mz}^{(i)} = \frac{1}{2t_m}\left[w_1^{(i+1)} - w_1^{(i)}\right]$$

$$\gamma_{myz}^{(i)} = \frac{1}{2t_m}\left[\left(\frac{t_f}{2} + t_m + \bar{z}\right)w_{1,y}^{(i+1)} + \left(\frac{t_f}{2} + t_m - \bar{z}\right)w_{1,y}^{(i)}\right]$$

$$\gamma_{mxz}^{(i)} = \frac{1}{2t_m}\left[\left(\frac{t_f}{2} + t_m + \bar{z}\right)w_{1,x}^{(i+1)} + \left(\frac{t_f}{2} + t_m - \bar{z}\right)w_{1,x}^{(i)}\right] \qquad (2.20)$$

Equations (2.20) show that the strains in the matrix-foundation are functions of the w displacements of the adjacent fiber-plates. The constitutive relations for the ith matrix-foundation are

$$\sigma_{mz}^{(i)} = \frac{E_m}{1-\nu_m^2}\varepsilon_{mz}^{(i)}$$

$$\tau_{myz}^{(i)} = G_m\,\gamma_{myz}^{(i)} \qquad (2.21)$$

$$\tau_{mxz}^{(i)} = G_m\,\gamma_{mxz}^{(i)}$$

where the matrix-foundation is a linear, elastic, homogeneous material and

E_m = Young's modulus of the matrix

G_m = shear modulus of the matrix

ν_m = Poisson's ratio of the matrix

The strain energy of the ith matrix-foundation $U_m^{(i)}$ is

$$U_m^{(i)} = \frac{1}{2}\int_0^a\int_0^b\int_{-t_m}^{t_m}\left[\sigma_{mz}^{(i)}\varepsilon_{mz}^{(i)} + \tau_{myz}^{(i)}\gamma_{myz}^{(i)} + \tau_{mxz}^{(i)}\gamma_{mxz}^{(i)}\right] d\tilde{z}\, dy\, dx \tag{2.22}$$

Using equations (2.20) and (2.21), equation (2.22) becomes

$$U_m^{(i)} = \frac{1}{2}\int_0^a\int_0^b\int_{-t_m}^{t_m}\left\{\frac{E_m}{1-\nu_m^2}\left[\frac{w_1^{(i+1)} - w_1^{(i)}}{2t_m}\right]^2 + \right.$$

$$\frac{G_m}{4t_m^2}\left[\left(\frac{t_f}{2} + t_m + \tilde{z}\right)w_{1,y}^{(i+1)} + \left(\frac{t_f}{2} + t_m - \tilde{z}\right)w_{1,y}^{(i)}\right]^2 +$$

$$\left.\frac{G_m}{4t_m^2}\left[\left(\frac{t_f}{2} + t_m + \tilde{z}\right)w_{1,x}^{(i+1)} + \left(\frac{t_f}{2} + t_m - \tilde{z}\right)w_{1,x}^{(i)}\right]^2\right\} d\tilde{z}\, dy\, dx \tag{2.23}$$

Equation (2.23) is integrated with respect to the through-the-thickness coordinate $\tilde{z}$ to obtain

$$U_m^{(i)} = \frac{1}{2}\int_0^a\int_0^b \{\frac{E_m}{2t_m(1-\nu_m^2)}\,[w_1^{(i+1)} + w_1^{(i)}]^2 +$$

$$\frac{G_m}{4t_m}\,[(\frac{t_f^2}{2} + 2t_f t_m + \frac{8t_m^2}{3})(w_{1,y}^{(i+1)^2} + w_{1,y}^{(i)^2} + w_{1,x}^{(i+1)^2} + w_{1,x}^{(i)^2})$$

$$+ 2(\frac{t_f^2}{2} + 2t_f t_m + \frac{4t_m^2}{3})(w_{1,y}^{(i+1)}w_{1,y}^{(i)} + w_{1,x}^{(i+1)}w_{1,x}^{(i)})]\}\,dy\,dx$$

(2.24)

The potential energy contribution of the ith matrix-foundation to the total potential energy of the model is given by equation (2.24) where $i = 1, 2, \ldots, (N-1)$ where N is the number of laminae in the laminate. The two outer-most matrix-foundation layers (figure 2.3) do not contribute to the potential energy of the model. The strains in the matrix-foundation result from differences in the w displacements of the fiber-plates. The outer-most matrix-foundation layers have a free surface on one side, and ε_{mz}, γ_{myz}, and γ_{mxz} are zero for these layers.

2.1.4 Governing Equations for the Model

The nonlinear equilibrium equations for the model are derived using the principle of stationary potential energy, i.e., the loaded model is in equilibrium if its total potential energy Π is

stationary. This principle is stated mathematically in terms of the first variation of the total potential energy as

$$\delta\Pi = 0 \tag{2.25}$$

The total potential energy of the model is the sum of the fiber-plate and the matrix-foundation contributions, or

$$\Pi = \sum_{i=1}^{N} U_{fp}^{(i)} + \sum_{i=1}^{N-1} U_{m}^{(i)} \tag{2.26}$$

where N is the number of laminae in the laminate. Using equations (2.6), (2.7), (2.15), (2.24), and (2.26), equation (2.25) becomes

$$\int_0^a \int_0^b \{ \sum_{i=1}^{N} [-(N_{x,x}^{(i)} + N_{xy,y}^{(i)})\delta u^{(i)^\circ} - (N_{y,y}^{(i)} + N_{xy,x}^{(i)})\delta v^{(i)^\circ}] +$$

$$[D_{11}^{(1)} w_{1,xxxx}^{(1)} + 2(D_{12}^{(1)} + 2D_{66}^{(1)}) w_{1,xxyy}^{(1)} + D_{22}^{(1)} w_{1,yyyy}^{(1)} +$$

$$4D_{16}^{(1)} w_{1,xxxy}^{(1)} + 4D_{26}^{(1)} w_{1,xyyy}^{(1)} - [N_x^{(1)}(w_{1,x}^{(1)} + w_{o,x}^{(1)})]_{,x} -$$

$$[N_y^{(1)}(w_{1,y}^{(1)} + w_{o,y}^{(1)})]_{,y} - [N_{xy}^{(1)}(w_{1,x}^{(1)} + w_{o,x}^{(1)})]_{,y} -$$

$$[N_{xy}^{(1)}(w_{1,y}^{(1)} + w_{o,y}^{(1)})]_{,x} + \frac{E_m}{2t_m(1-\nu_m^2)}(w_1^{(1)} - w_1^{(2)}) -$$

$$\frac{G_m}{4t_m}\left[\left(\frac{t_f^2}{2}+2t_ft_m+\frac{8t_m^2}{3}\right)\left(w_{1,yy}^{(1)}+w_{1,xx}^{(1)}\right)+\right.$$

$$\left.\left(\frac{t_f^2}{2}+2t_ft_m+\frac{4t_m^2}{3}\right)\left(w_{1,yy}^{(2)}+w_{1,xx}^{(2)}\right)\right]\delta w_1^{(1)}+$$

$$\sum_{i=2}^{N-1}\left[D_{11}^{(i)}w_{1,xxxx}^{(i)}+2\left(D_{12}^{(i)}+2D_{66}^{(i)}\right)w_{1,xxyy}^{(i)}+D_{22}^{(i)}w_{1,yyyy}\right.$$

$$+4D_{16}^{(i)}w_{1,xxxy}^{(i)}+4D_{26}^{(i)}w_{1,xyyy}^{(i)}-\left[N_x^{(i)}\left(w_{1,x}^{(i)}+w_{o,x}^{(i)}\right)\right]_{,x}-$$

$$\left[N_y^{(i)}\left(w_{1,y}^{(i}+w_{o,y}^{(i}\right)\right]_{,y}-\left[N_{xy}^{(i)}\left(w_{1,x}^{(i)}+w_{o,x}^{(i)}\right)\right]_{,y}-$$

$$-\left[N_{xy}^{(i)}\left(w_{1,y}^{(i)}+w_{o,y}^{(i)}\right)\right]_{,x}+$$

$$\frac{E_m}{2t_m(1-\nu_m^2)}\left(2w_1^{(i)}-w_1^{(i-1)}-w_1^{(i+1)}\right)$$

$$-\frac{G_m}{4t_m}\left[\left(\frac{t_f^2}{2}+2t_ft_m+\frac{8t_m^2}{3}\right)\left(2w_{1,yy}^{(i)}+2w_{1,xx}^{(i)}\right)+\right.$$

$$\left.\left(\frac{t_f^2}{2}+2t_ft_m+\frac{4t_m^2}{3}\right)\left(w_{1,yy}^{(i-1)}+w_{1,xx}^{(i-1)}+w_{1,yy}^{(i+1)}+\right.\right.$$

$$\left.\left.w_{1,xx}^{(i+1)}\right)\right]\delta w_1^{(i)}+\left[D_{11}^{(N)}w_{1,xxxx}^{(N)}+2\left(D_{12}^{(N)}+2D_{66}^{(N)}\right)w_{1,xxyy}^{(N)}\right.$$

$$+D_{22}^{(N)}w_{1,yyyy}+4D_{16}^{(N)}w_{1,xxxy}^{(N)}+D_{26}^{(N)}w_{1,xyyy}^{(N)}-$$

$$\left[N_x^{(N)}\left(w_{1,x}^{(N)}+w_{o,x}^{(N)}\right)\right]_{,x}-\left[N_y^{(N)}\left(w_{1,y}^{(N)}+w_{o,y}^{(N)}\right)\right]_{,y}$$

$$-\left[N_{xy}^{(N)}\left(w_{1,y}^{(N)}+w_{o,y}^{(N)}\right)\right]_{,x}$$

$$- [N_{xy}^{(N)}(w_{1,x}^{(N)} + w_{o,x}^{(N)})]_{,y} + \frac{E_m}{2t_m(1-\nu_m^2)}(w_1^{(N)} - w_1^{(N-1)}) -$$

$$\frac{G_m}{4t_m}[(\frac{t_f^2}{2} + 2t_f t_m + \frac{8t_m^2}{3})(w_{1,yy}^{(N)} + w_{1,xx}^{(N)}) +$$

$$(\frac{t_f^2}{2} + 2t_f t_m + \frac{4t_m^2}{3})(w_{1,yy}^{(N-1)} + w_{1,xx}^{(N-1)})]]\ \delta w_1^{(N)} \Big\} dy\, dx +$$

$$\sum_{i=1}^{N}[\int_0^b N_x^{(i)}\delta u^{(i)^\circ}\Big|_0^a dy + \int_0^a N_{xy}^{(i)}\delta u^{(i)^\circ}\Big|_0^b dx + \int_0^a N_y^{(i)}\delta v^{(i)^\circ}\Big|_0^b dx$$

$$+ \int_0^b N_{xy}^{(i)}\delta v^{(i)^\circ}\Big|_0^a dy - \int_0^b M_x^{(i)}\delta w_{1,x}^{(i)}\Big|_0^a dy - \int_0^a M_y^{(i)}\delta w_{1,y}^{(i)}\Big|_0^b dx$$

$$+ 2M_{xy}^{(i)}\delta w_1^{(i)}\Big|_0^a\Big|_0^b] + \int_0^b [M_{x,x}^{(1)} + 2M_{xy,y}^{(1)} + N_x^{(1)}(w_{1,x}^{(1)} + w_{o,x}^{(1)})$$

$$+ N_{xy}^{(1)}(w_{1,y}^{(1)} + w_{o,y}^{(1)}) + \frac{G_m}{4t_m}[(\frac{t_f^2}{2} + 2t_f t_m + \frac{8t_m^2}{3})w_{1,x}^{(1)} +$$

$$(\frac{t_f^2}{2} + 2t_f t_m + \frac{4t_m^2}{3})w_{1,x}^{(2)}]\delta w_1^{(1)}\Big|_0^a dy + \int_0^a [M_{y,y}^{(1)} + 2M_{xy,x}^{(1)} +$$

$$N_y^{(1)}(w_{1,y}^{(1)} + w_{o,y}^{(1)}) + N_{xy}^{(1)}(w_{1,x}^{(1)} + w_{o,x}^{(1)}) +$$

$$\frac{G_m}{4t_m}[(\frac{t_f^2}{2} + 2t_f t_m + \frac{8t_m^2}{3})w_{1,y}^{(1)} +$$

$$(\frac{t_f^2}{2} + 2t_f t_m + \frac{4t_m^2}{3})w_{1,y}^{(2)}]\delta w_1^{(1)}\Big|_0^b dx + \sum_{1=2}^{N-1}\{\int_0^b [M_{x,x}^{(i)} +$$

$$2M^{(i)}_{xy,y} + N^{(i)}_{x}(w^{(i)}_{1,x} + w^{(i)}_{o,x}) + N^{(i)}_{xy}(w^{(i)}_{1,y} + w^{(i)}_{o,y}) +$$

$$\frac{G_m}{4t_m}\left[\left(\frac{t_f^2}{2} + 2t_f t_m + \frac{8t_m^2}{3}\right)2w^{(i)}_{1,x} +\right.$$

$$\left.\left(\frac{t_f^2}{2} + 2t_f t_m + \frac{4t_m^2}{3}\right)(w^{(i+1)}_{1,x} + w^{(i-1)}_{1,x})\right]\delta w^{(i)}_{1}\Big|_0^a dy + \int_0^a \left[M^{(i)}_{y,y}\right.$$

$$+ 2M^{(i)}_{xy,x} + N^{(i)}_{y}(w^{(i)}_{1,y} + w^{(i)}_{o,y}) + N^{(i)}_{xy}(w^{(i)}_{1,x} + w^{(i)}_{o,x}) +$$

$$\frac{G_m}{4t_m}\left[\left(\frac{t_f^2}{2} + 2t_f t_m + \frac{8t_m^2}{3}\right)2w^{(i)}_{1,y} +\right.$$

$$\left.\left.\left(\frac{t_f^2}{2} + 2t_f t_m + \frac{4t_m^2}{3}\right)(w^{(i+1)}_{1,y} + w^{(i-1)}_{1,y})\right]\delta w^{(i)}_{1}\Big|_0^b dx\right\}$$

$$+ \int_0^b \left[M^{(N)}_{x,x} + 2M^{(N)}_{xy,y} + N^{(N)}_{x}(w^{(N)}_{1,x} + w^{(N)}_{o,x}) +\right.$$

$$N^{(N)}_{xy}(w^{(N)}_{1,y} + w^{(N)}_{o,y}) + \frac{G_m}{4t_m}\left[\left(\frac{t_f^2}{2} + 2t_f t_m + \frac{8t_m^2}{3}\right)w^{(N)}_{1,x} +\right.$$

$$\left.\left(\frac{t_f^2}{2} + 2t_f t_m + \frac{4t_m^2}{3}\right)w^{(N-1)}_{1,x}\right]\delta w^{(N)}_{1}\Big|_0^a dy + \int_0^a \left[M^{(N)}_{y,y} + 2M^{(N)}_{xy,x}\right.$$

$$+ N^{(N)}_{y}(w^{(N)}_{1,y} + w^{(N)}_{o,y}) + N^{(N)}_{xy}(w^{(N)}_{1,x} + w^{(N)}_{o,x}) +$$

$$\frac{G_m}{4t_m}\left[\left(\frac{t_f^2}{2} + 2t_f t_m + \frac{8t_m^2}{3}\right)w^{(N)}_{1,y} +\right.$$

$$\left(\frac{t_f^2}{2} + 2t_f t_m + \frac{4t_m^2}{3}\right) w_{1,y}^{(N-1)}\Big]\delta w_1^{(N)}\Big|_0^b dx = 0 \qquad (2.27)$$

where the stress resultants for the ith fiber-plate $N_x^{(i)}$, $N_y^{(i)}$, and $N_{xy}^{(i)}$ are defined by

$$\begin{aligned} N_x^{(i)} &= A_{11}^{(i)}\varepsilon_x^{(i)^\circ} + A_{12}^{(i)}\varepsilon_y^{(i)^\circ} + A_{16}^{(i)}\gamma_{xy}^{(i)^\circ} \\ N_y^{(i)} &= A_{12}^{(i)}\varepsilon_x^{(i)^\circ} + A_{22}^{(i)}\varepsilon_y^{(i)^\circ} + A_{26}^{(i)}\gamma_{xy}^{(i)^\circ} \\ N_{xy}^{(i)} &= A_{16}^{(i)}\varepsilon^{(i)^\circ} + A_{26}^{(i)}\varepsilon_y^{(i)^\circ} + A_{66}^{(i)}\gamma_{xy}^{(i)^\circ} \end{aligned} \qquad (2.28)$$

and the moment resultants for the ith fiber-plate $M_x^{(i)}$, $M_y^{(i)}$, and $M_{xy}^{(i)}$ are defined by

$$\begin{aligned} M_x^{(i)} &= -(D_{11}^{(i)}w_{1,xx}^{(i)} + D_{12}^{(i)}w_{1,yy}^{(i)} + 2D_{16}^{(i)}w_{1,xy}^{(i)}) \\ M_y^{(i)} &= -(D_{12}^{(i)}w_{1,xx}^{(i)} + D_{22}^{(i)}w_{1,yy}^{(i)} + 2D_{26}^{(i)}w_{1,xy}^{(i)}) \\ M_{xy}^{(i)} &= -(D_{16}^{(i)}w_{1,xx}^{(i)} + D_{26}^{(i)}w_{1,yy}^{(i)} + 2D_{66}^{(i)}w_{1,xy}^{(i)}) \end{aligned} \qquad (2.29)$$

The summations and integrations in equations (2.27) can be interchanged since the series of potential energy contributions

consists of continuous functions and is uniformly convergent over the region $0 \leq x \leq a$, $0 \leq y \leq b$ (see reference 55, p.589).

Equation (2.27) is satisfied when the integrand of the area integral and when the integrands of the boundary condition integrals equal zero independently. The governing nonlinear partial differential equations are obtained from the area integral and are stated below:

<u>for i = 1, 2, ..., N</u>

$$N^{(i)}_{x,x} + N^{(i)}_{xy,y} = 0$$

$$N^{(i)}_{y,y} + N^{(i)}_{xy,x} = 0 \qquad (2.30)$$

<u>for i = 1</u>

$$\bar{D}^{(1)}[w^{(1)}_1] - N^{(1)}_x(w^{(1)}_{1,xx} + w^{(1)}_{o,xx}) -$$

$$N^{(1)}_y(w^{(1)}_{1,yy} + w^{(1)}_{o,yy}) - 2N^{(1)}_{xy}(w^{(1)}_{1,xy} + w^{(1)}_{o,xy})$$

$$+ E^*(w^{(1)}_1 - w^{(2)}_1) - G^*_1(w^{(1)}_{1,yy} + w^{(1)}_{1,xx}) -$$

$$G^*_2(w^{(2)}_{1,yy} + w^{(2)}_{1,xx}) = 0 \qquad (2.31)$$

for i = 2, 3, ..., N-1

$$\bar{D}^{(i)}[w_1^{(i)}] - N_x^{(i)}(w_{1,xx}^{(i)} + w_{o,xx}^{(i)}) -$$

$$N_y^{(i)}(w_{1,yy}^{(i} + w_{o,yy}^{(i}) - 2N_{xy}^{(i)}(w_{1,xy}^{(i)} + w_{o,xy}^{(i)}) +$$

$$E^*(2w_1^{(i)} - w_1^{(i-1)} - w_1^{(i+1)}) - G_1^*(2w_{1,yy}^{(i)} + 2w_{1,xx}^{(i)}) -$$

$$G_2^*(w_{1,yy}^{(i-1)} + w_{1,xx}^{(i-1)} + w_{1,yy}^{(i+1)} + w_{1,xx}^{(i+1)}) = 0 \qquad (2.32)$$

for i = N

$$\bar{D}^{(N)}[w_1^{(N)}] - N_x^{(N)}(w_{1,xx}^{(N)} + w_{o,xx}^{(N)}) -$$

$$N_y^{(N)}(w_{1,yy}^{(N)} + w_{o,yy}^{(N)}) - 2N_{xy}^{(N)}(w_{1,xy}^{(N)} + w_{o,xy}^{(N)}) +$$

$$E^*(w_1^{(N)} - w_1^{(N-1)}) - G_1^*(w_{1,yy}^{(N)} + w_{1,xx}^{(N)}) -$$

$$G_2^*(w_{1,yy}^{(N)} + w_{1,xx}^{(N)}) = 0 \qquad (2.33)$$

where $\bar{D}^{(i)}[\ \cdot\ ]$ is an operator defined by

$$\bar{D}^{(i)}[w] = D_{11}^{(i)}w_{,xxxx} + 2(D_{12}^{(i)} + 2D_{66}^{(i)})w_{,xxyy} +$$

$$D_{22}^{(i)}w_{,yyyy} + 4D_{16}^{(i)}w_{,xxxy} + 4D_{26}^{(i)}w_{,xyyy} \qquad (2.34)$$

and the constants are defined by

$$E^* = \frac{E_m}{2t_m(1-\nu_m^2)}$$

$$G_1^* = \frac{G_m}{4t_m}\left(\frac{t_f^2}{2} + 2t_f t_m + \frac{8t_m^2}{3}\right) \qquad (2.35)$$

$$G_2^* = \frac{G_m}{4t_m}\left(\frac{t_f^2}{2} + 2t_f t_m + \frac{4t_m^2}{3}\right)$$

The equations for the boundary condition are obtained from the boundary condition integrals and are stated below:

<u>for i = 1, 2, ..., N</u>

$$N_x^{(i)}\delta u^{(i)^\circ}\Big|_0^a = 0 \qquad N_{xy}^{(i)}\delta u^{(i)^\circ}\Big|_0^b = 0$$

$$N_y^{(i)}\delta v^{(i)^\circ}\Big|_0^b = 0 \qquad N_{xy}^{(i)}\delta v^{(i)^\circ}\Big|_0^a = 0$$

$$M_x^{(i)}\delta w_{1,x}^{(i)}\Big|_0^a = 0 \qquad M_y^{(i)}\delta w_{1,y}^{(i)}\Big|_0^b = 0$$

$$2M_{xy}^{(i)}\delta w_1^{(i)}\Big|_0^a\Big|_0^b = 0 \qquad (2.36)$$

for i = 1

$$\left[M_{x,x}^{(1)} + 2M_{xy,y}^{(1)} + N_x^{(1)}(w_{1,x}^{(1)} + w_{o,x}^{(1)}) + \right.$$

$$\left. N_{xy}^{(1)}(w_{1,y}^{(1)} + w_{o,y}^{(1)}) + G_1^* w_{1,x}^{(1)} + G_2^* w_{1,x}^{(2)}\right]\delta w_1^{(1)}\Big|_0^a = 0$$

$$\left[M_{y,y}^{(1)} + 2M_{xy,x}^{(1)} + N_y^{(1)}(w_{1,y}^{(1)} + w_{o,y}^{(1)}) + \right.$$

$$\left. N_{xy}^{(1)}(w_{1,x}^{(1)} + w_{o,x}^{(1)}) + G_1^* w_{1,y}^{(1)} + G_2^* w_{1,y}^{(2)}\right]\delta w_1^{(1)}\Big|_0^b = 0 \qquad (2.37)$$

for i = 2, 3, ..., N-1

$$\left[M_{x,x}^{(i)} + 2M_{xy,y}^{(i)} + N_x^{(i)}(w_{1,x}^{(i)} + w_{o,x}^{(i)}) + N_{xy}^{(i)}(w_{1,y}^{(i)} + w_{o,y}^{(i)}) \right.$$

$$\left. + 2G_1^* w_{1,x}^{(i)} + G_2^*(w_{1,x}^{(i+1)} + w_{1,x}^{(i-1)})\right]\delta w_1^{(i)}\Big|_0^a = 0$$

$$\left[M_{y,y}^{(i)} + 2M_{xy,x}^{(i)} + N_y^{(i)}(w_{1,y}^{(i)} + w_{o,y}^{(i)}) + N_{xy}^{(i)}(w_{1,x}^{(i)} + w_{o,x}^{(i)}) \right.$$

$$\left. + 2G_1^* w_{1,y}^{(i)} + G_2^*(w_{1,y}^{(i+1)} + w_{1,y}^{(i-1)})\right]\delta w_1^{(i)}\Big|_0^b = 0 \qquad (2.38)$$

for i = N

$$\left[M_{x,x}^{(N)} + 2M_{xy,y}^{(N)} + N_x^{(N)}(w_{1,x}^{(N)} + w_{o,x}^{(N)}) + N_{xy}^{(N)}(w_{1,y}^{(N)} + w_{o,y}^{(N)}) \right.$$

$$\left. + G_1^* w_{1,x}^{(N)} + G_2^* w_{1,x}^{(N-1)}\right]\delta w_1^{(N)}\Big|_0^a = 0$$

$$\left[M_{y,y}^{(N)} + 2M_{xy,x}^{(N)} + N_{y}^{(N)}(w_{1,y}^{(N)} + w_{o,y}^{(N)}) + N_{xy}^{(N)}(w_{1,x}^{(N)} + w_{o,x}^{(N)})\right.$$

$$\left. + G_1^{*} w_{1,y}^{(N)} + G_2^{*} w_{1,y}^{(N-1)}\right]\delta w_1^{(N)}\Big|_0^b = 0 \qquad (2.39)$$

2.1.5 Model Loading, Boundary Conditions, and Solution Procedure

The model is loaded in compression by uniform end shortening. No external loads are applied to the model (hence, the potential energy of the applied loads is zero). This loading enters the analysis as a u displacement boundary condition for each fiber-plate and is expressed as

$$u^{(i)^{o}}(0,y) = 0$$

$$u^{(i)^{o}}(a,y) = -\bar{u}_o \quad , \; i = 1, 2, \ldots, N \qquad (2.40)$$

The u and v displacement boundary conditions are chosen to assure that the model remains rectangular during loading. A rectangular shape is typical for composite laminates in structural components. These boundary conditions for each fiber-plate are expressed as

$$u^{(i)^{\circ}}(x,0) = -\bar{u}_{\circ}\left(\frac{x}{a}\right)$$

$$u^{(i)^{\circ}}(x,b) = u^{(i)^{\circ}}(x,0)$$

$$v^{(i)^{\circ}}(0,y) = \left(\frac{A_{12}^{T}}{A_{22}^{T}}\right)\left(y - \frac{b}{2}\right)\frac{\bar{u}_{\circ}}{a}$$

$$v^{(i)^{\circ}}(a,y) = v^{(i)^{\circ}}(0,y)$$

$$v^{(i)^{\circ}}(x,0) = -\left(\frac{A_{12}^{T}}{A_{22}^{T}}\right)\left(\frac{b}{2}\right)\frac{\bar{u}_{\circ}}{a}$$

$$v^{(i)^{\circ}}(x,b) = -v^{(i)^{\circ}}(x,0)$$

$$i = 1, 2, \ldots, N \qquad (2.41)$$

where A_{12}^{T} and A_{22}^{T} are extensional stiffnesses for the total laminate and are defined by

$$(A_{12}^{T}, A_{22}^{T}) = \sum_{i=1}^{N} (A_{12}^{(i)}, A_{22}^{(i)}) \qquad (2.42)$$

The v displacement boundary conditions are the result of Poisson expansion during loading. These boundary conditions prevent an anisotropic lamina from deforming into a parallelogram-type shape.

The model is simply supported on the unloaded edges. These simple-support boundary conditions are expressed as

$$\underline{\text{at } y = 0 \text{ and } y = b}$$

$$w_1^{(i)} = 0 \qquad M_y^{(i)} = 0 \quad , \; i = 1, 2, \ldots, N \qquad (2.43)$$

The model with initial imperfections is loaded in the x direction and deforms into a short-wavelength buckling mode. The half-wavelength of the model's mode shape λ is a laminate property, and the calculation of λ is discussed in section 2.2 Linear Analysis. This half-wavelength is assumed to be much smaller than the laminate's length or the laminate's width. The fiber-plates in the model are assumed to behave as elastically supported semi-infinite strips causing the w displacement and moment boundary conditions at $x=0$ and at $x=a$ to have a negligible effect on the short-wavelength buckling behavior of the model. The w displacement and moment boundary conditions for this model are expressed along node lines of the mode shape and are

$$\underline{\text{at } \bar{x} = 0 \text{ and at } \bar{x} = \lambda}$$

$$w_1^{(i)} = 0 \qquad M_x^{(i)} = 0 \quad , \; i = 1, 2, \ldots, N \tag{2.44}$$

where the $\bar{x}$-axis is parallel to the x-axis and is illustrated in figure 2.5.

The Kantorovich method [56] is used throughout this study to obtain solutions to the governing equations that satisfy the boundary conditions. Each unknown is expressed as a kinematically admissible series of the $\bar{x}$ coordinate. An unknown function in this study has the general form

$$f(x,y) = f_o(x) + f_1(y) + f_s(y) \sin \frac{\pi \bar{x}}{\lambda} + f_c(y) \cos \frac{\pi \bar{x}}{\lambda} \tag{2.45}$$

where f_o and f_1 are known functions determined from the linear prebuckling analysis. Equation (2.45) is substituted into the governing equations, (2.30) to (2.33), and boundary conditions, (2.41), (2.43), and (2.44), to obtain ordinary differential equations for the unknowns f_s and f_c.

2.2 Linear Analysis

The nonlinear governing equations are linearized to determine the laminate end shortening when short-wavelength buckling occurs. This end shortening is also referred to as the critical end shortening $(\bar{u}_o)_{cr}$. The linearized equations are also used to determine the short-wavelength buckling mode shape. The linearized equations are derived using the adjacent-equilibrium criterion (see reference 57, p.27). The fiber-plates have no imperfections in the linear analysis (i.e., $w_o^{(i)} = 0$).

Adjacent equilibrium configurations for the fiber-plates are investigated by adding small increments to the fiber-plate displacements. The relationships between the displacements prior to buckling, $u_a^{(i)}$, $v_a^{(i)}$, and $w_a^{(i)}$, and the displacements of an adjacent equilibrium configuration, $u^{(i)}$, $v^{(i)}$, and $w^{(i)}$ are expressed by

$$\begin{aligned} u^{(i)} &= u_a^{(i)} + \varepsilon\bar{u} \\ v^{(i)} &= v_a^{(i)} + \varepsilon\bar{v} \\ w_1^{(i)} &= w_a^{(i)} + \varepsilon\bar{w}_1 \end{aligned} \qquad (2.46)$$

where the quantity ε is infinitesimally small. The prebuckling w displacement $w_a^{(i)}$ and its derivatives are zero for the flat ith fiber-plate loaded by uniform end shortening.

Equations (2.46) are substituted into equations (2.30) to (2.33), and the terms of like powers of ε sum to zero for arbitrary ε. The zeroth-order terms in ε combine to give the linear prebuckling equilibrium equations for the ith fiber-plate

$$N_{x^\circ,x}^{(i)} + N_{xy^\circ,y}^{(i)} = 0$$

$$N_{y^\circ,y}^{(i)} + N_{xy^\circ,x}^{(i)} = 0 \qquad (2.47)$$

where

$$N_{x^\circ}^{(i)} = A_{11}^{(i)} u_{a',x}^{(i)} + A_{12}^{(i)} v_{a',y}^{(i)} + A_{16}^{(i)} (u_{a',y}^{(i)} + v_{a',x}^{(i)})$$

$$N_{y^\circ}^{(i)} = A_{12}^{(i)} u_{a',x}^{(i)} + A_{22}^{(i)} v_{a',y}^{(i)} + A_{26}^{(i)} (u_{a',y}^{(i)} + v_{a',x}^{(i)}) \qquad (2.48)$$

$$N_{xy^\circ}^{(i)} = A_{16}^{(i)} u_{a',x}^{(i)} + A_{26}^{(i)} v_{a',y}^{(i)} + A_{66}^{(i)} (u_{a',y}^{(i)} + v_{a',x}^{(i)})$$

The prebuckling displacements that satisfy the governing equations (2.47) and the boundary condition equations (2.40) and (2.41) are

$$u_a^{(i)}(x,y) = -\bar{u}_o(\frac{x}{a})$$

$$v_a^{(i)}(x,y) = (\frac{A_{12}^T}{A_{22}^T})(y - \frac{b}{2})\frac{\bar{u}_o}{a} \qquad (2.49)$$

The first-order terms in ε combine to give the linear postbuckling equilibrium equations for the inplane loads in the ith fiber-plate

$$N_{x1}^{(i)}{}_{,x} + N_{xy1}^{(i)}{}_{,y} = 0$$

$$N_{y1}^{(i)}{}_{,y} + N_{xy1}^{(i)}{}_{,x} = 0 \qquad (2.50)$$

where

$$N_{x1}^{(i)} = A_{11}^{(i)}\bar{u}_{,x}^{(i)} + A_{12}^{(i)}\bar{v}_{,y}^{(i)} + A_{16}^{(i)}(\bar{u}_{,y}^{(i)} + \bar{v}_{,x}^{(i)})$$

$$N_{y1}^{(i)} = A_{12}^{(i)}\bar{u}_{,x}^{(i)} + A_{22}^{(i)}\bar{v}_{,y}^{(i)} + A_{26}^{(i)}(\bar{u}_{,y}^{(i)} + \bar{v}_{,x}^{(i)})$$

$$N_{xy1}^{(i)} = A_{16}^{(i)}\bar{u}_{,x}^{(i)} + A_{26}^{(i)}\bar{v}_{,y}^{(i)} + A_{66}^{(i)}(\bar{u}_{,y}^{(i)} + \bar{v}_{,x}^{(i)}) \qquad (2.51)$$

and the linear stability equations for the fiber-plates are stated below:

for i = 1

$$\bar{D}^{(1)}[\bar{w}_1^{(1)}] - N_{x^o}^{(1)}\bar{w}_{1,xx}^{(1)} - N_{y^o}^{(1)}\bar{w}_{1,yy}^{(1)} - 2N_{xy^o}^{(1)}\bar{w}_{1,xy}^{(1)}$$

$$+ E^*(\bar{w}_1^{(1)} - \bar{w}_1^{(2)}) - G_1^*(\bar{w}_{1,yy}^{(1)} + \bar{w}_{1,xx}^{(1)}) -$$

$$G_2^*(\bar{w}_{1,yy}^{(2)} + \bar{w}_{1,xx}^{(2)}) = 0 \qquad (2.52)$$

for i = 2, 3, ..., N-1

$$\bar{D}^{(i)}[\bar{w}_1^{(i)}] - N_{x^o}^{(i)}\bar{w}_{1,xx}^{(i)} - N_{y^o}^{(i)}\bar{w}_{1,yy}^{(i)} - 2N_{xy^o}^{(i)}\bar{w}_{1,xy}^{(i)}$$

$$+ E^*(2\bar{w}_1^{(i)} - \bar{w}_1^{(i-1)} - \bar{w}_1^{(i+1)}) - 2G_1^*(\bar{w}_{1,yy}^{(i)} + \bar{w}_{1,xx}^{(i)})$$

$$+ G_2^*(\bar{w}_{1,yy}^{(i-1)} + \bar{w}_{1,xx}^{(i-1)} + \bar{w}_{1,yy}^{(i+1)} + \bar{w}_{1,xx}^{(i+1)}) = 0 \qquad (2.53)$$

for i = N

$$\bar{D}^{(N)}[\bar{w}_1^{(N)}] - N_{x^o}^{(N)}\bar{w}_{1,xx}^{(N)} - N_{y^o}^{(N)}\bar{w}_{1,yy}^{(N)} - 2N_{xy^o}^{(N)}\bar{w}_{1,xy}^{(N)}$$

$$+ E^*(\bar{w}_1^{(N)} - \bar{w}_1^{(N-1)}) - G_1^*(\bar{w}_{1,yy}^{(N)} + \bar{w}_{1,xx}^{(N)}) -$$

$$G_2^*(\bar{w}_{1,yy}^{(N-1)} + \bar{w}_{1,xx}^{(N-1)}) = 0 \qquad (2.54)$$

where $N_{x^o}^{(i)}$, $N_{y^o}^{(i)}$, and $N_{xy^o}^{(i)}$ are determined from equations (2.48). The higher-order terms in ε are neglected since ε is small.

2.2.1 Orthotropic Fiber-Plates

The short-wavelength mode shape for an orthotropic fiber-plate is assumed to have half-waves that are normal to the direction of loading. These half-waves are referred to as "normal waves" and are illustrated in figure 2.5a. The linear stability equations and boundary conditions for a model composed of orthotropic fiber-plates are satisfied by

$$\bar{w}_1^{(i)} = \bar{w}_s^{(i)} \sin \frac{\pi \bar{x}}{\lambda} \sin \frac{\pi y}{b} \qquad (2.55)$$

where $\bar{w}_s^{(i)}$ is the amplitude of the normal wave for the ith fiber-plate. The coefficient of the cos $\frac{\pi \bar{x}}{\lambda}$ term is zero (see equation (2.45)), and the extensional stiffnesses, $A_{16}^{(i)}$ and $A_{26}^{(i)}$, and the bending stiffnesses, $D_{16}^{(i)}$ and $D_{26}^{(i)}$, are zero for orthotropic fiber-plates. Equation (2.55) is substituted into equations (2.51) to (2.53) to form a system of equations for calculating the model's critical end shortening and short-wavelength buckling mode shape. The system of equations is of the form

$$
\begin{aligned}
&[\tilde{D}^{(1)} + \bar{M} - k_1(\frac{\bar{u}_o}{a})]\bar{w}_s^{(1)} - \bar{N}\bar{w}_s^{(2)} = 0\\
&[\tilde{D}^{(2)} + 2\bar{M} - k_2(\frac{\bar{u}_o}{a})]\bar{w}_s^{(2)} - \bar{N}\bar{w}_s^{(1)} - \bar{N}\bar{w}_s^{(3)} = 0\\
&\qquad\vdots\\
&[\tilde{D}^{(N-1)} + 2\bar{M} - k_{N-1}(\frac{\bar{u}_o}{a})]\bar{w}_s^{(N-1)} - \bar{N}\bar{w}_s^{(N-2)} - \bar{N}\bar{w}_s^{(N)} = 0\\
&[\tilde{D}^{(N)} + \bar{M} - k_N(\frac{\bar{u}_o}{a})]\bar{w}_s^{(N)} - \bar{N}\bar{w}_s^{(N-1)} = 0
\end{aligned}
\qquad (2.56)
$$

for arbitrary $\bar{x}$ and y where the constants are defined by

$$
\begin{aligned}
\tilde{D}^{(i)} &= D_{11}^{(i)}(\tfrac{\pi}{\lambda})^4 + 2(D_{12}^{(i)} + 2D_{66}^{(i)})(\tfrac{\pi}{\lambda})^2(\tfrac{\pi}{b})^2 + D_{22}^{(i)}(\tfrac{\pi}{b})^4\\
\bar{M} &= E^* + G_1^*[(\tfrac{\pi}{b})^2 + (\tfrac{\pi}{\lambda})^2]\\
\bar{N} &= E^* - G_2^*[(\tfrac{\pi}{b})^2 + (\tfrac{\pi}{\lambda})^2]\\
k_i &= (A_{11}^{(i)} - \frac{A_{12}^T}{A_{22}^T}A_{12}^{(i)})(\tfrac{\pi}{\lambda})^2 + (A_{12}^{(i)} - \frac{A_{12}^T}{A_{22}^T}A_{22}^{(i)})(\tfrac{\pi}{b})^2
\end{aligned}
\qquad (2.57)
$$

Non-trivial solutions to equations (2.56) exist if the determinant of the matrix formed by the coefficients of $\bar{w}_s^{(i)}$ is zero. The smallest value of the normalized end shortening $\bar{u}_o/a$ for which this

determinate is zero is the critical normalized end shortening $(\bar{u}_o/a)_{cr}$. The end shortening is normalized by the laminate length, a. The value $(\bar{u}_o/a)_{cr}$ is an eigenvalue of this system of equations, and the corresponding eigenvector is the short-wavelength buckling mode shape of the model. The wavelength of the mode shape is determined by minimizing $(\bar{u}_o/a)_{cr}$ with respect to the wavelength.

2.2.2 Anisotropic Fiber-Plates

The short-wavelength mode shape for an anisotropic fiber-plate can have half-waves that are oriented at an angle ϕ to the orientation of a normal wave. These half-waves are referred to as "skewed waves" and are illustrated in figure 2.5b. The form of the w displacement that satisfies the linear stability equations and boundary conditions for a model composed of anisotropic fiber-plates is

$$\bar{w}_1^{(i)} = w_s^{(i)}(y) \sin \frac{\pi \bar{x}}{\lambda} + w_c^{(i)}(y) \cos \frac{\pi \bar{x}}{\lambda} \qquad (2.58)$$

The eigenvalues and eigenvectors for these fiber-plates are obtained using the Galerkin method [57]. The functions of y for the ith fiber-plate, $w_s^{(i)}$ and $w_c^{(i)}$, are expanded in a Fourier sine series.

These series satisfy the boundary conditions for $\bar{w}_1^{(i)}$ at $y=0$ and at $y=b$ and are expressed as

$$w_s^{(i)} = \sum_{m=1}^{M} \bar{w}_{sm}^{(i)} \sin \frac{m\pi y}{b}$$

$$w_c^{(i)} = \sum_{n=1}^{M} \bar{w}_{cn}^{(i)} \cos \frac{n\pi y}{b} \qquad (2.59)$$

where M is the number of terms in the series and is an even number. Equations (2.58) and (2.59) are substituted into equations (2.51) to (2.53), and the series expansions for $w_s^{(i)}$ and $w_c^{(i)}$ are solutions to these equations if the equations are orthogonal to $\sin \frac{m\pi y}{b}$ and to $\sin \frac{n\pi y}{b}$ for each m and n, respectively. The orthogonality conditions for the ith fiber-plate are stated below:

<u>for i = 1</u>

$$\int_0^b \{\bar{D}^{(1)}[\bar{w}_1^{(1)}] - N_{x^o}^{(1)}\bar{w}_{1,xx}^{(1)} - N_{y^o}^{(1)}\bar{w}_{1,yy}^{(1)} - 2N_{xy^o}^{(1)}\bar{w}_{1,xy}^{(1)}$$

$$+ E^*(\bar{w}_1^{(1)} - \bar{w}_1^{(2)}) - G_1^*(\bar{w}_{1,yy}^{(1)} + \bar{w}_{1,xx}^{(1)}) -$$

$$G_2^*(\bar{w}_{1,yy}^{(2)} + \bar{w}_{1,xx}^{(2)})\} \sin \frac{m\pi y}{b}\, dy = 0 \quad m = 1, 2, \ldots, M$$

for i = 2, 3, ..., N-1

$$\int_0^b \left(\bar{D}^{(i)}[\bar{w}_1^{(i)}] - N_{x^o}^{(i)}\bar{w}_{1,xx}^{(i)} - N_{y^o}^{(i)}\bar{w}_{1,yy}^{(i)} - 2N_{xy^o}^{(i)}\bar{w}_{1,xy}^{(i)}\right.$$

$$+ E^*(2\bar{w}_1^{(i)} - \bar{w}_1^{(i-1)} - \bar{w}_1^{(i+1)}) - 2G_1^*(\bar{w}_{1,yy}^{(i)} + \bar{w}_{1,xx}^{(i)})$$

$$\left. + G_2^*(\bar{w}_{1,yy}^{(i-1)} + \bar{w}_{1,xx}^{(i-1)} + \bar{w}_{1,yy}^{(i+1)} + \bar{w}_{1,xx}^{(i+1)})\right] \sin\frac{m\pi y}{b}\, dy = 0$$

$$m = 1, 2, \ldots, M$$

for i = N

$$\int_0^b \left(\bar{D}^{(N)}[\bar{w}_1^{(N)}] - N_{x^o}^{(N)}\bar{w}_{1,xx}^{(N)} - N_{y^o}^{(N)}\bar{w}_{1,yy}^{(N)} - 2N_{xy^o}^{(N)}\bar{w}_{1,xy}^{(N)}\right.$$

$$+ E^*(\bar{w}_1^{(N)} - \bar{w}_1^{(N-1)}) - G_1^*(\bar{w}_{1,yy}^{(N)} + \bar{w}_{1,xx}^{(N)}) -$$

$$\left. G_2^*(\bar{w}_{1,yy}^{(N-1)} + \bar{w}_{1,xx}^{(N-1)})\right] \sin\frac{m\pi y}{b}\, dy = 0$$

$$m = 1, 2, \ldots, M \qquad (2.60)$$

and

for i = 1

$$\int_0^b \left(\bar{D}^{(1)}[\bar{w}_1^{(1)}] - N_{x^o}^{(1)}\bar{w}_{1,xx}^{(1)} - N_{y^o}^{(1)}\bar{w}_{1,yy}^{(1)} - 2N_{xy^o}^{(1)}\bar{w}_{1,xy}^{(1)}\right.$$

$$+ E^*(\bar{w}_1^{(1)} - \bar{w}_1^{(2)}) - G_1^*(\bar{w}_{1,yy}^{(1)} + \bar{w}_{1,xx}^{(1)}) -$$

$$G_2^*(\bar{w}_{1,yy}^{(2)} + \bar{w}_{1,xx}^{(2)})] \sin \frac{n\pi y}{b}\, dy = 0 \quad n = 1, 2, \ldots, M$$

<u>for i = 2, 3, ..., N-1</u>

$$\int_0^b [\bar{D}^{(i)}[\bar{w}_1^{(i)}] - N_{x^\circ}^{(i)}\bar{w}_{1,xx}^{(i)} - N_{y^\circ}^{(i)}\bar{w}_{1,yy}^{(i)} - 2N_{xy^\circ}^{(i)}\bar{w}_{1,xy}^{(i)}$$

$$+ E^*(2\bar{w}_1^{(i)} - \bar{w}_1^{(i-1)} - \bar{w}_1^{(i+1)}) - 2G_1^*(\bar{w}_{1,yy}^{(i)} + \bar{w}_{1,xx}^{(i)})$$

$$+ G_2^*(\bar{w}_{1,yy}^{(i-1)} + \bar{w}_{1,xx}^{(i-1)} + \bar{w}_{1,yy}^{(i+1)} + \bar{w}_{1,xx}^{(i+1)})] \sin \frac{n\pi y}{b}\, dy = 0$$

$$n = 1, 2, \ldots, M$$

<u>for i = N</u>

$$\int_0^b [\bar{D}^{(N)}[\bar{w}_1^{(N)}] - N_{x^\circ}^{(N)}\bar{w}_{1,xx}^{(N)} - N_{y^\circ}^{(N)}\bar{w}_{1,yy}^{(N)} - 2N_{xy^\circ}^{(N)}\bar{w}_{1,xy}^{(N)}$$

$$+ E^*(\bar{w}_1^{(N)} - \bar{w}_1^{(N-1)}) - G_1^*(\bar{w}_{1,yy}^{(N)} + \bar{w}_{1,xx}^{(N)}) -$$

$$G_2^*(\bar{w}_{1,yy}^{(N-1)} + \bar{w}_{1,xx}^{(N-1)})] \sin \frac{n\pi y}{b}\, dy = 0$$

$$n = 1, 2, \ldots, M \qquad (2.61)$$

Equations (2.60) and (2.61) are integrated to obtain 2*M simultaneous homogeneous equations for each fiber-plate in terms of

the 2*M undetermined coefficients $\bar{w}_{sm}^{(i)}$ and $\bar{w}_{cn}^{(i)}$. The simultaneous equations for the ith fiber-plate can be expressed as

$$\begin{bmatrix} \bar{L}_{odd} & \bar{H} & 0 & 0 \\ \bar{H} & \bar{L}_{even} & 0 & 0 \\ 0 & 0 & \bar{L}_{even} & -\bar{H} \\ 0 & 0 & -\bar{H} & \bar{L}_{odd} \end{bmatrix}^{(i)} \begin{Bmatrix} (w_s)_{odd} \\ (w_c)_{even} \\ (w_s)_{even} \\ (w_c)_{odd} \end{Bmatrix}^{(i)} = \{0\} \tag{2.62}$$

where the submatrices for the ith fiber-plate are defined by

$$\bar{L}_{odd}^{(i)} = \begin{bmatrix} L_1 - k_1^*(\frac{\bar{u}_o}{a}) & 0 & 0 & \cdots & 0 \\ 0 & L_3 - k_3^*(\frac{\bar{u}_o}{a}) & 0 & \cdots & 0 \\ 0 & 0 & L_5 - k_5^*(\frac{\bar{u}_o}{a}) & \cdots & 0 \\ \vdots & \vdots & \vdots & \ddots & \vdots \\ 0 & 0 & \cdots & & L_{(M-1)} - k_{(M-1)}^*(\frac{\bar{u}_o}{a}) \end{bmatrix}^{(i)} \tag{2.63}$$

$$\bar{L}^{(i)}_{even} = \begin{bmatrix} L_2 - k_2^*(\frac{\bar{u}_o}{a}) & 0 & 0 & \cdots & 0 \\ 0 & L_4 - k_4^*(\frac{\bar{u}_o}{a}) & 0 & \cdots & 0 \\ 0 & 0 & L_6 - k_6^*(\frac{\bar{u}_o}{a}) & \cdots & 0 \\ \vdots & \vdots & \vdots & \ddots & \vdots \\ 0 & 0 & \cdots & & L_{(M)} - k^*_{(M)}(\frac{\bar{u}_o}{a}) \end{bmatrix} \quad (i) \qquad (2.64)$$

$$\bar{H}^{(i)} = \begin{bmatrix} H_{12} - h_{12}(\frac{\bar{u}_o}{a}) & H_{14} - h_{14}(\frac{\bar{u}_o}{a}) & \cdots & H_{1M} - h_{1M}(\frac{\bar{u}_o}{a}) \\ H_{32} - h_{32}(\frac{\bar{u}_o}{a}) & H_{34} - h_{34}(\frac{\bar{u}_o}{a}) & \cdots & H_{3M} - h_{3M}(\frac{\bar{u}_o}{a}) \\ \vdots & & & \vdots \\ H_{(M-1)2} - h_{(M-1)2}(\frac{\bar{u}_o}{a}) & \cdots & & H_{(M-1)M} - h_{(M-1)M}(\frac{\bar{u}_o}{a}) \end{bmatrix} \quad (i) \qquad (2.65)$$

with

$$L_m^{(i)} = D_{11}^{(i)}\left(\frac{\pi}{\lambda}\right)^4 + 2\left(D_{12}^{(i)} + 2D_{66}^{(i)}\right)\left(\frac{\pi}{\lambda}\right)^2\left(\frac{m\pi}{b}\right)^2 + D_{22}^{(i)}\left(\frac{m\pi}{b}\right)^4$$

$$+ c_1^{(i)}\left[E^* + G_1^*\left[\left(\frac{\pi}{\lambda}\right)^2 + \left(\frac{m\pi}{b}\right)^2\right]\right]$$

$$k_m^{(i)} = \left[\left(A_{11}^{(i)} - \frac{A_{12}^T}{A_{22}^T} A_{12}^{(i)}\right)\left(\frac{\pi}{\lambda}\right)^2 + \left(A_{12}^{(i)} - \frac{A_{12}^T}{A_{22}^T}\right)\left(\frac{m\pi}{b}\right)^2\right]$$

$$H_{mn}^{(i)} = \left[4D_{16}^{(i)}\left(\frac{\pi}{\lambda}\right)^3 + 4D_{26}^{(i)}\left(\frac{\pi}{\lambda}\right)\left(\frac{m\pi}{b}\right)^2\right] \frac{4mn}{b(m^2 - n^2)}$$

$$h_{mn}^{(i)} = \left(A_{16}^{(i)} - \frac{A_{12}^T}{A_{22}^T} A_{26}^{(i)}\right)\left(\frac{\pi}{\lambda}\right) \frac{8mn}{b(m^2 - n^2)}$$

$$c_1^{(i)} = 1, \quad i = 1 \text{ or } i = N$$

$$= 2, \quad \text{otherwise} \tag{2.66}$$

and the sub-vectors for the ith fiber-plate are defined by

$$(w_s)_{odd}^{(i)} = \begin{Bmatrix} w_{s1} \\ w_{s3} \\ w_{s5} \\ \vdots \\ w_{s(M-1)} \end{Bmatrix}^{(i)} \qquad (w_s)_{even}^{(i)} = \begin{Bmatrix} w_{s2} \\ w_{s4} \\ w_{s6} \\ \vdots \\ w_{sM} \end{Bmatrix}^{(i)} \tag{2.67}$$

$$(w_c)^{(i)}_{odd} = \begin{Bmatrix} w_{c1} \\ w_{c3} \\ w_{c5} \\ \vdots \\ w_{c(M-1)} \end{Bmatrix}^{(i)} \qquad (w_c)^{(i)}_{even} = \begin{Bmatrix} w_{c2} \\ w_{c4} \\ w_{c6} \\ \vdots \\ w_{cM} \end{Bmatrix}^{(i)}$$

The orthogonality of the trigonometric terms causes coupling between the $(w_s)^{(i)}_{odd}$ and the $(w_c)^{(i)}_{even}$ coefficients and between the $(w_s)^{(i)}_{even}$ and the $(w_c)^{(i)}_{odd}$ coefficients. Equations (2.62) lead to an eigenvalue problem of order $2*M*N$ for an N-lamina model. This $2*M*N$ system has only $M*N$ unique eigenvalues. The unique eigenvalues are obtained form equations for the fiber-plates of the form

$$\begin{bmatrix} \bar{L}_{odd} & \bar{H} \\ \bar{H} & \bar{L}_{even} \end{bmatrix}^{(i)} \begin{Bmatrix} (w_s)_{odd} \\ (w_c)_{even} \end{Bmatrix}^{(i)} = \{0\} \qquad (2.68)$$

The system of equations for the N-lamina model are shown in figure 2.6 and are labeled equations (2.69). The undefined sub-matrices in equations (2.69) are

$$\bar{N}_{odd} = \begin{bmatrix} N_1 & 0 & 0 & \cdots & 0 \\ 0 & N_3 & 0 & \cdots & 0 \\ 0 & 0 & N_5 & \cdots & 0 \\ \vdots & & & \ddots & \\ 0 & 0 & 0 & \cdots & N_{(M-1)} \end{bmatrix} \tag{2.70}$$

$$\bar{N}_{even} = \begin{bmatrix} N_2 & 0 & 0 & \cdots & 0 \\ 0 & N_4 & 0 & \cdots & 0 \\ 0 & 0 & N_6 & \cdots & 0 \\ \vdots & & & \ddots & \\ 0 & 0 & 0 & \cdots & N_M \end{bmatrix} \tag{2.71}$$

with

$$N_m = E^* + G_2^*[(\frac{m\pi}{b})^2 + (\frac{\pi}{\lambda})^2] \tag{2.72}$$

The $\bar{N}$ sub-matrix is the result of coupling between adjacent fiber-plates through the matrix-foundation. Non-trivial solutions to equations (2.69) exist if the determinant of the matrix of material properties is zero. The smallest value of $\bar{u}_o/a$ for which this determinate is zero is $(\bar{u}_o/a)_{cr}$, and this value is an eigenvalue of

equations (2.69). The eigenvector corresponding to $(\bar{u}_o/a)_{cr}$ is used to determine the short-wavelength buckling mode shape of the model. Similar to the model with orthotropic fiber-plates, the wavelength of the mode shape for a model with anisotropic fiber-plates is determined by minimizing $(\bar{u}_o/a)_{cr}$ with respect to the wavelength.

2.3 Nonlinear Analysis

The governing nonlinear differential equations are used to obtain displacements, strains, loads, and stresses for a model with initially imperfect fiber-plates. The initial imperfections for all fiber-plates are the same and have the shape of the short-wavelength buckling mode for the model. The Kantorovich method used in the linear analysis also is used to obtain solutions to the nonlinear equations. The unknown functions are expanded in kinematically admissible trigonometric series in the $\bar{x}$-coordinate, and the governing equations become nonlinear coupled ordinary differential equations.

An approximate solution to the nonlinear coupled ordinary differential equations is obtained using an algorithm developed by Lentini and Pereyra [58]. The algorithm is based on Newton's method and can be used to solve a system of simultaneous first-order nonlinear ordinary differential equations subject to two-point boundary conditions. The algorithm uses finite differences to solve

the differential equations, and adaptive mesh spacings are automatically produced so that mild boundary layers are detected and resolved. The difference between successive approximations for each unknown is calculated. The algorithm iterates until this difference is less than a specified tolerance.

2.3.1 Orthotropic Fiber-Plates

The nonlinear analysis for models with orthotropic fiber-plates is similar to the analysis used by Stein [59] for the postbuckling behavior of orthotropic plates. The displacements in the present analysis for the ith fiber-plate are expressed as

$$
\begin{aligned}
u^{(i)^\circ} &= \frac{-\bar{u}_o x}{a} + u_s^{(i)}(y) \sin \frac{2\pi\bar{x}}{\lambda} \\
v^{(i)^\circ} &= v_o^{(i)}(y) + v_c^{(i)}(y) \cos \frac{2\pi\bar{x}}{\lambda} \\
w^{(i)^\circ} &= w_o(y) \sin \frac{\pi\bar{x}}{\lambda} + w_s^{(i)}(y) \sin \frac{\pi\bar{x}}{\lambda}
\end{aligned}
\tag{2.73}
$$

Equations (2.73) are substituted into equations (2.6) and (2.7) to obtain these expressions for the strains and curvatures:

$$\varepsilon_x^{(i)^\circ} = -\frac{\bar{u}_o}{a} + \frac{2\pi}{\lambda} u_s^{(i)} \cos\frac{2\pi\bar{x}}{\lambda} + \frac{1}{4}(\frac{\pi}{\lambda})^2 w_s^{(i)^2}(1 + \cos\frac{2\pi\bar{x}}{\lambda})$$

$$+ \frac{1}{2}(\frac{\pi}{\lambda})^2 w_o w_s^{(i)}(1 + \cos\frac{2\pi\bar{x}}{\lambda})$$

$$\varepsilon_y^{(i)^\circ} = v_o^{(i)'} + v_c^{(i)'} \cos\frac{2\pi\bar{x}}{\lambda} + \frac{1}{4}(w_s^{(i)'})^2(1 - \cos\frac{2\pi\bar{x}}{\lambda})$$

$$+ \frac{1}{2} w_o' w_s^{(i)'}(1 - \cos\frac{2\pi\bar{x}}{\lambda})$$

$$\gamma_{xy}^{(i)^\circ} = u_s^{(i)'} \sin\frac{2\pi\bar{x}}{\lambda} - \frac{2\pi}{\lambda} v_c^{(i)} \sin\frac{2\pi\bar{x}}{\lambda} +$$

$$\frac{1}{2}(\frac{\pi}{\lambda}) w_s^{(i)} w_s^{(i)'} \sin\frac{2\pi\bar{x}}{\lambda} + \frac{1}{2}(\frac{\pi}{\lambda}) w_o w_s^{(i)'} \sin\frac{2\pi\bar{x}}{\lambda}$$

$$+ \frac{1}{2}(\frac{\pi}{\lambda}) w_o' w_s^{(i)} \sin\frac{2\pi\bar{x}}{\lambda}$$

$$\kappa_x^{(i)} = (\frac{\pi}{\lambda})^2 w_s^{(i)} \sin\frac{\pi\bar{x}}{\lambda}$$

$$\kappa_y^{(i)} = - w_s^{(i)''} \sin\frac{\pi\bar{x}}{\lambda}$$

$$\kappa_{xy}^{(i)} = -2(\frac{\pi}{\lambda}) w_s^{(i)'} \cos\frac{\pi\bar{x}}{\lambda} \qquad (2.74)$$

where $(\ )'$ denotes differentiation with respect to the y-coordinate. The stress and moment resultants are expressed as

$$N_x^{(i)} = N_{x^o}^{(i)}(y) + N_{xc}^{(i)}(y) \cos \frac{2\pi\bar{x}}{\lambda}$$

$$N_y^{(i)} = N_{y^o}^{(i)}(y) + N_{yc}^{(i)}(y) \cos \frac{2\pi\bar{x}}{\lambda}$$

$$N_{xy}^{(i)} = N_{xys}^{(i)}(y) \sin \frac{2\pi\bar{x}}{\lambda} \qquad (2.75)$$

$$M_x^{(i)} = M_{xs}^{(i)}(y) \sin \frac{\pi\bar{x}}{\lambda}$$

$$M_y^{(i)} = M_{ys}^{(i)}(y) \sin \frac{\pi\bar{x}}{\lambda}$$

$$M_{xy}^{(i)} = M_{xyc}^{(i)}(y) \cos \frac{\pi\bar{x}}{\lambda}$$

where

$$N_{x^o}^{(i)} = A_{11}^{(i)}\left[-\frac{\bar{u}_o}{a} + \frac{1}{4}\left(\frac{\pi}{\lambda}\right)^2 w_s^{(i)^2} + \frac{1}{2}\left(\frac{\pi}{\lambda}\right)^2 w_o w_s^{(i)}\right] +$$

$$A_{12}^{(i)}\left[v_o^{(i)'} + \frac{1}{4}\left(w_s^{(i)'}\right)^2 + \frac{1}{2} w_o' w_s^{(i)'}\right]$$

$$N_{xc}^{(i)} = A_{11}^{(i)}\left[\frac{2\pi}{\lambda} u_s^{(i)} + \frac{1}{4}\left(\frac{\pi}{\lambda}\right)^2 w_s^{(i)^2} + \frac{1}{2}\left(\frac{\pi}{\lambda}\right)^2 w_o w_s^{(i)}\right] +$$

$$A_{12}^{(i)}\left[v_c^{(i)'} - \frac{1}{4}\left(w_s^{(i)'}\right)^2 - \frac{1}{2} w_o' w_s^{(i)'}\right]$$

$$N_{y^o}^{(i)} = A_{22}^{(i)}\left[v_o^{(i)'} + \frac{1}{4}\left(w_s^{(i)'}\right)^2 + \frac{1}{2} w_o' w_s^{(i)'}\right] +$$

$$A_{12}^{(i)}\left[-\frac{\bar{u}_o}{a} + \frac{1}{4}\left(\frac{\pi}{\lambda}\right)^2 w_s^{(i)^2} + \frac{1}{2}\left(\frac{\pi}{\lambda}\right)^2 w_o w_s^{(i)}\right]$$

$$N_{yc}^{(i)} = A_{22}^{(i)}\left[v_c^{(i)'} - \frac{1}{4}\left(w_s^{(i)'}\right)^2 - \frac{1}{2} w_o' w_s^{(i)'}\right] +$$

$$A_{12}^{(i)}\left[\frac{2\pi}{\lambda} u_s^{(i)} + \frac{1}{4}\left(\frac{\pi}{\lambda}\right)^2 w_s^{(i)^2} + \frac{1}{2}\left(\frac{\pi}{\lambda}\right)^2 w_o w_s^{(i)}\right]$$

$$N_{xys}^{(i)} = A_{66}^{(i)}\left[u_s^{(i)\prime} - \frac{2\pi}{\lambda} v_c^{(i)} + \frac{1}{2}\left(\frac{\pi}{\lambda}\right) w_s^{(i)} w_s^{(i)\prime} + \right.$$

$$\left. \frac{1}{2}\left(\frac{\pi}{\lambda}\right) w_o w_s^{(i)\prime} + \frac{1}{2}\left(\frac{\pi}{\lambda}\right) w_o' w_s^{(i)}\right]$$

$$M_{xs}^{(i)} = D_{11}^{(i)}\left(\frac{\pi}{\lambda}\right)^2 w_s^{(i)} - D_{12}^{(i)} w_s^{(i)\prime\prime}$$

$$M_{ys}^{(i)} = -D_{22}^{(i)} w_s^{(i)\prime\prime} + D_{12}^{(i)}\left(\frac{\pi}{\lambda}\right)^2 w_s^{(i)}$$

$$M_{xyc}^{(i)} = -2D_{66}^{(i)}\left(\frac{\pi}{\lambda}\right) w_s^{(i)\prime} \qquad (2.76)$$

Equations (2.74) to (2.76) are used in equation (2.25) (principal of stationary potential energy), and the resulting equation is integrated over $0 \leq \bar{x} \leq \lambda$. For arbitrary $\delta u_2^{(i)}$, $\delta v_o^{(i)}$, $\delta v_2^{(i)}$, and $\delta w_s^{(i)}$, the principle of stationary potential energy requires that the following differential equations be satisfied:

<u>for i = 1, 2, ..., N</u>

$$\frac{2\pi}{\lambda} N_{xc}^{(i)} - N_{xys}^{(i)\prime} = 0$$

$$N_{yo}^{(i)\prime} = 0 \qquad (2.77)$$

$$\frac{2\pi}{\lambda} N_{xys}^{(i)} + N_{yc}^{(i)\prime} = 0$$

for i = 1

$$V_y^{(1)'} = -(\frac{\pi}{\lambda})^2 M_{xs}^{(1)} - (\frac{\pi}{\lambda})^2 (N_{x^o}^{(1)} + \frac{1}{2} N_{xc}^{(1)})(w_s^{(1)} + w_o) -$$

$$\frac{1}{2}(\frac{\pi}{\lambda}) N_{xys}^{(1)} (\beta^{(1)} + w_o') - G_1^* [-\beta^{(1)'} + (\frac{\pi}{\lambda})^2 w_s^{(1)}] -$$

$$G_2^* [-\beta^{(2)'} + (\frac{\pi}{\lambda})^2 w_s^{(2)}] - E^* (w_s^{(1)} - w_s^{(2)}) \qquad (2.78)$$

for i = 2, 3, ...,N

$$V_y^{(i)'} = -(\frac{\pi}{\lambda})^2 M_{xs}^{(i)} - (\frac{\pi}{\lambda})^2 (N_{x^o}^{(i)} + \frac{1}{2} N_{xc}^{(i)})(w_s^{(i)} + w_o) -$$

$$\frac{1}{2}(\frac{\pi}{\lambda}) N_{xys}^{(i)} (\beta^{(i)} + w_o') - 2G_1^* [-\beta^{(i)'} + (\frac{\pi}{\lambda})^2 w_s^{(i)}] -$$

$$G_2^* [-\beta^{(i-1)'} + (\frac{\pi}{\lambda})^2 w_s^{(i-1)} - \beta^{(i+1)'} + (\frac{\pi}{\lambda})^2 w_s^{(i+1)}]$$

$$- E^* (2w_s^{(i)} - w_s^{(i-1)} - w_s^{(i+1)}) \qquad (2.79)$$

for i = N

$$V_y^{(N)'} = -(\frac{\pi}{\lambda})^2 M_{xs}^{(N)} - (\frac{\pi}{\lambda})^2 (N_{x^o}^{(N)} + \frac{1}{2} N_{xc}^{(N)})(w_s^{(N)} + w_o) -$$

$$\frac{1}{2}(\frac{\pi}{\lambda}) N_{xys}^{(N)} (\beta^{(N)} + w_o') - G_1^* [-\beta^{(N)'} + (\frac{\pi}{\lambda})^2 w_s^{(N)}] -$$

$$G_2^* [-\beta^{(N-1)'} + (\frac{\pi}{\lambda})^2 w_s^{(N-1)}] - E^* (w_s^{(N)} - w_s^{(N-1)}) \qquad (2.80)$$

where the previously undefined functions for the ith fiber-plate are

$$V_y^{(i)} = -M_{ys}^{(i)} + \frac{2\pi}{\lambda} M_{xyc}^{(i)} - (N_{y^o}^{(i)} - \frac{1}{2} N_{yc}^{(i)})(\beta^{(i)} + w_o') -$$

$$\frac{1}{2}(\frac{\pi}{\lambda}) N_{xys}^{(i)}(w_s^{(i)} + w_o) \qquad (2.81)$$

$$\beta^{(i)} = w_s^{(i)'}$$

The boundary conditions for this energy formulation are

$$N_{xys}^{(i)} \delta u_s^{(i)} \Big|_0^b = 0 \qquad N_{y^o}^{(i)} \delta v_o^{(i)} \Big|_0^b = 0$$

$$N_{yc}^{(i)} \delta v_c^{(i)} \Big|_0^b = 0 \qquad M_{ys}^{(i)} \delta w_s^{(i)'} \Big|_0^b = 0 \qquad (2.82)$$

$$V_y^{(i)} \delta w_s^{(i)} \Big|_0^b = 0 \qquad i = 1, 2, \ldots, N$$

The model remains rectangular during loading and is simply-supported on the unloaded edges. These boundary conditions are expressed as

<u>at y = 0 and at y = b</u>

$$u_s^{(i)} = v_c^{(i)} = N_{y^o}^{(i)} = w_s^{(i)} = M_{ys}^{(i)} = 0 \qquad (2.83)$$

The equation (2.77) and boundary condition equation (2.83) for $N_{y^o}^{(i)}$ are satisfied by $N_{y^o}^{(i)} = 0$ for $1 \leq i \leq N$ throughout the region.

The first-order governing equations for a model with orthotropic fiber-plates can be expressed as a function of eight unknowns for each fiber-plate, and these unknowns are $u_s^{(i)}$, $v_c^{(i)}$, $w_s^{(i)}$, $\beta^{(i)}$, $N_{yc}^{(i)}$, $N_{xys}^{(i)}$, $M_{ys}^{(i)}$, and $V_y^{(i)}$. The other unknowns are expressed as functions of these eight. The eight differential equations for each fiber-plate are obtained by re-organizing equations (2.74) and (2.77) to (2.81) and are stated below:

<u>for i = 1, 2, ..., n</u>

$$u_s^{(i)'} = \frac{N_{xys}^{(i)}}{A_{66}^{(i)}} + \frac{2\pi}{\lambda} v_c^{(i)} - \frac{1}{2}\left(\frac{\pi}{\lambda}\right)\left(w_s^{(i)}\beta^{(i)} + w_o\beta^{(i)} + w_o' w_s^{(i)}\right)$$

$$v_c^{(i)'} = \frac{N_{yc}^{(i)}}{A_{22}^{(i)}} + \frac{1}{4}\beta^{(i)2} + \frac{1}{2} w_o'\beta^{(i)} - \frac{A_{12}^{(i)}}{A_{22}^{(i)}}\left[\frac{2\pi}{\lambda} u_s^{(i)} + \right.$$

$$\left. \frac{1}{4}\left(\frac{\pi}{\lambda}\right)^2 w_s^{(i)2} + \frac{1}{2}\left(\frac{\pi}{\lambda}\right)^2 w_o w_s^{(i)}\right]$$

$$\beta^{(i)'} = -\frac{M_{ys}^{(i)}}{D_{22}^{(i)}} + \frac{D_{12}^{(i)}}{D_{22}^{(i)}}\left(\frac{\pi}{\lambda}\right)^2 w_s^{(i)}$$

$$w_s^{(i)'} = \beta^{(i)} \qquad (2.84)$$

$$N_{xys}^{(i)'} = (\frac{2\pi}{\lambda})\{\frac{A_{12}^{(i)}}{A_{22}^{(i)}} N_{yc}^{(i)} + (A_{11}^{(i)} - \frac{A_{12}^{(i)^2}}{A_{22}^{(i)}})[\frac{2\pi}{\lambda} u_s^{(i)} +$$

$$\frac{1}{4}(\frac{\pi}{\lambda})^2 w_s^{(i)^2} + \frac{1}{2}(\frac{\pi}{\lambda})^2 w_o w_s^{(i)}]\}$$

$$N_{yc}^{(i)'} = -(\frac{2\pi}{\lambda}) N_{xys}^{(i)}$$

$$M_{ys}^{(i)'} = -V_y^{(i)} - 4D_{66}^{(i)}(\frac{\pi}{\lambda})^2 \beta^{(i)} + \frac{1}{2} N_{yc}^{(i)}(\beta^{(i)} + w_o') -$$

$$\frac{1}{2} N_{xys}^{(i)}(\frac{\pi}{\lambda})(w_s^{(i)} + w_o)$$

<u>for i = 1</u>

$$V_y^{(1)'} = -(\frac{\pi}{\lambda})^2[\frac{D_{12}^{(1)}}{D_{22}^{(1)}} M_{ys}^{(1)} + (D_{11}^{(1)} - \frac{D_{12}^{(1)^2}}{D_{22}^{(1)}})(\frac{\pi}{\lambda})^2 w_s^{(1)}] -$$

$$\frac{1}{2} N_{xys}^{(1)}(\frac{\pi}{\lambda})(\beta^{(1)} + w_o') - \frac{1}{2}(\frac{\pi}{\lambda})^2(w_s^{(1)} + w_o)\{\frac{A_{12}^{(1)}}{A_{22}^{(1)}} N_{yc}^{(1)}$$

$$+ (A_{11}^{(1)} - \frac{A_{12}^{(1)^2}}{A_{22}^{(1)}})[-\frac{2\bar{u}_o}{a} + \frac{2\pi}{\lambda} u_s^{(1)} +$$

$$\frac{3}{4}(\frac{\pi}{\lambda})^2(w_s^{(1)^2} + w_o^2)]\} - E^*(w_s^{(1)} - w_s^{(2)}) -$$

$$G_1^*[\frac{M_{ys}^{(1)}}{D_{22}^{(1)}} + (1 - \frac{D_{12}^{(1)}}{D_{22}^{(1)}})(\frac{\pi}{\lambda})^2 w_s^{(1)}] - G_2^*[\frac{M_{ys}^{(2)}}{D_{22}^{(2)}} +$$

$$(1 - \frac{D_{12}^{(2)}}{D_{22}^{(2)}})(\frac{\pi}{\lambda})^2 w_s^{(2)}] \qquad (2.85)$$

for i = 2, 3, ..., N-1

$$V_y^{(i)'} = -(\frac{\pi}{\lambda})^2[\frac{D_{12}^{(i)}}{D_{22}^{(i)}} M_{ys}^{(i)} + (D_{11}^{(i)} - \frac{D_{12}^{(i)^2}}{D_{22}^{(i)}})(\frac{\pi}{\lambda})^2 w_s^{(i)}] -$$

$$\frac{1}{2} N_{xys}^{(i)}(\frac{\pi}{\lambda})(\beta^{(i)} + w_o') - \frac{1}{2}(\frac{\pi}{\lambda})^2(w_s^{(i)} + w_o)\{\frac{A_{12}^{(i)}}{A_{22}^{(i)}} N_{yc}^{(i)}$$

$$+ (A_{11}^{(i)} - \frac{A_{12}^{(i)^2}}{A_{22}^{(i)}})[-\frac{2\bar{u}_o}{a} + \frac{2\pi}{\lambda} u_s^{(i)} +$$

$$\frac{3}{4}(\frac{\pi}{\lambda})^2(w_s^{(i)^2} + w_o^2)]\} - E^*(2w_s^{(i)} - w_s^{(i-1)} - w_s^{(i+1)})$$

$$- 2G_1^*[\frac{M_{ys}^{(i)}}{D_{22}^{(i)}} + (1 - \frac{D_{12}^{(i)}}{D_{22}^{(i)}})(\frac{\pi}{\lambda})^2 w_s^{(i)}] - G_2^*[\frac{M_{ys}^{(i-1)}}{D_{22}^{(i-1)}} +$$

$$(1 - \frac{D_{12}^{(i-1)}}{D_{22}^{(i-1)}})(\frac{\pi}{\lambda})^2 w_s^{(i-1)} + \frac{M_{ys}^{(i+1)}}{D_{22}^{(i+1)}} +$$

$$(1 - \frac{D_{12}^{(i+1)}}{D_{22}^{(i+1)}})(\frac{\pi}{\lambda})^2 w_s^{(i+1)}] \qquad (2.86)$$

for i = N

$$V_y^{(N)'} = -(\frac{\pi}{\lambda})^2[\frac{D_{12}^{(N)}}{D_{22}^{(N)}} M_{ys}^{(N)} + (D_{11}^{(N)} - \frac{D_{12}^{(N)2}}{D_{22}^{(N)}})(\frac{\pi}{\lambda})^2 w_s^{(N)}] -$$

$$\frac{1}{2} N_{xys}^{(N)}(\frac{\pi}{\lambda})(\beta^{(N)} + w_o') - \frac{1}{2}(\frac{\pi}{\lambda})^2(w_s^{(N)} + w_o)\{\frac{A_{12}^{(N)}}{A_{22}^{(N)}} N_{yc}^{(N)}$$

$$+ (A_{11}^{(N)} - \frac{A_{12}^{(N)2}}{A_{22}^{(N)}})[-\frac{2\bar{u}_o}{a} + \frac{2\pi}{\lambda} u_s^{(N)} +$$

$$\frac{3}{4}(\frac{\pi}{\lambda})^2(w_s^{(N)2} + w_o^2)]\} - E^*(w_s^{(N)} - w_s^{(N-1)}) -$$

$$G_1^*[\frac{M_{ys}^{(N)}}{D_{22}^{(N)}} + (1 - \frac{D_{12}^{(N)}}{D_{22}^{(N)}})(\frac{\pi}{\lambda})^2 w_s^{(N)}] - G_2^*[\frac{M_{ys}^{(N-1)}}{D_{22}^{(N-1)}} +$$

$$(1 - \frac{D_{12}^{(N-1)}}{D_{22}^{(N-1)}})(\frac{\pi}{\lambda})^2 w_s^{(N-1)}] \qquad (2.87)$$

The function of y for the initial imperfection w_o is expressed as

$$w_o(y) = \bar{w}_o \sin \frac{\pi y}{b} \qquad (2.88)$$

where $\bar{w}_o$ is a constant that is input to the analysis.

2.3.2 Anisotropic Fiber-Plates

The nonlinear analysis for compression-loaded models with anisotropic fiber-plates is similar to the analysis used by Stein [60] for the postbuckling behavior of orthotropic plates loaded in combined compression and shear. The equations in the present analysis for the *ith anisotropic fiber-plate* are general forms of the equations for the ith orthotropic fiber-plate. The displacements for the ith anisotropic fiber-plate are expressed as

$$
\begin{aligned}
u^{(i)^{\circ}} &= \frac{-\bar{u}_o x}{a} + u_o^{(i)}(y) + u_s^{(i)}(y) \sin \frac{2\pi\bar{x}}{\lambda} + \\
&\quad u_c^{(i)}(y) \cos \frac{2\pi\bar{x}}{\lambda} \\
v^{(i)^{\circ}} &= v_o^{(i)}(y) + v_s^{(i)}(y) \sin \frac{2\pi\bar{x}}{\lambda} \\
&\quad + v_c^{(i)}(y) \cos \frac{2\pi\bar{x}}{\lambda} \\
w^{(i)^{\circ}} &= w_{o_s}(y) \sin \frac{\pi\bar{x}}{\lambda} + w_{o_c}(y) \sin \frac{\pi\bar{x}}{\lambda} + \\
&\quad w_s^{(i)}(y) \sin \frac{\pi\bar{x}}{\lambda} + w_c^{(i)}(y) \cos \frac{\pi\bar{x}}{\lambda}
\end{aligned}
\tag{2.89}
$$

Equations (2.89) are substituted into equations (2.6) and (2.7) to obtain the following expressions for the strains and curvatures:

$$\varepsilon_x^{(i)^\circ} = -\frac{\bar{u}_o}{a} + \frac{2\pi}{\lambda} u_s^{(i)} \cos\frac{2\pi\bar{x}}{\lambda} - \frac{2\pi}{\lambda} u_c^{(i)} \sin\frac{2\pi\bar{x}}{\lambda} +$$

$$\frac{1}{4}(\frac{\pi}{\lambda})^2[w_s^{(i)^2} + w_c^{(i)^2} + (w_s^{(i)^2} - w_c^{(i)^2}) \cos\frac{2\pi\bar{x}}{\lambda}$$

$$- 2w_s^{(i)} w_c^{(i)} \sin\frac{2\pi\bar{x}}{\lambda}] + \frac{1}{2}(\frac{\pi}{\lambda})^2[w_s^{(i)} w_{o_s} + w_c^{(i)} w_{o_c}$$

$$+ (w_s^{(i)} w_{o_s} - w_c^{(i)} w_{o_c}) \cos\frac{2\pi\bar{x}}{\lambda} - (w_s^{(i)} w_{o_s} +$$

$$w_c^{(i)} w_{o_c}) \sin\frac{2\pi\bar{x}}{\lambda}]$$

$$\varepsilon_y^{(i)^\circ} = v_o^{(i)'} + v_s^{(i)'} \sin\frac{2\pi\bar{x}}{\lambda} + v_c^{(i)'} \cos\frac{2\pi\bar{x}}{\lambda} +$$

$$\frac{1}{4}\{(w_s^{(i)'})^2 + (w_c^{(i)'})^2 - [(w_s^{(i)'})^2 -$$

$$(w_c^{(i)'})^2] \cos\frac{2\pi\bar{x}}{\lambda} + 2w_s^{(i)'} w_c^{(i)'} \sin\frac{2\pi\bar{x}}{\lambda}\} +$$

$$\frac{1}{2}[w_s^{(i)'} w_{o_s}' + w_c^{(i)'} w_{o_c}' - (w_s^{(i)'} w_{o_s}' -$$

$$w_c^{(i)'} w_{o_c}') \cos\frac{2\pi\bar{x}}{\lambda} + (w_s^{(i)'} w_{o_c}' +$$

$$w_c^{(i)'} w_{o_s}') \sin\frac{2\pi\bar{x}}{\lambda}]$$

$$\gamma_{xy}^{(i)^{\circ}} = u_o^{(i)'} + u_s^{(i)'} \sin \frac{2\pi\bar{x}}{\lambda} + u_c^{(i)'} \cos \frac{2\pi\bar{x}}{\lambda} +$$

$$\frac{2\pi}{\lambda} v_s^{(i)} \cos \frac{2\pi\bar{x}}{\lambda} - \frac{2\pi}{\lambda} v_c^{(i)} \sin \frac{2\pi\bar{x}}{\lambda} +$$

$$\frac{1}{2}(\frac{\pi}{\lambda})[w_s^{(i)} w_c^{(i)'} - w_s^{(i)'} w_c^{(i)} + (w_s^{(i)} w_c^{(i)'} +$$

$$w_s^{(i)'} w_c^{(i)}) \cos \frac{2\pi\bar{x}}{\lambda} + (w_s^{(i)} w_s^{(i)'} -$$

$$w_c^{(i)} w_c^{(i)'}) \sin \frac{2\pi\bar{x}}{\lambda}] + \frac{1}{2}(\frac{\pi}{\lambda})[w_c^{(i)'} w_{os} - w_s^{(i)'} w_{oc}$$

$$+ (w_c^{(i)'} w_{os} + w_s^{(i)'} w_{oc}) \cos \frac{2\pi\bar{x}}{\lambda} + (w_s^{(i)'} w_{os} -$$

$$+ w_c^{(i)'} w_{oc}) \sin \frac{2\pi\bar{x}}{\lambda}] + \frac{1}{2}(\frac{\pi}{\lambda})[w_s^{(i)} w_{oc}' - w_c^{(i)} w_{os}'$$

$$+ (w_s^{(i)} w_{oc}' + w_c^{(i)} w_{os}') \cos \frac{2\pi\bar{x}}{\lambda} + (w_s^{(i)} w_{os}' -$$

$$w_c^{(i)} w_{oc}') \sin \frac{2\pi\bar{x}}{\lambda}]$$

$$\kappa_x^{(i)} = (\frac{\pi}{\lambda})^2 [w_s^{(i)} \sin \frac{\pi\bar{x}}{\lambda} + w_c^{(i)} \cos \frac{\pi\bar{x}}{\lambda}]$$

$$\kappa_y^{(i)} = -[w_s^{(i)''} \sin \frac{\pi\bar{x}}{\lambda} + w_c^{(i)''} \cos \frac{\pi\bar{x}}{\lambda}]$$

$$\kappa_{xy}^{(i)} = -2(\frac{\pi}{\lambda})[w_s^{(i)'} \cos \frac{\pi\bar{x}}{\lambda} - w_c^{(i)'} \sin \frac{\pi\bar{x}}{\lambda}] \qquad (2.90)$$

The stress and moment resultants are written as

$$N_x^{(i)} = N_{x^o}^{(i)}(y) + N_{xs}^{(i)}(y) \sin\frac{2\pi\bar{x}}{\lambda} + N_{xc}^{(i)}(y) \cos\frac{2\pi\bar{x}}{\lambda}$$

$$N_y^{(i)} = N_{y^o}^{(i)}(y) + N_{ys}^{(i)}(y) \sin\frac{2\pi\bar{x}}{\lambda} + N_{yc}^{(i)}(y) \cos\frac{2\pi\bar{x}}{\lambda}$$

$$N_{xy}^{(i)} = N_{xy^o}^{(i)}(y) + N_{xys}^{(i)}(y) \sin\frac{2\pi\bar{x}}{\lambda} + N_{xyc}^{(i)}(y) \cos\frac{2\pi\bar{x}}{\lambda}$$

$$M_x^{(i)} = M_{xs}^{(i)}(y) \sin\frac{\pi\bar{x}}{\lambda} + M_{xc}^{(i)}(y) \cos\frac{\pi\bar{x}}{\lambda}$$

$$M_y^{(i)} = M_{ys}^{(i)}(y) \sin\frac{\pi\bar{x}}{\lambda} + M_{yc}^{(i)}(y) \cos\frac{\pi\bar{x}}{\lambda}$$

$$M_{xy}^{(i)} = M_{xys}^{(i)}(y) \sin\frac{\pi\bar{x}}{\lambda} + M_{xyc}^{(i)}(y) \cos\frac{\pi\bar{x}}{\lambda} \qquad (2.91)$$

where

$$N_{x^o}^{(i)} = A_{11}^{(i)}\Big[-\frac{\bar{u}_o}{a} + \frac{1}{4}(\frac{\pi}{\lambda})^2(w_s^{(i)^2} + w_c^{(i)^2}) + \frac{1}{2}(\frac{\pi}{\lambda})^2(w_{o_s}w_s^{(i)} + w_{o_c}w_c^{(i)})\Big] + A_{12}^{(i)}\Big[v_o^{(i)'} + \frac{1}{4}[(w_s^{(i)'})^2 + (w_c^{(i)'})^2] + \frac{1}{2}(w'_{o_s}w_s^{(i)'} + w'_{o_c}w_c^{(i)'})\Big\} + A_{16}^{(i)}\Big[u_o^{(i)'} + \frac{1}{2}(\frac{\pi}{\lambda})(w_s^{(i)}w_c^{(i)'} - w_s^{(i)'}w_c^{(i)} + w_{o_s}w_c^{(i)'} - w_{o_c}w_s^{(i)'} + w'_{o_c}w_s^{(i)} - w'_{o_s}w_c^{(i)})\Big]$$

C-2

$$N_{xs}^{(i)} = A_{11}^{(i)}[-(\frac{2\pi}{\lambda})u_c^{(i)} - \frac{1}{2}(\frac{\pi}{\lambda})^2(w_s^{(i)}w_c^{(i)} + w_s^{(i)}w_{oc} + w_c^{(i)}w_{os})] + A_{12}^{(i)}[v_s^{(i)'} + \frac{1}{2}(w_s^{(i)'}w_c^{(i)'} + w_s^{(i)'}w_{oc}' + w_c^{(i)'}w_{os}')] + A_{16}^{(i)}[u_s^{(i)'} - \frac{2\pi}{\lambda}v_c^{(i)} + \frac{1}{2}(\frac{\pi}{\lambda})(w_s^{(i)}w_s^{(i)'} - w_c^{(i)}w_c^{(i)'} + w_s^{(i)'}w_{os} - w_c^{(i)'}w_{oc} + w_s^{(i)}w_{os}' - w_c^{(i)}w_{oc}')]$$

$$N_{xc}^{(i)} = A_{11}^{(i)}[\frac{2\pi}{\lambda}u_s^{(i)} + \frac{1}{4}(\frac{\pi}{\lambda})^2(w_s^{(i)2} - w_c^{(i)2}) + \frac{1}{2}(\frac{\pi}{\lambda})^2(w_{os}w_s^{(i)} - w_{oc}w_c^{(i)})] + A_{12}^{(i)}\{v_c^{(i)'} - \frac{1}{4}[(w_s^{(i)'})^2 - (w_c^{(i)'})^2] - \frac{1}{2}(w_{os}'w_s^{(i)'} - w_{oc}'w_c^{(i)'})\} + A_{16}^{(i)}[u_c^{(i)'} + \frac{2\pi}{\lambda}v_s^{(i)} + \frac{1}{2}(\frac{\pi}{\lambda})(w_s^{(i)}w_c^{(i)'} + w_s^{(i)'}w_c^{(i)} + w_{os}w_c^{(i)'} + w_{oc}w_s^{(i)'} + w_{oc}'w_s^{(i)} + w_{os}'w_c^{(i)})]$$

$$N_{y^o}^{(i)} = A_{12}^{(i)}[-\frac{\bar{u}_o}{a} + \frac{1}{4}(\frac{\pi}{\lambda})^2(w_s^{(i)2} + w_c^{(i)2}) + \frac{1}{2}(\frac{\pi}{\lambda})^2(w_{os}w_s^{(i)} + w_{oc}w_c^{(i)})] + A_{22}^{(i)}\{v_o^{(i)'} + \frac{1}{4}[(w_s^{(i)})^2 + (w_c^{(i)'})^2] + \frac{1}{2}(w_{os}'w_s^{(i)'} + w_{oc}'w_c^{(i)'})\} + A_{26}^{(i)}[u_o^{(i)'} + \frac{1}{2}(\frac{\pi}{\lambda})(w_s^{(i)}w_c^{(i)'} - w_s^{(i)'}w_c^{(i)} + w_{os}w_c^{(i)'} - w_{oc}w_s^{(i)'} + w_{oc}'w_s^{(i)} - w_{os}'w_c^{(i)}]$$

$$N_{ys}^{(i)} = A_{12}^{(i)}[-(\frac{2\pi}{\lambda})u_c^{(i)} - \frac{1}{2}(\frac{\pi}{\lambda})^2(w_s^{(i)}w_c^{(i)} + w_s^{(i)}w_{oc} + w_c^{(i)}w_{os})] + A_{22}^{(i)}[v_s^{(i)'} + \frac{1}{2}(w_s^{(i)'}w_c^{(i)'} + w_s^{(i)'}w_{oc}' + w_c^{(i)'}w_{os}')] + A_{26}^{(i)}[u_s^{(i)'} - \frac{2\pi}{\lambda}v_c^{(i)} + \frac{1}{2}(\frac{\pi}{\lambda})(w_s^{(i)}w_s^{(i)'} - w_c^{(i)}w_c^{(i)'} + w_s^{(i)'}w_{os} - w_c^{(i)'}w_{oc} + w_s^{(i)}w_{os}' - w_c^{(i)}w_{oc}')]$$

$$N_{yc}^{(i)} = A_{12}^{(i)}[\frac{2\pi}{\lambda}u_s^{(i)} + \frac{1}{4}(\frac{\pi}{\lambda})^2(w_s^{(i)2} - w_c^{(i)2}) + \frac{1}{2}(\frac{\pi}{\lambda})^2(w_{os}w_s^{(i)} - w_{oc}w_c^{(i)})] + A_{22}^{(i)}\{v_c^{(i)'} - \frac{1}{4}[(w_s^{(i)'})^2 - (w_c^{(i)'})^2] - \frac{1}{2}(w_{os}'w_s^{(i)'} - w_{oc}'w_c^{(i)'})\} + A_{26}^{(i)}[u_c^{(i)'} + \frac{2\pi}{\lambda}v_s^{(i)} + \frac{1}{2}(\frac{\pi}{\lambda})(w_s^{(i)}w_c^{(i)'} + w_s^{(i)'}w_c^{(i)} + w_{os}w_c^{(i)'} + w_{oc}w_s^{(i)'} + w_{oc}'w_s^{(i)} + w_{os}'w_c^{(i)})]$$

$$N_{xyo}^{(i)} = A_{16}^{(i)}[-\frac{\bar{u}_o}{a} + \frac{1}{4}(\frac{\pi}{\lambda})^2(w_s^{(i)2} + w_c^{(i)2}) + \frac{1}{2}(\frac{\pi}{\lambda})^2(w_{os}w_s^{(i)} + w_{oc}w_c^{(i)})] + A_{26}^{(i)}\{v_o^{(i)'} + \frac{1}{4}[(w_s^{(i)'})^2 + (w_c^{(i)'2})] + \frac{1}{2}(w_{os}'w_s^{(i)'} + w_{oc}'w_c^{(i)'})\} + A_{66}^{(i)}[u_o^{(i)'} + \frac{1}{2}(\frac{\pi}{\lambda})(w_s^{(i)}w_c^{(i)'} - w_s^{(i)'}w_c^{(i)} + w_{os}w_c^{(i)'} - w_{oc}w_s^{(i)'} + w_{oc}'w_s^{(i)} - w_{os}'w_c^{(i)}]$$

$$N_{xys}^{(i)} = A_{16}^{(i)}[-(\frac{2\pi}{\lambda})u_c^{(i)} - \frac{1}{2}(\frac{\pi}{\lambda})^2(w_s^{(i)}w_c^{(i)} + w_s^{(i)}w_{oc} + w_c^{(i)}w_{os})] + A_{26}^{(i)}[v_s^{(i)'} + \frac{1}{2}(w_s^{(i)'}w_c^{(i)'} + w_s^{(i)'}w_{oc}' + w_c^{(i)'}w_{os}')] + A_{66}^{(i)}[u_s^{(i)'} - \frac{2\pi}{\lambda}v_c^{(i)} + \frac{1}{2}(\frac{\pi}{\lambda})(w_s^{(i)}w_s^{(i)'} - w_c^{(i)}w_c^{(i)'} + w_s^{(i)'}w_{os} - w_c^{(i)'}w_{oc} + w_s^{(i)}w_{os}' - w_c^{(i)}w_{oc}')]$$

$$N_{xyc}^{(i)} = A_{16}^{(i)}[\frac{2\pi}{\lambda}u_s^{(i)} + \frac{1}{4}(\frac{\pi}{\lambda})^2(w_s^{(i)2} - w_c^{(i)2}) + \frac{1}{2}(\frac{\pi}{\lambda})^2(w_{os}w_s^{(i)} - w_{oc}w_c^{(i)})] + A_{26}^{(i)}\{v_c^{(i)'} - \frac{1}{4}[(w_s^{(i)'})^2 - (w_c^{(i)'})^2] - \frac{1}{2}(w_{os}'w_s^{(i)'} - w_{oc}'w_c^{(i)'})\} + A_{66}^{(i)}[u_c^{(i)'} + \frac{2\pi}{\lambda}v_s^{(i)} + \frac{1}{2}(\frac{\pi}{\lambda})(w_s^{(i)}w_c^{(i)'} + w_s^{(i)'}w_c^{(i)} + w_{os}w_c^{(i)'} + w_{oc}w_s^{(i)'} + w_{oc}'w_s^{(i)} + w_{os}'w_c^{(i)})]$$

$$M_{xs}^{(i)} = D_{11}^{(i)}(\frac{\pi}{\lambda})^2 w_s^{(i)} - D_{12}^{(i)}w_s^{(i)''} + 2D_{16}^{(i)}(\frac{\pi}{\lambda})\,w_c^{(i)'}$$

$$M_{xc}^{(i)} = D_{11}^{(i)}(\frac{\pi}{\lambda})^2 w_c^{(i)} - D_{12}^{(i)}w_c^{(i)''} - 2D_{16}^{(i)}(\frac{\pi}{\lambda})\,w_s^{(i)'}$$

$$M_{ys}^{(i)} = D_{12}^{(i)}(\frac{\pi}{\lambda})^2 w_s^{(i)} - D_{22}^{(i)}w_s^{(i)''} + 2D_{26}^{(i)}(\frac{\pi}{\lambda})\,w_c^{(i)'}$$

$$M_{yc}^{(i)} = D_{12}^{(i)}(\frac{\pi}{\lambda})^2 w_c^{(i)} - D_{22}^{(i)}w_c^{(i)''} - 2D_{26}^{(i)}(\frac{\pi}{\lambda})\,w_s^{(i)'}$$

$$M_{xys}^{(i)} = D_{16}^{(i)}\left(\frac{\pi}{\lambda}\right)^2 w_s^{(i)} - D_{26}^{(i)} w_s^{(i)''} + 2D_{66}^{(i)}\left(\frac{\pi}{\lambda}\right) w_c^{(i)'}$$

$$M_{xyc}^{(i)} = D_{16}^{(i)}\left(\frac{\pi}{\lambda}\right)^2 w_c^{(i)} - D_{26}^{(i)} w_c^{(i)''} - 2D_{66}^{(i)}\left(\frac{\pi}{\lambda}\right) w_s^{(i)'} \qquad (2.92)$$

Equations (2.90) to (2.92) are used in equation (2.25), and the resulting equation is integrated with respect to $\bar{x}$. For arbitrary $\delta u_o^{(i)}$, $\delta u_s^{(i)}$, $\delta u_c^{(i)}$, $\delta v_o^{(i)}$, $\delta v_s^{(i)}$, $\delta v_c^{(i)}$, $\delta w_s^{(i)}$, and $\delta w_c^{(i)}$, the principle of stationary potential energy requires that these differential equations are satisfied:

<u>for i = 1, 2, ..., N</u>

$$N_{xyo}^{(i)'} = 0$$

$$\frac{2\pi}{\lambda} N_{xc}^{(i)} - N_{xys}^{(i)'} = 0$$

$$\frac{2\pi}{\lambda} N_{xs}^{(i)} + N_{xyc}^{(i)'} = 0$$

$$N_{yo}^{(i)'} = 0$$

$$\frac{2\pi}{\lambda} N_{xyc}^{(i)} - N_{ys}^{(i)'} = 0$$

$$\frac{2\pi}{\lambda} N_{xys}^{(i)} + N_{yc}^{(i)'} = 0 \qquad (2.93)$$

for i = 1

$$V_{ys}^{(1)'} = -(\tfrac{\pi}{\lambda})^2 M_{xs}^{(1)} - (\tfrac{\pi}{\lambda})^2 (N_{x^o}^{(1)} + \tfrac{1}{2} N_{xc}^{(1)})(w_s^{(1)} + w_{o_s}) +$$

$$\tfrac{1}{2}(\tfrac{\pi}{\lambda})^2 N_{xs}^{(1)}(w_c^{(1)} + w_{o_c}) - (\tfrac{\pi}{\lambda})[(N_{xy^o}^{(1)} +$$

$$\tfrac{1}{2} N_{xyc}^{(1)})(\beta_c^{(1)} + w_{o_c}') + \tfrac{1}{2} N_{xys}^{(1)}(\beta_s^{(1)} + w_{o_s}')] -$$

$$G_1^*[-\beta_s^{(1)'} + (\tfrac{\pi}{\lambda})^2 w_s^{(1)}] -$$

$$G_2^*[-\beta_s^{(2)'} + (\tfrac{\pi}{\lambda})^2 w_s^{(2)}] - E^*(w_s^{(1)} - w_s^{(2)})$$

$$V_{yc}^{(1)'} = -(\tfrac{\pi}{\lambda})^2 M_{xc}^{(1)} - (\tfrac{\pi}{\lambda})^2 (N_{x^o}^{(1)} - \tfrac{1}{2} N_{xc}^{(1)})(w_c^{(1)} + w_{o_c}) +$$

$$\tfrac{1}{2}(\tfrac{\pi}{\lambda})^2 N_{xs}^{(1)}(w_s^{(1)} + w_{o_s}) + (\tfrac{\pi}{\lambda})[(N_{xy^o}^{(1)} -$$

$$\tfrac{1}{2} N_{xyc}^{(1)})(\beta_s^{(1)} + w_{o_s}') + \tfrac{1}{2} N_{xys}^{(1)}(\beta_c^{(1)} + w_{o_c}')] -$$

$$G_1^*[-\beta_c^{(1)'} + (\tfrac{\pi}{\lambda})^2 w_c^{(1)}] -$$

$$G_2^*[-\beta_c^{(2)'} + (\tfrac{\pi}{\lambda})^2 w_c^{(2)}] - E^*(w_c^{(1)} - w_c^{(2)}) \qquad (2.94)$$

for i = 2, 3, ...,N

$$V_{ys}^{(i)'} = -(\tfrac{\pi}{\lambda})^2 M_{xs}^{(i)} - (\tfrac{\pi}{\lambda})^2 (N_{x^o}^{(i)} + \tfrac{1}{2} N_{xc}^{(i)})(w_s^{(i)} + w_{o_s}) +$$

$$\tfrac{1}{2}(\tfrac{\pi}{\lambda})^2 N_{xs}^{(i)}(w_c^{(i)} + w_{o_c}) - (\tfrac{\pi}{\lambda})[(N_{xy^o}^{(i)} +$$

$$\tfrac{1}{2} N_{xyc}^{(i)})(\beta_c^{(i)} + w_{o_c}') + \tfrac{1}{2} N_{xys}^{(i)}(\beta_s^{(i)} + w_{o_s}')] -$$

$$2G_1^*[-\beta_s^{(i)'} + (\tfrac{\pi}{\lambda})^2 w_s^{(i)}] -$$

$$G_2^*[-\beta_s^{(i-1)'} + (\tfrac{\pi}{\lambda})^2 w_s^{(i-1)} - \beta_s^{(i+1)'} + (\tfrac{\pi}{\lambda})^2 w_s^{(i+1)}]$$

$$- E^*(2w_s^{(i)} - w_s^{(i-1)} - w_s^{(i+1)})$$

$$V_{yc}^{(i)'} = -(\tfrac{\pi}{\lambda})^2 M_{xc}^{(i)} - (\tfrac{\pi}{\lambda})^2 (N_{x^\circ}^{(i)} - \tfrac{1}{2} N_{xc}^{(i)})(w_c^{(i)} + w_{\circ c}) +$$

$$\tfrac{1}{2}(\tfrac{\pi}{\lambda})^2 N_{xs}^{(i)}(w_s^{(i)} + w_{\circ s}) + (\tfrac{\pi}{\lambda})[(N_{xy^\circ}^{(i)} -$$

$$\tfrac{1}{2} N_{xyc}^{(i)})(\beta_s^{(i)} + w_{\circ s}') + \tfrac{1}{2} N_{xys}^{(i)}(\beta_c^{(i)} + w_{\circ c}')] -$$

$$2G_1^*[-\beta_c^{(i)'} + (\tfrac{\pi}{\lambda})^2 w_c^{(i)}] -$$

$$G_2^*[-\beta_c^{(i-1)'} + (\tfrac{\pi}{\lambda})^2 w_c^{(i-1)} - \beta_c^{(i+1)'} + (\tfrac{\pi}{\lambda})^2 w_c^{(i+1)}]$$

$$- E^*(2w_c^{(i)} - w_c^{(i-1)} - w_c^{(i+1)}) \qquad (2.95)$$

<u>for i = N</u>

$$V_{ys}^{(N)'} = -(\tfrac{\pi}{\lambda})^2 M_{xs}^{(N)} - (\tfrac{\pi}{\lambda})^2 (N_{x^\circ}^{(N)} + \tfrac{1}{2} N_{xc}^{(N)})(w_s^{(N)} + w_{\circ s}) +$$

$$\tfrac{1}{2}(\tfrac{\pi}{\lambda})^2 N_{xs}^{(N)}(w_c^{(N)} + w_{\circ c}) - (\tfrac{\pi}{\lambda})[(N_{xy^\circ}^{(N)} +$$

$$\tfrac{1}{2} N_{xyc}^{(N)})(\beta_c^{(N)} + w_{\circ c}') + \tfrac{1}{2} N_{xys}^{(N)}(\beta_s^{(N)} + w_{\circ s}')] -$$

$$G_1^*[-\beta_s^{(N)'} + (\tfrac{\pi}{\lambda})^2 w_s^{(N)}] -$$

$$G_2^*[-\beta_s^{(N-1)'} + (\tfrac{\pi}{\lambda})^2 w_s^{(N-1)}] - E^*(w_s^{(N)} - w_s^{(N-1)})$$

$$V_{yc}^{(N)'} = -(\frac{\pi}{\lambda})^2 M_{xc}^{(N)} - (\frac{\pi}{\lambda})^2 (N_{x^o}^{(N)} - \frac{1}{2} N_{xc}^{(N)})(w_c^{(N)} + w_{oc}) +$$

$$\frac{1}{2}(\frac{\pi}{\lambda})^2 N_{xs}^{(N)}(w_s^{(N)} + w_{os}) + (\frac{\pi}{\lambda})[(N_{xy^o}^{(N)} -$$

$$\frac{1}{2} N_{xyc}^{(N)})(\beta_s^{(N)} + w_{os}') + \frac{1}{2} N_{xys}^{(N)}(\beta_c^{(N)} + w_{oc}')] -$$

$$G_1^*[-\beta_c^{(N)'} + (\frac{\pi}{\lambda})^2 w_c^{(N)}] -$$

$$G_2^*[-\beta_c^{(N-1)'} + (\frac{\pi}{\lambda})^2 w_c^{(N-1)}] - E^*(w_c^{(N)} - w_c^{(N-1)})$$

(2.96)

where the previously undefined functions for the ith fiber-plate are

$$V_{ys}^{(i)} = -M_{ys}^{(i)} + \frac{2\pi}{\lambda} M_{xyc}^{(i)} - (N_{y^o}^{(i)} - \frac{1}{2} N_{yc}^{(i)})(\beta_s^{(i)} + w_{os}') -$$

$$\frac{1}{2} N_{ys}^{(i)}(\beta_c^{(i)} + w_{oc}') + (\frac{\pi}{\lambda})[(N_{xy^o}^{(i)} - \frac{1}{2} N_{xyc}^{(i)})(w_c^{(i)}$$

$$+ w_{oc}) - \frac{1}{2} N_{xys}^{(i)}(w_s^{(i)} + w_{os})]$$

$$V_{yc}^{(i)} = -M_{yc}^{(i)} - \frac{2\pi}{\lambda} M_{xys}^{(i)} - (N_{y^o}^{(i)} + \frac{1}{2} N_{yc}^{(i)})(\beta_c^{(i)} + w_{oc}') -$$

$$\frac{1}{2} N_{ys}^{(i)}(\beta_s^{(i)} + w_{os}') - (\frac{\pi}{\lambda})[(N_{xy^o}^{(i)} + \frac{1}{2} N_{xyc}^{(i)})(w_s^{(i)}$$

$$+ w_{os}) - \frac{1}{2} N_{xys}^{(i)}(w_c^{(i)} + w_{oc})]$$

$$\beta_s^{(i)} = w_s^{(i)'}$$

$$\beta_c^{(i)} = w_c^{(i)'} \qquad (2.97)$$

The boundary conditions for this energy formulation are

$$N_{xy^o}^{(i)}\delta u_o^{(i)}\Big|_0^b = 0 \qquad N_{xys}^{(i)}\delta u_s^{(i)}\Big|_0^b = 0$$

$$N_{xyc}^{(i)}\delta u_c^{(i)}\Big|_0^b = 0 \qquad N_{y^o}^{(i)}\delta v_o^{(i)}\Big|_0^b = 0$$

$$N_{ys}^{(i)}\delta v_s^{(i)}\Big|_0^b = 0 \qquad N_{yc}^{(i)}\delta v_c^{(i)}\Big|_0^b = 0$$

$$M_{ys}^{(i)}\delta w_s^{(i)'}\Big|_0^b = 0 \qquad M_{yc}^{(i)}\delta w_c^{(i)'}\Big|_0^b = 0$$

$$V_{ys}^{(i)}\delta w_s^{(i)}\Big|_0^b = 0 \qquad V_{yc}^{(i)}\delta w_c^{(i)}\Big|_0^b = 0$$

$$i = 1, 2, \ldots, N \tag{2.98}$$

The model remains rectangular during loading and is simply supported on the unloaded edges. The boundary conditions are expressed as

<u>at y = 0 and at y = b</u>

$$u_o^{(i)} = u_s^{(i)} = u_c^{(i)} = v_s^{(i)} = v_c^{(i)} = w_s^{(i)} = w_c^{(i)} = 0$$

$$N_{y^o}^{(i)} = M_{ys}^{(i)} = M_{yc}^{(i)} = 0 \tag{2.99}$$

The first-order governing equations for a model with anisotropic fiber-plates can be expressed as a function of twenty unknowns for each fiber-plate. These unknowns for the ith fiber-plate are $u_o^{(i)}$, $u_s^{(i)}$, $u_c^{(i)}$, $v_o^{(i)}$, $v_s^{(i)}$, $v_c^{(i)}$, $w_s^{(i)}$, $w_c^{(i)}$, $\beta_s^{(i)}$, $\beta_c^{(i)}$, $N_{y^o}^{(i)}$, $N_{ys}^{(i)}$, $N_{yc}^{(i)}$, $N_{xy^o}^{(i)}$, $N_{xys}^{(i)}$, $N_{xyc}^{(i)}$, $M_{ys}^{(i)}$, $M_{yc}^{(i)}$, $V_{ys}^{(i)}$, and $V_{yc}^{(i)}$. The other unknowns are expressed as functions of these twenty. The twenty differential equations for each fiber-plate are obtained by re-organizing equations (2.90) and (2.93) to (2.97) and are stated below:

<u>for i = 1, 2, ..., N</u>

$$u_o^{(i)\prime} = -\frac{1}{2}\left(\frac{\pi}{\lambda}\right)\left(w_s^{(i)}\beta_c^{(i)} - \beta_s^{(i)}w_c^{(i)} + w_{o_s}\beta_c^{(i)} - w_{o_c}\beta_s^{(i)} + w_{o_c}'w_s^{(i)} - w_{o_s}'w_c^{(i)}\right) + \left(A_{66}^{(i)} - \frac{A_{26}^{(i)^2}}{A_{22}^{(i)}}\right)^{-1}\left\{N_{xy^o}^{(i)} - \frac{A_{26}^{(i)}}{A_{22}^{(i)}}N_{y^o}^{(i)} - \left(A_{16}^{(i)} - \frac{A_{26}^{(i)}A_{12}^{(i)}}{A_{22}^{(i)}}\right)\left[-\frac{\bar{u}_o}{a} + \frac{1}{4}\left(\frac{\pi}{\lambda}\right)^2\left(w_s^{(i)^2} + w_c^{(i)^2} + 2w_{o_s}w_s^{(i)} + 2w_{o_c}w_c^{(i)}\right)\right]\right\}$$

$$u_s^{(i)\prime} = \frac{2\pi}{\lambda}v_c^{(i)} - \frac{1}{2}\left(\frac{\pi}{\lambda}\right)\left(w_s^{(i)}\beta_s^{(i)} - w_c^{(i)}\beta_c^{(i)} + \beta_s^{(i)}w_{o_s} - \beta_c^{(i)}w_{o_c} + w_s^{(i)}w_{o_s}' - w_c^{(i)}w_{o_c}'\right) +$$

$$(A_{66}^{(i)} - \frac{A_{26}^{(i)2}}{A_{22}^{(i)}})^{-1}\{N_{xys}^{(i)} - \frac{A_{26}^{(i)}}{A_{22}^{(i)}} N_{ys}^{(i)} -$$

$$(A_{16}^{(i)} - \frac{A_{26}^{(i)}A_{12}^{(i)}}{A_{22}^{(i)}})[-(\frac{2\pi}{\lambda})u_c^{(i)} - \frac{1}{2}(\frac{\pi}{\lambda})^2(w_s^{(i)}w_c^{(i)}$$

$$+ w_s^{(i)}w_{oc} + w_c^{(i)}w_{os})]\}$$

$$u_c^{(i)'} = -\frac{2\pi}{\lambda} v_s^{(i)} - \frac{1}{2}(\frac{\pi}{\lambda})(w_s^{(i)}\beta_c^{(i)} + \beta_s^{(i)}w_c^{(i)} + w_{os}\beta_c^{(i)}$$

$$+ w_{oc}\beta_s^{(i)} + w_{oc}'w_s^{(i)} + w_{os}'w_c^{(i)}) +$$

$$(A_{66}^{(i)} - \frac{A_{26}^{(i)2}}{A_{22}^{(i)}})^{-1}\{N_{xyc}^{(i)} - \frac{A_{26}^{(i)}}{A_{22}^{(i)}} N_{yc}^{(i)} -$$

$$(A_{16}^{(i)} - \frac{A_{26}^{(i)}A_{12}^{(i)}}{A_{22}^{(i)}})[\frac{2\pi}{\lambda} u_s^{(i)} + \frac{1}{4}(\frac{\pi}{\lambda})^2(w_s^{(i)2} - w_c^{(i)2}$$

$$+ 2w_{os}w_s^{(i)} - 2w_{oc}w_c^{(i)})]\}$$

$$v_o^{(i)'} = -\frac{1}{4}(\beta_s^{(i)2} + \beta_c^{(i)2} + 2w_{os}'\beta_s^{(i)} + 2w_{oc}'\beta_c^{(i)})$$

$$(A_{22}^{(i)} - \frac{A_{26}^{(i)2}}{A_{66}^{(i)}})^{-1}\{N_{yo}^{(i)} - \frac{A_{26}^{(i)}}{A_{66}^{(i)}} N_{xyo}^{(i)} -$$

$$(A_{12}^{(i)} - \frac{A_{26}^{(i)}A_{16}^{(i)}}{A_{66}^{(i)}})[-\frac{\bar{u}_o}{a} + \frac{1}{4}(\frac{\pi}{\lambda})^2(w_s^{(i)2} + w_c^{(i)2}$$

$$+ 2w_{os}w_s^{(i)} + 2w_{oc}w_c^{(i)})]\}$$

$$v_s^{(i)'} = -\frac{1}{2}(\beta_s^{(i)}\beta_c^{(i)} + \beta_s^{(i)}w_{oc}' + \beta_c^{(i)}w_{os}') +$$

$$(A_{22}^{(i)} - \frac{A_{26}^{(i)^2}}{A_{66}^{(i)}})^{-1}\{N_{ys}^{(i)} - \frac{A_{26}^{(i)}}{A_{66}^{(i)}}N_{xys}^{(i)} -$$

$$(A_{12}^{(i)} - \frac{A_{26}^{(i)}A_{16}^{(i)}}{A_{66}^{(i)}})[-(\frac{2\pi}{\lambda})u_c^{(i)} - \frac{1}{2}(\frac{\pi}{\lambda})^2(w_s^{(i)}w_c^{(i)}$$

$$+ w_s^{(i)}w_{oc} + w_c^{(i)}w_{os})]\}$$

$$v_c^{(i)'} = \frac{1}{4}(\beta_s^{(i)^2} - \beta_c^{(i)^2} + 2w_{os}'\beta_s^{(i)} - 2w_{oc}'\beta_c^{(i)}) +$$

$$(A_{22}^{(i)} - \frac{A_{26}^{(i)^2}}{A_{66}^{(i)}})^{-1}\{N_{yc}^{(i)} - \frac{A_{26}^{(i)}}{A_{66}^{(i)}}N_{xyc}^{(i)} -$$

$$(A_{12}^{(i)} - \frac{A_{26}^{(i)}A_{16}^{(i)}}{A_{66}^{(i)}})[\frac{2\pi}{\lambda}u_s^{(i)} + \frac{1}{4}(\frac{\pi}{\lambda})^2(w_s^{(i)^2} - w_c^{(i)^2}$$

$$+ 2w_{os}w_s^{(i)} - 2w_{oc}w_c^{(i)})]\}$$

$$w_s^{(i)'} = \beta_s^{(i)}$$

$$w_c^{(i)'} = \beta_c^{(i)}$$

$$\beta_s^{(i)'} = \frac{1}{D_{22}^{(i)}}[D_{12}^{(i)}(\frac{\pi}{\lambda})^2 w_s^{(i)} + 2D_{26}^{(i)}(\frac{\pi}{\lambda})\beta_c^{(i)} - M_{ys}^{(i)}]$$

$$\beta_c^{(i)'} = \frac{1}{D_{22}^{(i)}}[D_{12}^{(i)}(\frac{\pi}{\lambda})^2 w_c^{(i)} - 2D_{26}^{(i)}(\frac{\pi}{\lambda})\beta_s^{(i)} - M_{yc}^{(i)}]$$

$$N_{y_o}^{(i)'} = 0$$

$$N_{ys}^{(i)'} = (\frac{2\pi}{\lambda})\, N_{xyc}^{(i)}$$

$$N_{yc}^{(i)'} = -(\frac{2\pi}{\lambda})\, N_{xys}^{(i)}$$

$$N_{xy_o}^{(i)'} = 0$$

$$N_{xys}^{(i)'} = (A_{11}^{(i)} - \frac{A_{12}^{(i)^2} A_{66}^{(i)} + A_{16}^{(i)^2} A_{22}^{(i)} - 2A_{12}^{(i)} A_{16}^{(i)} A_{26}^{(i)}}{A_{22}^{(i)} A_{66}^{(i)} - A_{26}^{(i)^2}}) *$$

$$(\frac{2\pi}{\lambda})[\frac{2\pi}{\lambda}\, u_s^{(i)} + \frac{1}{4}(\frac{\pi}{\lambda})^2 (w_s^{(i)^2} - w_c^{(i)^2} + 2w_{o_s} w_s^{(i)}$$

$$- 2w_{o_c} w_c^{(i)})] + (\frac{2\pi}{\lambda})[(\frac{A_{12}^{(i)} A_{66}^{(i)} - A_{16}^{(i)} A_{26}^{(i)}}{A_{22}^{(i)} A_{66}^{(i)} - A_{26}^{(i)^2}}) N_{yc}^{(i)} +$$

$$(\frac{A_{16}^{(i)} A_{22}^{(i)} - A_{12}^{(i)} A_{26}^{(i)}}{A_{22}^{(i)} A_{66}^{(i)} - A_{26}^{(i)^2}}) N_{xyc}^{(i)}]$$

$$N_{xyc}^{(i)'} = -(A_{11}^{(i)} - \frac{A_{12}^{(i)^2} A_{66}^{(i)} + A_{16}^{(i)^2} A_{22}^{(i)} - 2A_{12}^{(i)} A_{16}^{(i)} A_{26}^{(i)}}{A_{22}^{(i)} A_{66}^{(i)} - A_{26}^{(i)^2}}) *$$

$$(\frac{2\pi}{\lambda})[-(\frac{2\pi}{\lambda}) u_c^{(i)} - \frac{1}{2}(\frac{\pi}{\lambda})^2 (w_s^{(i)} w_c^{(i)} + w_s^{(i)} w_{o_c} +$$

$$w_c^{(i)} w_{os})] - (\frac{2\pi}{\lambda})[(\frac{A_{12}^{(i)}A_{66}^{(i)} - A_{16}^{(i)}A_{26}^{(i)}}{A_{22}^{(i)}A_{66}^{(i)} - A_{26}^{(i)2}})N_{ys}^{(i)} +$$

$$(\frac{A_{16}^{(i)}A_{22}^{(i)} - A_{12}^{(i)}A_{26}^{(i)}}{A_{22}^{(i)}A_{66}^{(i)} - A_{26}^{(i)2}})N_{xys}^{(i)}]$$

$$M_{ys}^{(i)'} = -V_{ys}^{(i)} + (\frac{2\pi}{\lambda})[(\frac{\pi}{\lambda})^2(D_{16}^{(i)} - \frac{D_{12}^{(i)}D_{26}^{(i)}}{D_{22}^{(i)}})w_c^{(i)} -$$

$$2(\frac{\pi}{\lambda})(D_{66}^{(i)} - \frac{D_{26}^{(i)2}}{D_{22}^{(i)}})\beta_s^{(i)} + \frac{D_{26}^{(i)}}{D_{22}^{(i)}} M_{yc}^{(i)}] -$$

$$(N_{y^o}^{(i)} - \frac{1}{2} N_{yc}^{(i)})(\beta_s^{(i)} + w_{os}') - \frac{1}{2} N_{ys}^{(i)}(\beta_c^{(i)} + w_{oc}')$$

$$+ (\frac{\pi}{\lambda})[(N_{xy^o}^{(i)} - \frac{1}{2} N_{xyc}^{(i)})(w_c^{(i)} + w_{oc}) -$$

$$\frac{1}{2} N_{xys}^{(i)}(w_s^{(i)} + w_{os})]$$

$$M_{yc}^{(i)'} = -V_{yc}^{(i)} + (\frac{2\pi}{\lambda})[(\frac{\pi}{\lambda})^2(D_{16}^{(i)} - \frac{D_{12}^{(i)}D_{26}^{(i)}}{D_{22}^{(i)}})w_s^{(i)} +$$

$$2(\frac{\pi}{\lambda})(D_{66}^{(i)} - \frac{D_{26}^{(i)2}}{D_{22}^{(i)}})\beta_c^{(i)} + \frac{D_{26}^{(i)}}{D_{22}^{(i)}} M_{ys}^{(i)}] -$$

$$(N_{y^o}^{(i)} + \frac{1}{2} N_{yc}^{(i)})(\beta_c^{(i)} + w_{oc}') - \frac{1}{2} N_{ys}^{(i)}(\beta_s^{(i)} + w_{os}')$$

$$- (\frac{\pi}{\lambda})[(N_{xy^o}^{(i)} + \frac{1}{2} N_{xyc}^{(i)})(w_s^{(i)} + w_{os}) -$$

$$\frac{1}{2} N_{xys}^{(i)}(w_c^{(i)} + w_{oc})] \qquad (2.100)$$

for i = 1

$$V_{ys}^{(1)'} = -(\frac{\pi}{\lambda})^2[\frac{D_{12}^{(1)}}{D_{22}^{(1)}} M_{ys}^{(1)} + 2(\frac{\pi}{\lambda})(D_{16}^{(1)} - \frac{D_{12}^{(1)}D_{26}^{(1)}}{D_{22}^{(1)}})\beta_c^{(1)}$$

$$+ (D_{11}^{(1)} - \frac{D_{12}^{(1)2}}{D_{22}^{(1)}})(\frac{\pi}{\lambda})^2 w_s^{(1)}] - (\frac{\pi}{\lambda})^2(w_s^{(1)} + w_{os}) *$$

$$\{(A_{11}^{(1)} - \frac{A_{12}^{(1)2}A_{66}^{(1)} + A_{16}^{(1)2}A_{22}^{(1)} - 2A_{12}^{(1)}A_{16}^{(1)}A_{26}^{(1)}}{A_{22}^{(1)}A_{66}^{(1)} - A_{26}^{(1)2}}) *$$

$$[-\frac{\bar{u}_o}{a} + (\frac{\pi}{\lambda})u_s^{(1)} + \frac{1}{8}(\frac{\pi}{\lambda})^2(3w_s^{(1)2} + w_c^{(1)2} +$$

$$6w_s^{(1)}w_{os} + 2w_c^{(1)}w_{oc})] + (\frac{A_{12}^{(1)}A_{66}^{(1)} - A_{16}^{(1)}A_{26}^{(1)}}{A_{22}^{(1)}A_{66}^{(1)} - A_{26}^{(1)2}}) *$$

$$(N_{yo}^{(1)} + \frac{1}{2} N_{yc}^{(1)}) + (\frac{A_{16}^{(1)}A_{22}^{(1)} - A_{12}^{(1)}A_{26}^{(1)}}{A_{22}^{(1)}A_{66}^{(1)} - A_{26}^{(1)2}})(N_{xyo}^{(1)} +$$

$$\frac{1}{2} N_{xyc}^{(1)})\} + \frac{1}{2}(\frac{\pi}{\lambda})^2(w_c^{(1)} + w_{oc}) *$$

$$\{(A_{11}^{(1)} - \frac{A_{12}^{(1)2}A_{66}^{(1)} + A_{16}^{(1)2}A_{22}^{(1)} - 2A_{12}^{(1)}A_{16}^{(1)}A_{26}^{(1)}}{A_{22}^{(1)}A_{66}^{(1)} - A_{26}^{(1)2}}) *$$

$$[-(\frac{2\pi}{\lambda})u_c^{(1)} - \frac{1}{2}(\frac{\pi}{\lambda})^2(w_s^{(1)}w_c^{(1)} + w_s^{(1)}w_{oc} +$$

$$w_c^{(1)}w_{os})] + (\frac{A_{12}^{(1)}A_{66}^{(1)} - A_{16}^{(1)}A_{26}^{(1)}}{A_{22}^{(1)}A_{66}^{(1)} - A_{26}^{(1)^2}})N_{ys}^{(1)} +$$

$$(\frac{A_{16}^{(1)}A_{22}^{(1)} - A_{12}^{(1)}A_{26}^{(1)}}{A_{22}^{(1)}A_{66}^{(1)} - A_{26}^{(1)^2}})N_{xys}^{(1)}\} - (\frac{\pi}{\lambda})[(N_{xyo}^{(1)} +$$

$$\frac{1}{2}N_{xyc}^{(1)})(\beta_c^{(1)} + w_{oc}') + \frac{1}{2}N_{xys}^{(1)}(\beta_s^{(1)} + w_{os}')] -$$

$$G_1^*[\frac{M_{ys}^{(1)}}{D_{22}^{(1)}} - 2\frac{D_{26}^{(1)}}{D_{22}^{(1)}}\beta_c^{(1)} + (1 - \frac{D_{12}^{(1)}}{D_{22}^{(1)}})(\frac{\pi}{\lambda})^2 w_s^{(1)}]$$

$$- G_2^*[\frac{M_{ys}^{(2)}}{D_{22}^{(1)}} - 2\frac{D_{26}^{(2)}}{D_{22}^{(2)}}\beta_c^{(2)} + (1 - \frac{D_{12}^{(2)}}{D_{22}^{(2)}})(\frac{\pi}{\lambda})^2 w_s^{(2)}]$$

$$- E^*(w_s^{(1)} - w_s^{(2)})$$

$$V_{yc}^{(1)'} = -(\frac{\pi}{\lambda})^2[\frac{D_{12}^{(1)}}{D_{22}^{(1)}}M_{yc}^{(1)} - 2(\frac{\pi}{\lambda})(D_{16}^{(1)} - \frac{D_{12}^{(1)}D_{26}^{(1)}}{D_{22}^{(1)}})\beta_s^{(1)}$$

$$+ (D_{11}^{(1)} - \frac{D_{12}^{(1)^2}}{D_{22}^{(1)}})(\frac{\pi}{\lambda})^2 w_c^{(1)}] - (\frac{\pi}{\lambda})^2(w_c^{(1)} + w_{oc}) *$$

$$\{(A_{11}^{(1)} - \frac{A_{12}^{(1)^2}A_{66}^{(1)} + A_{16}^{(1)^2}A_{22}^{(1)} - 2A_{12}^{(1)}A_{16}^{(1)}A_{26}^{(1)}}{A_{22}^{(1)}A_{66}^{(1)} - A_{26}^{(1)^2}}) *$$

$$[-\frac{\bar{u}_o}{a} - (\frac{\pi}{\lambda})u_s^{(1)} + \frac{1}{8}(\frac{\pi}{\lambda})^2(w_s^{(1)^2} + 3w_c^{(1)^2} +$$

$$2w_s^{(1)}w_{os} + 6w_c^{(1)}w_{oc})] + \left(\frac{A_{12}^{(1)}A_{66}^{(1)} - A_{16}^{(1)}A_{26}^{(1)}}{A_{22}^{(1)}A_{66}^{(1)} - A_{26}^{(1)2}}\right) *$$

$$(N_{yo}^{(1)} - \frac{1}{2}N_{yc}^{(1)}) + \left(\frac{A_{16}^{(1)}A_{22}^{(1)} - A_{12}^{(1)}A_{26}^{(1)}}{A_{22}^{(1)}A_{66}^{(1)} - A_{26}^{(1)2}}\right)(N_{xyo}^{(1)} -$$

$$\frac{1}{2}N_{xyc}^{(1)})\} + \frac{1}{2}\left(\frac{\pi}{\lambda}\right)^2(w_s^{(1)} + w_{os}) *$$

$$\{(A_{11}^{(1)} - \frac{A_{12}^{(1)2}A_{66}^{(1)} + A_{16}^{(1)2}A_{22}^{(1)} - 2A_{12}^{(1)}A_{16}^{(1)}A_{26}^{(1)}}{A_{22}^{(1)}A_{66}^{(1)} - A_{26}^{(1)2}}) *$$

$$[-\left(\frac{2\pi}{\lambda}\right)u_c^{(1)} - \frac{1}{2}\left(\frac{\pi}{\lambda}\right)^2(w_s^{(1)}w_c^{(1)} + w_s^{(1)}w_{oc} +$$

$$w_c^{(1)}w_{os})] + \left(\frac{A_{12}^{(1)}A_{66}^{(1)} - A_{16}^{(1)}A_{26}^{(1)}}{A_{22}^{(1)}A_{66}^{(1)} - A_{26}^{(1)2}}\right)N_{ys}^{(1)} +$$

$$\left(\frac{A_{16}^{(1)}A_{22}^{(1)} - A_{12}^{(1)}A_{26}^{(1)}}{A_{22}^{(1)}A_{66}^{(1)} - A_{26}^{(1)2}}\right)N_{xys}^{(1)}\} + \left(\frac{\pi}{\lambda}\right)[(N_{xyo}^{(1)} -$$

$$\frac{1}{2}N_{xyc}^{(1)})(\beta_s^{(1)} + w'_{os}) + \frac{1}{2}N_{xys}^{(1)}(\beta_c^{(1)} + w'_{oc})] -$$

$$G_1^*\left[\frac{M_{yc}^{(1)}}{D_{22}^{(1)}} + 2\frac{D_{26}^{(1)}}{D_{22}^{(1)}}\beta_s^{(1)} + \left(1 - \frac{D_{12}^{(1)}}{D_{22}^{(1)}}\right)\left(\frac{\pi}{\lambda}\right)^2 w_c^{(1)}\right]$$

$$- G_2^*\left[\frac{M_{yc}^{(2)}}{D_{22}^{(1)}} + 2\frac{D_{26}^{(2)}}{D_{22}^{(2)}}\beta_s^{(2)} + \left(1 - \frac{D_{12}^{(2)}}{D_{22}^{(2)}}\right)\left(\frac{\pi}{\lambda}\right)^2 w_c^{(2)}\right]$$

$$- E^*(w_c^{(1)} - w_c^{(2)}) \qquad (2.101)$$

for i = 2, 3, ..., N-1

$$V_{ys}^{(i)'} = -(\frac{\pi}{\lambda})^2[\frac{D_{12}^{(i)}}{D_{22}^{(i)}} M_{ys}^{(i)} + 2(\frac{\pi}{\lambda})(D_{16}^{(i)} - \frac{D_{12}^{(i)}D_{26}^{(i)}}{D_{22}^{(i)}})\beta_c^{(i)}$$

$$+ (D_{11}^{(i)} - \frac{D_{12}^{(i)^2}}{D_{22}^{(i)}})(\frac{\pi}{\lambda})^2 w_s^{(i)}] - (\frac{\pi}{\lambda})^2(w_s^{(i)} + w_{os}) *$$

$$\{(A_{11}^{(i)} - \frac{A_{12}^{(i)^2}A_{66}^{(i)} + A_{16}^{(i)^2}A_{22}^{(i)} - 2A_{12}^{(i)}A_{16}^{(i)}A_{26}^{(i)}}{A_{22}^{(i)}A_{66}^{(i)} - A_{26}^{(i)^2}}) *$$

$$[-\frac{\bar{u}_o}{a} + (\frac{\pi}{\lambda})u_s^{(i)} + \frac{1}{8}(\frac{\pi}{\lambda})^2(3w_s^{(i)^2} + w_c^{(i)^2} +$$

$$6w_s^{(i)}w_{os} + 2w_c^{(i)}w_{oc})] + (\frac{A_{12}^{(i)}A_{66}^{(i)} - A_{16}^{(i)}A_{26}^{(i)}}{A_{22}^{(i)}A_{66}^{(i)} - A_{26}^{(i)^2}}) *$$

$$(N_{yo}^{(i)} + \frac{1}{2} N_{yc}^{(i)}) + (\frac{A_{16}^{(i)}A_{22}^{(i)} - A_{12}^{(i)}A_{26}^{(i)}}{A_{22}^{(i)}A_{66}^{(i)} - A_{26}^{(i)^2}})(N_{xyo}^{(i)} +$$

$$\frac{1}{2} N_{xyc}^{(i)})\} + \frac{1}{2}(\frac{\pi}{\lambda})^2(w_c^{(i)} + w_{oc}) *$$

$$\{(A_{11}^{(i)} - \frac{A_{12}^{(i)^2}A_{66}^{(i)} + A_{16}^{(i)^2}A_{22}^{(i)} - 2A_{12}^{(i)}A_{16}^{(i)}A_{26}^{(i)}}{A_{22}^{(i)}A_{66}^{(i)} - A_{26}^{(i)^2}}) *$$

$$[-(\frac{2\pi}{\lambda})u_c^{(i)} - \frac{1}{2}(\frac{\pi}{\lambda})^2(w_s^{(i)}w_c^{(i)} + w_s^{(i)}w_{oc} +$$

$$w_c^{(i)} w_{os})] + \left(\frac{A_{12}^{(i)}A_{66}^{(i)} - A_{16}^{(i)}A_{26}^{(i)}}{A_{22}^{(i)}A_{66}^{(i)} - A_{26}^{(i)2}}\right)N_{ys}^{(i)} +$$

$$\left(\frac{A_{16}^{(i)}A_{22}^{(i)} - A_{12}^{(i)}A_{26}^{(i)}}{A_{22}^{(i)}A_{66}^{(i)} - A_{26}^{(i)2}}\right)N_{xys}^{(i)}\} - \left(\frac{\pi}{\lambda}\right)[(N_{xyo}^{(i)} +$$

$$\frac{1}{2} N_{xyc}^{(i)})(\beta_c^{(i)} + w'_{oc}) + \frac{1}{2} N_{xys}^{(i)}(\beta_s^{(i)} + w'_{os})] -$$

$$2G_1^*\left[\frac{M_{ys}^{(i)}}{D_{22}^{(i)}} - 2\frac{D_{26}^{(i)}}{D_{22}^{(i)}}\beta_c^{(i)} + \left(1 - \frac{D_{12}^{(i)}}{D_{22}^{(i)}}\right)\left(\frac{\pi}{\lambda}\right)^2 w_s^{(i)}\right]$$

$$- G_2^*\left[\frac{M_{ys}^{(i-1)}}{D_{22}^{(i-1)}} - 2\frac{D_{26}^{(i-1)}}{D_{22}^{(i-1)}}\beta_c^{(i-1)} +\right.$$

$$\left(1 - \frac{D_{12}^{(i-1)}}{D_{22}^{(i-1)}}\right)\left(\frac{\pi}{\lambda}\right)^2 w_s^{(i-1)} + \frac{M_{ys}^{(i+1)}}{D_{22}^{(i+1)}} -$$

$$\left.2\frac{D_{26}^{(i+1)}}{D_{22}^{(i+1)}}\beta_c^{(i+1)} + \left(1 - \frac{D_{12}^{(i+1)}}{D_{22}^{(i+1)}}\right)\left(\frac{\pi}{\lambda}\right)^2 w_s^{(i+1)}\right]$$

$$- E^*(2w_s^{(i)} - w_s^{(i-1)} - w_s^{(i+1)})$$

$$V_{yc}^{(i)'} = -\left(\frac{\pi}{\lambda}\right)^2\left[\frac{D_{12}^{(i)}}{D_{22}^{(i)}} M_{yc}^{(i)} - 2\left(\frac{\pi}{\lambda}\right)\left(D_{16}^{(i)} - \frac{D_{12}^{(i)}D_{26}^{(i)}}{D_{22}^{(i)}}\right)\beta_s^{(i)}\right.$$

$$\left. + \left(D_{11}^{(i)} - \frac{D_{12}^{(i)2}}{D_{22}^{(i)}}\right)\left(\frac{\pi}{\lambda}\right)^2 w_c^{(i)}\right] - \left(\frac{\pi}{\lambda}\right)^2(w_c^{(i)} + w_{oc}) *$$

$$\{(A_{11}^{(i)} - \frac{A_{12}^{(i)2}A_{66}^{(i)} + A_{16}^{(i)2}A_{22}^{(i)} - 2A_{12}^{(i)}A_{16}^{(i)}A_{26}^{(i)}}{A_{22}^{(i)}A_{66}^{(i)} - A_{26}^{(i)2}}) *$$

$$[-\frac{\bar{u}_o}{a} - (\frac{\pi}{\lambda})u_s^{(i)} + \frac{1}{8}(\frac{\pi}{\lambda})^2(w_s^{(i)2} + 3w_c^{(i)2} +$$

$$2w_s^{(i)}w_{os} + 6w_c^{(i)}w_{oc})] + (\frac{A_{12}^{(i)}A_{66}^{(i)} - A_{16}^{(i)}A_{26}^{(i)}}{A_{22}^{(i)}A_{66}^{(i)} - A_{26}^{(i)2}}) *$$

$$(N_{yo}^{(i)} - \frac{1}{2}N_{yc}^{(i)}) + (\frac{A_{16}^{(i)}A_{22}^{(i)} - A_{12}^{(i)}A_{26}^{(i)}}{A_{22}^{(i)}A_{66}^{(i)} - A_{26}^{(i)2}})(N_{xyo}^{(i)} -$$

$$\frac{1}{2}N_{xyc}^{(i)})\} + \frac{1}{2}(\frac{\pi}{\lambda})^2(w_s^{(i)} + w_{os}) *$$

$$\{(A_{11}^{(i)} - \frac{A_{12}^{(i)2}A_{66}^{(i)} + A_{16}^{(i)2}A_{22}^{(i)} - 2A_{12}^{(i)}A_{16}^{(i)}A_{26}^{(i)}}{A_{22}^{(i)}A_{66}^{(i)} - A_{26}^{(i)2}}) *$$

$$[-(\frac{2\pi}{\lambda})u_c^{(i)} - \frac{1}{2}(\frac{\pi}{\lambda})^2(w_s^{(i)}w_c^{(i)} + w_s^{(i)}w_{oc} +$$

$$w_c^{(i)}w_{os})] + (\frac{A_{12}^{(i)}A_{66}^{(i)} - A_{16}^{(i)}A_{26}^{(i)}}{A_{22}^{(i)}A_{66}^{(i)} - A_{26}^{(i)2}})N_{ys}^{(i)} +$$

$$(\frac{A_{16}^{(i)}A_{22}^{(i)} - A_{12}^{(i)}A_{26}^{(i)}}{A_{22}^{(i)}A_{66}^{(i)} - A_{26}^{(i)2}})N_{xys}^{(i)}\} + (\frac{\pi}{\lambda})[(N_{xyo}^{(i)} -$$

$$\frac{1}{2}N_{xyc}^{(i)})(\beta_s^{(i)} + w'_{os}) + \frac{1}{2}N_{xys}^{(i)}(\beta_c^{(i)} + w'_{oc})] -$$

$$2G_1^*\left[\frac{M_{yc}^{(i)}}{D_{22}^{(i)}} + 2\frac{D_{26}^{(i)}}{D_{22}^{(i)}}\beta_s^{(i)} + \left(1 - \frac{D_{12}^{(i)}}{D_{22}^{(i)}}\right)\left(\frac{\pi}{\lambda}\right)^2 w_c^{(i)}\right]$$

$$- G_2^*\left[\frac{M_{yc}^{(i-1)}}{D_{22}^{(i-1)}} + 2\frac{D_{26}^{(i-1)}}{D_{22}^{(i-1)}}\beta_s^{(i-1)} +\right.$$

$$\left(1 - \frac{D_{12}^{(i-1)}}{D_{22}^{(i-1)}}\right)\left(\frac{\pi}{\lambda}\right)^2 w_c^{(i-1)} + \frac{M_{yc}^{(i+1)}}{D_{22}^{(i+1)}} +$$

$$\left.2\frac{D_{26}^{(i+1)}}{D_{22}^{(i+1)}}\beta_s^{(i+1)} + \left(1 - \frac{D_{12}^{(i+1)}}{D_{22}^{(i+1)}}\right)\left(\frac{\pi}{\lambda}\right)^2 w_c^{(i+1)}\right]$$

$$- E^*\left(2w_c^{(i)} - w_c^{(i-1)} - w_c^{(i+1)}\right) \qquad (2.102)$$

<u>for i = N</u>

$$V_{ys}^{(N)'} = -\left(\frac{\pi}{\lambda}\right)^2\left[\frac{D_{12}^{(N)}}{D_{22}^{(N)}} M_{ys}^{(N)} + 2\left(\frac{\pi}{\lambda}\right)\left(D_{16}^{(N)} - \frac{D_{12}^{(N)} D_{26}^{(N)}}{D_{22}^{(N)}}\right)\beta_c^{(N)}\right.$$

$$\left. + \left(D_{11}^{(N)} - \frac{D_{12}^{(N)^2}}{D_{22}^{(N)}}\right)\left(\frac{\pi}{\lambda}\right)^2 w_s^{(N)}\right] - \left(\frac{\pi}{\lambda}\right)^2\left(w_s^{(N)} + w_{os}\right) *$$

$$\left\{\left(A_{11}^{(N)} - \frac{A_{12}^{(N)^2} A_{66}^{(N)} + A_{16}^{(N)^2} A_{22}^{(N)} - 2A_{12}^{(N)} A_{16}^{(N)} A_{26}^{(N)}}{A_{22}^{(N)} A_{66}^{(N)} - A_{26}^{(N)^2}}\right) *\right.$$

$$\left[-\frac{u_o}{a} + \left(\frac{\pi}{\lambda}\right) u_s^{(N)} + \frac{1}{8}\left(\frac{\pi}{\lambda}\right)^2 \left(3w_s^{(N)^2} + w_c^{(N)^2} +\right.\right.$$

$$6w_s^{(N)}w_{o_s} + 2w_c^{(N)}w_{o_c})] + \left(\frac{A_{12}^{(N)}A_{66}^{(N)} - A_{16}^{(N)}A_{26}^{(N)}}{A_{22}^{(N)}A_{66}^{(N)} - A_{26}^{(N)^2}}\right) *$$

$$(N_{y^o}^{(N)} + \frac{1}{2}N_{yc}^{(N)}) + \left(\frac{A_{16}^{(N)}A_{22}^{(N)} - A_{12}^{(N)}A_{26}^{(N)}}{A_{22}^{(N)}A_{66}^{(N)} - A_{26}^{(N)^2}}\right)(N_{xy^o}^{(N)} +$$

$$\frac{1}{2}N_{xyc}^{(N)})\} + \frac{1}{2}\left(\frac{\pi}{\lambda}\right)^2(w_c^{(N)} + w_{o_c}) *$$

$$\{(A_{11}^{(N)} - \frac{A_{12}^{(N)^2}A_{66}^{(N)} + A_{16}^{(N)^2}A_{22}^{(N)} - 2A_{12}^{(N)}A_{16}^{(N)}A_{26}^{(N)}}{A_{22}^{(N)}A_{66}^{(N)} - A_{26}^{(N)^2}}) *$$

$$[-\left(\frac{2\pi}{\lambda}\right)u_c^{(N)} - \frac{1}{2}\left(\frac{\pi}{\lambda}\right)^2(w_s^{(N)}w_c^{(N)} + w_s^{(N)}w_{o_c} +$$

$$w_c^{(N)}w_{o_s})] + \left(\frac{A_{12}^{(N)}A_{66}^{(N)} - A_{16}^{(N)}A_{26}^{(N)}}{A_{22}^{(N)}A_{66}^{(N)} - A_{26}^{(N)^2}}\right)N_{ys}^{(N)} +$$

$$\left(\frac{A_{16}^{(N)}A_{22}^{(N)} - A_{12}^{(N)}A_{26}^{(N)}}{A_{22}^{(N)}A_{66}^{(N)} - A_{26}^{(N)^2}}\right)N_{xys}^{(N)}\} - \left(\frac{\pi}{\lambda}\right)[(N_{xy^o}^{(N)} +$$

$$\frac{1}{2}N_{xyc}^{(N)})(\beta_c^{(N)} + w'_{o_c}) + \frac{1}{2}N_{xys}^{(N)}(\beta_s^{(N)} + w'_{o_s})] -$$

$$G_1^*\left[\frac{M_{ys}^{(N)}}{D_{22}^{(N)}} - 2\frac{D_{26}^{(N)}}{D_{22}^{(N)}}\beta_c^{(N)} + \left(1 - \frac{D_{12}^{(N)}}{D_{22}^{(N)}}\right)\left(\frac{\pi}{\lambda}\right)^2 w_s^{(N)}\right]$$

$$- G_2^*\left[\frac{M_{ys}^{(N-1)}}{D_{22}^{(N-1)}} - 2\frac{D_{26}^{(N-1)}}{D_{22}^{(N-1)}}\beta_c^{(N-1)} + (1 -\right.$$

$$\frac{D_{12}^{(N-1)}}{D_{22}^{(N-1)}})(\frac{\pi}{\lambda})^2 w_s^{(N-1)}] - E^*(w_s^{(N)} - w_s^{(N-1)})$$

$$V_{yc}^{(N)'} = -(\frac{\pi}{\lambda})^2[\frac{D_{12}^{(N)}}{D_{22}^{(N)}} M_{yc}^{(N)} + 2(\frac{\pi}{\lambda})(D_{16}^{(N)} - \frac{D_{12}^{(N)} D_{26}^{(N)}}{D_{22}^{(N)}})\beta_s^{(N)}$$

$$+ (D_{11}^{(N)} - \frac{D_{12}^{(N)^2}}{D_{22}^{(N)}})(\frac{\pi}{\lambda})^2 w_c^{(N)}] - (\frac{\pi}{\lambda})^2(w_c^{(N)} + w_{oc}) *$$

$$\{(A_{11}^{(N)} - \frac{A_{12}^{(N)^2} A_{66}^{(N)} + A_{16}^{(N)^2} A_{22}^{(N)} - 2A_{12}^{(N)} A_{16}^{(N)} A_{26}^{(N)}}{A_{22}^{(N)} A_{66}^{(N)} - A_{26}^{(N)^2}}) *$$

$$[-\frac{\bar{u}_o}{a} - (\frac{\pi}{\lambda})u_s^{(N)} + \frac{1}{8}(\frac{\pi}{\lambda})^2(w_s^{(N)^2} + 3w_c^{(N)^2} +$$

$$2w_s^{(N)} w_{os} + 6w_c^{(N)} w_{oc})] + (\frac{A_{12}^{(N)} A_{66}^{(N)} - A_{16}^{(N)} A_{26}^{(N)}}{A_{22}^{(N)} A_{66}^{(N)} - A_{26}^{(N)^2}}) *$$

$$(N_{yo}^{(N)} - \frac{1}{2} N_{yc}^{(N)}) + (\frac{A_{16}^{(N)} A_{22}^{(N)} - A_{12}^{(N)} A_{26}^{(N)}}{A_{22}^{(N)} A_{66}^{(N)} - A_{26}^{(N)^2}})(N_{xyo}^{(N)} -$$

$$\frac{1}{2} N_{xyc}^{(N)})\} + \frac{1}{2}(\frac{\pi}{\lambda})^2(w_s^{(N)} + w_{os}) *$$

$$\{(A_{11}^{(N)} - \frac{A_{12}^{(N)^2} A_{66}^{(N)} + A_{16}^{(N)^2} A_{22}^{(N)} - 2A_{12}^{(N)} A_{16}^{(N)} A_{26}^{(N)}}{A_{22}^{(N)} A_{66}^{(N)} - A_{26}^{(N)^2}}) *$$

$$[-(\frac{2\pi}{\lambda})u_c^{(N)} - \frac{1}{2}(\frac{\pi}{\lambda})^2(w_s^{(N)} w_c^{(N)} + w_s^{(N)} w_{oc} +$$

$$w_c^{(N)} w_{os})] + \left(\frac{A_{12}^{(N)} A_{66}^{(N)} - A_{16}^{(N)} A_{26}^{(N)}}{A_{22}^{(N)} A_{66}^{(N)} - A_{26}^{(N)2}}\right) N_{ys}^{(N)} +$$

$$\left(\frac{A_{16}^{(N)} A_{22}^{(N)} - A_{12}^{(N)} A_{26}^{(N)}}{A_{22}^{(N)} A_{66}^{(N)} - A_{26}^{(N)2}}\right) N_{xys}^{(N)}\} + \left(\frac{\pi}{\lambda}\right)[(N_{xyo}^{(N)} -$$

$$\frac{1}{2} N_{xyc}^{(N)})(\beta_c^{(N)} + w'_{oc}) + \frac{1}{2} N_{xys}^{(N)}(\beta_c^{(N)} + w'_{oc})] -$$

$$G_1^*\left[\frac{M_{yc}^{(N)}}{D_{22}^{(N)}} + 2\frac{D_{26}^{(N)}}{D_{22}^{(N)}} \beta_s^{(N)} + \left(1 - \frac{D_{12}^{(N)}}{D_{22}^{(N)}}\right)\left(\frac{\pi}{\lambda}\right)^2 w_c^{(N)}\right]$$

$$- G_2^*\left[\frac{M_{yc}^{(N-1)}}{D_{22}^{(N-1)}} + 2\frac{D_{26}^{(N-1)}}{D_{22}^{(N-1)}} \beta_s^{(N-1)} + \left(1 -\right.\right.$$

$$\left.\left.\frac{D_{12}^{(N-1)}}{D_{22}^{(N-1)}}\right)\left(\frac{\pi}{\lambda}\right)^2 w_c^{(N-1)}\right] - E^*(w_c^{(N)} - w_c^{(N-1)}) \qquad (2.103)$$

The functions of y for w_{os} and w_{oc} are expressed as

$$w_{os}(y) = \bar{w}_{os} \sin \frac{\pi y}{b}$$

$$w_{oc}(y) = \bar{w}_{oc} \sin \frac{\pi y}{b} \qquad (2.104)$$

Chapter 3

RESULTS AND DISCUSSION

This chapter presents results from the analytical model described in Chapter 2 Analysis for compression-loaded laminates. Short-wavelength buckling results obtained using the linear analysis are discussed. These results are compared to the results obtained by Rosen [7] for unidirectional $[0]_s$-class laminates. Laminate end shortening and stress data for short-wavelength buckling are presented for several multi-directional laminates. The short-wavelength buckling mode shapes for the laminates are described. Results obtained using the nonlinear analysis also are discussed. Each laminate has laminae with short-wavelength out-of-plane initial imperfections. The nonlinear behavior of a laminate is described using laminate end shortening, compressive load, and maximum w displacement. Shear stress and strain distributions within the laminate are presented.

The last section of this chapter discusses failure prediction for compression-loaded laminates. A failure criterion is described and applied to the analytical results from the present model. The failure mode is predicted for several laminates. Approximate

equations for predicting the compressive failure of 0°-dominated laminates are presented.

All results were obtained using the central scientific computing complex at NASA Langley Research Center. The results of the linear analysis were obtained using Cyber 170 series computers. The analysis of an eight-layer model required a maximum execution time of 1000 seconds. This long execution time is the result of the number of iterations required by the solution algorithm to determine the minimum compressive stress for short-wavelength buckling and the corresponding half-wavelength of the mode shape. The analysis of the eight-layer model required approximately 39,500 decimal memory locations. The results of the nonlinear analysis were obtained using a Cyber 205 vector processing computer. This analysis had a maximum of forty-one finite difference stations. The ratio of the maximum distance between adjacent stations to the plate width was 0.05 when using all forty-one stations. An error tolerance was specified for each unknown in the nonlinear analysis since the results of this analysis are approximate. This specified tolerance was approximately one percent of the maximum calculated value for each unknown. The execution time for a nonlinear analysis for a single load case of a four-layer model with orthotropic fiber-plates was approximately twenty-five seconds. The execution time for a single load case of a eight-layer model with anisotropic fiber-plates was approximately 390 seconds. Ten incremental load cases were used for a typical nonlinear analysis. The analysis of

these four-layer and eight-layer models required approximately 1 X 10^6 memory locations and 4 X 10^6 memory locations, respectively.

3.1 Short-Wavelength Buckling

3.1.1 Comparison with Rosen's Results

Rosen's studies [7] included the short-wavelength buckling of the $[0]_s$-class laminates used in structural applications. These laminates had fiber volume fractions greater than 0.30 and buckled into the shear mode shape shown in figure 1.1. He assumed that the laminates failed when short-wavelength buckling occurred and suggested that the compressive strength for these laminates was proportional to the matrix shear modulus as indicated in equation (1.3). The fiber's elastic properties had a negligible effect on the predicted strength.

The analysis used in this study can be simplified to obtain Rosen's results. All fiber-plates have the same w displacement for the shear mode shape; equation (2.55) becomes

$$\bar{w}_1^{(i)}(x,y) = \bar{w}_s \sin \frac{\pi \bar{x}}{\lambda} \sin \frac{\pi y}{b} \qquad (3.1)$$

where $\bar{w}_s$ is a constant. The characteristic equation for determining the short-wavelength buckling of an N-lamina $[0]_s$-class laminate is obtained from equations (2.56) and is expressed as

$$\left[D_{11}^{(1)}\left(\frac{\pi}{\lambda}\right)^4 + 2\left(D_{12}^{(1)} + 2D_{66}^{(1)}\right)\left(\frac{\pi}{\lambda}\right)^2\left(\frac{\pi}{b}\right)^2 + D_{22}^{(1)}\left(\frac{\pi}{b}\right)^4 + \left(\frac{\bar{u}_o}{a}\right)\left(\frac{A_{12}^T}{A_{22}^T}A_{12}^{(1)} - A_{11}^{(1)}\right)\left(\frac{\pi}{\lambda}\right)^2 + \frac{G_m}{4t_m}\left(t_f + 2t_m\right)^2\left[\left(\frac{\pi}{\lambda}\right)^2 + \left(\frac{\pi}{b}\right)^2\right]\right]^2\left[D_{11}^{(i)}\left(\frac{\pi}{\lambda}\right)^4 + 2\left(D_{12}^{(i)} + 2D_{66}^{(i)}\right)\left(\frac{\pi}{\lambda}\right)^2\left(\frac{\pi}{b}\right)^2 + D_{22}^{(i)}\left(\frac{\pi}{b}\right)^4 + \left(\frac{\bar{u}_o}{a}\right)\left(\frac{A_{12}^T}{A_{22}^T}A_{12}^{(i)} - A_{11}^{(i)}\right)\left(\frac{\pi}{\lambda}\right)^2 + \frac{G_m}{2t_m}\left(t_f + 2t_m\right)^2\left[\left(\frac{\pi}{\lambda}\right)^2 + \left(\frac{\pi}{b}\right)^2\right]\right]^{(N-2)} = 0 \tag{3.2}$$

Equation (3.2) is satisfied if

$$D_{11}^{(i)}\left(\frac{\pi}{\lambda}\right)^4 + 2\left(D_{12}^{(i)} + 2D_{66}^{(i)}\right)\left(\frac{\pi}{\lambda}\right)^2\left(\frac{\pi}{b}\right)^2 + D_{22}^{(i)}\left(\frac{\pi}{b}\right)^4 + \left(\frac{\bar{u}_o}{a}\right)\left(\frac{A_{12}^T}{A_{22}^T}A_{12}^{(i)} - A_{11}^{(i)}\right)\left(\frac{\pi}{\lambda}\right)^2 + \frac{G_m}{2t_m}\left(t_f + 2t_m\right)^2\left[\left(\frac{\pi}{\lambda}\right)^2 + \left(\frac{\pi}{b}\right)^2\right] = 0 \tag{3.3}$$

or if

$$D_{11}^{(1)}\left(\frac{\pi}{\lambda}\right)^4 + 2\left(D_{12}^{(1)} + 2D_{66}^{(1)}\right)\left(\frac{\pi}{\lambda}\right)^2\left(\frac{\pi}{b}\right)^2 + D_{22}^{(1)}\left(\frac{\pi}{b}\right)^4 +$$

$$\left(\frac{\bar{u}_o}{a}\right)\left(\frac{A_{12}^T}{A_{22}^T}A_{12}^{(1)} - A_{11}^{(1)}\right)\left(\frac{\pi}{\lambda}\right)^2 + \frac{G_m}{4t_m}\left(t_f + 2t_m\right)^2\left[\left(\frac{\pi}{\lambda}\right)^2 +\right.$$

$$\left.\left(\frac{\pi}{b}\right)^2\right] = 0 \qquad (3.4)$$

Equation (3.3) determines the critical end shortening for short-wavelength buckling of the ith fiber-plate when i = 2, 3, ..., N-1, i.e., interior fiber-plates. Rosen's analysis considers interior fibers. The bending stiffness terms in equation (3.3) are negligible compared to the loading and matrix-foundation terms, and the critical normalized end shortening is expressed as

$$-\left(\frac{\bar{u}_o}{a}\right)_{cr} = \left(\frac{A_{12}^T}{A_{22}^T}A_{12}^{(i)} - A_{11}^{(i)}\right)^{-1}\left\{\frac{G_m}{2t_m}\left(t_f + 2t_m\right)^2\left[1 + \left(\frac{\lambda}{b}\right)^2\right]\right\} \qquad (3.5)$$

where this negative normalized end shortening corresponds to a compressive strain. The half-wavelength of the buckling mode shape λ is much smaller than the laminate width b so that the $\left(\frac{\lambda}{b}\right)^2$ term in equation (3.5) is negligible. The half-wavelength is discussed in

detail in section 3.1.1 Laminate Mode Shapes. Equations (2.1) and (2.2) for thicknesses and fiber volume fraction are substituted into equation (3.5). The constitutive equation for the ith fiber-plate also is substituted into equation (3.5), and the compressive stress in the ith fiber-plate is

$$\sigma_x^{(i)} = \frac{V_f G_m}{1 - V_f} \tag{3.6}$$

The compressive stress in the composite laminate is

$$\sigma_c = \frac{G_m}{1 - V_f} \tag{3.7}$$

Equation (3.7) is the same as the equation (1.3) obtained by Rosen.

The analysis used in this study both simplifies to Rosen's classic results and provides new results for the short-wavelength buckling of compression-loaded laminates. Equation (3.4) determines the critical end shortening for short-wavelength buckling of the ith fiber-plate when i = 1 or when i = N, i.e., the outer-most fiber-plates in the model. Rosen's analysis does not specifically consider the outer-most fibers. The compressive stress in the composite laminate when the outer laminae buckle in a short-wavelength mode is

derived using the same procedure as used above. This compressive stress is expressed as

$$\sigma_c = \frac{G_m}{2(1 - V_f)} \tag{3.8}$$

Equations (3.7) and (3.8) show the dominant role of the matrix in determining short-wavelength buckling response. The fiber-plates are so thin that their bending stiffnesses are negligible compared to the foundation extensional and shearing stiffnesses of the matrix. The compressive stress for short-wavelength buckling is a function of how the fiber-plate is supported. An interior fiber-plate is supported on two sides by matrix-foundation. The compressive stress determined by equation (3.8) is half the compressive stress determined by equation (3.7) because the outer-most fiber-plates are supported on only one side by matrix-foundation.

The short-wavelength buckling of a $[0]_s$-class laminate may be a sequence of buckling of the outer laminae. Outer-lamina buckling can occur when the outer-most laminae are not supported by test fixtures or specimen end tabs. The amplitude of the short-wavelength buckling mode shape may be large enough to cause matrix failure that leads to delamination. When one pair of outer laminae buckles and delaminates, the adjacent laminae become the "new" outer laminae and

subsequently buckle and delaminate. The failure of a $[0]_s$-class laminate is characterized by this progressive short-wavelength buckling and delamination of the outer laminae. The characteristic "brooming" failure mode for these laminates is evidence of progressive buckling and delamination.

3.1.2 Laminate Compressive Stresses and Strains

The discussion in the previous section describes values that bound the compressive stress from the present model for the short-wavelength buckling of $[0]_s$-class laminates. The bounds for the compressive stress result from allowing the interior laminae and the outer-most laminae to buckle independently. The general form for the present analysis requires all laminae to buckle simultaneously into the laminate's short-wavelength mode. The normalized compressive stress from the present analysis as a function of the number of laminae in the laminate is shown figure 3.1. The compressive stress is normalized by the stress obtained from Rosen's analysis given by equation (3.7), and the laminate fiber volume fraction is 0.55. A two-lamina model focuses on outer-laminae buckling and gives the same value as equation (3.8) for the compressive stress from the present analysis. As the number of laminae in the laminate increases, the normalized compressive stress for short-wavelength buckling asymptotically approaches unity. A twenty-lamina model is similar to

Rosen's model and predicts a compressive stress at short-wavelength buckling within five percent of the compressive stress from equation (3.7). The significance of the behavior in figure 3.1 is that consistent results using the present analysis for determining the stress at short-wavelength buckling in different laminates require the laminates to have the same number of laminae.

The laminate compressive stresses and strains for short-wavelength buckling of several two-lamina, four-lamina, and eight-lamina laminates are presented in Tables 3.1, 3.2, and 3.3, respectively. The critical normalized end shortening $\bar{u}_o/a$ is equal to the laminate compressive strain for short-wavelength buckling. The half-wavelengths for the mode shapes are also included in the tables and are discussed in the next section on laminate mode shapes. The results in Table 3.1 show that these stresses are affected by laminate anisotropy. A combination of bending and inplane stiffnesses (see $H_{mn}^{(i)}$ and $h_{mn}^{(i)}$, respectively, in equations (2.66)) cause the compressive stress for a $[+30]_s$ laminate to be thirteen percent less than the compressive stress for a $[0]_s$ laminate. Similar laminates with more than two laminae have the same differences in compressive stresses observed in Table 3.1. The compressive stress for a $[90]_s$ laminate is approximately the same as the compressive stress for a $[0]_s$ laminate. These two specially-orthotropic laminates demonstrate

that matrix-foundation components dominate the laminate compressive stress. All compressive stresses for the four-lamina laminates (Table 3.2) are approximately the same. These laminates do not have the A_{16}^{T} and A_{26}^{T} inplane stiffness terms that affect the compressive stress of some two-lamina laminates. The matrix-foundation components dominate the compressive stresses for the four-lamina laminates. The compressive stresses in Table 3.3 for the $[0_4]_s$, $[(\pm 45)]_s$, $[+45/0/-45/90]_s$, and $[90/+45/0/-45]_s$ laminates are approximately the same. The matrix-foundation components dominate the compressive stress for these laminates. The compressive stresses for the $[0/\pm 45/90]_s$ and $[0/+45/90/-45]_s$ laminates are thirteen percent lower than the compressive stress for the $[0_4]_s$ laminate. These lower stresses may be due to the laminates having 0° laminae as the outer-most laminae and not having any interior 0° laminae.

The effect of fiber volume fraction on the normalized compressive stress for short-wavelength buckling is shown in figure 3.2. The compressive stress is normalized by the compressive stress for short-wavelength buckling of a laminate with fiber volume fraction equal to 0.55. The normalized compressive stress is determined for $0.25 \leq V_f \leq 0.85$ which includes most all composite laminates in structural applications. These results agree with similar results by

Rosen [7]. The results from the present analysis show that the curve in figure 3.2 determines the compressive stress for short-wavelength buckling of a laminate with any stacking sequence and any thickness.

3.1.3 Laminate Mode Shapes

The laminate mode shape at short-wavelength buckling has half-waves that are either normal or skewed to the direction of loading. Also, the shear mode (see figure 1.1) is predicted for all the symmetric laminates in this study. The mode shapes for several laminates are shown in figures 3.3 to 3.9. The skew angle is denoted as ϕ. The mode shape for the $[0]_s$ laminate has normal waves and is illustrated in figure 3.3. A similar mode shape is predicted for all balanced, symmetric laminates. The only difference among these mode shapes is the half-wavelength λ. The mode shapes for the $[+10]_s$, $[+20]_s$, $[+30]_s$, $[+45]_s$, $[+60]_s$, and $[+80]_s$ laminates have skewed waves and are illustrated in figures 3.4 to 3.9, respectively. The skew angle is plotted as a function of the fiber orientation in figure 3.10 for these laminates. Generally, the skew angle is not the same as the fiber orientation. The skew angle increases to a maximum at approximately $\theta = 45^{\circ}$. The laminate mode shape at short-wavelength buckling is affected by the fiber-plate bending stiffnesses in

contrast to the compressive stress which is unaffected by these bending stiffnesses. The bending stiffness contribution to the mode shape is discussed in the next paragraphs.

The half-wavelength of the mode shape for a $[0]_s$-class laminate is determined exactly using equations (3.3) and (3.4). The compressive strain (normalized end shortening) in these equations is minimized with respect to the half-wavelength λ to obtain

$$\lambda = \pi\left[(D_{11})^{-1}\left[D_{22}\left(\frac{\pi}{b}\right)^4 + \frac{c_1^{(i)} G_m}{2(1-V_f)}\left(\frac{\pi}{b}\right)^2\right]\right]^{-1/4} \tag{3.9}$$

where $c_1^{(i)}$ is defined as (see equation (2.6))

$$\begin{aligned} c_1^{(i)} &= 1, \text{ outer-lamina buckling} \\ &= 2, \text{ inner-lamina buckling} \end{aligned} \tag{3.10}$$

The half-wavelength of the mode shape for any laminate can be determined approximately by numerically minimizing the compressive strain with respect to λ. The compressive strain as a function of λ is shown in figure 3.11 for several laminates. The compressive strain for the four-lamina laminates decreases rapidly to a minimum and increases very gradually as the half-wavelength increases. The

minimum compressive strains are observed easily by expanding the ordinate in the region of interest and re-plotting the results as shown in figure 3.12 for a $[0_2]_s$ laminate. The compressive strain for the $[0/\pm45/90]_s$ laminate in figure 3.11 decreases rapidly to a minimum and then increases rapidly in the neighborhood of the minimum as the half-wavelength increases. The minimum compressive strain for this laminate is clearly shown in figure 3.11. The half-wavelengths for two-, four-, and eight-lamina laminates are presented in Tables 3.1, 3.2, and 3.3, respectively.

The half-wavelength as a function of fiber orientation θ is shown in figures 3.13 and 3.14 for $[+\theta]_s$ laminates and $[\pm\theta]_s$ laminates, respectively. The results in figure 3.13 for $0^\circ \leq \theta \leq 90^\circ$ show that the half-wavelength increases slightly and decreases. The slight increase may be the effect of anisotropy on laminate behavior discussed previously for compressive stress. The decrease is similar to the behavior of D_{11} as a function of θ. Equation (3.9) shows that D_{11} is used to calculate the half-wavelength. The results in figure 3.14 for $0^\circ \leq \theta \leq 90^\circ$ show that the half-wavelength decreases. The $[\pm\theta]_s$ laminate behavior is not affected by the inplane anisotropic terms that influence the $[+\theta]_s$ laminate behavior. The behavior in figure 3.14 may also reflect the influence of D_{11} on the

half-wavelength. The half-wavelength as a function of the laminate fiber volume fraction is shown in figure 3.15. The response for the $[0_2]_s$ and $[\pm 45]_s$ laminates is used in the figure as typical behavior. The half-wavelength increases with increasing fiber volume fraction for both laminates. Specifically, the half-wavelength for these laminates with $V_f = 0.85$ is approximately twice the half-wavelength for the corresponding laminates with $V_f = 0.25$.

The half-wavelength results of the present study may explain the scatter in compressive strength data for composite laminates. The range of half-wavelengths for the buckling of laminates with $V_f = 0.55$ in this study is from 0.0140 inches to 0.2255 inches. Most of the half-wavelengths are on the order of $O(10^{-1})$ inches. Some compression test methods for composite laminates use specimens with short test sections (e.g., 0.50 in., [61]) or require elaborate fixtures that completely support the test specimen along the length [62]. These methods may inhibit the natural failure mode for a laminate that deforms in a short-wavelength buckling mode shape. These methods may cause the half-wavelength to be less than the half-wavelength corresponding to the minimum compressive strain if short-wavelength buckling ever occurs. The results in figure 3.11 show that significantly higher compressive strains can occur if the half-wavelength is 0.1 inch less than the half-wavelength corresponding to the minimum compressive strain.

3.2 Nonlinear Behavior

The nonlinear behavior of four laminates is presented in this section. The laminate nonlinear behavior is the result of short-wavelength out-of-plane initial imperfections in each lamina. The laminate orientations are $[0_2]_s$, $[0/90]_s$, $[\pm 45]_s$, and $[+45/0/-45/90]_s$. These laminates illustrate the range of application for the present analysis. Specifically, these laminates illustrate:

$[0_2]_s$	Orthotropic laminae, unidirectional laminate
$[0/90]_s$	Orthotropic laminae, multi-directional laminate
$[\pm 45]_s$	Anisotropic laminae, multi-directional laminate
$[+45/0/-45/90]_s$	Orthotropic and anisotropic laminae, multi-directional laminate

The nonlinear laminate behavior is discussed for two imperfection-amplitude-to-lamina-thickness ratios $\bar{w}_o/t$. These ratios are $\bar{w}_o/t = 0.1$ and $\bar{w}_o/t = 0.5$. The imperfection amplitudes for anisotropic fiber-plates, $\bar{w}_{o_S}$ and $\bar{w}_{o_C}$, are simplified by letting

$\bar{w}_{o_s} = w_{o_c} = \bar{w}_o$. All fiber-plates have the same imperfection. The shape of the imperfection is the same as the short-wavelength buckling mode shape for the laminate.

3.2.1 Displacements and Inplane Stresses

The nonlinear behavior of a $[0_2]_s$ laminate with initial imperfections is shown in figure 3.16. The ordinate is the laminate compressive stress normalized by the laminate compressive stress for short-wavelength buckling. The abscissa is the laminate end shortening normalized by the laminate end shortening for short-wavelength buckling. The laminate response for $\bar{w}_o/t = 0.$ (no initial imperfections) is included for comparison with the laminate response for $\bar{w}_o/t = 0.1$ and 0.5. The results in the figure show that this laminate behaves like a wide column, i.e., the slope of each response curve (laminate stiffness) approaches zero as the end shortening is increased. This change in stiffness is dramatic for the laminate with $\bar{w}_o/t = 0.$ but is more gradual for the laminates with $\bar{w}_o/t = 0.1$ and 0.5. A maximum compressive stress that corresponds to the maximum load-carrying capacity of the laminate is defined by this wide-column response. The maximum stresses for laminates with $\bar{w}_o/t = 0.1$ and 0.5

are approximately five and twenty-five percent lower, respectively, than the maximum stress for the laminate with $\bar{w}_o/t = 0.$

The stress resultant N_x for a 0° lamina is plotted in figure 3.17 for $\bar{u}_o/(\bar{u}_o)_{cr} = 0.5$, 0.8, and 1.0. The laminate end shortening for short-wavelength buckling is $(\bar{u}_o)_{cr}$. The initial imperfection for the $[0_2]_s$ laminate is $\bar{w}_o/t = 0.5$. The results in the figure are typical of a plate with an out-of-plane initial imperfection. The stress resultant at the edges of the lamina ($y/b = 0.$ and $y/b = 1.$) is greater than the stress resultant at the center of the lamina ($y/b = 0.5$). The difference between the stress resultants for these locations increases as the laminate end shortening increases. The stress resultant at the edges is more than twenty-five percent greater than the stress resultant at the center when $\bar{u}_o/(\bar{u}_o)_{cr} = 1.0.$

The w displacement for the outer-most 0° lamina along $\bar{x} = \lambda/2$ is plotted in figure 3.18 for $\bar{u}_o/(\bar{u}_o)_{cr} = 0.5$, 0.8, and 1.0. The initial imperfection for this laminate is $\bar{w}_o/t = 0.5$. Again, the results in the figure are typical for a plate with an out-of-plane initial imperfection. The shape of this w-displacement curve is approximately parabolic for $\bar{u}_o/(\bar{u}_o)_{cr} = 0.5$. This shape changes as

$\bar{u}_o/(\bar{u}_o)_{cr}$ increases. For $\bar{u}_o/(\bar{u}_o)_{cr} = 1.0$, the magnitude of the slope, $w_{,y}^{(1)}$, is very large near the lamina edges and the w displacement is approximately constant for $0.3 \leq y/b \leq 0.7$.

The maximum w displacement as a function of end shortening for a $[0_2]_s$ laminate is shown in figure 3.19. The laminate response for $\bar{w}_o/t = 0.$ is included for comparison with the laminate response for $\bar{w}_o/t = 0.1$ and 0.5. The maximum w displacement occurs at $y = b/2$ as illustrated in figure 3.18. The results in figure 3.19 show that significantly large w displacements occur for the imperfect laminates. The w displacement is approximately equal to a lamina thickness for the laminate with $\bar{w}_o/t = 0.1$ for $\bar{u}_o/(\bar{u}_o)_{cr} = 1.0$ and almost equal to two lamina thicknesses for the laminate with $\bar{w}_o/t = 0.5$ for $\bar{u}_o/(\bar{u}_o)_{cr} = 1.0$. These large w displacements produce large interlaminar shear stresses as discussed in section 3.2.2 Interlaminar Strains.

The nonlinear behavior for a $[0/90]_s$ laminate with initial imperfections is shown in figures 3.20 and 3.21. Laminate compressive stress as a function of laminate end shortening is plotted in figure 3.20. This multi-directional laminate has the same wide-column behavior as the unidirectional laminate (cf., figure 3.16). The maximum stresses for $[0/90]_s$ laminates with $\bar{w}_o/t = 0.1$ and 0.5 are

approximately seven and twenty-eight percent lower, respectively, than the maximum stress for this laminate with $\bar{w}_o/t = 0$. These differences are similar to those observed for the corresponding $[0_2]_s$ laminates. The maximum w displacement as a function of end shortening for a $[0/90]_s$ laminate is shown in figure 3.21. The results in this figure for the multi-directional laminate are approximately the same as the results in figure 3.19 for the unidirectional laminate. Generally, the results for the $[0/90]_s$ laminates are approximately the same as the corresponding results for the $[0_2]_s$ laminates.

The nonlinear behavior for a $[\pm 45]_s$ laminate with initial imperfections is shown in figure 3.22. The normalized laminate compressive stress is plotted as a function of normalized laminate end shortening for $\bar{u}_o/(\bar{u}_o)_{cr} \leq 1.0$. Results for $\bar{u}_o/(\bar{u}_o)_{cr} > 1.0$ did not converge to within the specified tolerances. The mode shape for short-wavelength buckling of this laminate changes from having normal waves to having skewed waves for $\bar{u}_o/(\bar{u}_o)_{cr} > 1.0$. The lack of convergence is caused by the changing mode shape. The results in the figure approach the wide-column behavior discussed previously. The maximum compressive stresses in the figure for $[\pm 45]_s$ laminates with $\bar{w}_o/t = 0.1$ and 0.5 are approximately five and twelve percent lower, respectively, than the compressive stress for short-wavelength

buckling of this laminate with $\bar{w}_o/t = 0$. The results for the $[\pm 45]_s$ laminate with $\bar{w}_o/t = 0.1$ are approximately the same as the results for similar $[0_2]_s$ and $[0/90]_s$ laminates. The results for the $[\pm 45]_s$ laminate with $\bar{w}_o/t = 0.5$ suggest that this imperfection has less effect on the compressive stress of a $[\pm 45]_s$ laminate than on the compressive stresses of $[0_2]_s$ and $[0/90]_s$ laminates.

The N_x and N_{xy} stress resultants for a 45° lamina are plotted in figure 3.23 for $\bar{u}_o/(\bar{u}_o)_{cr} = 0.25$ and 0.50. The initial imperfection for this $[\pm 45]_s$ laminate is $\bar{w}_o/t = 0.5$. Laminates with $\bar{u}_o/(\bar{u}_o)_{cr} > 0.50$ have compressive stresses more than an order of magnitude greater than the typical compressive strength for a $[\pm 45]_s$ laminate, and results for these laminates are not included in the figure. The maximum N_x occurs at the laminate edges although N_x is approximately constant across the laminate width. The stress resultant N_{xy} is constant across the laminate width. The stress resultant N_x is more than twice N_{xy} for both values of $\bar{u}_o/(\bar{u}_o)_{cr}$; however, N_{xy} is sufficient to initiate failure within the laminate, and this failure is discussed in the section on laminate failure predictions.

Results for the w displacements in the $[\pm 45]_s$ laminates are presented in figures 3.24 and 3.25. The w displacement for the outer-most 45° lamina along $\bar{x} = \lambda/2$ is plotted in figure 3.24 for $\bar{u}_o/(\bar{u}_o)_{cr} = 0.25$ and 0.50. The initial imperfection for this laminate is $\bar{w}_o/t = 0.5$. The shape of these w-displacement curves is approximately parabolic for both values of $\bar{u}_o/(\bar{u}_o)_{cr}$. The maximum w displacement as a function of end shortening is shown in figure 3.25. The laminate response for $\bar{w}_o/t = 0.$ is coincident with the ordinate. The laminate response for $\bar{w}_o/t = 0.1$ and for $\bar{w}_o/t = 0.5$ are presented also. Significantly large w displacements occur for the imperfect laminates. The maximum w displacement is greater than 1.5 lamina thicknesses for the laminate with $\bar{w}_o/t = 0.1$ for $\bar{u}_o/(\bar{u}_o)_{cr} = 1.0$ and is approximately equal to two lamina thicknesses for the laminate with $\bar{w}_o/t = 0.5$ for $\bar{u}_o/(\bar{u}_o)_{cr} = 0.9$. These w displacements are larger than the corresponding w displacements for the $[0_2]_s$ and $[0/90]_s$ laminates because the axial bending stiffness for the $[\pm 45]_s$ laminates is less than the axial bending stiffness for the 0°-dominated laminates.

The nonlinear behavior for a $[+45/0/-45/90]_s$ laminate with initial imperfections is shown in figure 3.26. The normalized

laminate compressive stress is plotted as a function of normalized laminate end shortening for $\bar{u}_o/(\bar{u}_o)_{cr} \leq 1.0$. Results for $\bar{u}_o/(\bar{u}_o)_{cr} > 1.0$ did not converge to within the specified tolerances. The lack of convergence is caused by changes in the laminate short-wavelength mode shape and is similar to the lack of convergence noted for the $[\pm 45]_s$ results. The results in the figure approach the wide-column behavior discussed previously. The maximum compressive stresses in the figure for $[+45/0/-45/90]_s$ laminates with $\bar{w}_o/t = 0.1$ and 0.5 are approximately seventeen and thirty-six percent lower, respectively than the compressive stress for short-wavelength buckling of this laminate with $\bar{w}_o/t = 0$. These differences for an eight-lamina laminate are larger than the corresponding differences for the four-lamina laminates and are related to laminate thickness.

The N_x and N_{xy} stress resultants for a 45° lamina are plotted for $\bar{u}_o/(\bar{u}_o)_{cr} = 0.25$ in figure 3.27 and for $\bar{u}_o/(\bar{u}_o)_{cr} = 0.50$ in figure 3.28. The corresponding N_x values for a 0° lamina also are plotted in the figures. The initial imperfection for the laminate is $\bar{w}_o/t = 0.5$. The maximum N_x in the 0° and 45° laminae occurs at the laminate edges. For the 45° lamina N_x is approximately constant across the laminate width, and N_{xy} is constant across the laminate

width. The difference between N_x for the 0° lamina and N_x for the 45° lamina is approximately the same as the difference between the corresponding axial stiffnesses.

Results for the w displacements in the $[+45/0/-45/90]_s$ laminates are presented in figures 3.29 and 3.30. The w displacement for the outer-most lamina (45° lamina) along $\bar{x} = \lambda/2$ is plotted in figure 3.29 for $\bar{u}_o/(\bar{u}_o)_{cr} = 0.25$ and 0.50. The initial imperfection for this laminate is $\bar{w}_o/t = 0.5$. The shape of these w-displacement curves is approximately parabolic for both values of $\bar{u}_o/(\bar{u}_o)_{cr}$. The maximum w displacement as a function of end shortening is shown in figure 3.30. The laminate response for $\bar{w}_o/t = 0.$ is coincident with the ordinate. The laminate response for $\bar{w}_o/t = 0.1$ and for $\bar{w}_o/t = 0.5$ are presented also. The results are plotted using the same scale as that in figures 3.19, 3.21, and 3.25 and indicate that the w displacements for the eight-lamina laminate are much smaller than the w displacements for the four-lamina laminates. The w displacements for the eight-lamina laminate are only one-quarter to one-third the w displacements for the four-lamina laminates. The w displacements for the eight-lamina laminate are smaller than the w displacements for the four-lamina laminates

because the axial bending stiffness for the eight-lamina laminate is greater than the axial bending stiffness for the four-lamina laminate.

3.2.2 Interlaminar Strains

The strains in each matrix-foundation are expressed in equations (2.20) as functions of the w displacements of the adjacent fiber-plates. These strains are interlaminar normal and shearing strains. The interlaminar normal strain $\varepsilon_{mz}^{(i)}$ is negligible for all the cases in this study since the deformation of every laminate is dominated by the shear mode (see figure 1.1). This deformation also causes the interlaminar shear strains $\gamma_{myz}^{(i)}$ and $\gamma_{mxz}^{(i)}$ to be constant within each matrix-foundation region. These strains are largest at the interface between the two outer laminae because the gradients of the w displacements are largest at this interface. The interlaminar shear strains are represented by γ_{yz} and γ_{xz} and are reported for the interface between the two outer laminae in subsequent discussion. The maximum γ_{yz} occurs along $\bar{x} = m\lambda/2$, $m = 1, 2, 3, \ldots$ (see figure 2.5a) since the $w_{,y}$ component to this shear strain has a maximum along these lines. The maximum γ_{xz} occurs along nodal lines, $\bar{x} = n\lambda$, $n = 0, 1, 2, \ldots$ (see figure 2.5a) since the $w_{,x}$ component to this shear strain has a maximum along these

lines. These interlaminar strains are caused by the geometrically nonlinear behavior of the laminae and are different from the interlaminar strains that result from lamina material property differences [63].

Interlaminar shear strain distributions in a $[0_2]_s$ laminate are shown in figures 3.31, 3.32, and 3.33. The strains in figures 3.31 and 3.32 are for $\bar{u}_o/(\bar{u}_o)_{cr} = 0.30$ and 0.60, respectively, and for $\bar{w}_o/t = 0.1$. The results in the figures show that the magnitude of γ_{yz} is a maximum at the laminate edges. The maximum and minimum values for $w_{,y}$ occur at $y/b = 0.$ and $1.$, respectively. The results in the figures also show that γ_{xz} has a parabolic distribution across the laminate width and is a maximum at the laminate center. The maximum value for $w_{,x}$ occurs at $y/b = 0.5$. The strains in figure 3.33 are for $\bar{u}_o/(\bar{u}_o)_{cr} = 0.30$ and for $\bar{w}_o/t = 0.5$. The behavior for γ_{yz} and γ_{xz} for $\bar{w}_o/t = 0.5$ is approximately the same as the behavior for γ_{yz} and γ_{xz} for $\bar{w}_o/t = 0.1$; however, the maximum γ_{yz} and the maximum γ_{xz} at $\bar{w}_o/t = 0.5$ are greater than the maximum γ_{yz} and the maximum γ_{xz}, respectively, for both load cases at $\bar{w}_o/t = 0.1$. The $\bar{w}_o/t = 0.5$ imperfection causes interlaminar strains for $\bar{u}_o/(\bar{u}_o)_{cr} = 0.3$ that are greater than the interlaminar strains

for $\bar{w}_o/t = 0.1$ at twice the load level. The maximum γ_{xz} approaches four percent at an end shortening that is only thirty percent of the end shortening at short-wavelength buckling. The results in figures 3.31 to 3.33 also illustrate that the maximum γ_{xz} is more than an order of magnitude greater than the maximum γ_{yz}. Results for γ_{xz} only are presented subsequently.

The γ_{xz} distribution at the $0^\circ/90^\circ$ interface in a $[0/90]_s$ laminate is shown in figure 3.34 and at the $+45^\circ/-45^\circ$ interface in a $[\pm 45]_s$ laminate is shown in figure 3.35. Both laminates are loaded to $\bar{u}_o/(\bar{u}_o)_{cr} = 0.20$, and the results in the figures are similar. These results are also similar to the γ_{xz} results in figures 3.31 and 3.33 for a $[0_2]_s$ laminate with $\bar{u}_o/(\bar{u}_o)_{cr} = 0.30$.

The γ_{xz} distribution at the $+45^\circ/0^\circ$ interface in a $[+45/0/-45/90]_s$ laminate is shown in figure 3.36. The laminate is loaded to $\bar{u}_o/(\bar{u}_o)_{cr} = 0.10$. The results in the figure are similar to those reported for the four-lamina laminates except that this laminate is loaded only to $\bar{u}_o/(\bar{u}_o)_{cr} = 0.10$. The $w_{,x}$ component to γ_{xz} for the $[+45/0/-45/90]_s$ laminate is large because the wavelength of the mode shape for this laminate is extremely small, i.e., $\lambda = 0.0477$ in.

(Table 3.3). The w-gradients for this laminate are large although the w displacements are small (figure 3.30) when compared to similar results for the four-lamina laminates.

3.2.3 Effects of Fiber Volume Fraction

The fiber volume fraction V_f affects the short-wavelength buckling behavior of compression-loaded laminates. The effect of V_f on the compressive stress at short-wavelength buckling and on the half-wavelength of the buckling mode are illustrated in figures 3.2 and 3.15, respectively.

The fiber volume fraction also affects the nonlinear behavior of compression-loaded laminates with short-wavelength imperfections. The nonlinear results reported in the preceeding paragraphs are for laminates with $V_f = 0.55$. This section examines the behavior of laminates with $V_f = 0.45$ and with $V_f = 0.65$. These V_f bound the typical laminates with structural applications. Typical results are presented in the following paragraphs for $[0_2]_s$ and $[\pm 45]_s$ laminates.

The effect of V_f on the behavior of $[0_2]_s$ laminates is shown in figures 3.37 to 3.39. Laminate compressive stress as a function of the laminate end shortening is presented in figure 3.37. The laminate

response for $\bar{w}_o/t = 0.$ is included for comparison with the laminate response for $\bar{w}_o/t = 0.1$ and 0.5. The results for $V_f = 0.45$ and $V_f = 0.65$ in this figure bound the results for $V_f = 0.55$ in figure 3.16. The laminates with $V_f = 0.65$ are the stiffest, as expected. The effect of fiber volume fraction on laminate compressive-stress versus end-shortening response is more significant for $\bar{w}_o/t = 0.5$ than for $\bar{w}_o/t = 0.1$. The compressive stress for $V_f = 0.65$ with $\bar{u}_o/(\bar{u}_o)_{cr} = 1.0$ is more than ten percent greater than the compressive stress for $V_f = 0.45$ with $\bar{u}_o/(\bar{u}_o)_{cr} = 1.0$ when $\bar{w}_o/t = 0.5$. Similar results differ by two percent when $\bar{w}_o/t = 0.1$. The maximum w displacement as a function of laminate end shortening is shown in figure 3.38. These results also bound the results for $V_f = 0.55$ in figure 3.19. Significantly large w displacements are observed for this laminate at each fiber volume fraction. The w displacements for $V_f = 0.45$ are greater than or equal to a lamina thickness for $\bar{w}_o/t = 0.1$. The w displacements for $V_f = 0.65$ are greater than or equal to 1.5 lamina thicknesses for $\bar{w}_o/t = 0.5$. The laminates with $V_f = 0.65$ have the largest w displacements of the laminates studied because the matrix-foundation regions are thinnest for $V_f = 0.65$. This thin region may allow large w displacements for the fiber-plates. The interlaminar shear strain distribution across the

laminate is plotted in figure 3.39 for $\bar{u}_o/(\bar{u}_o)_{cr} = 0.30$. The corresponding results for $V_f = 0.55$ are plotted in figures 3.31 and 3.33. The effect of fiber volume fraction on γ_{xz} is more significant for $\bar{w}_o/t = 0.5$ than for $\bar{w}_o/t = 0.1$. The γ_{xz} for $V_f = 0.65$ at $y/b = 0.5$ is more than forty-three percent greater than γ_{xz} for $V_f = 0.45$ at $y/b = 0.5$ when $\bar{w}_o/t = 0.5$. Similar results differ by twenty-eight percent when $\bar{w}_o/t = 0.1$. The large w displacements shown in figure 3.38 may lead to large w-gradients that contribute to γ_{xz}.

The effect of V_f on the behavior of $[\pm 45]_s$ laminates is shown in figures 3.40 to 3.42. Laminate compressive stress as a function of the laminate end shortening is presented in figure 3.40. The results in this figure for $V_f = 0.45$ and $V_f = 0.65$ are within five percent of the results in figure 3.22 for $V_f = 0.55$. The laminates with $V_f = 0.65$ are the stiffest. The effect of fiber volume fraction on the results in figure 3.40 is noticeable but not significant because a change in V_f has a noticeable but not significant change in the axial extensional stiffness for this laminate. The maximum w displacement as a function of laminate end shortening is shown in figure 3.41. The laminate response for $\bar{w}_o/t = 0.$ is coincident with the ordinate. These results are also very similar to the results in

figure 3.25 for $V_f = 0.55$. Significantly large w displacements are observed for this laminate at each fiber volume fraction, and the largest w displacements occur in laminates with $V_f = 0.65$. The interlaminar shear strain distribution across the laminate at the $+45^\circ/-45^\circ$ interface is plotted in figure 3.42 for $\bar{u}_o/(\bar{u}_o)_{cr} = 0.30$. The corresponding results for $V_f = 0.55$ are plotted in figure 3.35. The γ_{xz} for $V_f = 0.65$ at $y/b = 0.5$ is more than thirty percent greater than the γ_{xz} for $V_f = 0.65$ at $y/b = 0.5$ when $\bar{w}_o/t = 0.5$. Similar results are observed when $\bar{w}_o/t = 0.1$. The large w displacements shown in figure 3.41 may lead to large w-displacement gradients that contribute to γ_{xz}.

3.3 Laminate Failure Predictions

3.3.1 Dominant Mechanisms

This section applies the results of the present analysis for the short-wavelength buckling response and for the geometrically nonlinear response of a laminate to the failure of compression-loaded laminates. Specifically, laminate failure initiated by outer-lamina buckling, by interlaminar shear strains from lamina imperfections, or by inplane shearing stresses is considered. Outer-lamina buckling

occurs at an outer-lamina stress determined by equation (3.8). This phenomenon is independent of the fiber orientation of the outer laminae since short-wavelength buckling behavior is dominated by the matrix contributions. This phenomenon is not observed for many laminates because other mechanisms dominate their failure. An example of such a mechanism is interlaminar shearing caused by lamina short-wavelength imperfections. A simple maximum-shear-strain criterion is used in this study to predict failure due to this mechanism. The shear strain for matrix failure is used for this maximum shear strain. The nonlinear analysis is used to calculate the laminate compressive stress for this interlaminar shearing failure. Another mechanism that may dominate laminate failure is the inplane shearing at the fiber-matrix interface and in the epoxy matrix between fibers. This inplane shearing has been referred to as matrix shearing and has been shown to initiate failure in compression-loaded $[\pm 45]_s$-class laminates [64]. A simple maximum-shear-stress criterion is used in this study to predict failure due to matrix shearing. The nonlinear analysis derived herein also is used to calculate the laminate compressive stress for inplane shear failure.

The compressive strength σ_c is shown as a function of lamina orientation in figure 3.43 for $[\pm\theta]_s$ laminates. The laminate compressive strength is normalized by the compressive stress for short-wavelength buckling of a $[0_2]_s$ laminate, i.e., $\sigma_o = 433.5$ ksi

(Table 3.2). Short-wavelength buckling of the outer laminae occurs at $\sigma_c/\sigma_o = 0.66$ (289.6 ksi) for all θ and is indicated by the horizontal line in the figure. The axial compressive stress for laminate failure by short-wavelength buckling of the outer laminae is less than five percent greater than the compressive stress for interlaminar shear failure when $0^\circ \leq \theta \leq 15^\circ$. Laminate failure due to interlaminar shearing for laminates with $\bar{w}_o/t = 0.1$ and for laminates with $\bar{w}_o/t = 0.5$ is plotted in the figure for a maximum shear strain $(\gamma_{xz})_{max} = 0.036$ [54]. The laminate compressive strength due to interlaminar shearing decreases as θ increases. Laminate failure due to matrix shearing is plotted in the figure for a maximum shear stress in the principal material coordinate system $(\tau_{12})_{max} = 13.8$ ksi [64]. The laminate compressive strength due to matrix shearing approaches infinity for θ near 0° and for θ near 90°. Results for inplane matrix shearing are plotted for $10^\circ \leq \theta \leq 85^\circ$. The results in figure 3.43 suggest that laminate failure for $[\pm\theta]_s$ laminates may be due to short-wavelength buckling of the outer laminae for $0^\circ \leq \theta < 15^\circ$ when $\bar{w}_o/t < 0.1$. The initial imperfections $\bar{w}_o/t < 0.1$ are very small and may rarely occur in typical laminates. Laminate failure for $[\pm\theta]_s$ laminates is due to interlaminar shearing for $0^\circ \leq \theta < 15^\circ$ when $\bar{w}_o/t \geq 0.1$. The compressive strength due to

interlaminar shearing is a function of $\bar{w}_o/t$. The results in the figure also suggest that laminate failure is due to inplane matrix shearing for $15^\circ \leq \theta \leq 75^\circ$. The compressive strength due to matrix shearing is not a function of $\bar{w}_o/t$. Results from the present model for $75^\circ < \theta \leq 90^\circ$ are not applicable to laminate failure. Typical failure in these laminates appears to be initiated by compressive failure of the matrix. The present model treats the matrix as an elastic foundation and axial loading of the matrix-foundation is not considered. Nevertheless, the present model predicts laminate failures initiated by outer-lamina buckling, by interlaminar shearing, or by inplane matrix shearing for $0^\circ \leq \theta \leq 75^\circ$. The present model is unique in its ability to predict the compressive strength as a function of short-wavelength buckling and shear failures for such a variety of laminates.

3.3.2 Simple Equations for 0°-Dominated Laminates

Many laminates used in structural applications have 0° laminae, and the behavior of these laminae often dominates the behavior of the laminate. Such laminates are referred to as 0°-dominated laminates. Some examples of 0°-dominated laminates are $[0/90]_s$ and $[0/\pm45/90]_s$. The compressive failure of a 0°-dominated

laminate can be predicted by determining the failure of the 0° laminae. The present analysis can be used to determine the compressive strength of 0° laminae, and the results in figure 3.43 show that many $[0]_s$-class laminates fail due to interlaminar shearing. This failure mode can cause failure of 0° laminae in a laminate.

A simple method can be used to predict the compressive failure of 0°-dominated laminates. The method is referred to herein as the stiffness-ratio method and is outlined as follows:

1. Determine the compressive strength of a 0° lamina by using the results from the present analysis in figure 3.43;
2. Calculate the load in the 0° laminae of the given laminate when the 0° laminae will fail;
3. Calculate the load in all other lamina of the given laminate when the 0° laminae will fail by using

$$\frac{P_{\theta}}{P_{o}} = \frac{E_{x\theta}}{E_{11}} \tag{3.11}$$

where

P_θ = load in a θ-oriented lamina

P_o = load in a 0° lamina

$E_{x\theta}$ = Young's modulus in the x-direction for a θ-oriented lamina (see figure 2.4)

$E_{x\theta}$ is determined from [12]

$$\frac{1}{E_{x\theta}} = \frac{1}{E_{11}}\cos^4\theta + \left(\frac{1}{G_{12}} - \frac{2\nu_{12}}{E_{11}}\right)\cos^2\theta \sin^2\theta + \frac{1}{E_{22}}\sin^4\theta \qquad (3.12)$$

where E_{11}, E_{22}, G_{12}, and ν_{12} are lamina properties in the principal material coordinate system;

4. Sum the loads of all laminae to determine the laminate failure load;
5. Calculate the laminate compressive strength.

The stiffness-ratio method assumes that the laminate is loaded by uniform end shortening (i.e., constant strain) and that the laminate has linear stress-strain behavior.

The stiffness-ratio method results in a simple equation for the compressive strength of a 0°-dominated laminate

$$\sigma_{lam} = \frac{\sigma_0}{N\, E_{11}} \sum_{i=1}^{N} E_{x\theta}^{(i)} \qquad (3.13)$$

where

σ_{lam} = compressive strength of the laminate

σ_0 = compressive strength of a 0° lamina

N = number of laminae in the laminate

The predicted laminate strength using equation (3.13) is compared to the experimental strength for three 0°-dominated laminates in Table 3.4. All laminates have $V_f = 0.55$, and the compressive strength of a 0° lamina is determined using figure 3.43 with $\sigma_{\theta}/\sigma_{o} = 0.45$. The experimental strengths are typical results from extensive testing. The agreement between predicted strength and experimental strength for this limited number of laminates is excellent. The maximum difference between the predicted strengths and the experimental strengths is less than five percent.

Chapter 4

CONCLUSIONS

4.1 Concluding Remarks

This investigation studies the short-wavelength buckling (or microbuckling) of multi-directional composite laminates loaded in uniaxial compression. This investigation also studies the interlaminar shear failures due to short-wavelength initial imperfections for the laminae and the inplane shear failures in these laminates. A laminate model is presented that idealizes each lamina. The fibers in the lamina are modeled as a plate, and the matrix in the lamina is modeled as an elastic foundation. The model is applied to symmetric laminates having linear material behavior. The laminates are loaded in uniform end shortening and are simply supported on all edges.

The present model is used to determine linear and nonlinear laminate responses. A linear analysis is derived to determine the short-wavelength buckling response of composite laminates. The out-of-plane w displacement for each plate is expressed as a trigonometric series in the half-wavelength of the mode shape for

laminate short-wavelength buckling. Results from this linear analysis are also compared to previous results for unidirectional laminates. The present linear analysis for laminates with no initial imperfections is generalized to obtain a nonlinear analysis for the response of laminates with short-wavelength initial imperfections. This nonlinear analysis is derived using nonlinear strain-displacement relations. The results of the present linear and nonlinear analyses are used to develop a compressive failure criterion for composite laminates.

The present linear analysis is used to determine the laminate stresses, strains, and mode shape for short-wavelength buckling of several different laminates. The compressive stress that corresponds to short-wavelength buckling from this analysis for any symmetric laminate simplifies to the critical compressive stress for short-wavelength buckling from previous studies for unidirectional laminates. The equations for the laminate compressive stress corresponding to short-wavelength buckling are dominated by matrix contributions. The compressive stress corresponding to short-wavelength buckling of the outer laminae is half the compressive stress that corresponds to short-wavelength buckling of the interior laminae. The short-wavelength buckling and delamination of these outer laminae characterize the compression failure of $[0]_s$-class laminates. The compressive stress that corresponds to short-wavelength buckling of some quasi-isotropic laminates is lower than

the compressive stress that corresponds to short-wavelength buckling of unidirectional laminates with the same number of laminae. This lower stress may be due to these quasi-isotropic laminates having 0° laminae as the outer-most laminae and not having any interior 0° laminae. The compressive stress that corresponds to short-wavelength buckling is a function of fiber volume fraction, and this compressive stress is determined from a single curve. All laminates in this study buckle into the short-wavelength shear mode. This mode shape is dominated by interlaminar shearing, and extensional deformations between laminae are negligible. All balanced, symmetric laminates have mode shapes with half-waves oriented normal to the direction of applied load. Most of the half-wavelengths for short-wavelength buckling are on the order of $O(10^{-1})$. The magnitude of these half-wavelengths may influence the experimental compressive strengths for composite materials. Some compressive test methods for composite materials may inhibit the natural failure mode for a laminate by supporting the test specimen along the length in a manner that suppresses or prevents short-wavelength buckling. The degree of specimen support for different test methods may contribute to the scatter in compressive strength data for composite laminates.

The nonlinear analysis for laminae with short-wavelength initial imperfections is used to determine laminate stresses and interlaminar strains. This analysis provides the capability to

calculate these stresses and strains for a variety of laminates. The nonlinear behavior of four laminates with orientations of $[0_2]_s$, $[0/90]_s$, $[\pm 45]_s$, and $[+45/0/-45/90]_s$ is discussed. The initial imperfection for each lamina have the same shape as the laminate's short-wavelength buckling mode, and results are presented for imperfection-amplitude-to-lamina-thickness ratios of 0.1 and 0.5. The compressive-stress verses end-shortening behavior for all laminates is similar to the behavior of a wide column. The wide-column response for each composite laminate defines a maximum compressive stress that corresponds to the maximum load-carrying capacity of the laminate. The distribution of the lamina inplane stress resultants, N_x and N_{xy}, across each lamina is discussed. The stress resultant N_x at the edges of the lamina is greater than N_x at the center of the lamina. The stress resultant N_{xy} is constant across the lamina width. The stress resultant N_x is larger than the stress resultant N_{xy}, as expected; however, N_{xy} is sufficient to initiate failure within some laminates. The interlaminar shear strains due to the initial imperfections are calculated. The $w_{,x}$ displacement gradients cause significant interlaminar shear strains γ_{xz}. The interlaminar shear strains γ_{xz} are greater than 0.03 for laminate compressive loadings that are less than thirty percent of the laminate loading for short-wavelength buckling of some laminates. The γ_{xz}

for each laminate is largest between the outer two laminae. The effects of fiber volume fraction on the nonlinear laminate response are presented for $[0_2]_s$ and $[\pm 45]_s$ laminates. The laminate stiffness and the maximum γ_{xz} in the laminate increase as the fiber volume fraction increases.

A failure criterion for compression-loaded laminates is presented. Laminate failures that initiate by outer-lamina buckling, by interlaminar shear strains from lamina imperfections, or by inplane matrix shearing are included in the criterion. The present linear analysis is used to calculate the compressive stress that corresponds to outer-lamina buckling, and the present nonlinear analysis is used to calculate the compressive stress that corresponds to the interlaminar and inplane shear failures. The laminate strength is calculated as a function of lamina orientation for $[\pm\theta]_s$ laminates. Compressive failure of $[\pm\theta]_s$ laminates for $0^\circ \leq \theta < 15^\circ$ is due to outer-lamina buckling when $\bar{w}_o/t < 0.1$ and is due to interlaminar shearing when $\bar{w}_o/t \geq 0.1$. Compressive failure of these laminates for $15^\circ \leq \theta \leq 75^\circ$ is due to inplane matrix shearing. Results from the present analysis are not applicable for $\theta > 75^\circ$. The failure of $[\pm\theta]_s$ laminates with $\theta > 75^\circ$ appears to be initiated by compressive failure of the matrix, and this type of failure is not considered in

the present model. A simple method called the stiffness-ratio method is introduced for predicting the strength of 0°-dominated laminates. The stiffness-ratio method uses results from the present nonlinear analysis, and the difference between predicted strengths and experimental strengths is less than five percent for a limited number of laminates.

4.2 Recommendations for Future Studies

An analytical study of short-wavelength buckling and shear failures in symmetric composite laminates has been described. Recommendations for future studies are grouped in three categories: analytical extensions; additional experimental verification; and applications of the present theory. A useful analytical extension to this study would be to generalize the present theory to unsymmetric laminates. Such laminates are being considered for use in the next generation of commercial transport aircraft structures. Another useful analytical extension would be to include material nonlinearity in the present theory. Material properties may be a function of the compressive load level. These properties are also affected by the residual thermal stresses in the laminate and the operating temperature of the composite structure. The formulation of the present theory is sufficiently general that these analytical

extensions could be included by modifying the strain energy expressions.

Additional experimental verification of the present analytical results is needed. The effect of the compression test method on a laminate's compressive strength and failure mode should be evaluated. A study of compression-loaded $[\pm\theta]_s$ laminates might focus on the short-wavelength buckling and shear failure mechanisms that were described for these laminates. An experimental study of 0°-dominated laminates is needed to better evaluate the stiffness-ratio method for predicting the compressive strength of these laminates.

The present theory may be applied in current research. Interleaved materials are currently being considered as one of the next generation of composite materials. These materials have soft adhesive layers that are used (or interleaved) between stiff composite layers. Laminates of interleaved materials are similar to the model in the present analysis, i.e., alternating soft and stiff layers. The present theory may be very useful for predicting the failure mechanisms in laminates of interleaved materials. The present theory also may be useful for understanding the compressive behavior of woven composite laminates. The initial imperfections due to weaving are known and may dominate the compressive response of these laminates. An investigation of the unique failure mechanisms of woven composite laminates needs to be conducted.

REFERENCES

1. Dow, N. F.; and Gruntfest, I. J.: Determination of Most-Needed, Potentially Possible Improvements in Materials for Ballistic and Space Vehicles. T. I. S. R60SD389, General Electric Company, Air Force Contract AF 04 (647)-269, June 1960.

2. Timoshenko, S. P.; and Gere, J. M.: Theory of Elastic Stability. Second edition, McGraw-Hill, 1961.

3. Fried, N.: The Compressive Strength of Parallel Filament Reinforced Plastics - The Role of the Resin. Proceedings of the 18th Annual Meeting of the Reinforced Plastics Division, Society of the Plastics Industry, Inc., February 1963, pp. (9-A) 1-10.

4. Fried, N.; and Kaminetsky, J.: The Influence of Material Variables on the Compressive Properties of Parallel Filament Reinforced Plastics. Proceedings of the 19th Annual Technical and Management Conference, Reinforced Plastics Division, Society of the Plastics Industry, Inc., February 1964, pp. (9-A) 1-10.

5. Fried, N.: The Response of Orthogonal Filament Wound Materials to Compressive Stress. Proceedings of the 20th Anniversary Technical Conference, Reinforced Plastics Division, Society of the Plastics Industry, Inc., February 1965, pp. (1-C) 1-8.

6. Levenetz, B.: Compressive Applications of Large Diameter Fiber Reinforced Plastics. Proceedings of the 19th Annual Technical and Management Conference, Reinforced Plastics Division, Society of the Plastics Industry, Inc., February 1964, pp. (14-D) 1-18.

7. Rosen, B. W.: Mechanics of Composite Strengthening. Fiber Composite Materials, American Society for Metals, 1965, pp. 37-75.

8. Dow, Norris F.; and Rosen, B. Walter: Evaluations of Filament-Reinforced Composites for Aerospace Structural Applications. NASA CR-207, April 1965.

9. Dow, N. F.; Rosen, B. W.; and Hashin, Z.: Studies of Mechanics of Filamentary Composites. NASA CR-492, June 1966.

10. Ekvall, J. C.: Structural Behavior of Monofilament Composites. Proceedings of AIAA 6th Structures and Materials Conference, 1965, pp. 250-263.

11. Hayashi, T.: On the Shear Instability of Structures Caused by Compressive Load. AIAA Paper No. 65-770, 1965.

12. Jones, Robert M.: Mechanics of Composite Materials. Scripta Book Co., 1975.

13. Schuerch, H.: Prediction of Compressive Strength in Uniaxial Boron Fiber - Metal Matrix Composite Materials. AIAA Journal, vol. 4, no. 1, January 1966, pp. 102-106.

14. Foye, R. L.: Compression Strength of Unidirectional Composites. AIAA Paper No. 66-143, 1966.

15. Herrmann, L. R.; Mason, W. E.; and Chan, S. T. K.: Response of Reinforcing Wires to Compressive States of Stress. Journal of Composite Materials, vol. 1, no. 3, 1967, pp. 212-226.

16. Sadowsky, M. A.; Pa, S. L.; and Hussain, M. A.: Buckling of Microfibers. Journal of Applied Mechanics, vol. 34, no.4, December 1967, pp. 1011-1016.

17. Crawford, R. F.: An Evaluation of Boron-Polymer Film Layer Composites for High-Performance Structures. NASA CR-1114, 1968.

18. Yue, A. S.; Crossman, F. W.; Vidoz, A. E.; and Jacobson, M. I.: Controlled Microstructures of Aℓ-$CuAℓ_2$ Eutectic Composites and Their Compressive Properties. Transactions of the Metallurgical Society of AIME, vol. 242, no. 12, December 1968, pp. 2441-2452.

19. Lager, J. B.; and June, R. R.: Compressive Strength of Boron-Epoxy Composites. Journal of Composite Materials, vol. 3, no. 1, January 1969, pp. 48-56.

20. Chung, W.; and Testa, R. B.: The Elastic Stability of Fibers in a Composite Plate. Journal of Composite Materials, vol. 3, no. 1, January 1969, pp. 58-80.

21. Biot, M. A.: Mechanics of Incremental Deformations. John Wiley and Sons, Inc., 1965.

22. Guz', A. N.: On Setting Up a Stability Theory of Unidirectional Fibrous Materials. Prikladnaya Mekhanika, vol. 5, no. 2, February 1969, pp. 62-70.

23. Guz', A. N.; Kritsuk, A. A.; and Yemel'yanov, R. F.: Nature of the Failure of a Unidirectional Fiberglass-Reinforced Plastic Under Compression. Prikladnaya Mekhanika, vol. 5, no. 9, September 1969, pp. 118-121. (Also available as NASA TT F-13,442.)

24. Guz', A. N.: Constructing a Theory for the Strength of Unidirectionally Reinforced Materials in Compression. Problemy Prochnosti, vol. 3, no. 3, March 1971, pp. 37-39.

25. Skudra, A. M.; Kalnays, A. A.; and Bulavs, F. Ya.: Creep-Rupture Strength of Reinforced Plastics Under Uniaxial Compression. Mekhanika Polimerov, vol. 5, 1969, pp. 621-628. (Also available as NASA TT F-13,441.)

26. Guz', O. M.: Determination of the Theoretical Compression Strength of Reinforced Materials. Dopovidi Akademii Nauk Ukrayns'koy RSR, Seriya A, Fiziko-Technichni i Matematichni Nauki, vol. 31, March 1969, pp. 236-238. (Also available as NASA TT F-13,443.)

27. Babich, I. Yu.; Garashchuk, I. N.; and Guz', A. N.: Stability of a Fiber in an Elastic Matrix with a Nonuniform Subcritical State. Soviet Applied Mechanics, vol. 19, no. 11, 1983, pp. 941-947.

28. De Ferran, E. M.; and Harris, B.: Compression Strength of Polyester Resin Reinforced with Steel Wires. Journal of Composite Materials, vol. 4, no. 1, January 1970, pp. 62-72.

29. Kiusalaas, J.; and Jaunzemis, W.: Internal Buckling of a Laminated Medium. Developments in Theoretical and Applied Mechanics, vol. 5, Proceedings of the 5th Southeastern Conference on Theoretical and Applied Mechanics, Grover L. Rogers, ed., The University of North Carolina Press, 1970, pp. 151-173.

30. Hayashi, T.: Compressive Strength of Unidirectionally Fibre Reinforced Composite Materials. Seventh International Reinforced Plastics Conference, British Plastics Federation, October 1970, pp. 11/1-11/3.

31. Hayashi, T.; and Koyama, K.: Theory and Experiments of Compressive Strength of Unidirectionally Fiber-Reinforced Composite Materials. Mechanical Behavior of Materials; Proceedings of the First International Conference, vol. 5, Japanese Society of Materials Science, 1972, pp. 104-112.

32. Orringer, O.: Compressive Behavior of Fiber Composites. AFOSR-TR-71-3098, 1971.

33. Greszczuk. L. B.: Microbuckling of Unidirectional Composites, AFML-TR-71-231, U. S. Air Force, January 1972.

34. Greszczuk. L. B.: Failure Mechanics of Composites Subjected to Compressive Loading. AFML-TR-72-107, U. S. Air Force, August 1972.

35. Greszczuk, L. B.: Compressive Strength and Failure Modes of Unidirectional Composites. Analysis of the Test Methods for High Modulus Fibers and Composites, ASTM STP 521, American Society for Testing and Materials, 1973, pp. 192-217.

36. Greszczuk, L. B.: Microbuckling of Lamina-Reinforced Composites. Composite Materials: Testing and Design (Third Conference), ASTM STP 546. American Society for Testing and Materials, 1974, pp. 5-29.

37. Greszczuk, L. B.: Microbuckling Failure of Circular Fiber-Reinforced Composites. AIAA Paper No. 74-354, 1974.

38. Greszczuk, L. B.: On Failure Modes of Unidirectional Composites Under Compressive Loading. Fracture of Composite Materials; Proceedings of the 2nd USA-USSR Symposium, Martinus Nijhoff Publishers, 1982, pp. 231-244.

39. Greszczuk, L. B.: Prediction of Strength Properties of Multilayer, Multidirectional Composites from Properties of Constituents-Fibers and Matrix. AIAA Paper No. 83-0836-CP, 1983.

40. Suarez, J. A.; Whiteside, J. B.; and Hadcock, R. N.: The Influence of Local Failure Modes on the Compressive Strength of Boron/Epoxy Composites. Composite Materials: Testing and Design (Second Conference), ASTM STP 497, American Society for Testing and Materials, 1972, pp. 237-256.

41. Hackett, R. M.; Tarpy, T. S., Jr.; and Wood, J. L.: An Analysis of Fiber Buckling. Polymer Engineering and Science, vol. 12, no. 4, July 1972, pp. 272-276.

42. Lanir, Y.; and Fung, Y. C. B.: Fiber Composite Columns Under Compression. Journal of Composite Materials, vol. 6, no. 3, July 1972, pp. 387-401.

43. Kao, B.; and Pipkin, A. C.: Finite Buckling of Fiber-Reinforced Columns. Acta Mechanica, vol. 13, no. 3-4, 1972, pp. 265-280.

44. Kulkarni, S. V.; Rice, J. S.; and Rosen, B. W.: An Investigation of the Compressive Strength of PRD-49-III/Epoxy Composites. NASA CR-112334, June 1973.

45. Kulkarni, S. V.; Rice, J. S.; and Rosen, B. W.: An Investigation of the Compressive Strength of Kevlar 49/Epoxy Composites. Composites, vol. 6, no. 5, Sept. 1975, pp. 217-225.

46. Davis, J. G., Jr.: Compressive Strength of Lamina Reinforced and Fiber Reinforced Composite Materials. Ph.D. Dissertation, Virginia Polytechnic Institute and State University, May 1973.

47. Davis, J. G., Jr.: Compressive Strength of Fiber-Reinforced Composite Materials. Composite Reliability, ASTM STP 580, American Society for Testing and Materials, 1975, pp. 364-377.

48. Hanasaki, S.; and Hasegawa, Y.: Compressive Strength of Unidirectional Fibrous Composites. Journal of Composite Materials, vol. 8, no. 3, July 1974, pp. 306-309.

49. Wang, A. S. D.: A Nonlinear Microbuckling Model Predicting the Compressive Strength of Unidirectional Composites. ASME Paper No. 78-WA/AERO-1, 1978.

50. Evans, A. G.; and Adler, W. F.: Kinking as a Mode of Structural Degradation in Carbon Fiber Composites. Acta Metallurgica, vol. 26, no. 5, May 1978, pp. 725-738.

51. Maewal, A.: Postbuckling Behavior of a Periodically Laminated Medium in Compression. International Journal of Solids and Structures, vol. 17, no. 3, 1981, pp. 335-344.

52. Budiansky, B.: Micromechanics. Computers and Structures, vol. 16, no. 1-4, 1983, pp. 3-12.

53. Hahn, H. T.; and Williams, J. G.: Compression Failure Mechanisms in Undirectional Composites. NASA TM 85834, 1984.

54. Zimmerman, R. S.; Adams, D. F.; and Walrath, D. E.: Investigation of the Relations Between Neat Resin and Advanced Composite Mechanical Properties, Volume I - Results. NASA CR-172303, 1984.

55. Kreyszig, E.: Advanced Engineering Mathematics, Third ed. John Wiley and Sons, Inc., 1972.

56. Kantorovich, L. V.; and Krylov, V. I. (C. D. Benster, transl.): Approximate Methods of Higher Analysis. Interscience Publishers, Inc., 1964, pp. 304-327.

57. Ashton, J. E.; and Whitney, J. M.: Theory of Laminated Plates. Technomic Publishing Co., 1970.

58. Lentini, M.; and Pereyra, V.: An Adaptive Finite Difference Solver for Nonlinear Two-Point Boundary Problems with Mild Boundary Layers. SIAM Journal on Numerical Analysis, vol. 14, no. 1, March 1977, pp. 91-111.

59. Stein, M.: Postbuckling of Orthortropic Composite Plates Loaded in Compression. AIAA Journal, vol. 21, no. 12, December 1983, pp. 1729-1735.

60. Stein, M.: Postbuckling of Long Orthotropic Plates Under Combined Loading. AIAA Journal, vol. 23, no. 8, August 1985, pp. 1267-1272.

61. D 3410-75 Standard Test Method for Compressive Properties of Unidirectional or Crossply Fiber-Resin Composites. 1982 Annual Book of ASTM Standards, Part 36, American Society for Testing and Materials, 1982, pp. 872-880.

62. Sandorff, P. E.; Ryder, J. T.; and Lauraitis, K. N.: Experimental Evaluation of Column Compression Properties of Graphite/Epoxy Composites. Composites Technology Review, vol. 3, no. 1, Spring 1981, pp. 6-16.

63. Pipes, R. B.: Solution of Certain Problems in the Theory of Elasticity for Laminated Anisotropic Systems. Ph.D. Dissertation, University of Texas at Arlington, March 1972.

64. Shuart, Mark J.; and Williams, Jerry G.: Compression Failure Characteristics of ±45°-Dominated Laminates with a Circular Hole and Impact Damage. AIAA Paper No. 84-0848, 1984.

Table 2.1. Typical elastic properties for the graphite-epoxy fiber-plate and matrix-foundation.

Fiber - Plate	
Longitudinal Young's modulus, E_{11}, Msi	18.50
Transverse Young's modulus, E_{22}, Msi	1.64
Shear modulus, G_{12}, Msi	0.87
Major Poisson's ratio, ν_{12}	0.30
Minor Poisson's ratio, ν_{21}	0.03†
Matrix - Foundation [54]	
Young's modulus, E_m, Msi	0.59
Shear modulus, G_m, Msi	0.26
Poisson's ratio, ν_m	0.36

†calculated using the reciprocal relation

$$\frac{\nu_{12}}{E_{11}} = \frac{\nu_{21}}{E_{22}}$$

Table 3.1. Short-wavelength buckling results for selected two-lamina laminates.

Laminate Orientation	Compressive Stress, ksi	Compressive Strain	Half-Wavelength, in.
$[0]_s$	289.6	0.0157	0.2158
$[+10]_s$	283.1	.0165	.2188
$[+30]_s$	251.4	.0342	.2255
$[+45]_s$	253.7	.0848	.2066
$[+60]_s$	279.7	.1484	.1544
$[+80]_s$	287.4	.1741	.1189
$[90]_s$	287.5	.1753	.1177

Table 3.2. Short-wavelength buckling results for selected four-lamina laminates.

Laminate Orientation	Compressive Stress, ksi	Compressive Strain	Half-Wavelength, in.
$[0_2]_s$	433.5	0.0234	0.1905
$[\pm 10]_s$	433.4	.0253	.1910
$[\pm 30]_s$	432.7	.0589	.1703
$[\pm 45]_s$	431.9	.1444	.1450
$[\pm 60]_s$	431.2	.2289	.1173
$[\pm 80]_s$	430.8	.2610	.0969
$[90]_s$	430.8	.2627	.0973
$[0/90]_s$	431.6	.0426	.1336

Table 3.3. Short-wavelength buckling results for selected eight-lamina laminates.

Laminate Orientation	Compressive Stress, ksi	Compressive Strain	Half Wavelength, in.
$[0_4]_s$	505.4	0.0273	0.1854
$[(\pm 45)_2]_s$	503.7	.1684	.1371
$[0/\pm 45/90]_s$	438.8	.0589	.0140
$[0/+45/90/-45]_s$	437.2	.0587	.0182
$[+45/0/-45/90]_s$	501.2	.0675	.0477
$[90/+45/0/-45]_s$	503.6	.0678	.1336

Table 3.4. Laminate compressive strengths.

Laminate Orientation	Predicted Strength, ksi	Experimental Strength, ksi	Difference†, percent
$[0]_T$	195.1	204	- 4.4
$[0/90]_s$	106.2	110	- 3.5
$[0/\pm45/90]_s$	64.9	66	- 1.7

† $\frac{\text{(predicted) - (experimental)}}{\text{(experimental)}}$

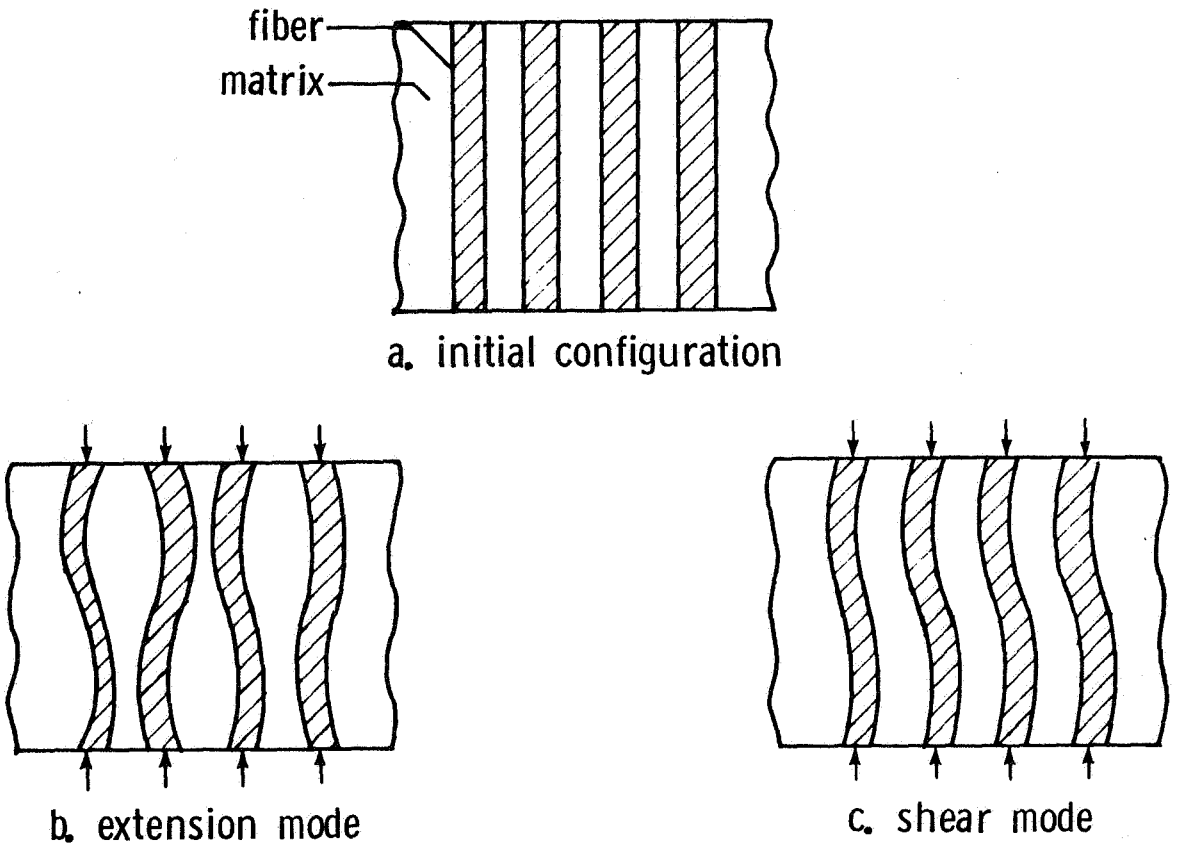

Figure 1.1. Initial configuration and buckling mode shapes.

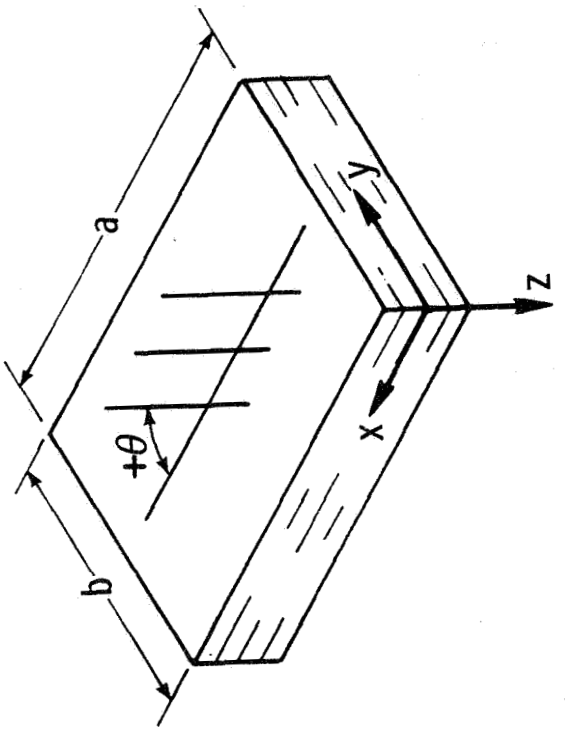

Figure 2.1. Coordinate system and dimensions for a typical laminate.

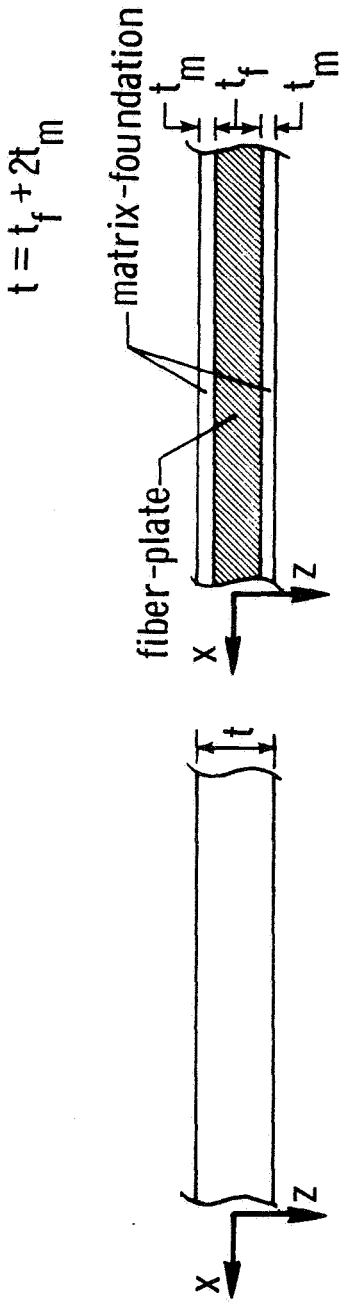

Figure 2.2. Typical and idealized lamina geometry.

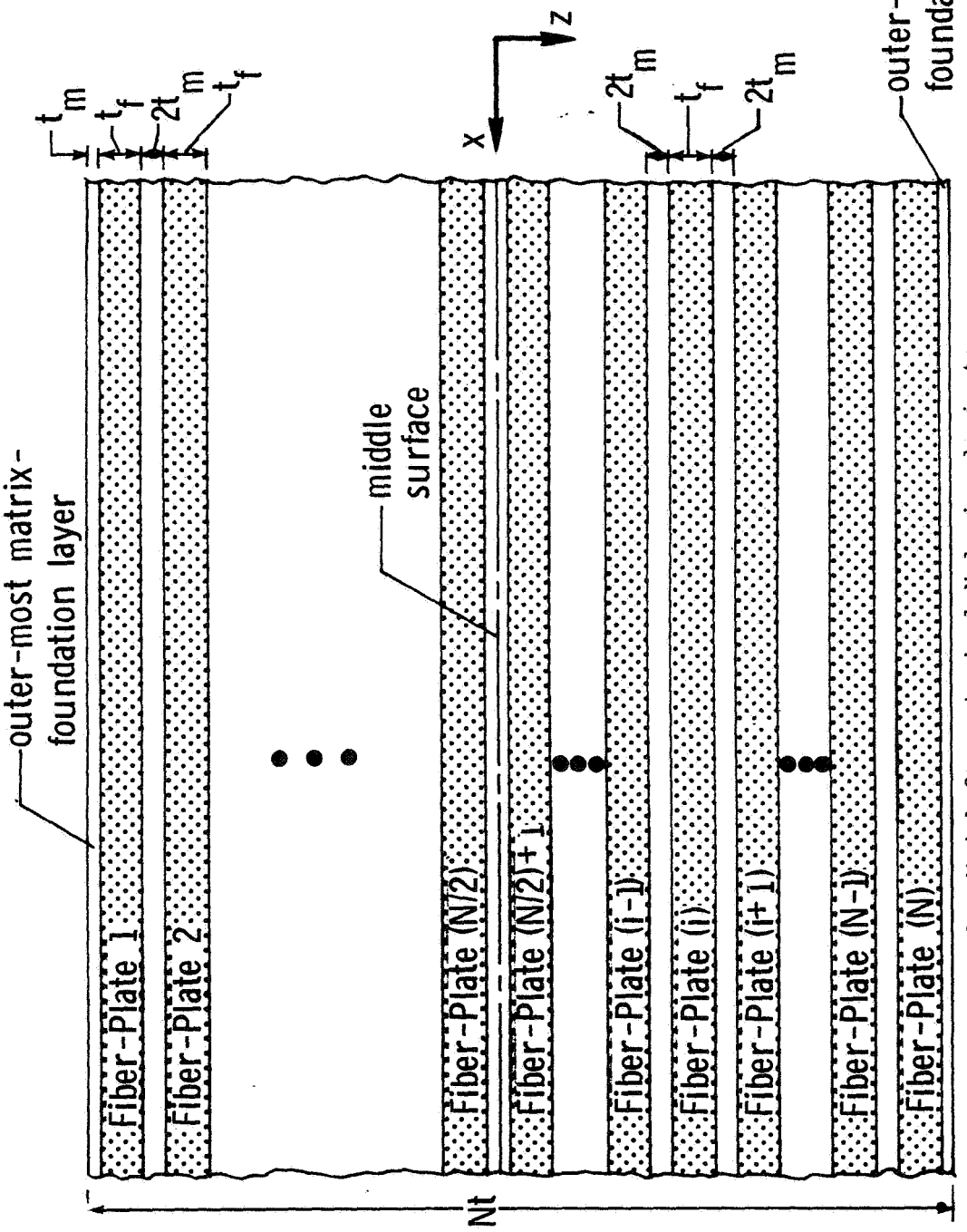

Figure 2.3. Model for a typical N-lamina laminate.

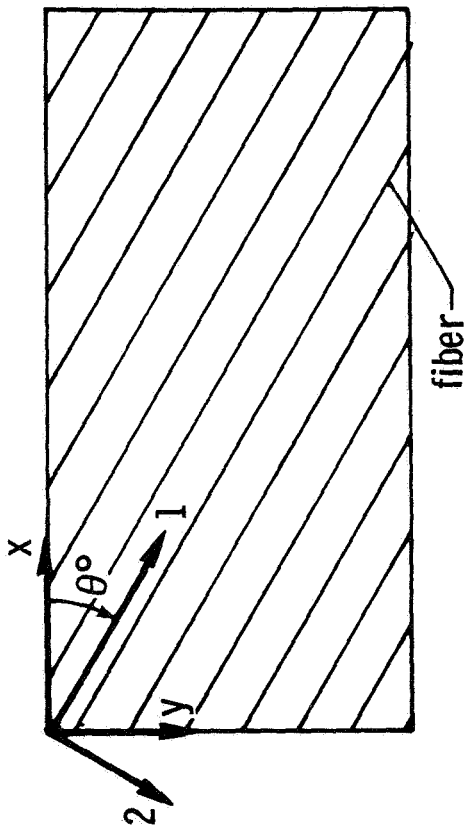

Figure 2.4. Principal material axes (1,2) and laminate axes (x,y) for a lamina with a +θ fiber orientation.

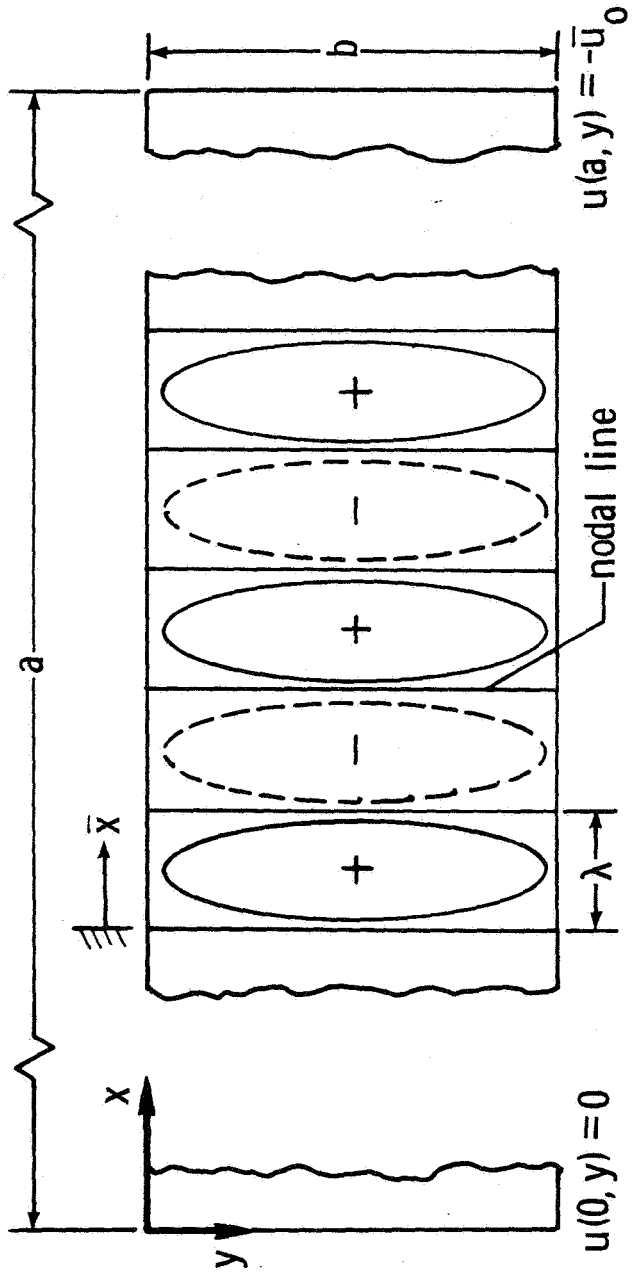

Figure 2.5. Short-wavelength buckling mode shapes.

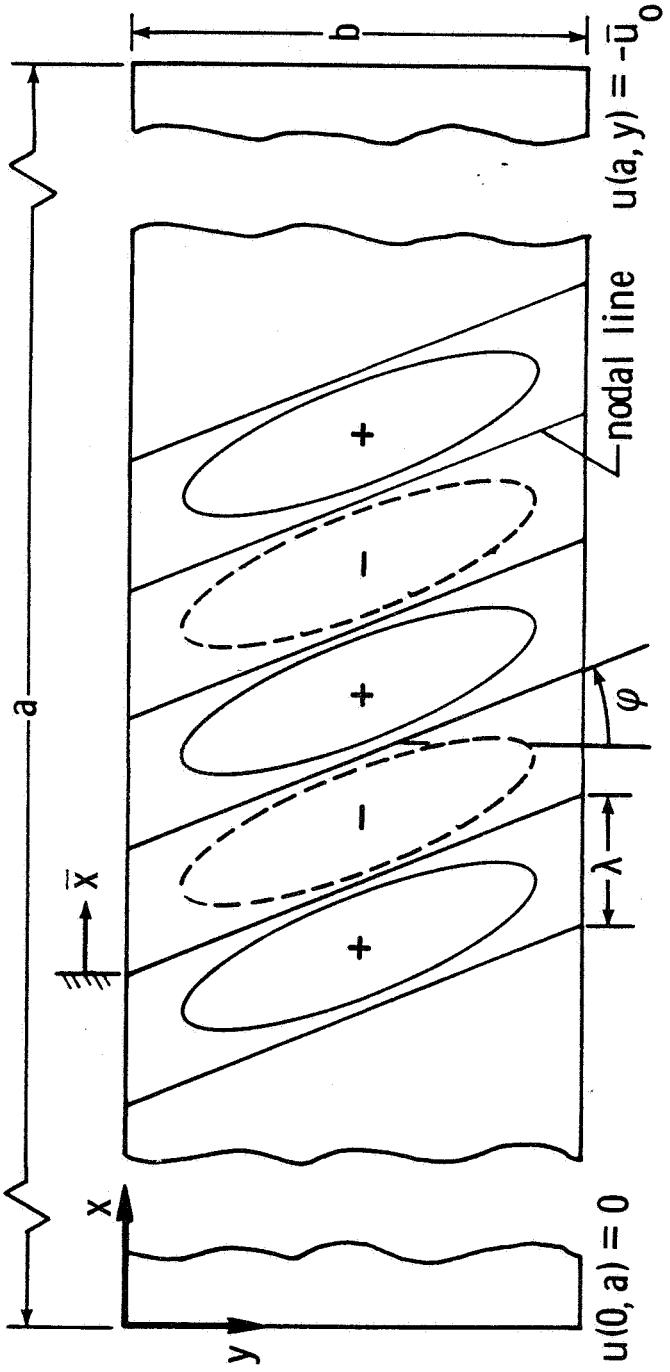

Figure 2.5. Concluded.

$$
\begin{bmatrix}
\bar{L}^{(1)}_{odd} & \bar{H}^{(1)} & -\bar{N}_{odd} & 0 & 0 & 0 & \cdots & 0 & 0 & 0 & 0 \\
\bar{H}^{(1)} & \bar{L}^{(1)}_{even} & 0 & \bar{N}_{even} & 0 & 0 & \cdots & 0 & 0 & 0 & 0 \\
-\bar{N}_{odd} & 0 & \bar{L}^{(2)}_{odd} & \bar{H}^{(2)} & -\bar{N}_{odd} & 0 & \cdots & 0 & 0 & 0 & 0 \\
0 & -\bar{N}_{even} & \bar{H}^{(2)} & \bar{L}^{(2)}_{even} & 0 & -\bar{N}_{even} & \cdots & 0 & 0 & 0 & 0 \\
0 & 0 & -\bar{N}_{odd} & 0 & \bar{L}^{(3)}_{odd} & \bar{H}^{(3)} & \cdots & 0 & 0 & 0 & 0 \\
0 & 0 & 0 & -\bar{N}_{even} & \bar{H}^{(3)} & \bar{L}^{(3)}_{even} & \cdots & 0 & 0 & 0 & 0 \\
\vdots & \vdots & \vdots & \vdots & \vdots & \vdots & & \vdots & \vdots & \vdots & \vdots \\
0 & 0 & 0 & 0 & 0 & 0 & \cdots & \bar{L}^{(n-1)}_{odd} & \bar{H}^{(n-1)} & -\bar{N}_{odd} & 0 \\
0 & 0 & 0 & 0 & 0 & 0 & \cdots & \bar{H}^{(n-1)} & \bar{L}^{(n-1)}_{even} & 0 & -\bar{N}_{even} \\
0 & 0 & 0 & 0 & 0 & 0 & \cdots & -\bar{N}_{odd} & 0 & \bar{L}^{(n)}_{odd} & \bar{H}^{(n)} \\
0 & 0 & 0 & 0 & 0 & 0 & \cdots & 0 & -\bar{N}_{even} & \bar{H}^{(n)} & \bar{L}^{(n)}_{even}
\end{bmatrix}
\begin{Bmatrix}
(w_s)^{(1)}_{odd} \\
(w_c)^{(1)}_{even} \\
(w_s)^{(2)}_{odd} \\
(w_c)^{(2)}_{even} \\
(w_s)^{(3)}_{odd} \\
(w_c)^{(3)}_{even} \\
\vdots \\
(w_s)^{(n-1)}_{odd} \\
(w_c)^{(n-1)}_{even} \\
(w_s)^{(n)}_{odd} \\
(w_c)^{(n)}_{even}
\end{Bmatrix}
= \{0\}
$$

Figure 2.6 . Equations (2.69) for the linear analysis of a model with anisotropic fiber-plates.

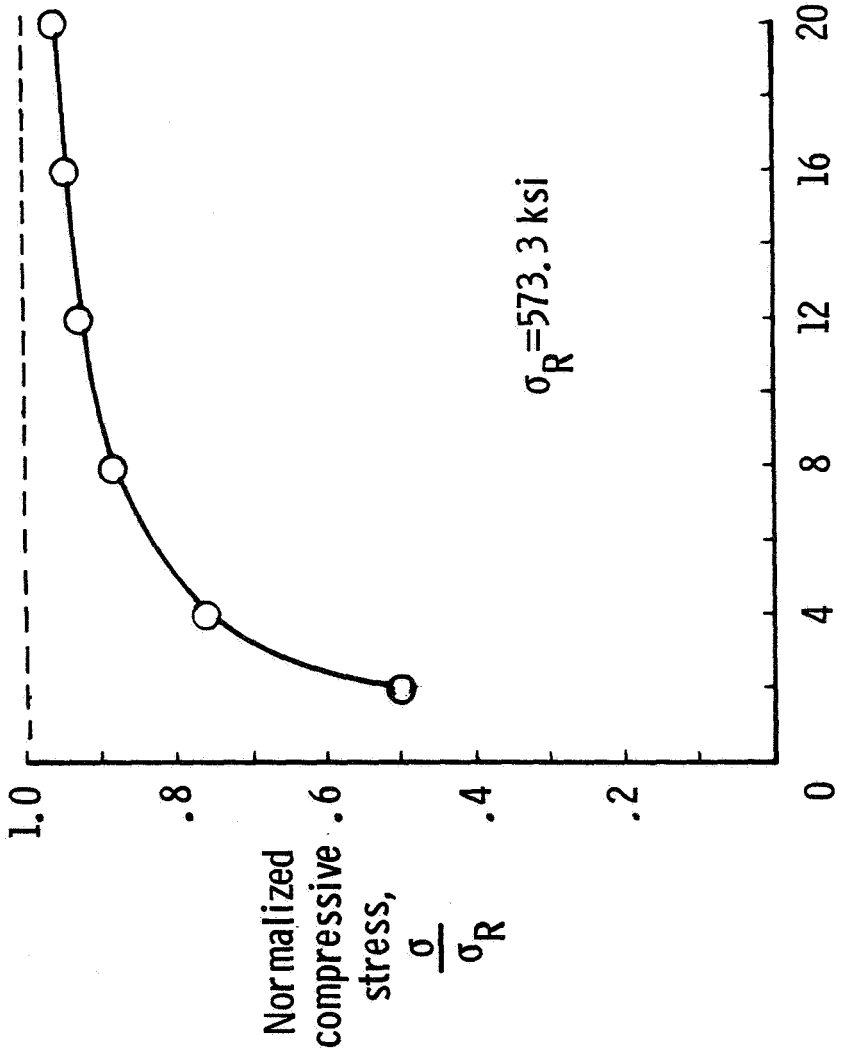

Figure 3.1. Normalized compressive stress for short-wavelength buckling of a $[0]_s$-class laminate as a function of the number of laminae.

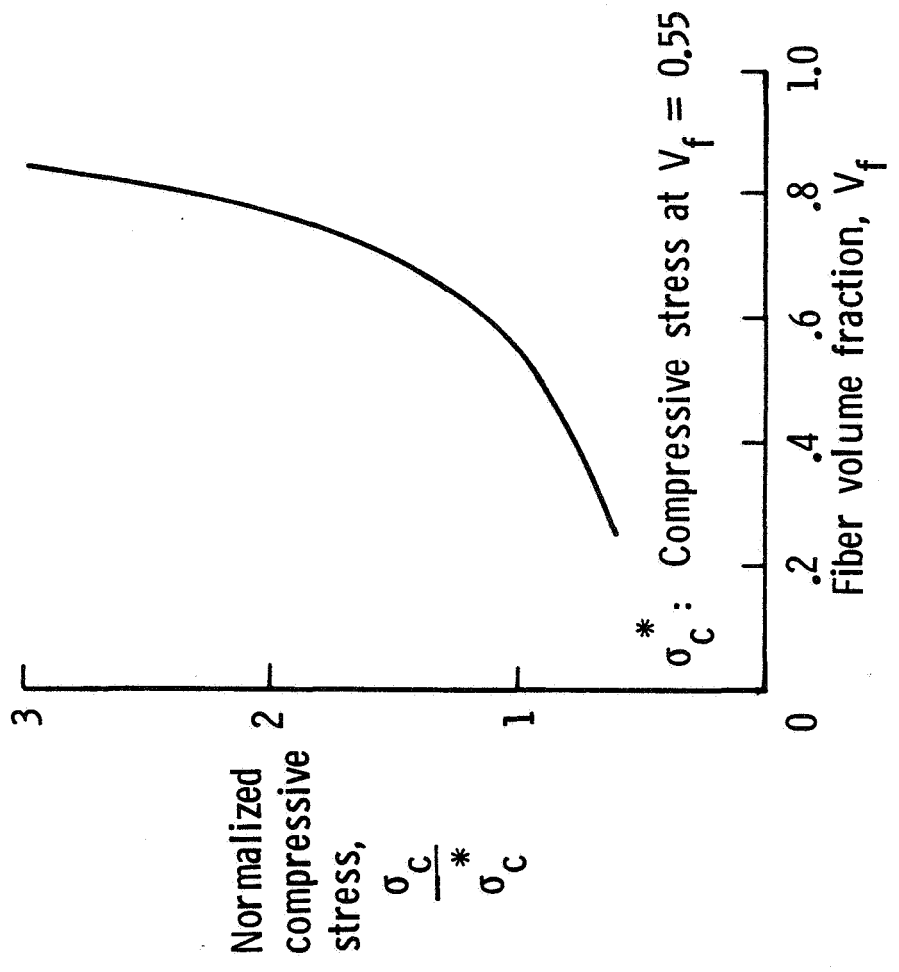

Figure 3.2. Normalized laminate compressive stress for short-wavelength buckling as a function of fiber volume fraction.

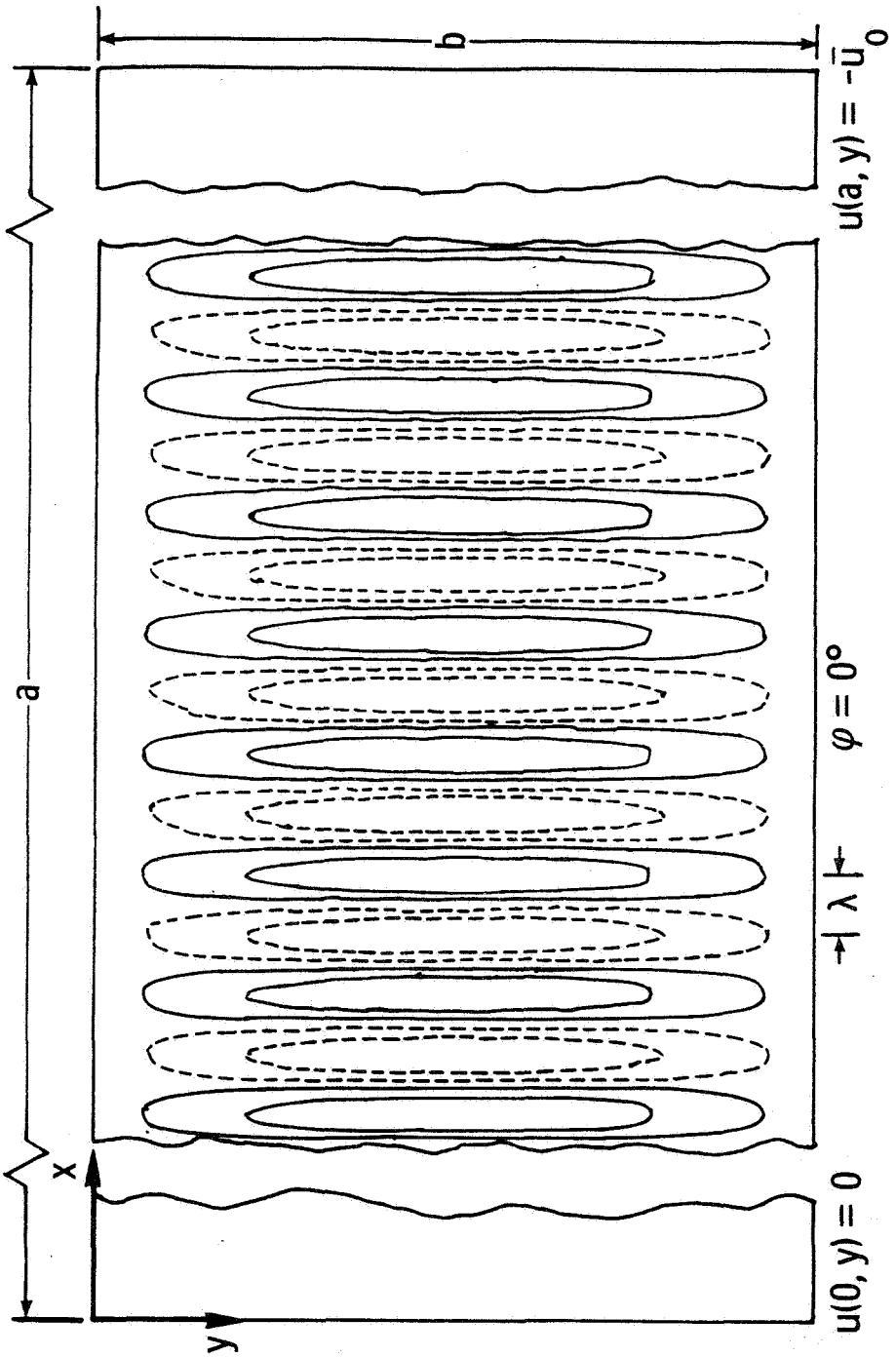

Figure 3.3. Mode shape for short-wavelength buckling of a $[0]_s$ laminate (normal waves).

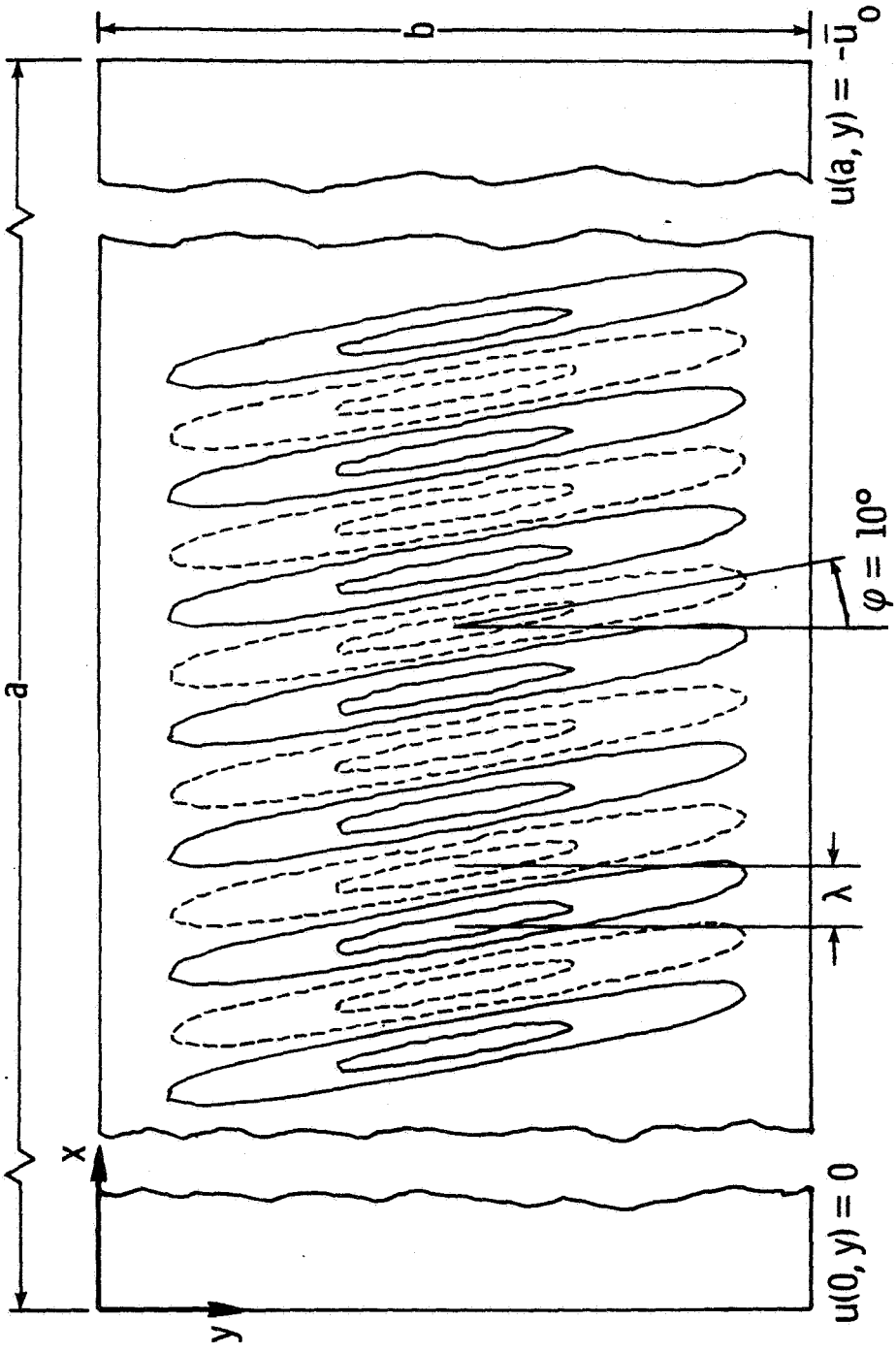

Figure 3.4. Mode shape for short-wavelength buckling of a $[+10]_s$ laminate (skewed waves).

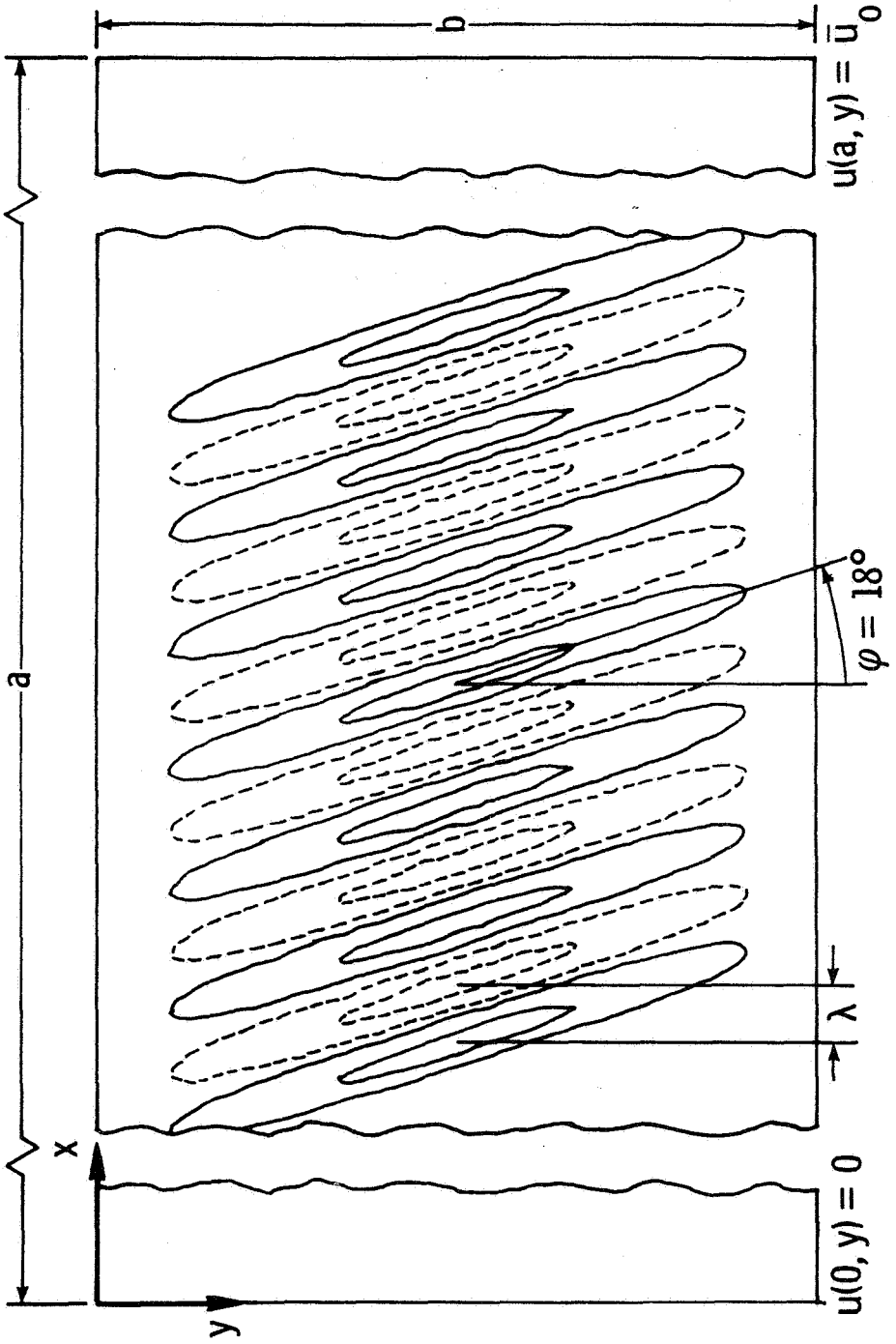

Figure 3.5. Mode shape for short-wavelength buckling of a $[+20]_s$ laminate (skewed waves)

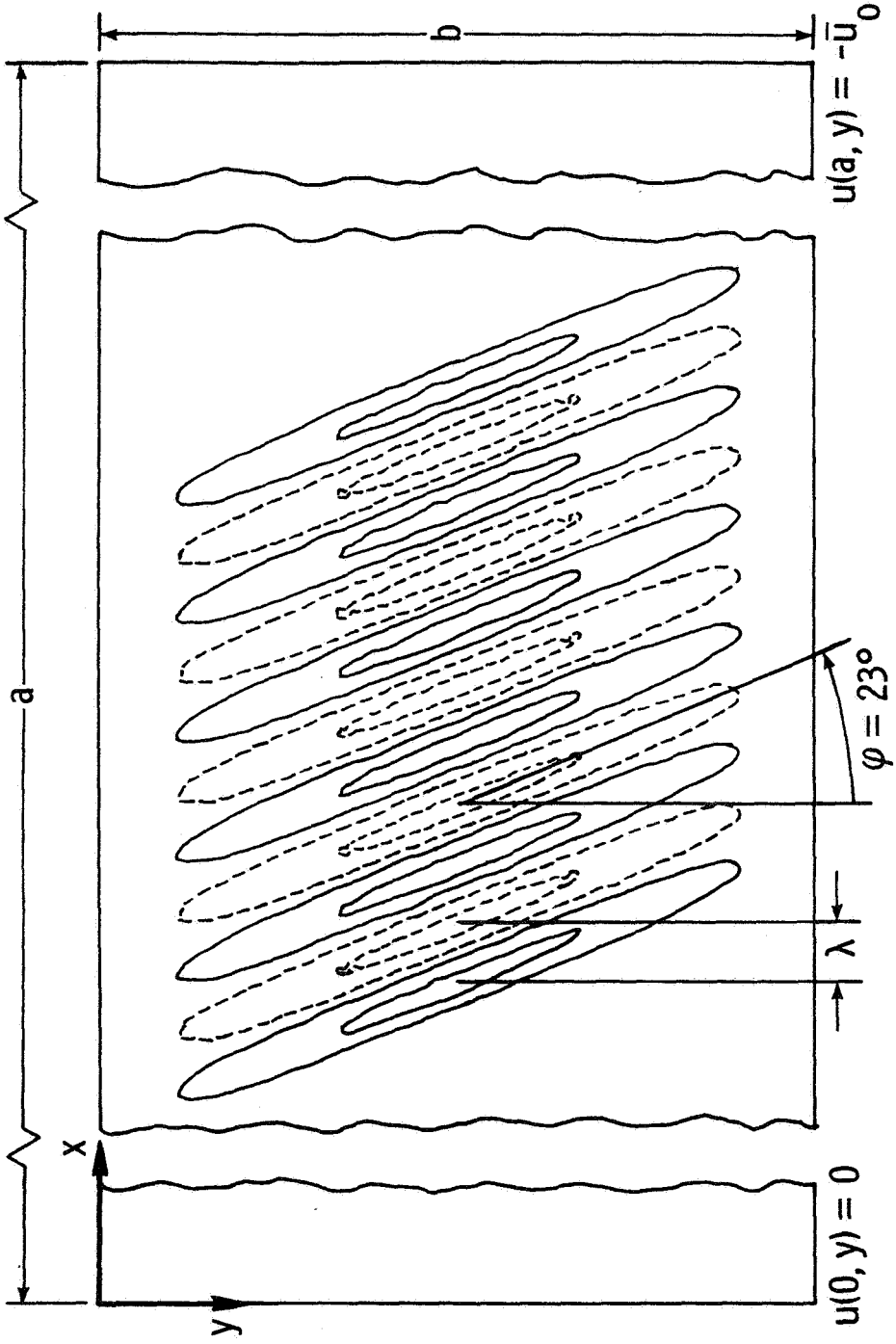

Figure 3.6. Mode shape for short-wavelength buckling of a $[+30]_s$ laminate (skewed waves).

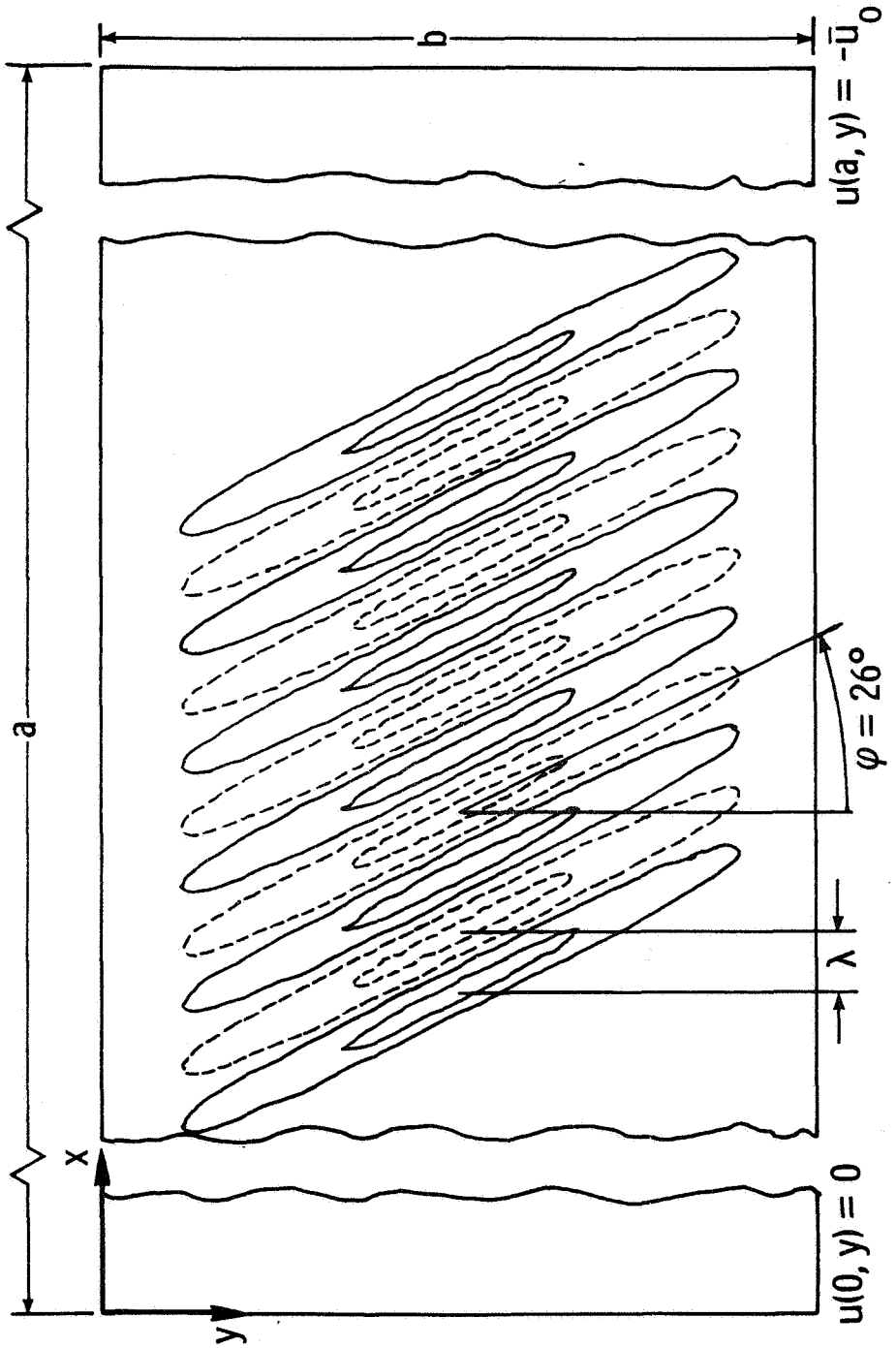

Figure 3.7. Mode shape for short-wavelength buckling of a $[+45]_s$ laminate (skewed waves).

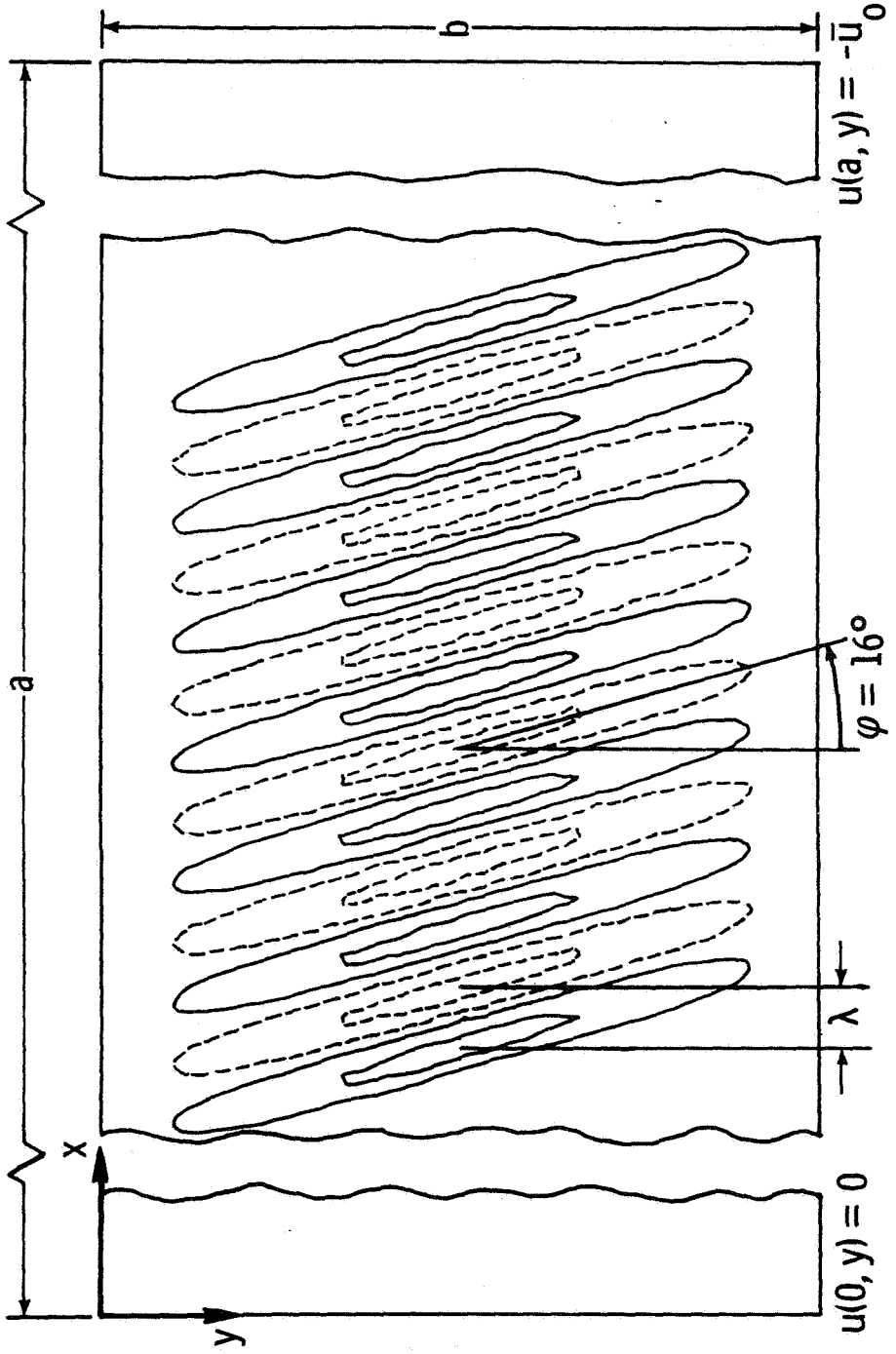

Figure 3.8. Mode shape for short-wavelength buckling of a $[+60]_s$ laminate (skewed waves).

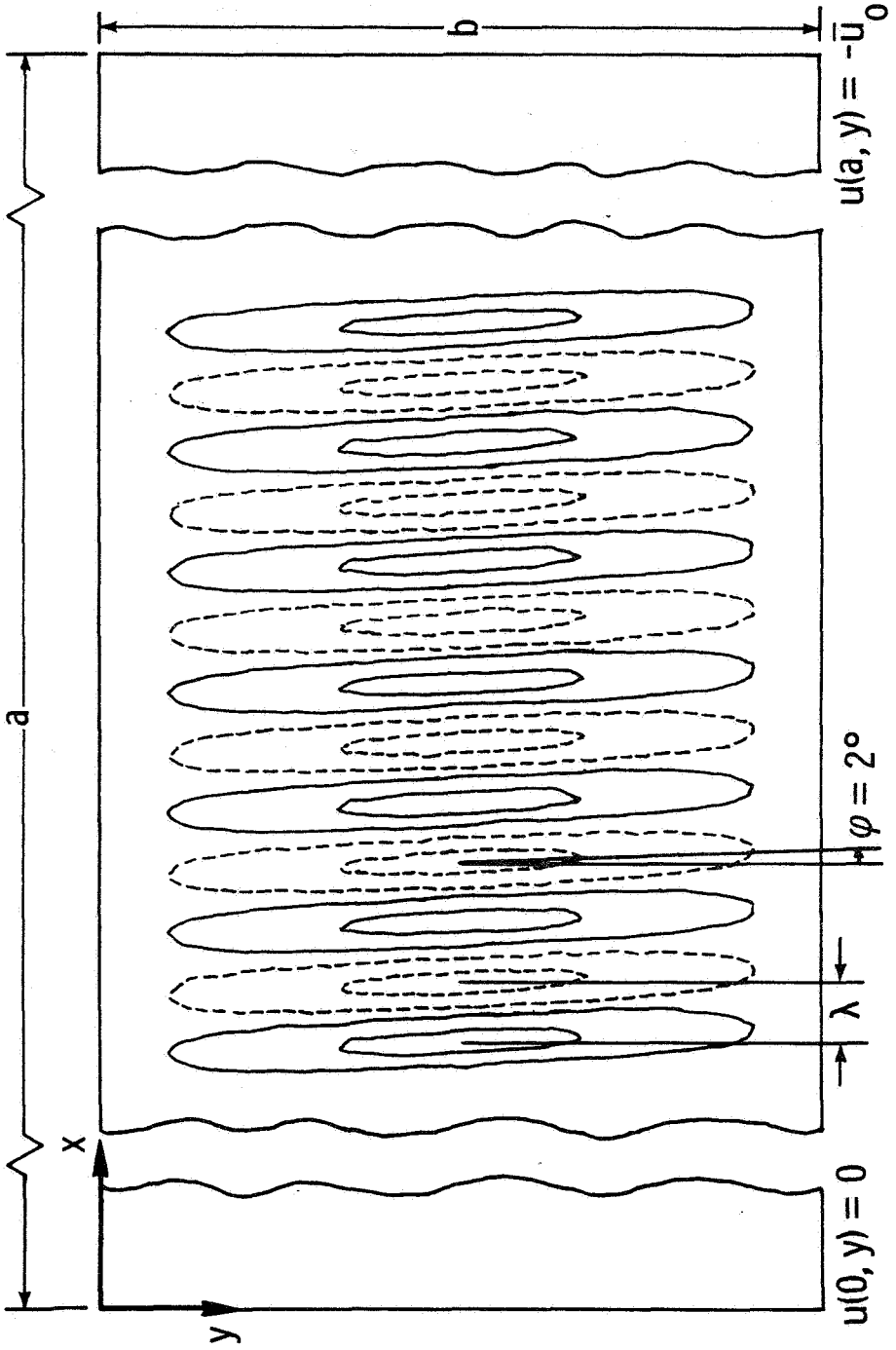

Figure 3.9. Mode shape for short-wavelength buckling of a $[+80]_s$ laminate (skewed waves).

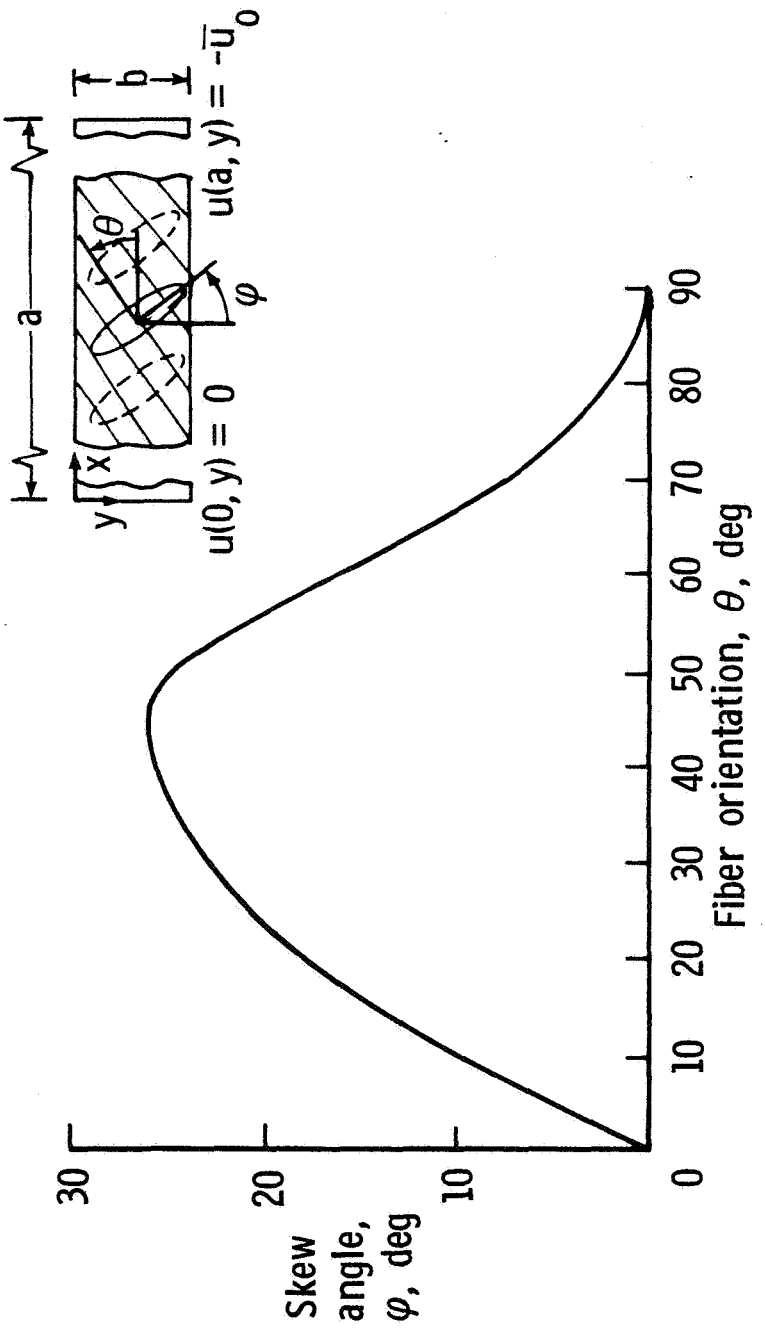

Figure 3.10. Skew angle for the laminate mode shape as a function of fiber orientation.

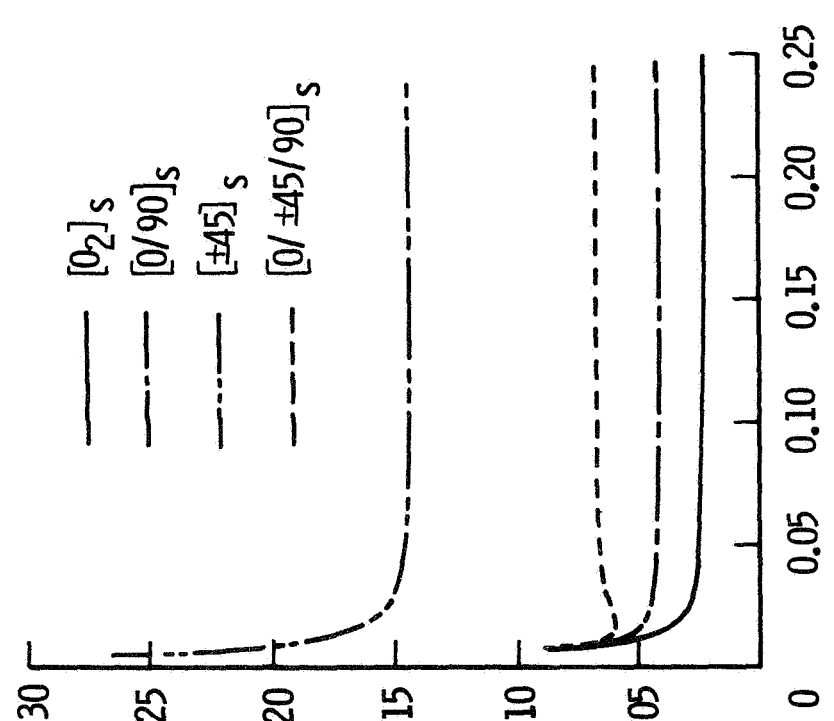

Figure 3.11. Compressive strain for short-wavelength buckling as a function of laminate half-wavelength.

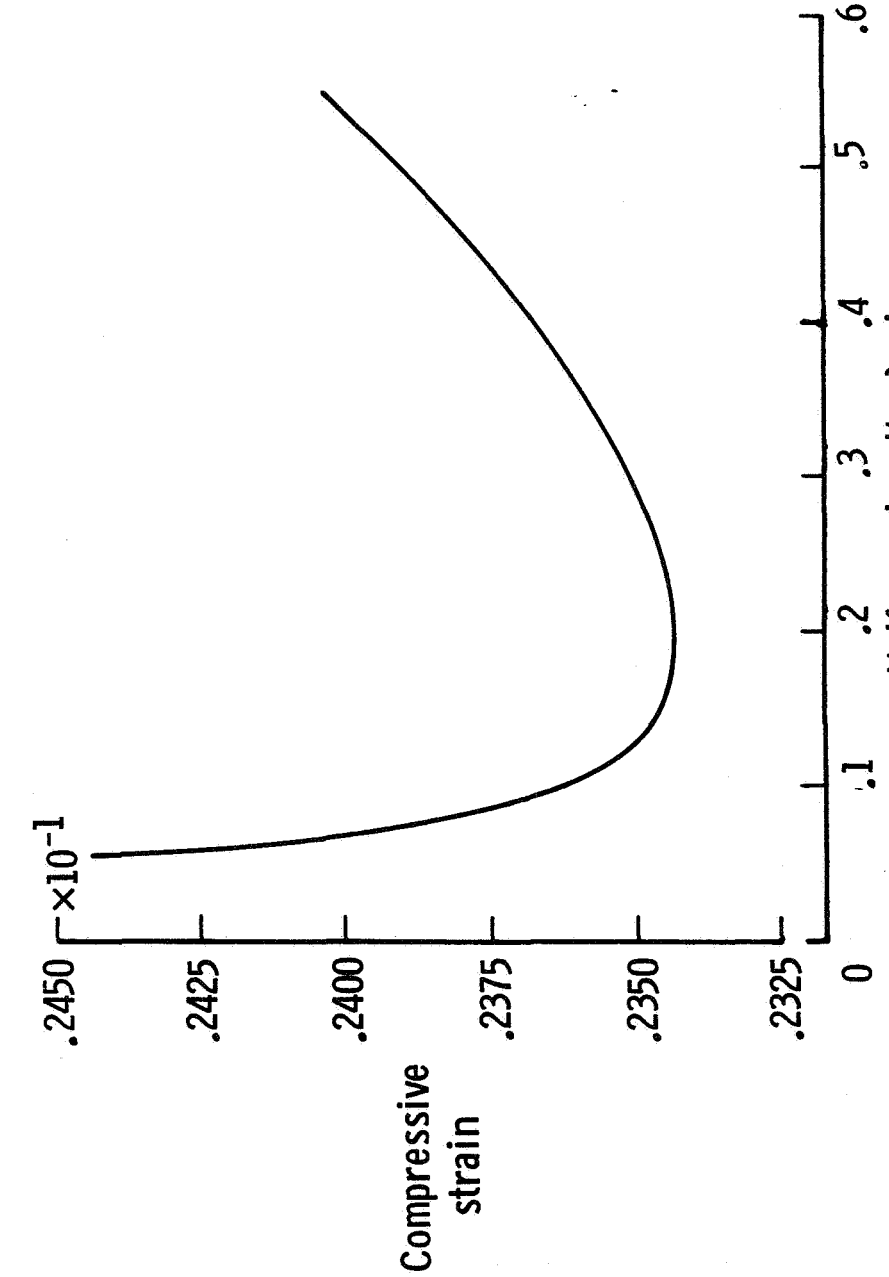

Figure 3.12. Compressive strain for short-wavelength buckling as a function of laminate half-wavelength for a $[0_2]_s$ laminate (expanded ordinate).

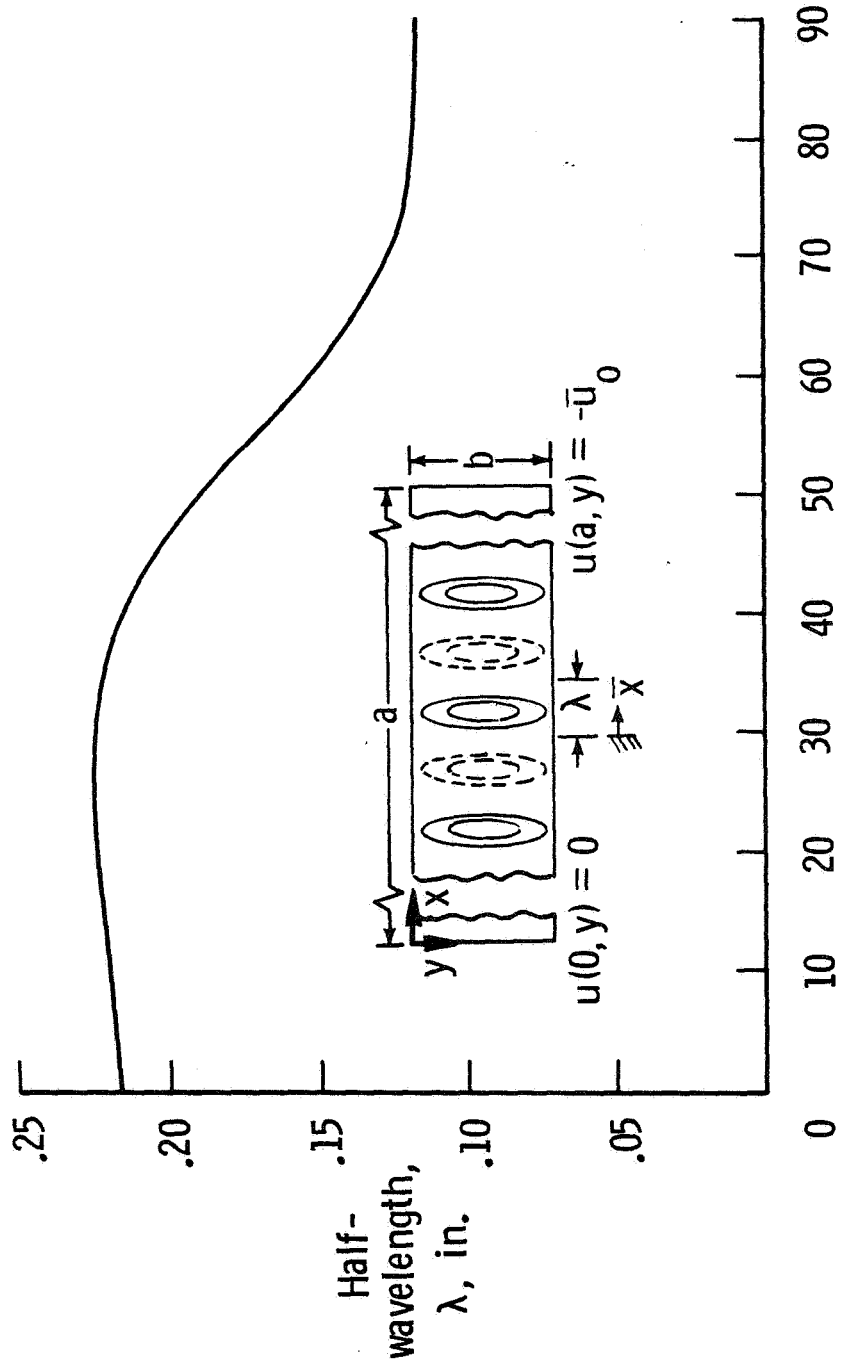

Figure 3.13. Half-wavelength of the buckling mode as a function of lamina orientation for a $[+\theta]_s$ laminate.

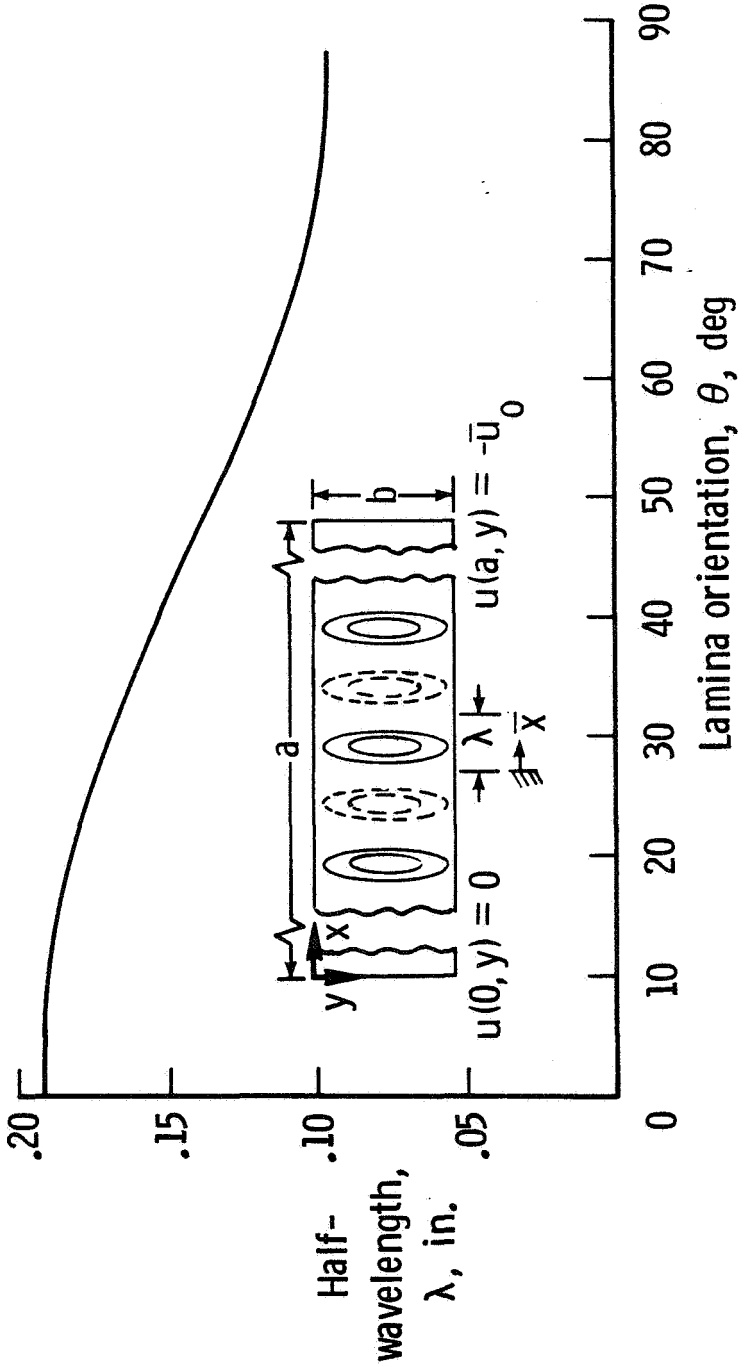

Figure 3.14. Half-wavelength of the buckling mode as a function of lamina orientation for a $[\pm\theta]_s$ laminate.

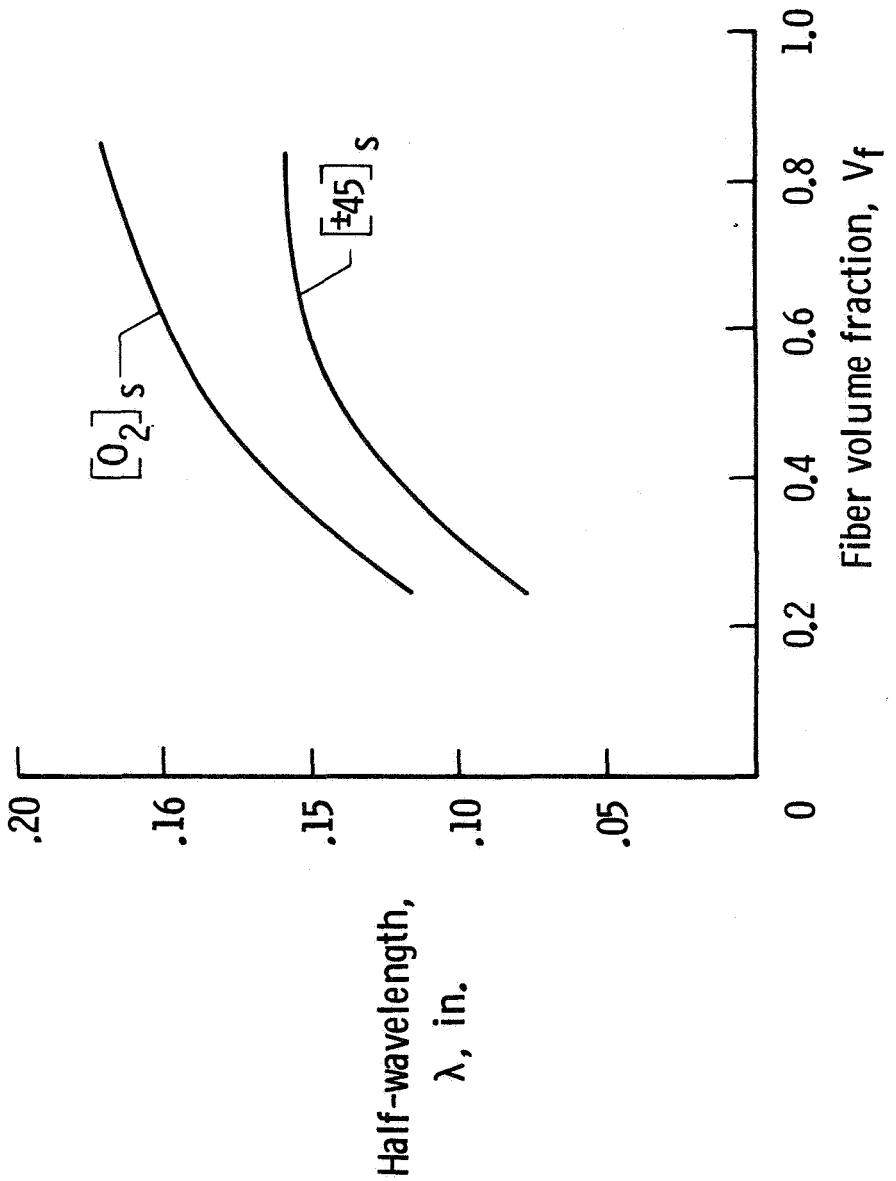

Figure 3.15. Half-wavelength for short-wavelength buckling as a function of laminate fiber volume fraction.

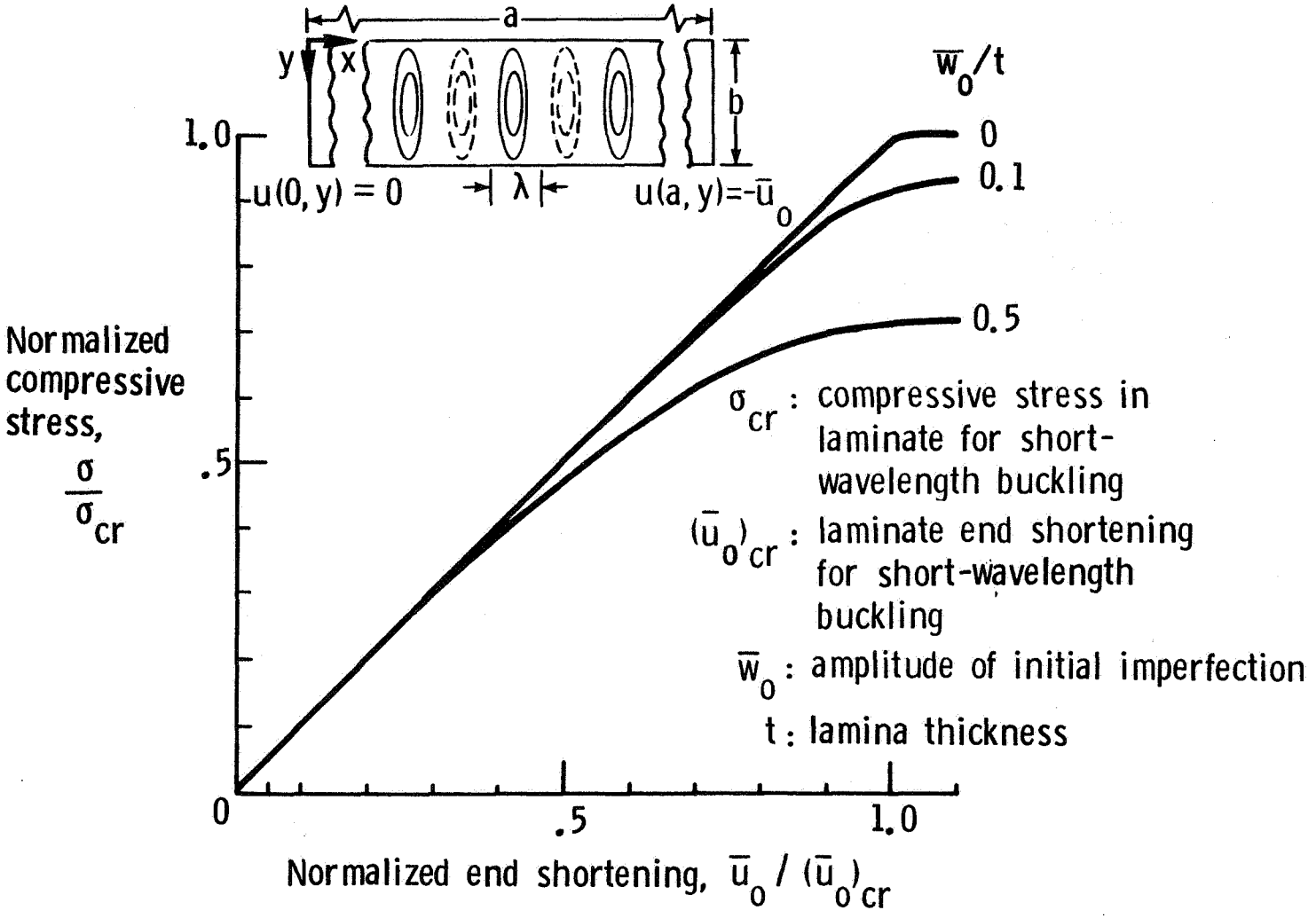

Figure 3.16. Normalized compressive stress versus end shortening for a $[0_2]_s$ laminate.

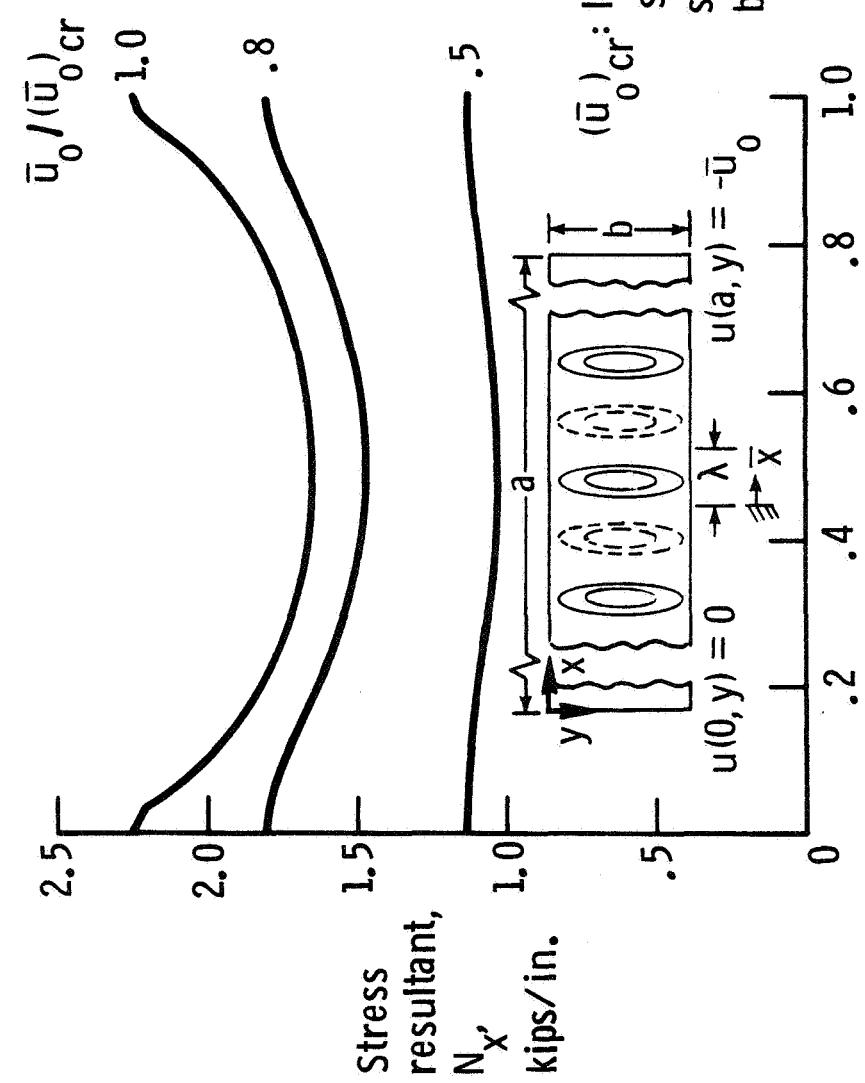

Figure 3.17. Stress resultant for a 0° lamina in a $[0_2]_s$ laminate ($\bar{w}_o/t = 0.5$).

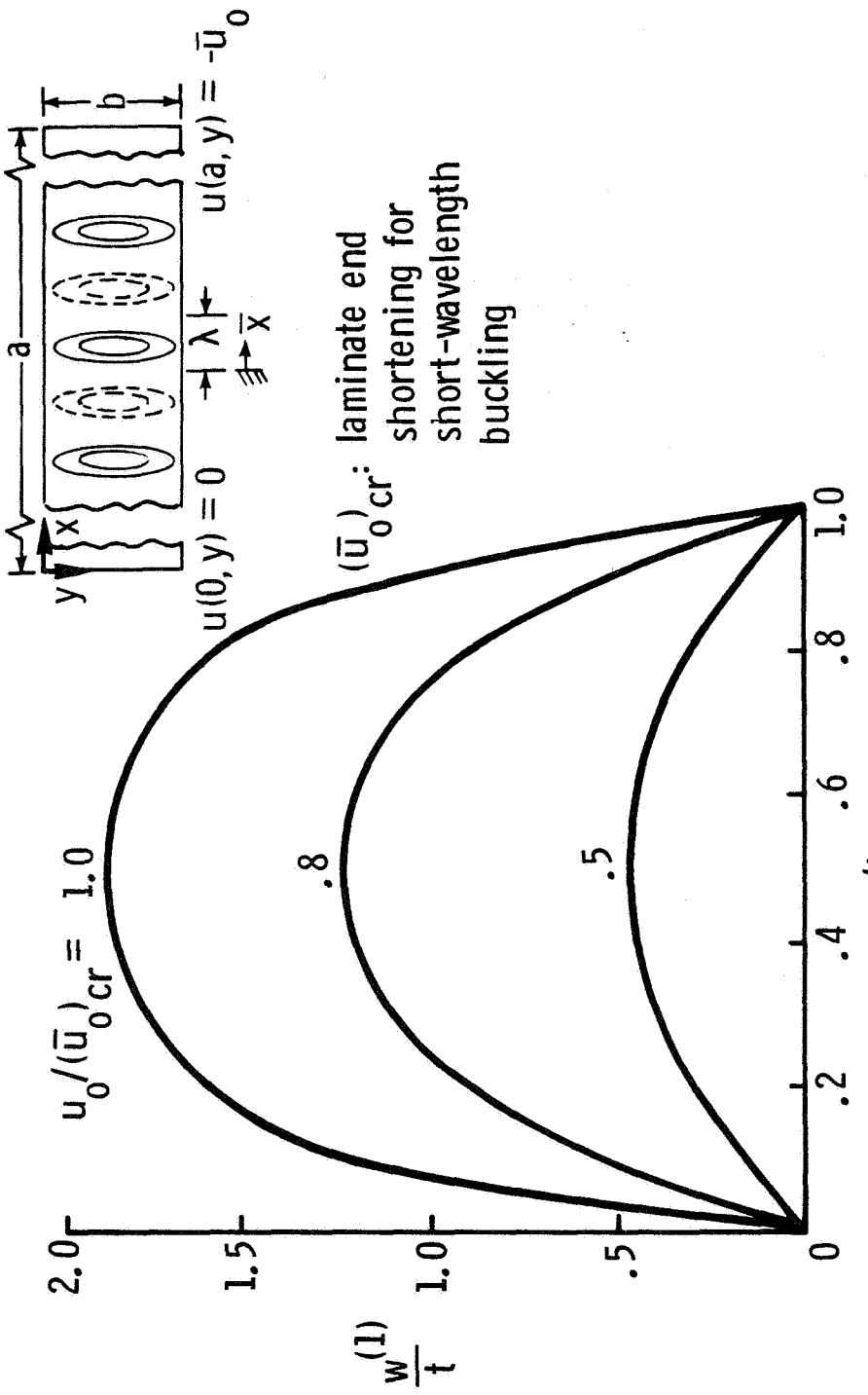

Figure 3.18. Distribution of the w displacement for the outer-most 0° lamina in a $[0_2]_s$ laminate along $\bar{x} = \lambda/2$ ($\bar{w}_o/t = 0.5$).

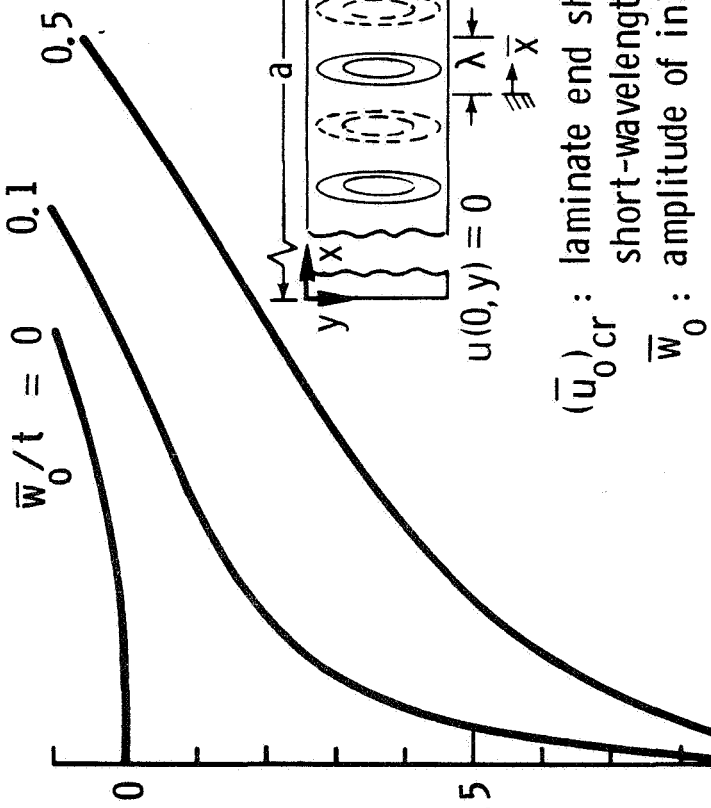

Figure 3.19. Maximum w displacement as a function of end shortening for a $[0_2]_s$ laminate.

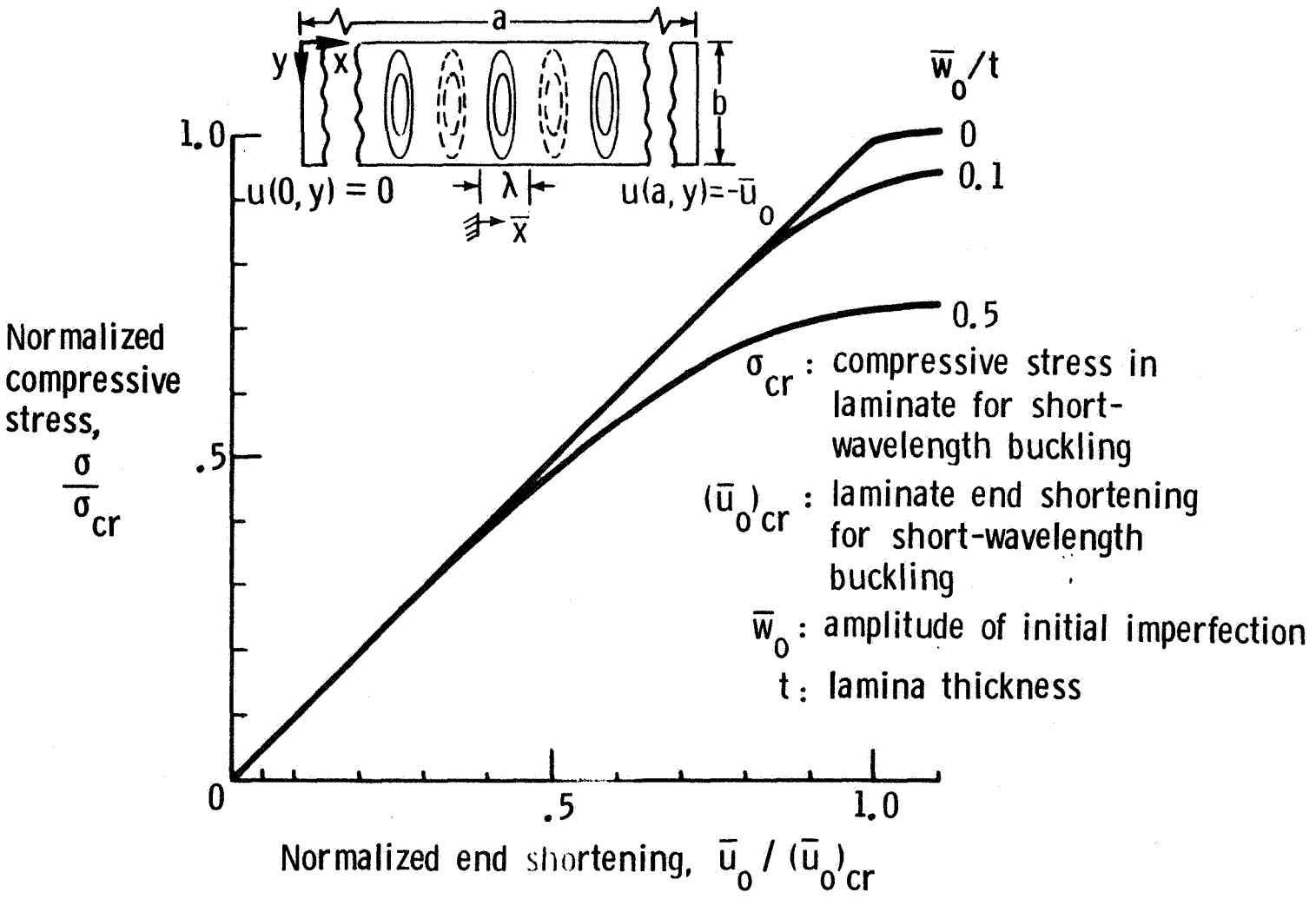

Figure 3.20. Normalized compressive stress versus end shortening for a $[0/90]_s$ laminate.

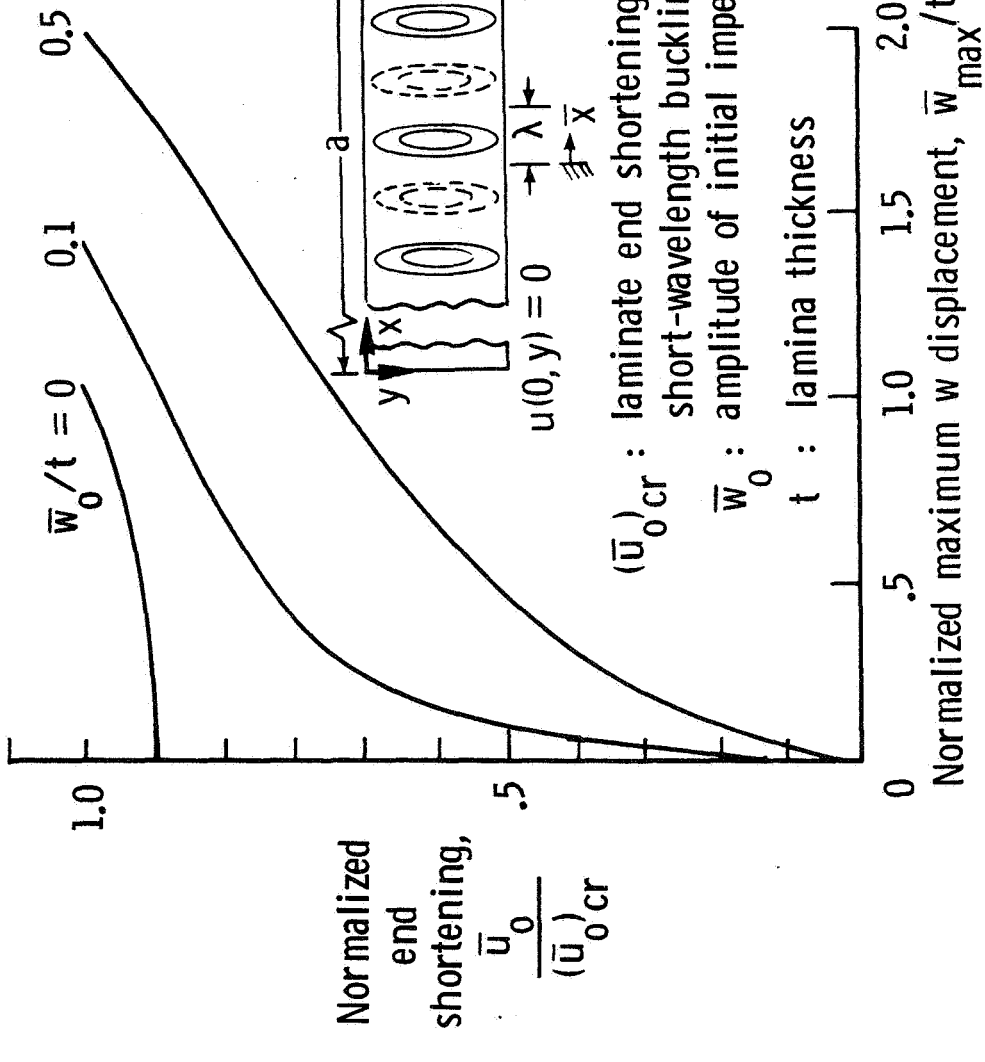

Figure 3.21. Maximum w displacement as a function of end shortening for a $[0/90]_s$ laminate.

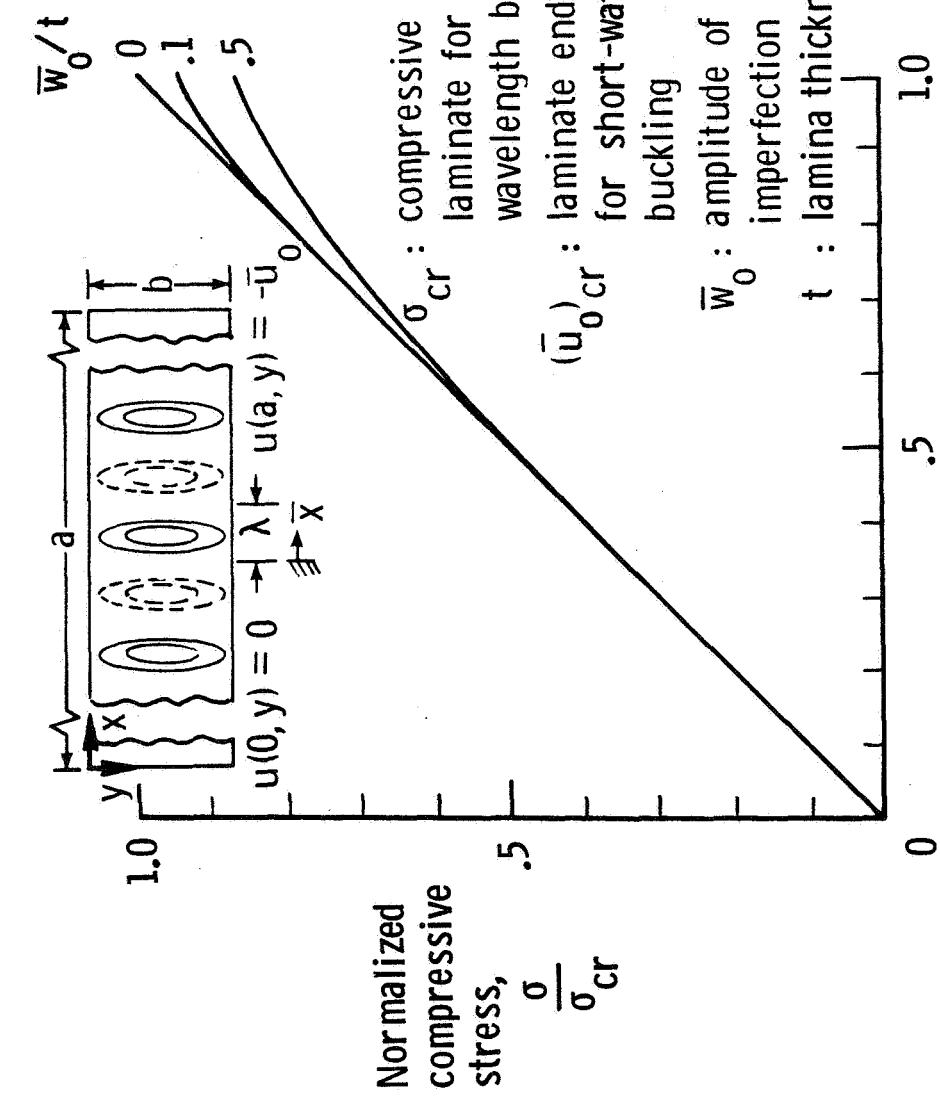

Figure 3.22. Normalized compressive stress versus end shortening for a $[\pm 45]_s$ laminate.

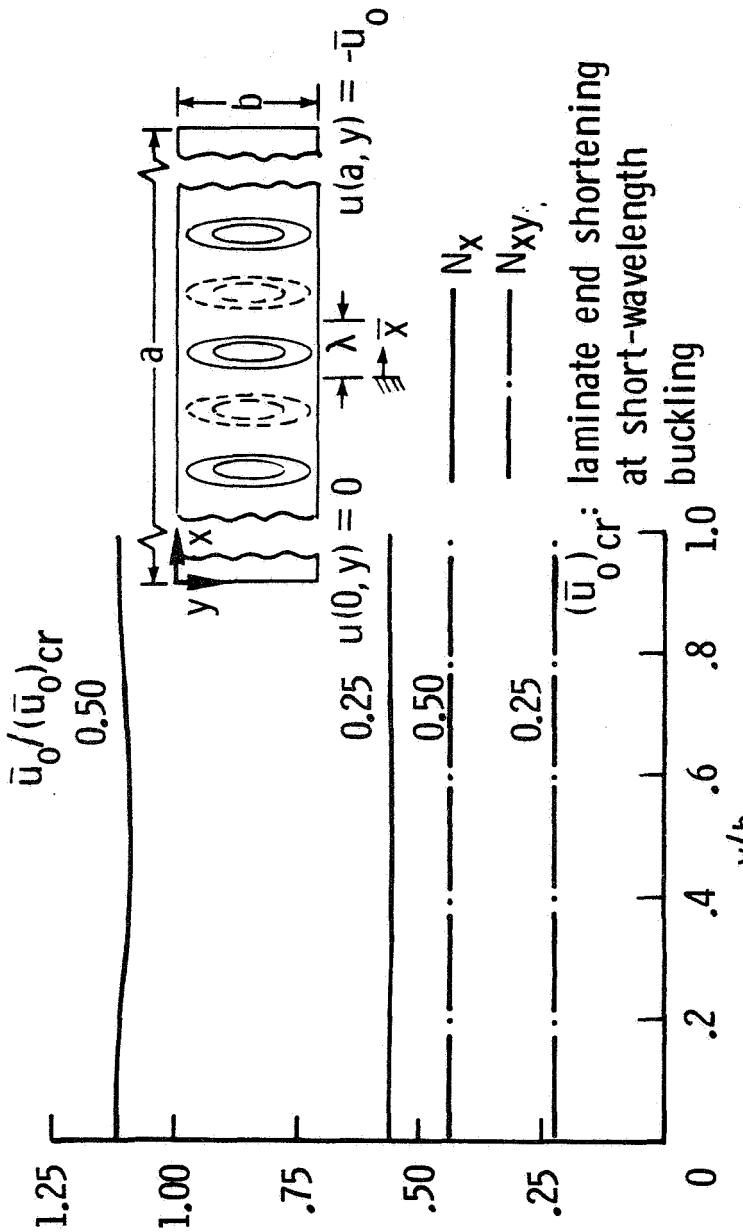

Figure 3.23. Stress resultants for a 45° lamina in a $[\pm 45]_s$ laminate ($\bar{w}_o/t = 0.5$).

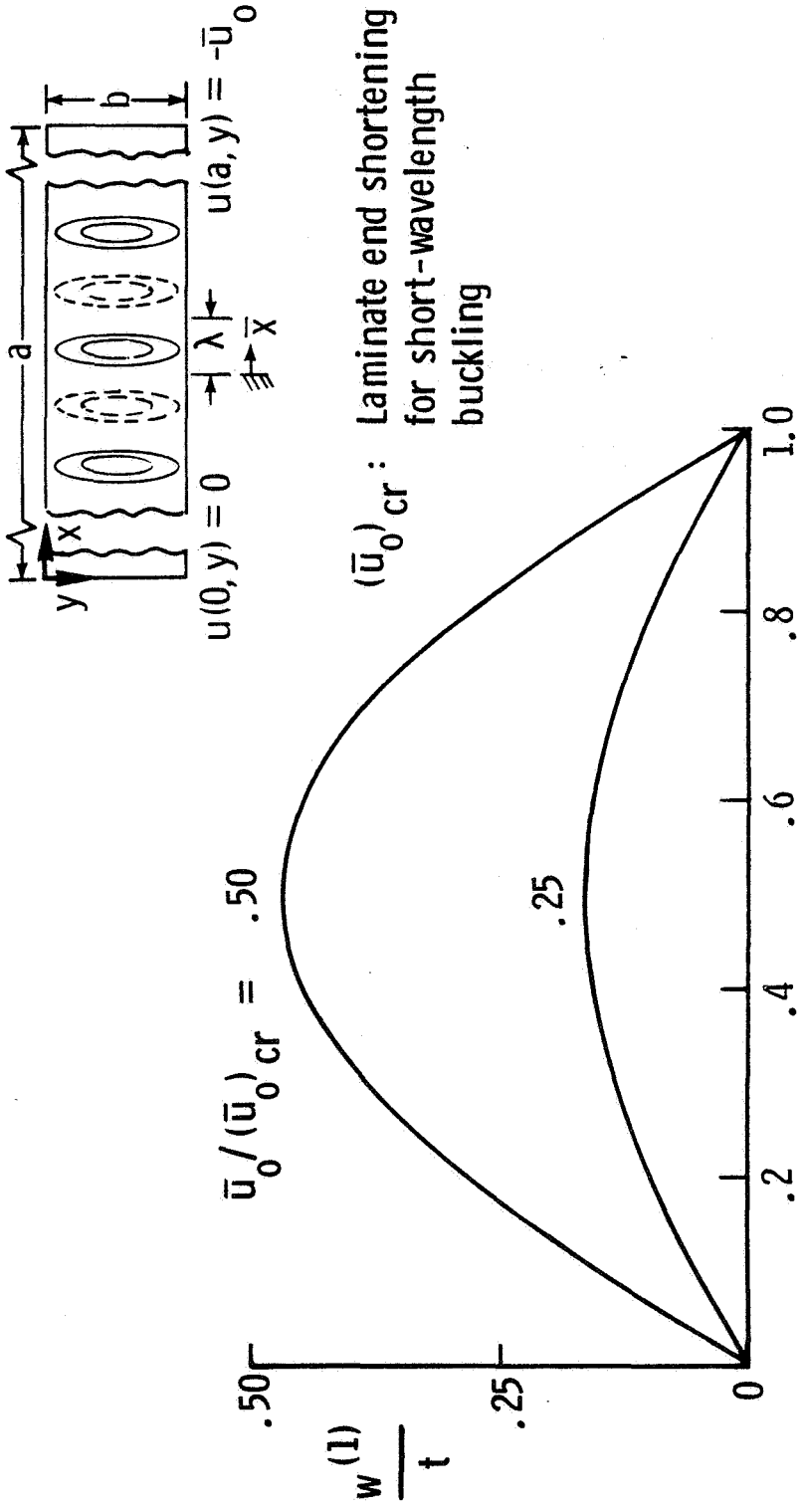

Figure 3.24. Distribution of the w displacement for the outer-most 45° lamina in a $[\pm 45]_s$ laminate along $\bar{x} = \lambda/2$ ($\bar{w}_o/t = 0.5$).

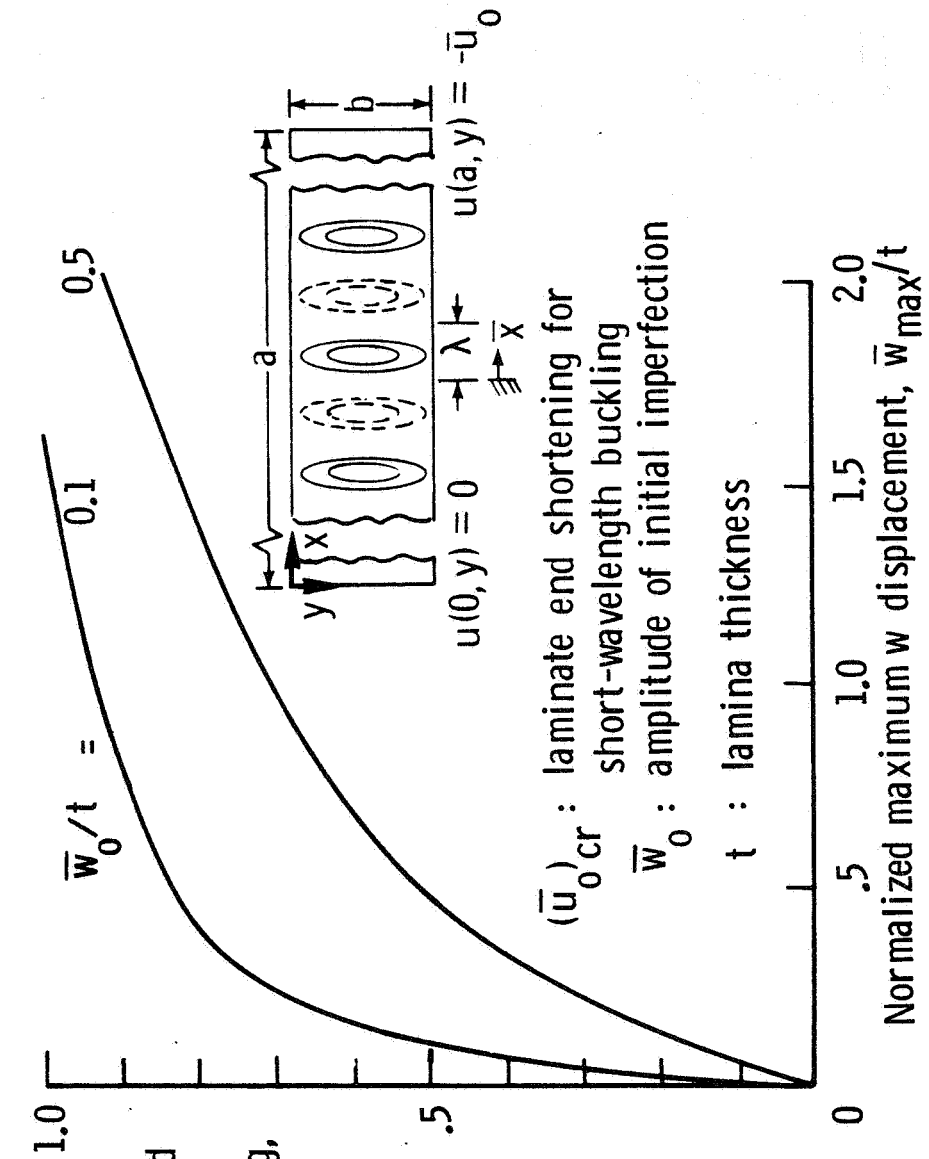

Figure 3.25. Maximum w displacement as a function of end shortening for a $[\pm 45]_s$ laminate.

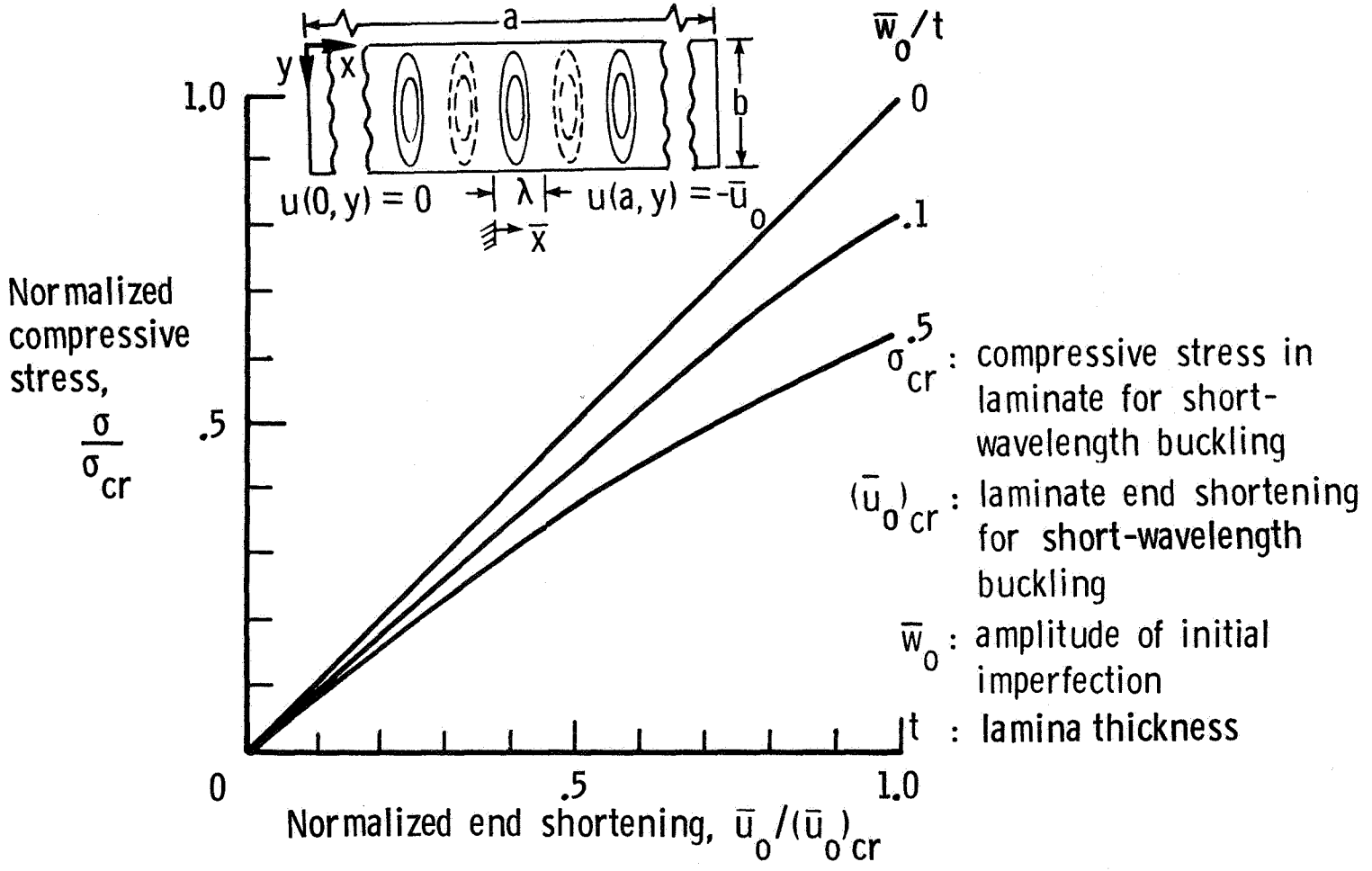

Figure 3.26. Normalized compressive stress versus end shortening for a $[+45/0/-45/90]_s$ laminate.

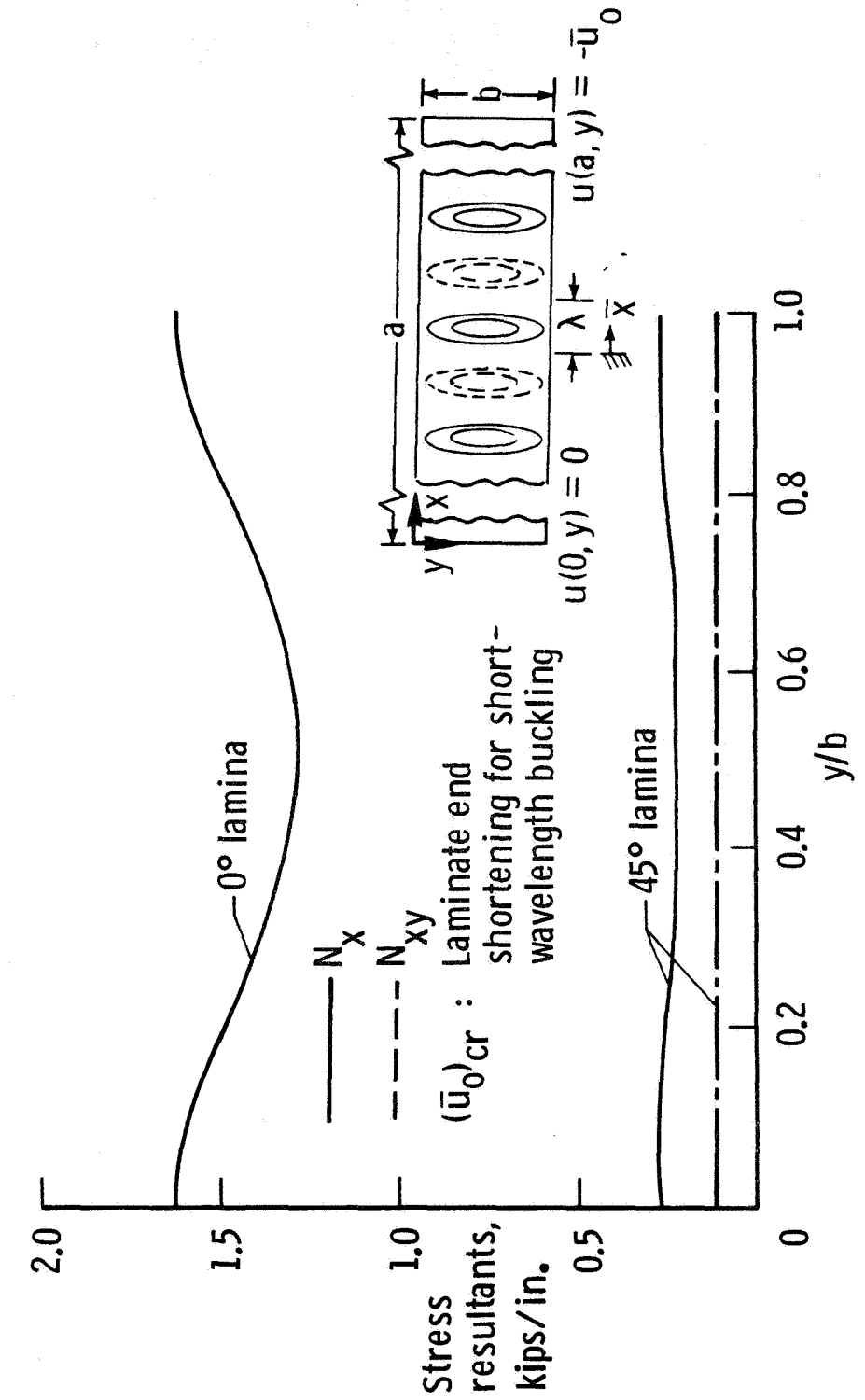

Figure 3.27. Stress resultants for 0° and 45° laminae in a $[+45/0/-45/90]_s$ laminate for $\bar{u}_o/(\bar{u}_o)_{cr} = 0.25$ ($\bar{w}_o/t = 0.5$).

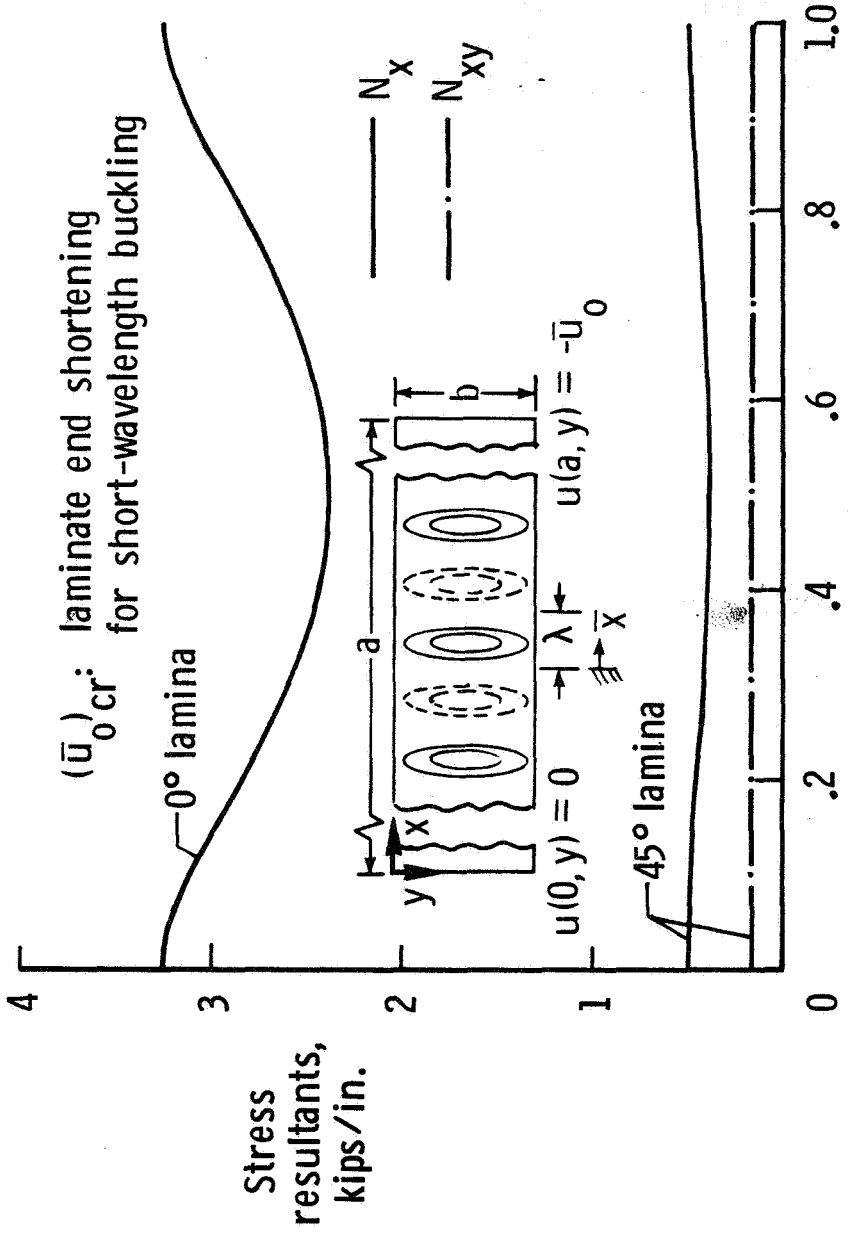

Figure 3.28. Stress resultants for 0° and 45° laminae in a $[+45/0/-45/90]_s$ laminate for $\bar{u}_o/(\bar{u}_o)_{cr} = 0.50$ ($\bar{w}_o/t = 0.5$).

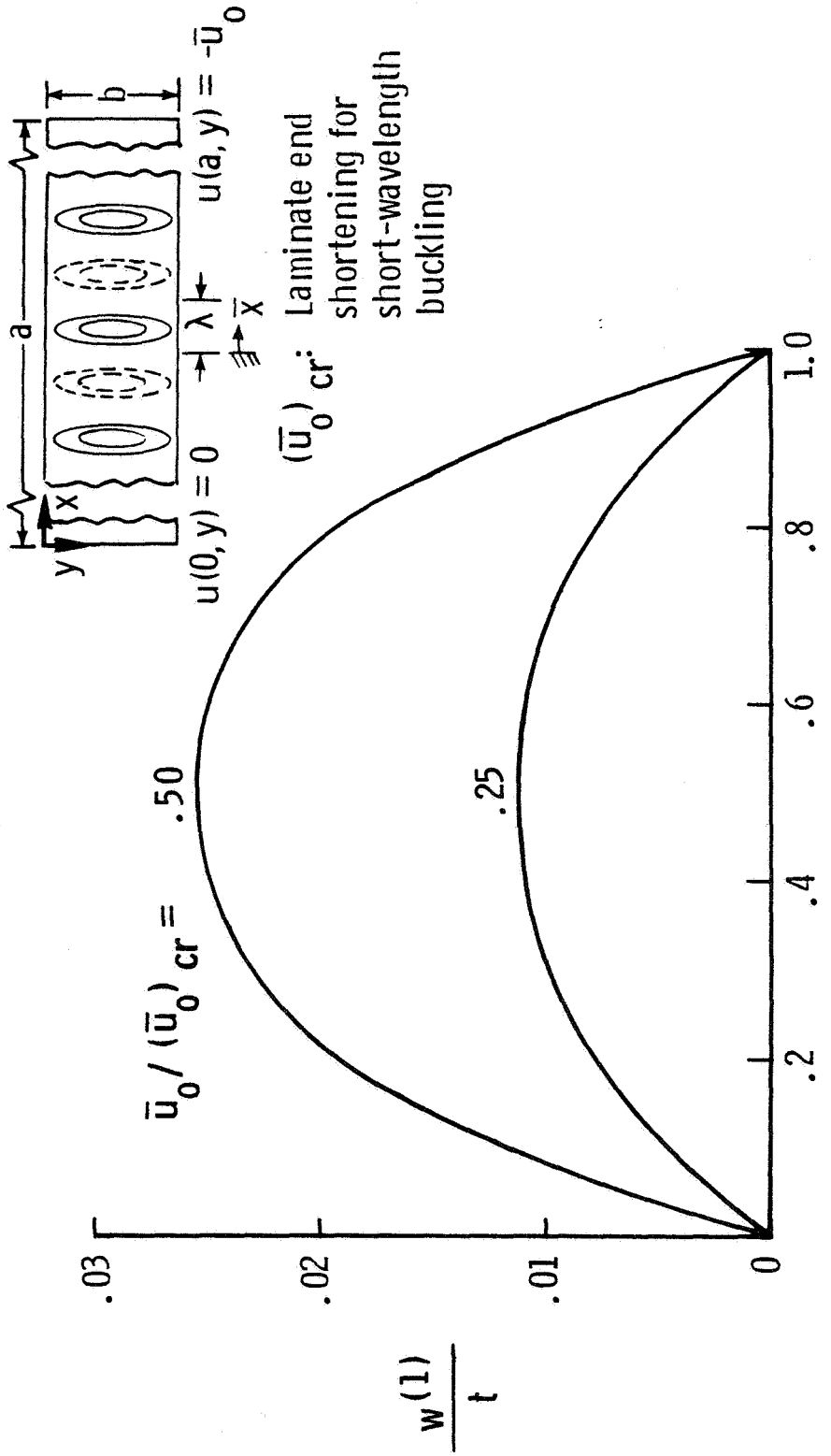

Figure 3.29. Distribution of the w displacement for the outer-most lamina ($+45^{\circ}$ lamina) in a $[+45/0/-45/90]_s$ laminate along $\bar{x} = \lambda/2$ ($\bar{w}_o/t = 0.5$).

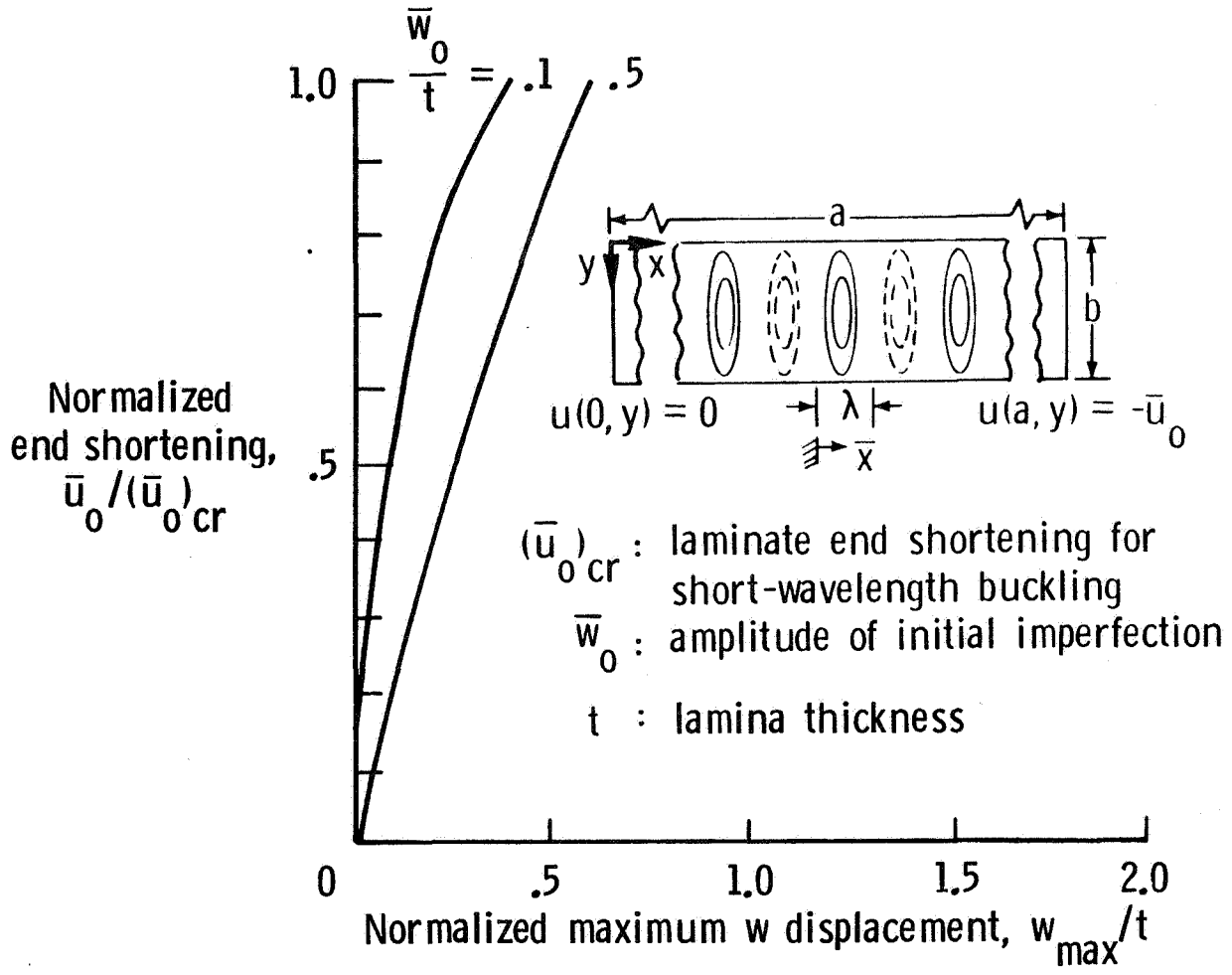

Figure 3.30. Maximum w displacement as a function of end shortening for a $[+45/0/-45/90]_s$ laminate.

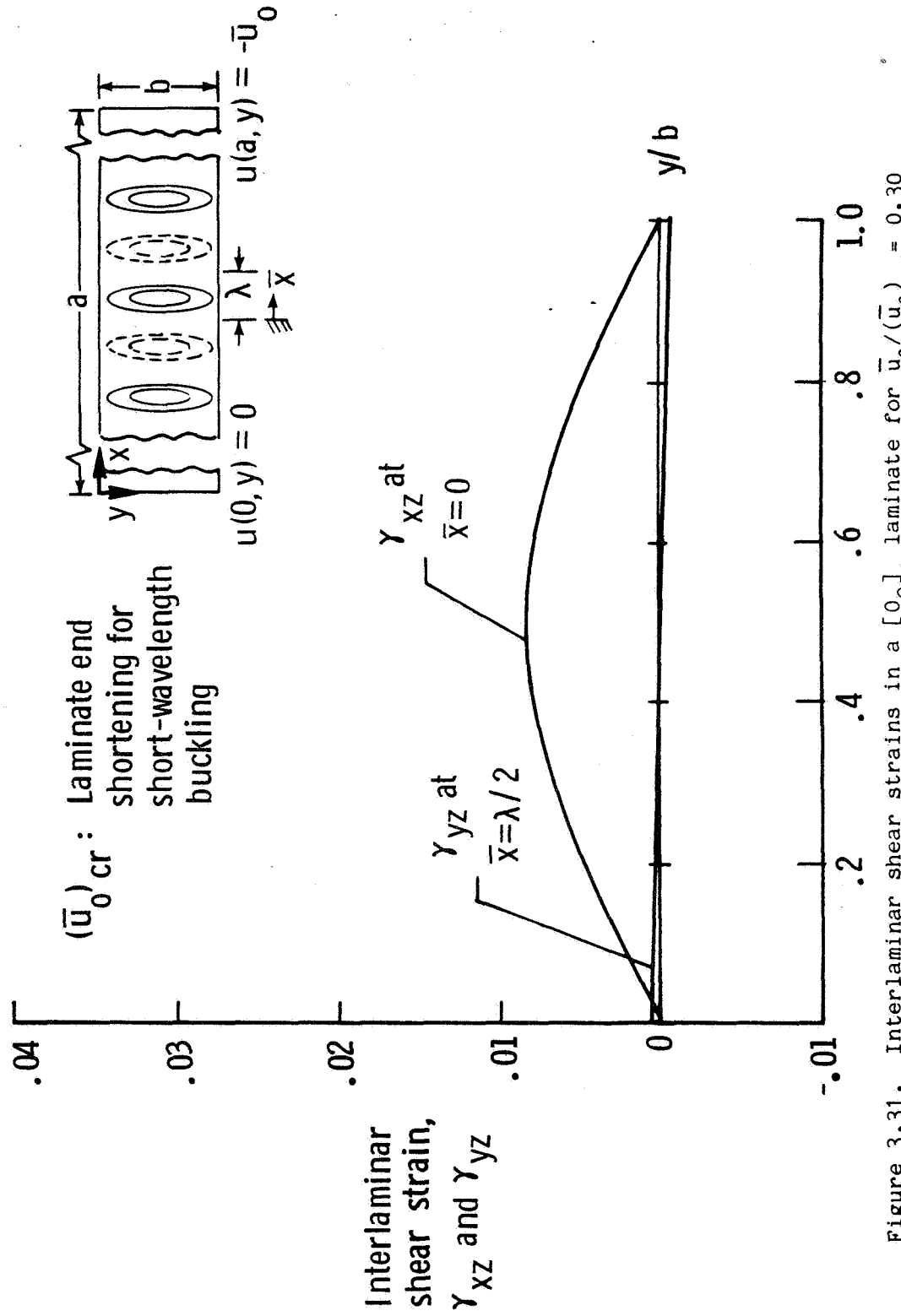

Figure 3.31. Interlaminar shear strains in a $[0_2]_s$ laminate for $\bar{u}_o/(\bar{u}_o)_{cr} = 0.30$ ($\bar{w}_o/t = 0.1$).

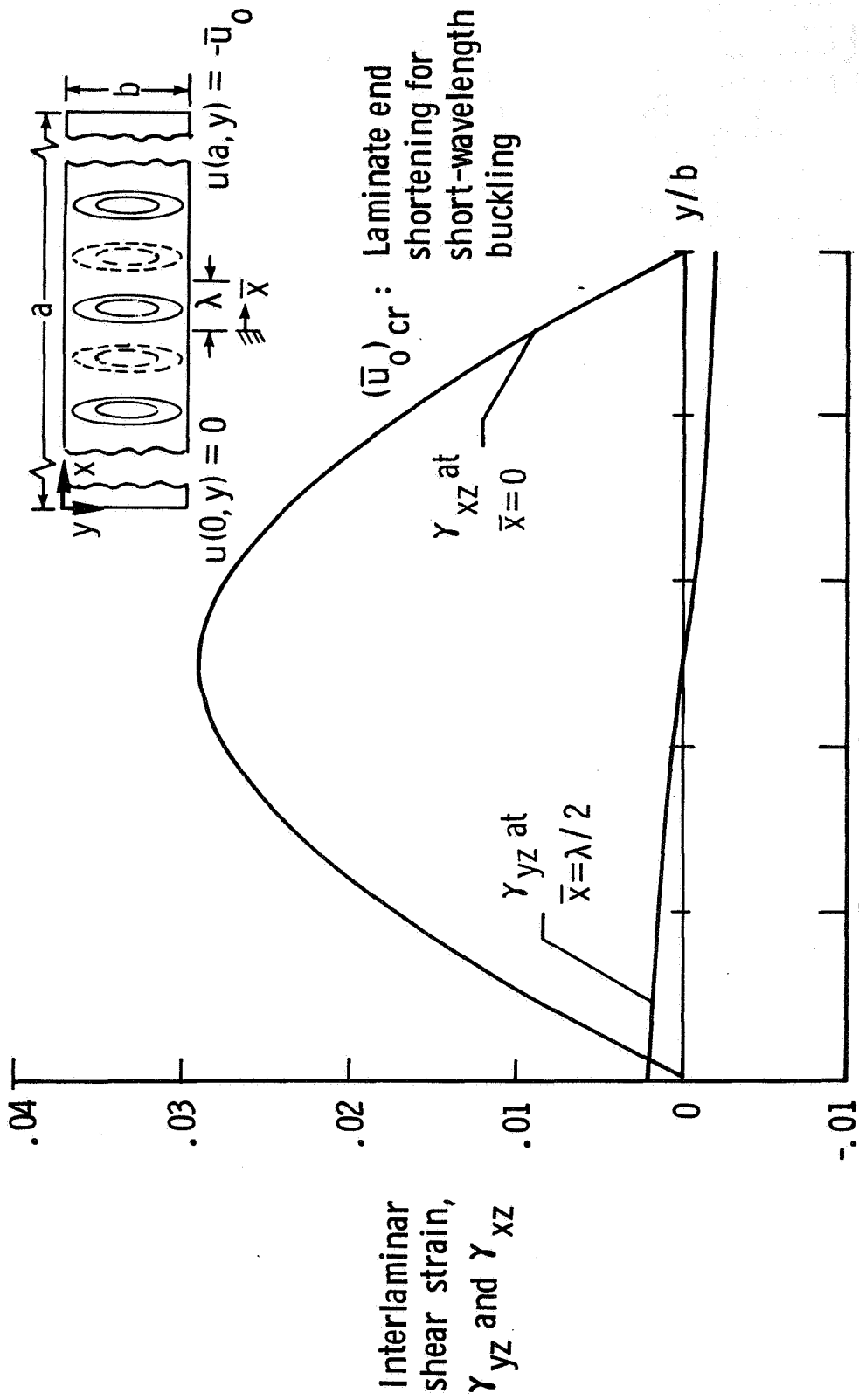

Figure 3.32. Interlaminar shear strains in a $[0_2]_s$ laminate for $\bar{u}_o/(\bar{u}_o)_{cr} = 0.60$ ($\bar{w}_o/t = 0.1$).

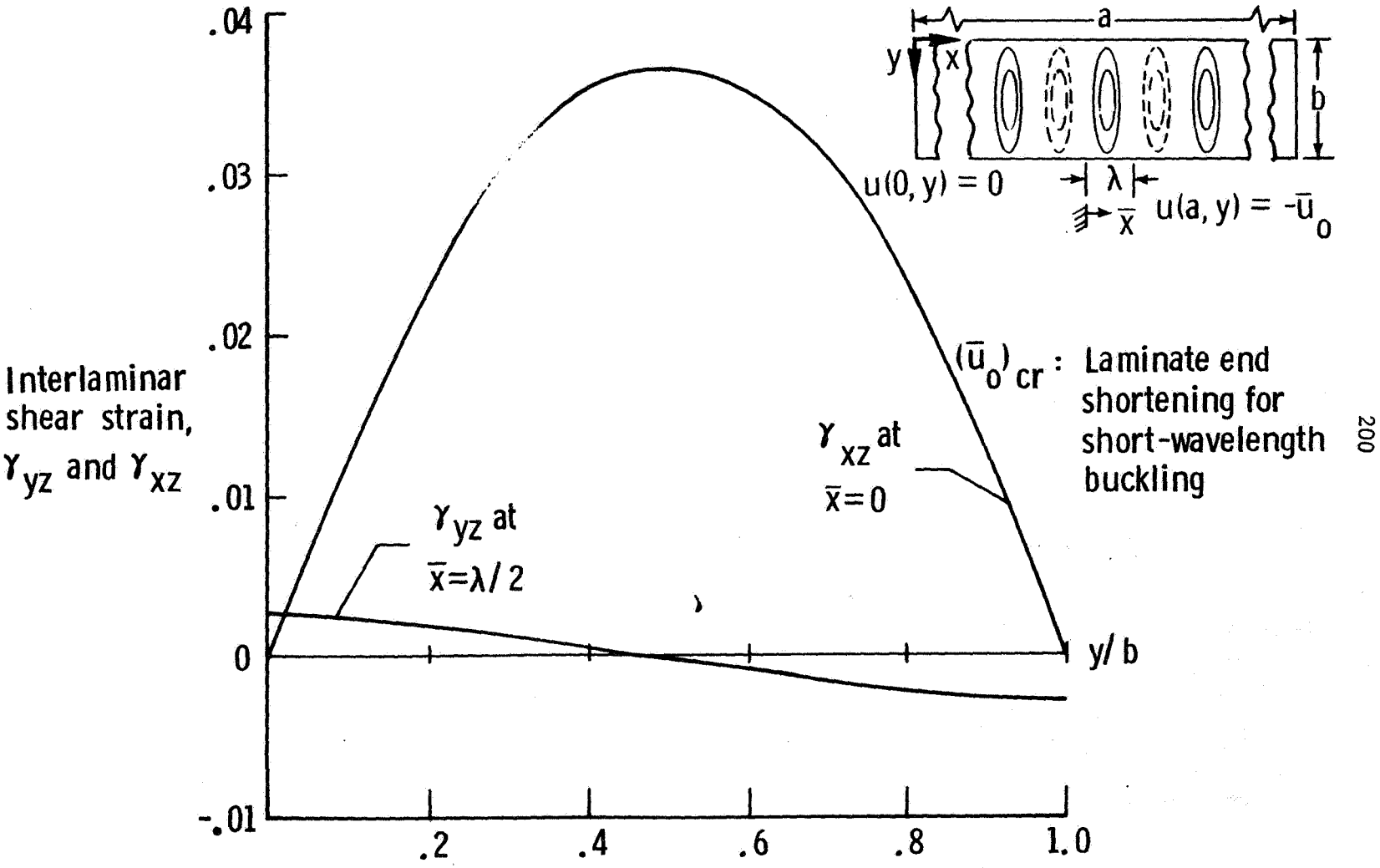

Figure 3.33. Interlaminar shear strains in a $[0_2]_s$ laminate for $\bar{u}_o/(\bar{u}_o)_{cr}$ = 0.30 ($\bar{w}_o/t$ = 0.5).

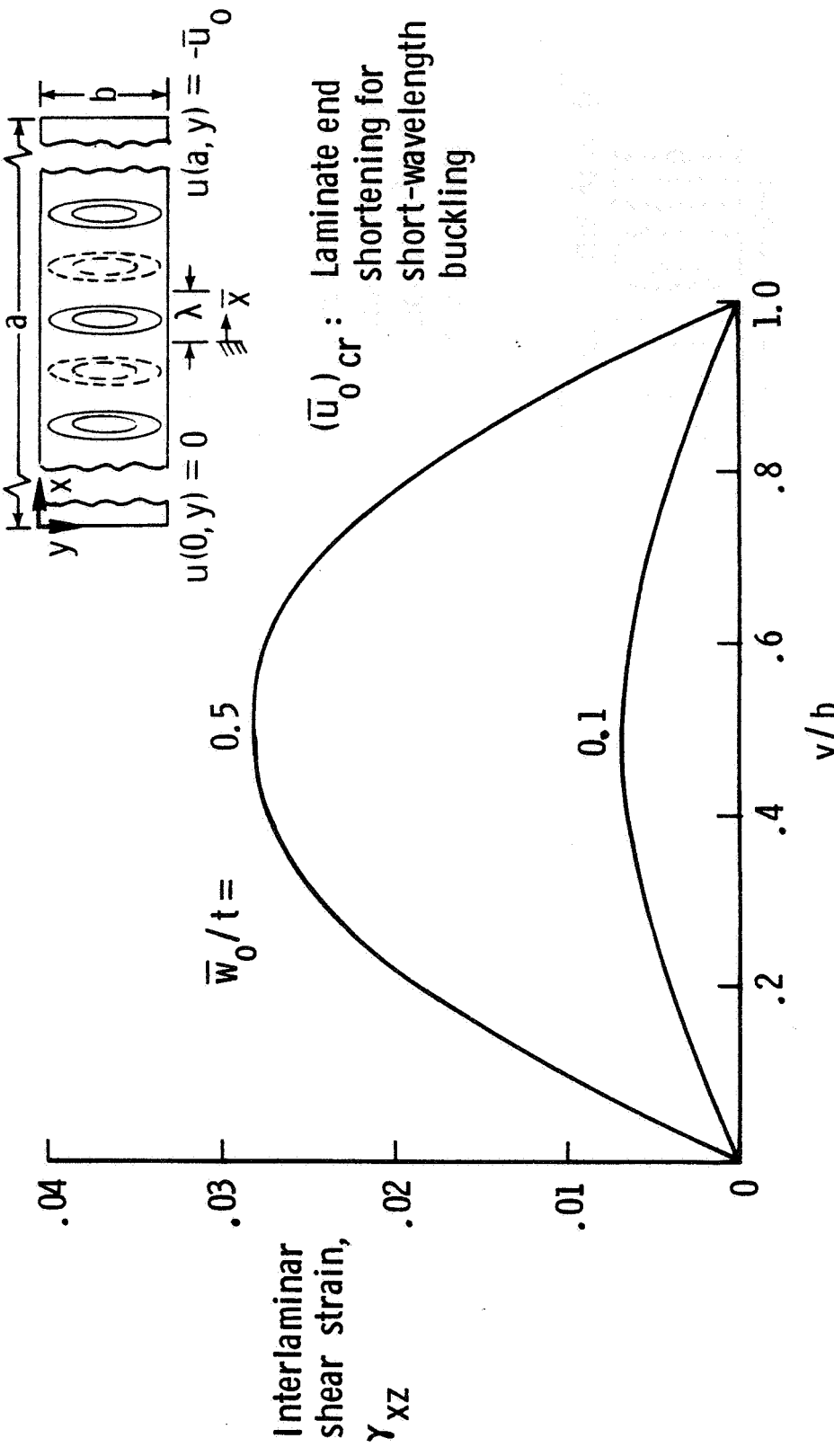

Figure 3.34. Interlaminar shear strain at the $0^\circ/90^\circ$ interface along $\bar{x} = 0$. for $[0/90]_s$ laminates for $\bar{u}_o/(\bar{u}_o)_{cr} = 0.20$.

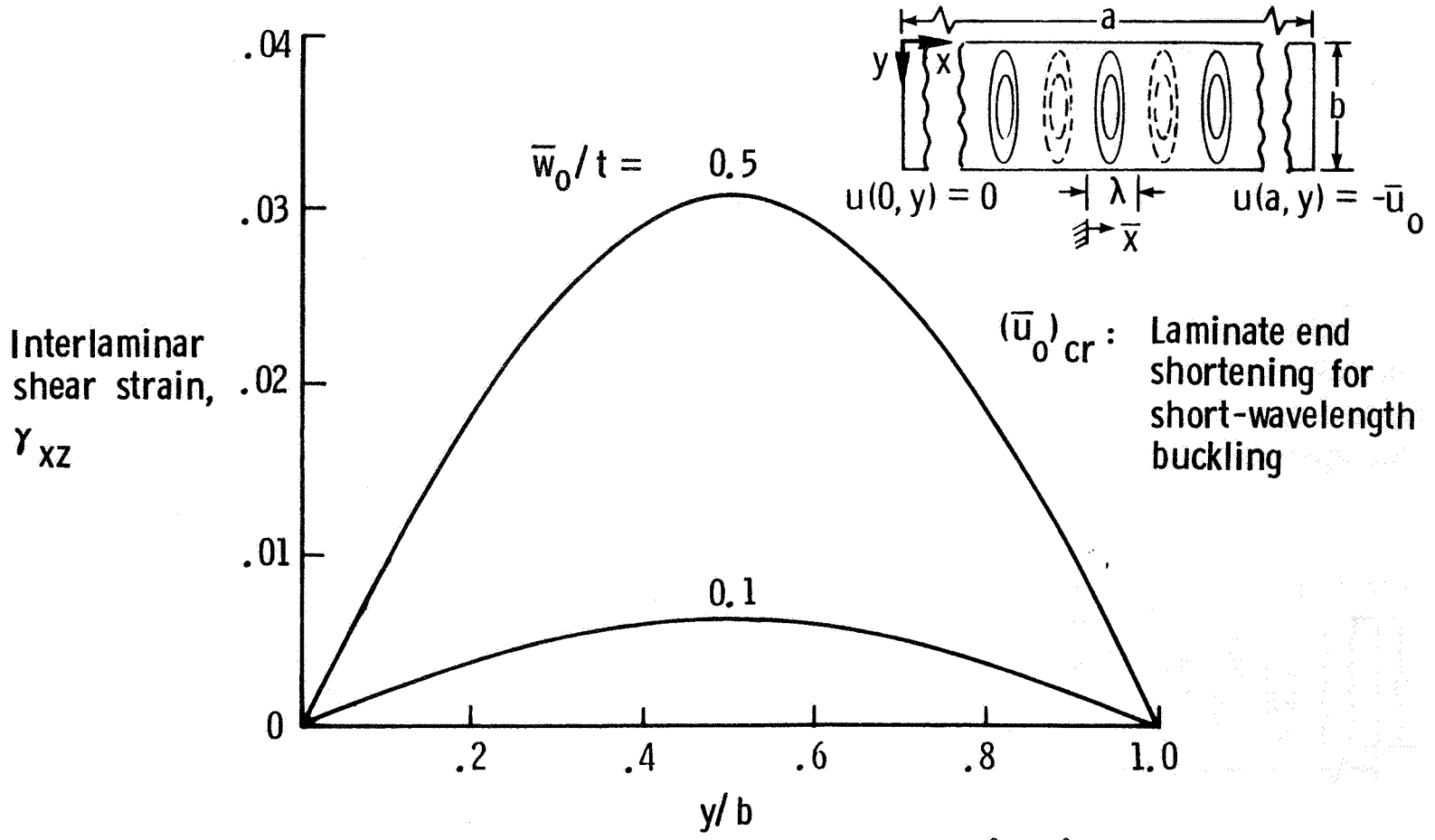

Figure 3.35. Interlaminar shear strain at the +45°/-45° interface along $\bar{x} = 0$. for $[\pm 45]_s$ laminates for $\bar{u}_o/(\bar{u}_o)_{cr} = 0.20$.

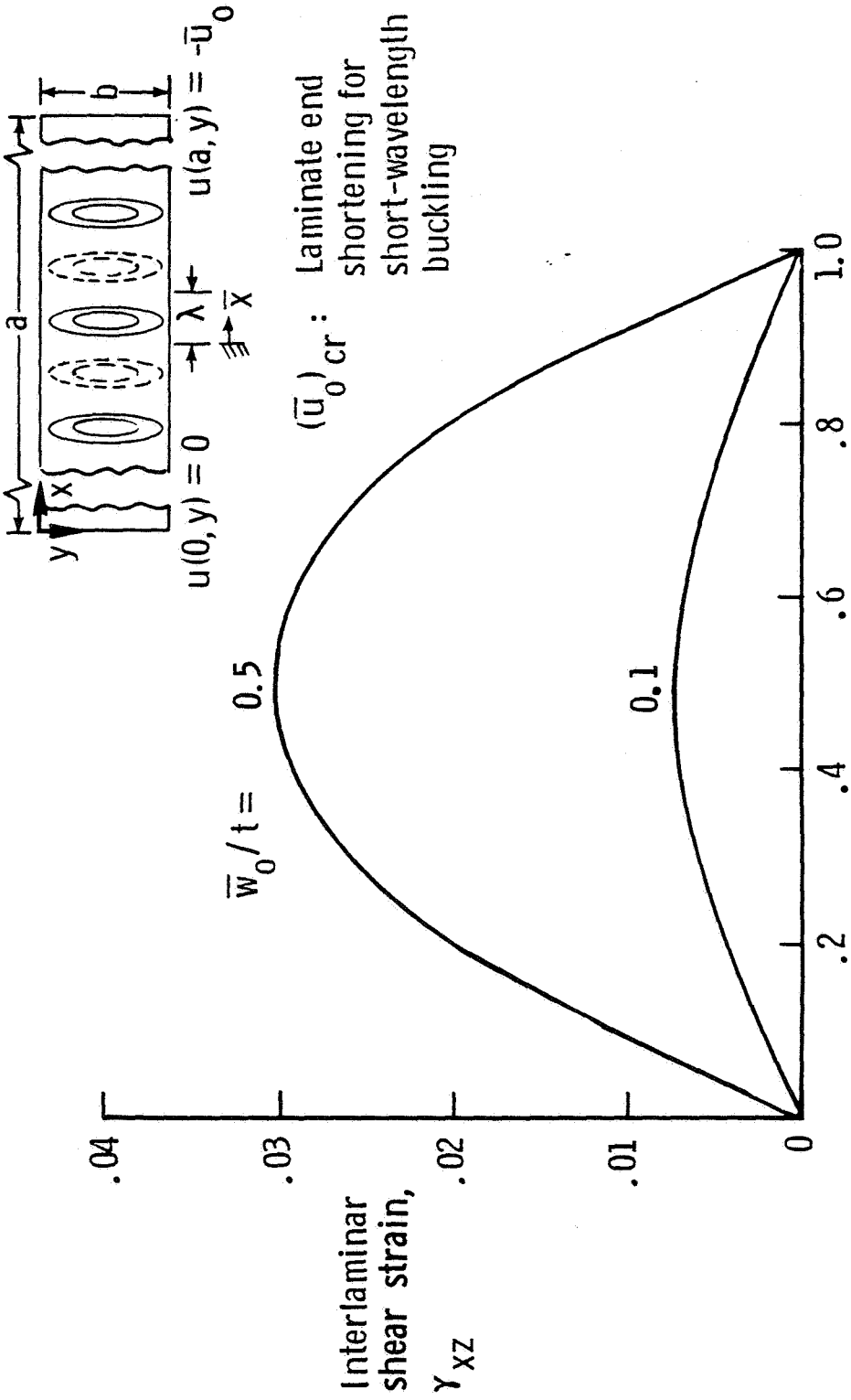

Figure 3.36. Interlaminar shear strain at the $+45^{\circ}/\underline{0}^{\circ}$ interface along $\bar{x} = 0$. for $[+45/0/-45/90]_s$ laminates for $\bar{u}_o/(\bar{u}_o)_{cr} = 0.10$.

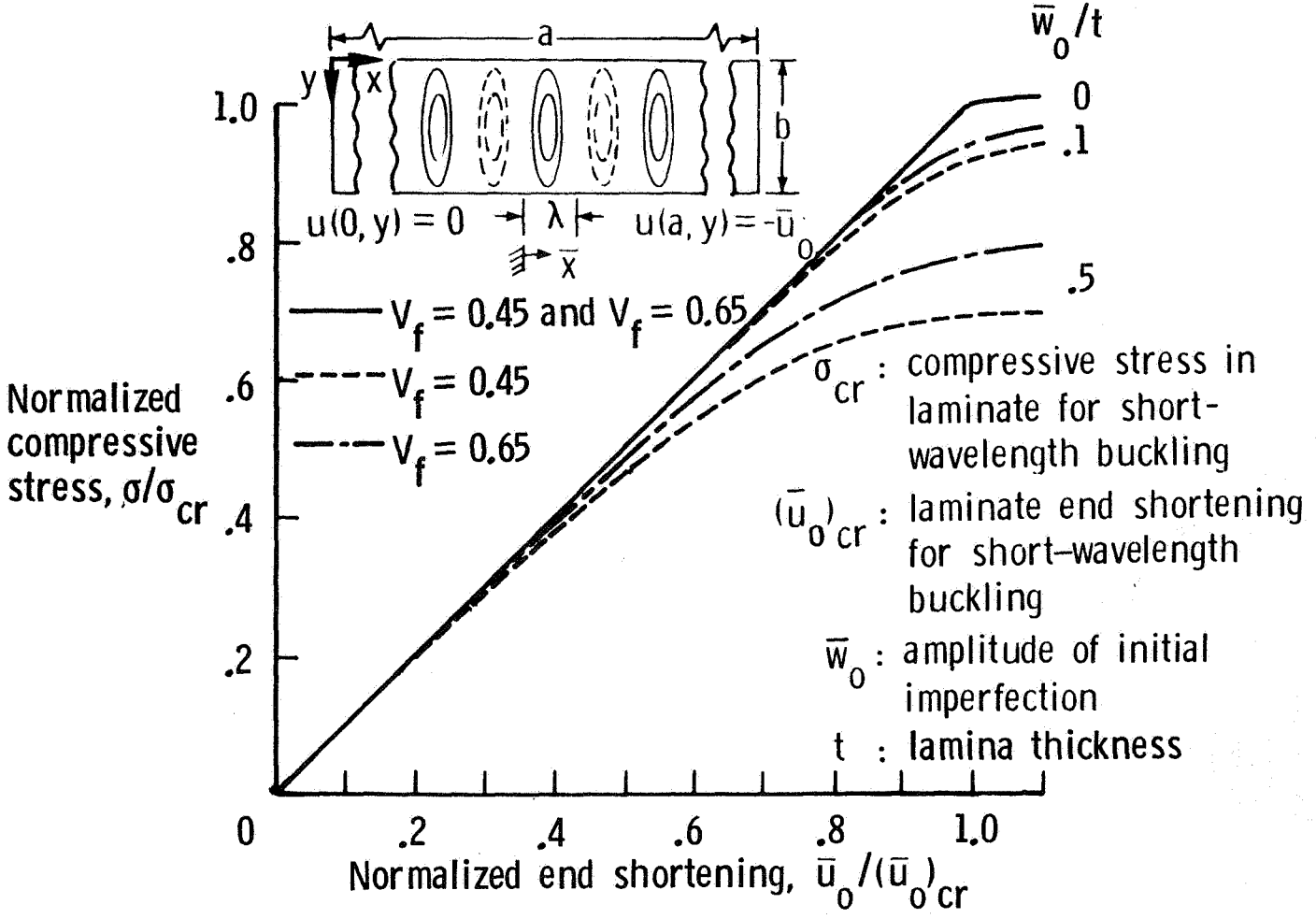

Figure 3.37. Effects of fiber volume fraction on the normalized compressive-stress - end-shortening behavior for a $[0_2]_s$ laminate.

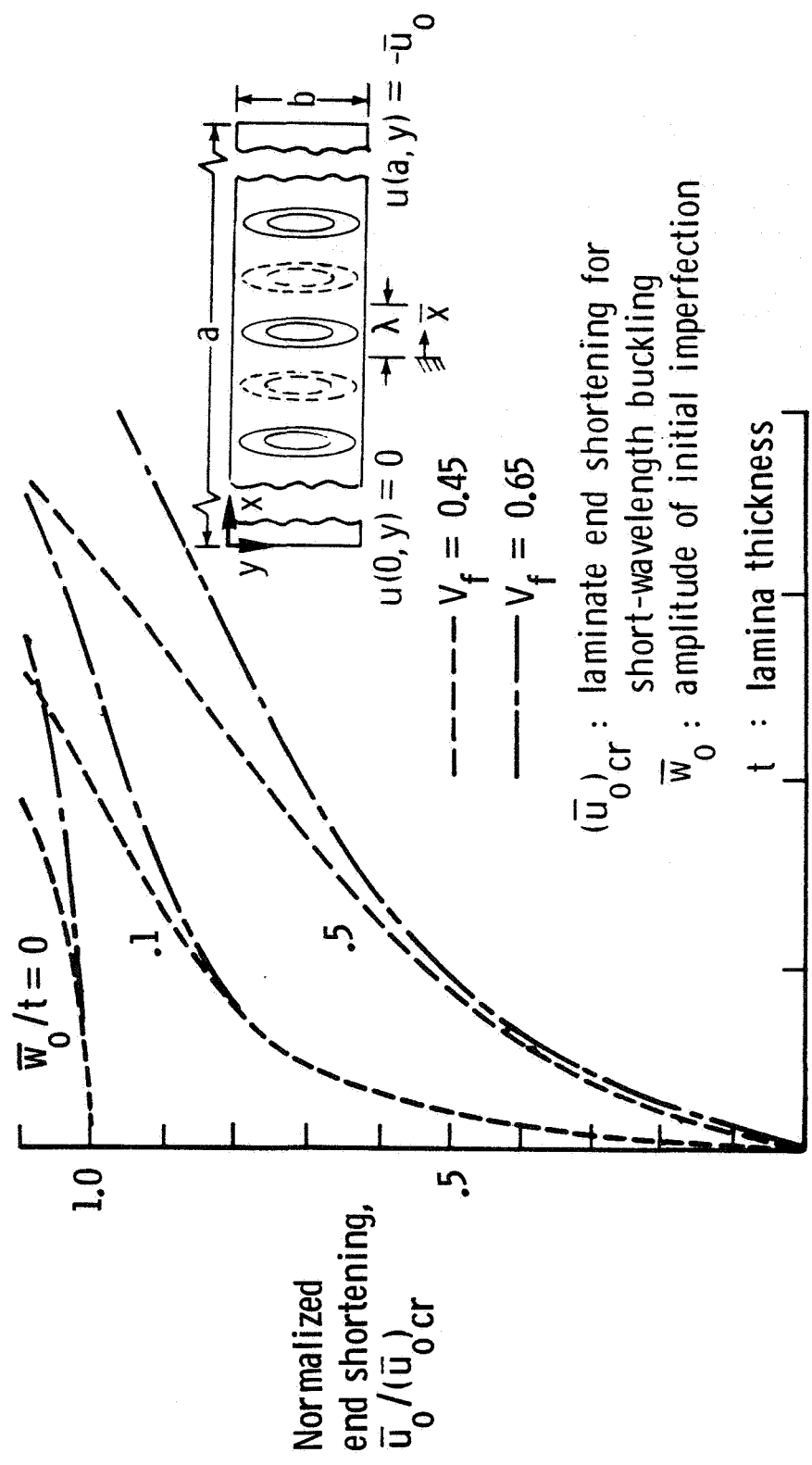

Figure 3.38. Effects of fiber volume fraction on the maximum w displacement as a function of the end shortening for a $[0_2]_s$ laminate.

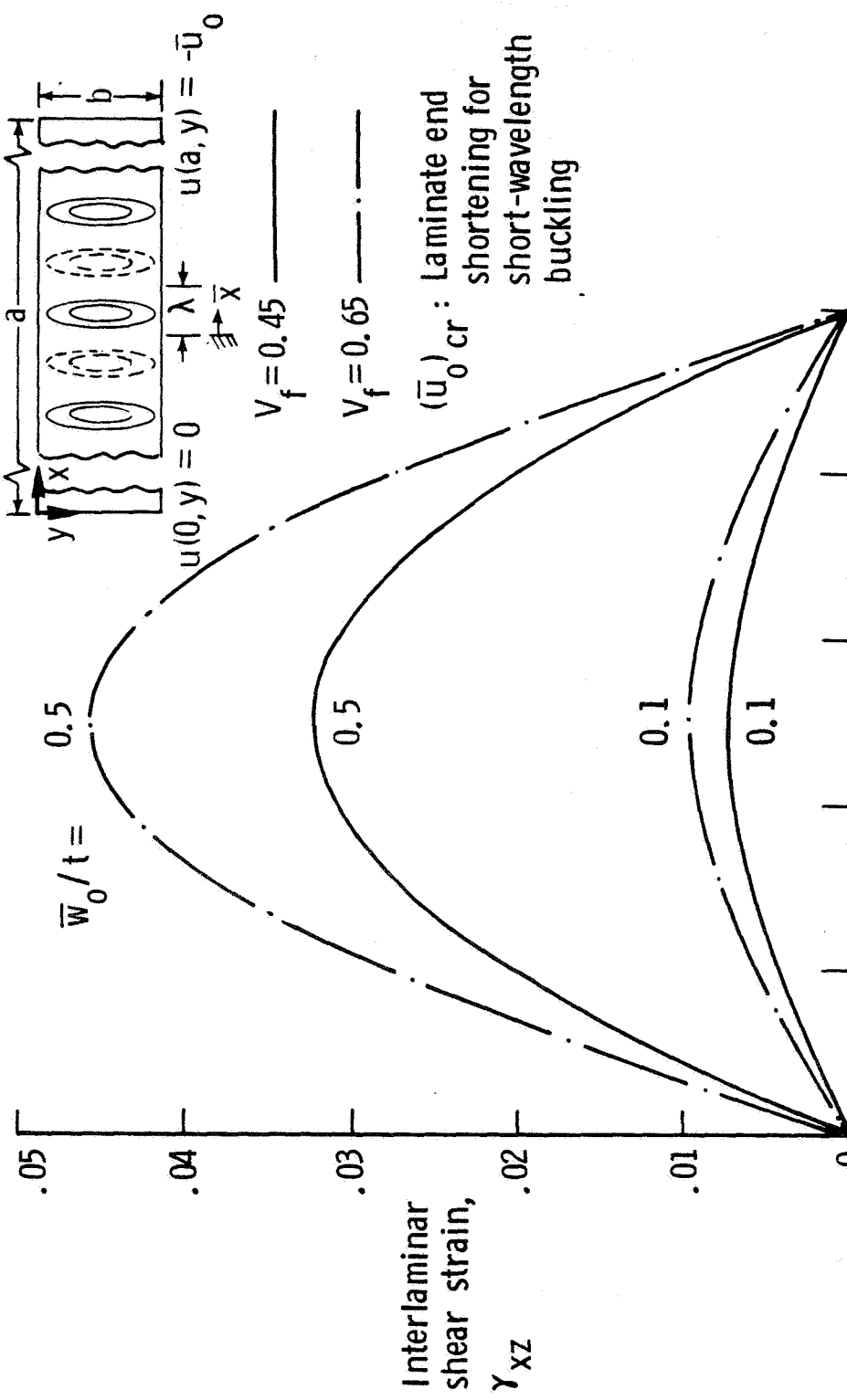

Figure 3.39. Effects of fiber volume fraction on γ_{xz} along $\bar{x} = 0.$ for $[0_2]_s$ laminates for $\bar{u}_o/(\bar{u}_o)_{cr} = 0.30$.

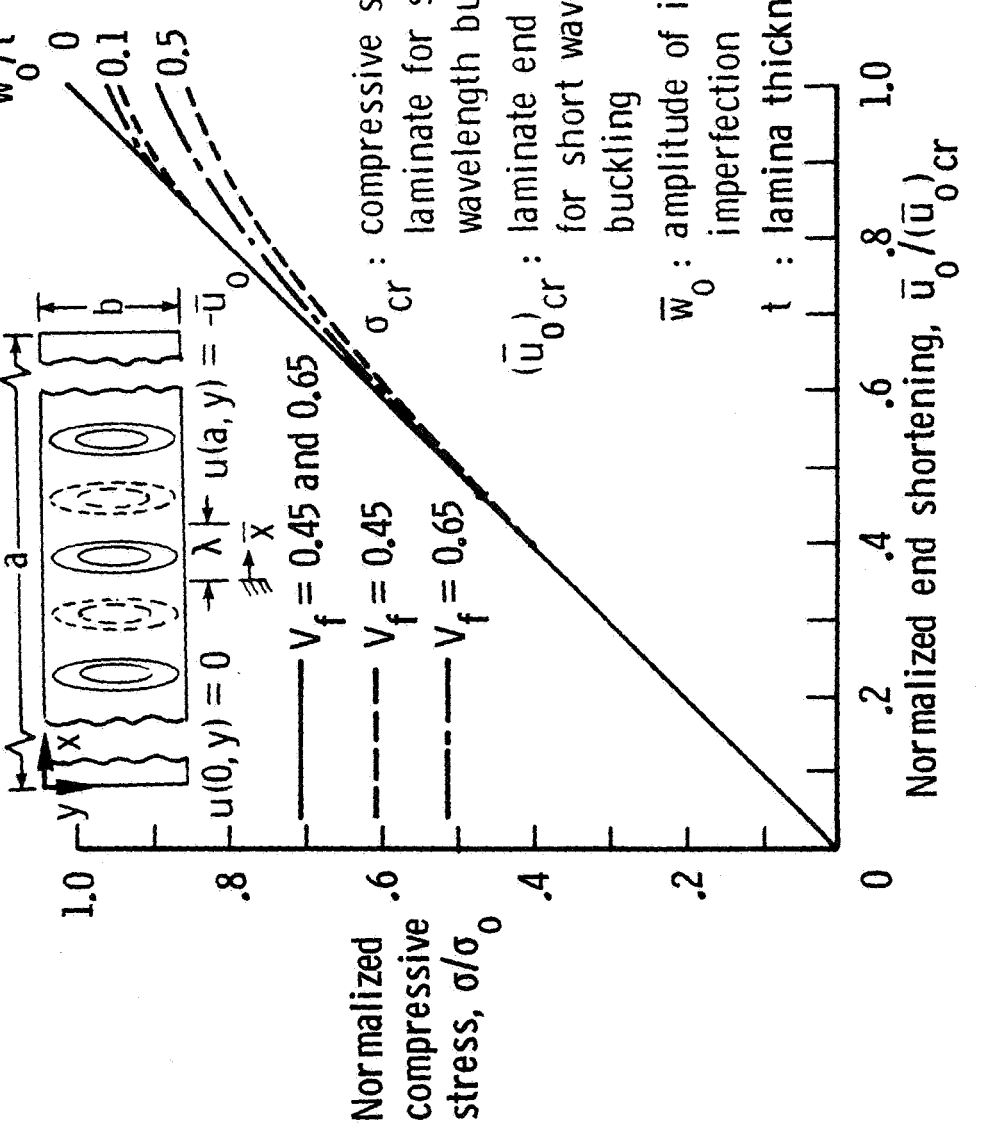

Figure 3.40. Effects of fiber volume fraction on the normalized compressive-stress - end-shortening behavior for a $[\pm 45]_s$ laminate.

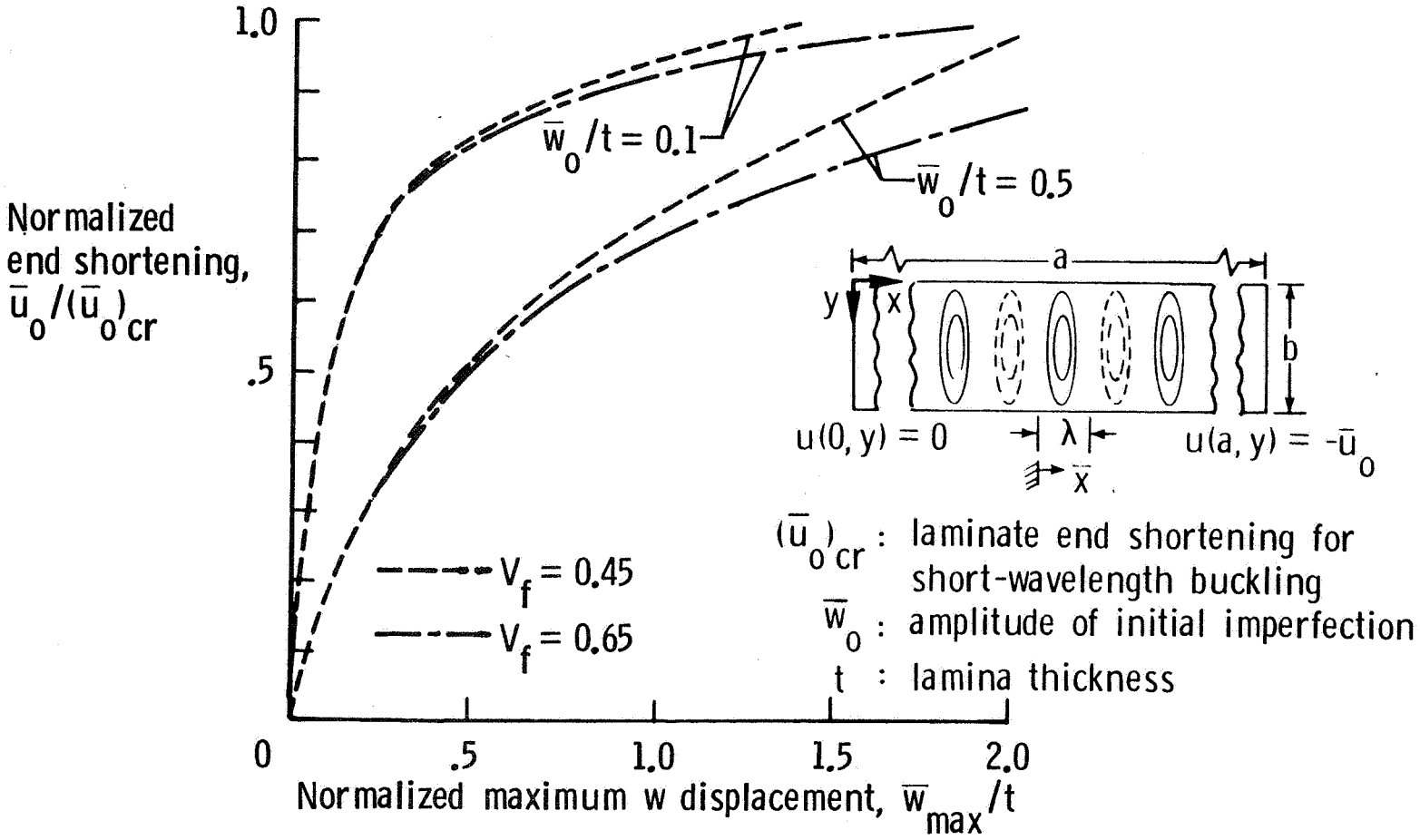

Figure 3.41. Effects of fiber volume fraction on the maximum w displacement as a function of the end shortening for a $[\pm 45]_s$ laminate.

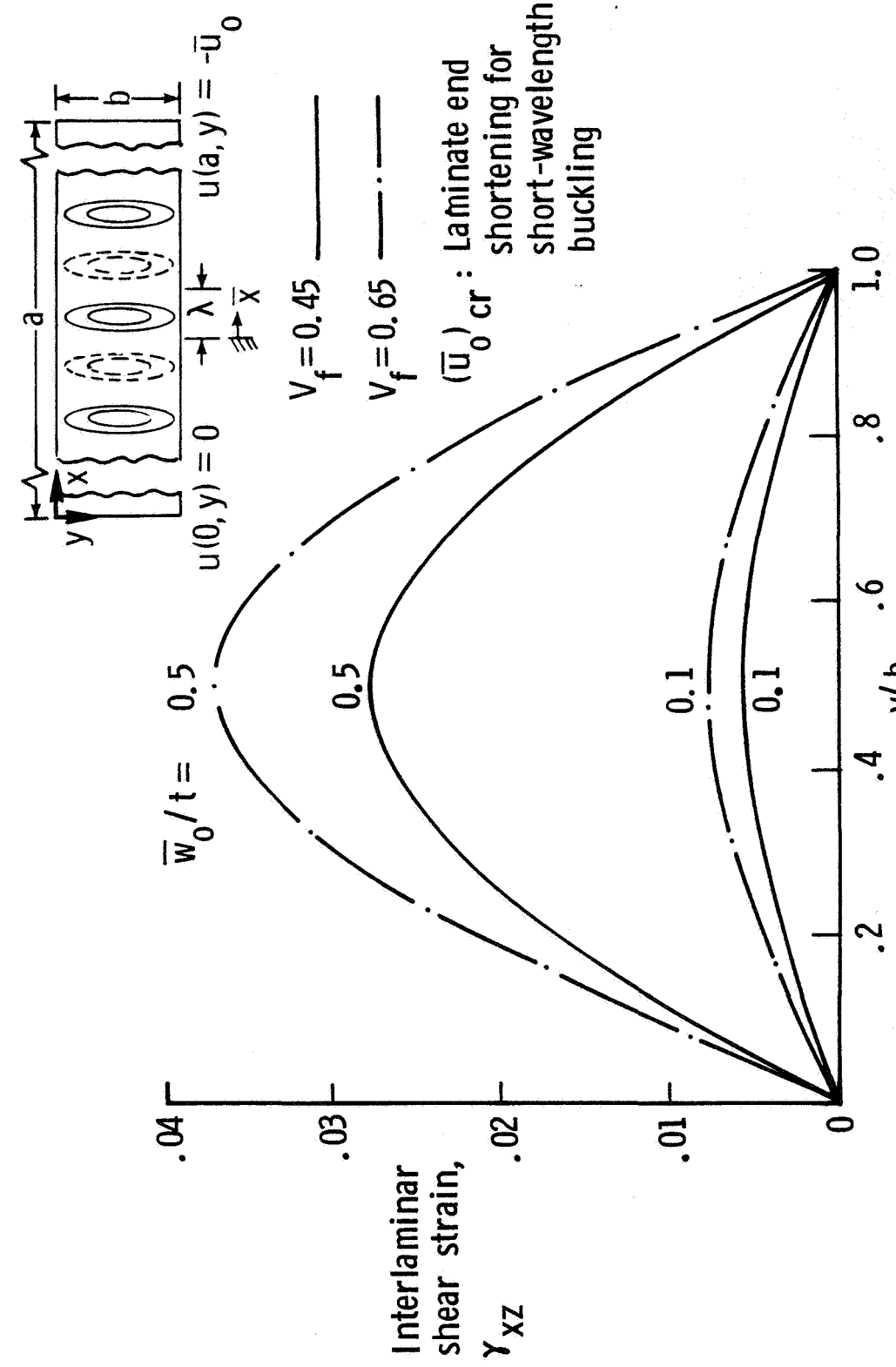

Figure 3.42. Effects of fiber volume fraction on γ_{xz} at the $+45^{\circ}/45^{\circ}$ interface along $\bar{x} = 0.$ for $[\pm 45]_s$ laminates for $\bar{u}_o/(\bar{u}_o)_{cr} = 0.20$

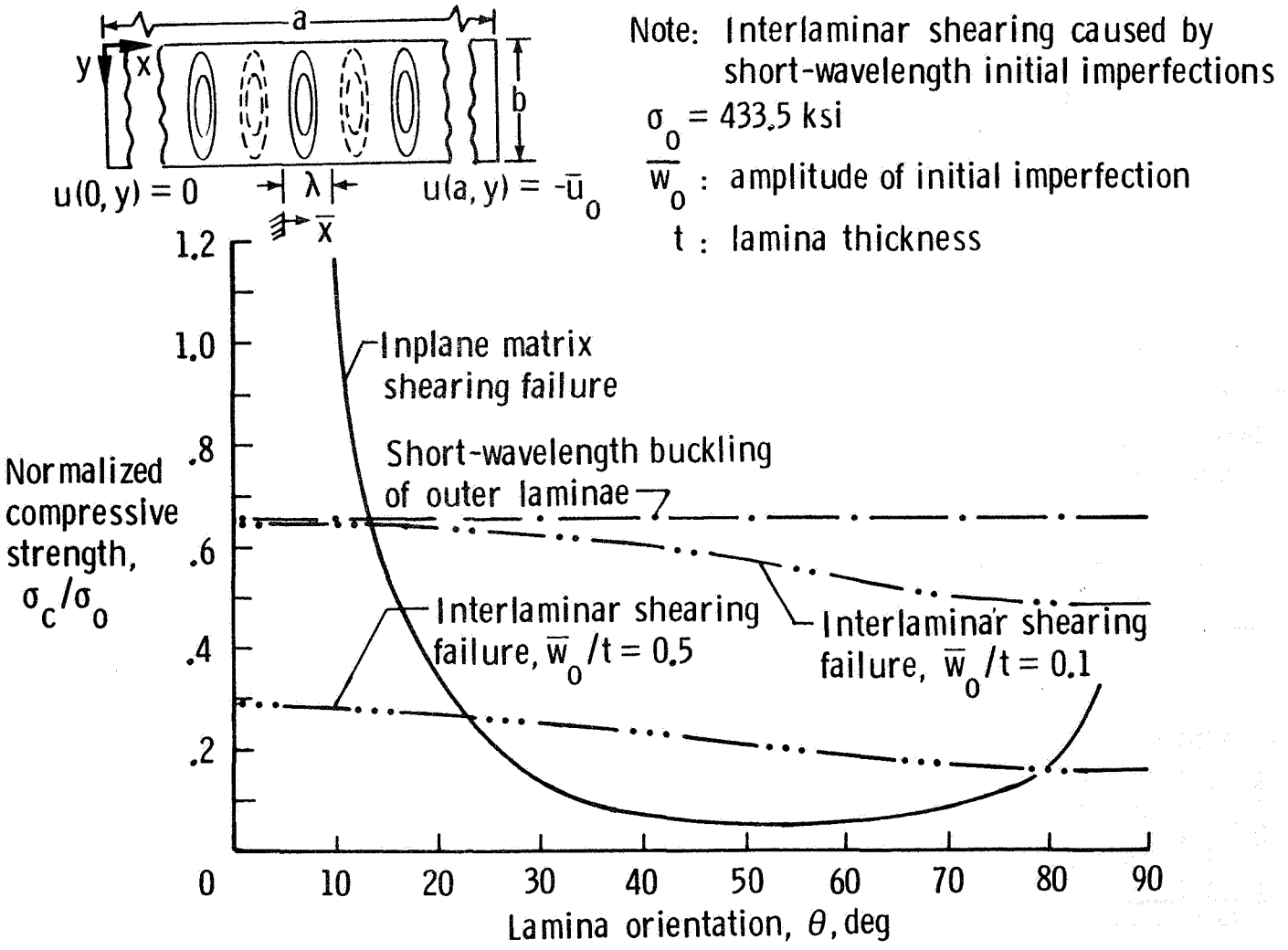

Figure 3.43. Compressive strength for a $[\pm\theta]_s$ laminate as a function of lamina orientation.

Standard Bibliographic Page

1. Report No.	2. Government Accession No.	3. Recipient's Catalog No.
NASA TM-87640		

4. Title and Subtitle	5. Report Date
Short-Wavelength Buckling and Shear Failures for Compression-Loaded Composite Laminates	November 1985
	6. Performing Organization Code: 534-06-23-08
7. Author(s): Mark J. Shuart	8. Performing Organization Report No.
9. Performing Organization Name and Address: NASA Langley Research Center, Hampton, VA 23665-5225	10. Work Unit No.
	11. Contract or Grant No.
12. Sponsoring Agency Name and Address: National Aeronautics and Space Administration, Washington, DC 20546	13. Type of Report and Period Covered: Technical Memorandum
	14. Sponsoring Agency Code

15. Supplementary Notes

Author's Ph.D. Dissertation, University of Delaware, Newark, DE

16. Abstract

This investigation studies the short-wavelength buckling (or the microbuckling) and the interlaminar and inplane shear failures of multi-directional composite laminates loaded in uniaxial compression. A laminate model is presented that idealizes each lamina. The fibers in the lamina are modeled as a plate, and the matrix in the lamina is modeled as an elastic foundation. The out-of-plane w displacement for each plate is expressed as a trigonometric series in the half-wavelength of the mode shape for laminate short-wavelength buckling. Nonlinear strain-displacement relations are used. The model is applied to symmetric laminates having linear material behavior. The laminates are loaded in uniform end shortening and are simply supported. A linear analysis is used to determine the laminate stress, strain, and mode shape when short-wavelength buckling occurs. A nonlinear analysis for laminae with initial imperfections is used to determine laminate stresses and interlaminar strains. A failure criterion for compression-loaded laminates is discussed.

17. Key Words (Suggested by Authors(s))	18. Distribution Statement
Composite Materials Compression Failure Interlaminar stresses Microbuckling	Unclassified - Unlimited Subject Category 24

19. Security Classif.(of this report)	20. Security Classif.(of this page)	21. No. of Pages	22. Price
Unclassified	Unclassified	227	A11

For sale by the National Technical Information Service, Springfield, Virginia 22161

NASA Langley Form 63 (June 1985)